2015

Catalytic Synthesis of Higher Alcohols from Syngas

Ranjan Kumar Sahoo
Lehigh University

Catalytic Synthesis of Higher Alcohols from Syngas

by

Ranjan Kumar Sahoo

Presented to the Graduate and Research Committee
of Lehigh University
in Candidacy for the degree of
Doctor of Philosophy

in
Chemical Engineering

Lehigh University
January, 2015

January, 2015

Approved and recommended for acceptance as a dissertation in partial fulfillment of the requirements for the degree of Doctor of Philosophy in Chemical Engineering.

"Catalytic Synthesis of Higher Alcohols from Syngas"

Ranjan Kumar Sahoo

_____
Date

_____
Hugo S. Caram, Ph.D., Dissertation Adviser

_____
Accepted Date

_____
Mark A. Snyder, Ph.D., Committee Member

_____
Divyanshu Acharya, Ph.D., Committee Member

_____
Richard G. Herman, Ph.D., Committee Member

_____
James T. Hsu, Ph.D., Committee Member

_____
Steven McIntosh, Ph.D., Committee Member

Acknowledgments

I would like to express my sincere gratitude to my thesis advisor, Professor Hugo S. Caram for his excellent guidance, support, and constant encouragement throughout my research work.

I am extremely grateful to Dr. Richard G. Herman and Dr. Divyanshu Acharya, member of my research committee, for their help in conducting experiments and useful suggestions throughout my research work. The willingness of the other committee members, Prof. Steven McIntosh, Prof. Mark A. Snyder, and Prof. James T. Hsu, to assist me in their personal fields of expertise is greatly appreciated. I am also thankful to Dr. Alfred Miller and Dr. Henry Luftman for conducting XPS experiments.

Many other people have contributed in various ways to my education and social happiness during my studies at Lehigh University. Special mention to, Wesley Michaels, Brad Carnish, Paul S. Dimick, Paul Bader, John Caffrey, Fan Ni, Kathleen S. Hutnik, and Bill Hunter. I am also grateful to the Chemical engineering faculty for their support throughout my coursework, and department secretaries, especially Barbara for always sure that my paperwork proceed quickly and timely.

Finally, but most lovingly, I would like to thank my parents, brother, and sister, for their consistent support, encouragement, love, understanding, and sacrifices all the way. Without you I could not have achieved my PhD.

Table of Contents

List of Tables

List of Figures

Abbreviations

AC	Activated Carbon
AMT	Ammonium Molybdate Tetrahydrate
ASF	Anderson-Schultz-Flory
BET	Brunauer-Emmett-Teller
DI	Deionized
EDS or EDX	Energy Dispersive X-ray Spectroscopy
EMP	Empirical
EXAFS	Extended X-ray Absorption Fine Structure
FFVs	Flexible Fuel Vehicles
FGA	Float Genetic Algorithm
GA	Genetic Algorithm
GC	Gas Chromatograph
GHSV	Gas Hourly Space Velocity
GSAS	General Structure Analysis System
HAS	Higher Alcohol Synthesis
HCs	Hydrocarbon
ICP-MS	Inductively Coupled Plasma Mass Spectroscopy
IR	Infrared
LH	Langmuir-Hinshelwood
$MoO_2(acac)_2$	Molybdenum Dioxydiacetylacetonate
PFR	Plug Flow Reactor

SEM	Scanning Electron Microscopy
SVD	Singular Value Decomposition
TCD	Thermal Conductivity Detector
TEM	Transmission Electron Microscopy
TPR	Temperature Programmed Reduction
TRFs	Thermal Response Factors
WGS	Water Gas Shift
XPS	X-ray Photoelectron Spectroscopy
XRD	X-Ray Diffraction
XRF	X-Ray Fluorescence

Publications from the Thesis

Patent published (1)

Caram, H. S., Sahoo, R. K., Herman, G. H., and Acharya, D. R. "Catalyst composition formulated for synthesis of alcohols and method of preparing the same." U.S. Patent No. 8,815,963 B1, 26 Aug. 2014.

Patent in preparation (1)

Caram, H. S., Sahoo, R. K., Herman, G. H., and Acharya, D. R. "An Improved Method for the Preparation of Novel Catalyst for Ethanol and Higher Alcohols Synthesis." *in preparation*

Participation in International Conferences (1)

Caram, H. S., Sahoo, R. K., Herman, G. H., and Acharya, D. R. "Supported Cesium-Promoted Molybdenum Sulfide Catalyst and Reaction Kinetics for Higher Alcohol Synthesis." *AIChE annual meeting*, San Francisco, November 2013.

Manuscript in preparation (4)

Sahoo, R. K., Caram, H. S., Herman, G. H., and Acharya, D. R. “Activated Carbon Supported Cesium-Promoted Molybdenum Sulfide Catalysts for Higher Alcohol Synthesis from Syngas” *manuscript in preparation.*

Sahoo, R. K., Caram, H. S., Herman, G. H., and Acharya, D. R. "Effect of Sulfidation Temperature on Activated Carbon Supported Cesium-Promoted Molybdenum Sulfide Catalysts for Higher Alcohol Synthesis from Syngas" *manuscript in preparation.*

Sahoo, R. K., Caram, H. S., Herman, G. H., and Acharya, D. R. "Steady-State Kinetic Analysis of Higher Alcohol Synthesis from Syngas over Activated Carbon Supported Cesium-Promoted Molybdenum Sulfide Catalysts" *manuscript in preparation.*

Sahoo, R. K., Caram, H. S., Herman, G. H., and Acharya, D. R. "Modeling and Simulation of Fixed-Bed Higher Alcohol Synthesis Reactor from Syngas over Activated Carbon Supported Cesium-Promoted Molybdenum Sulfide Catalysts" *manuscript in preparation.*

Abstract

This work has been an investigation of the catalytic conversion of syngas into mixed alcohols over molybdenum based catalysts. The primary focus has been on the cesium promoted molybdenum disulfide catalysts supported on activated carbon. The catalyst was selected because of its excellent sulfur tolerance and water gas shift properties. The alcohol synthesis is a possibility for the production of gasoline additives or replacements to cater the growing demand of alcohols as a motor fuel.

A catalyst preparation method has been developed for the production of cesium promoted molybdenum sulfide catalysts supported on activated carbon and its application for mixed alcohol synthesis was demonstrated. The basic steps involved in catalyst preparation are formation of crystalline molybdenum dioxide upon thermal decomposition of highly dispersed molybdenum precursor on activated carbon support, followed by transformation to sulfide complexes upon sulfidation, and cesium promotion being the last step. The catalyst composition (cesium to molybdenum ratio), catalyst preparation process parameters (temperature, promotion rate, etc.), alcohol synthesis reaction conditions (reaction temperature, pressure, gas hourly space velocity, and hydrogen to carbon monoxide feed ratio) were optimized with respect to alcohol yields, alcohol selectivity, and carbon monoxide conversion. The catalyst maintains its activity for more than 500 hours under higher alcohol synthesis conditions. The sulfur products and water were not detected in the products during this period.

The x-ray diffraction (XRD) and x-ray photoelectron spectroscopy (XPS) analyses were performed after each stage of catalyst preparation and testing process. The combined XRD and XPS studies reveal that, the sulfidation (conversion of molybdenum dioxide to molybdenum disulfide) was not complete at a sulfidation temperature of 723.15 °K. The effect of sulfidation temperature on catalyst performance was investigated. It was found that the alcohol yields, alcohol selectivity, and carbon monoxide conversion increases with increase in suilfidation temperature, up to a maximum sulfidation temperature of 923.15 °K employed for our studies. The increase in catalyst activity was attributed to the increase in molybdenum disulfide phase and decrease in molybdenum dioxide phase in the catalyst. A complete conversion to molybdenum disulfide was achieved at 923.15 °K.

Another attempt was made to prepare the catalyst by direct sulfidation of highly dispersed molybdenum precursor on activated carbon support. The catalyst was tested extensively for more than 600 hours under higher alcohol synthesis conditions. The loss of catalyst activity and the presence of water and sulfur compounds were not observed in the product during this period. An increase in alcohol selectivity was observed for this catalyst compared to the catalyst prepared by previous method.

Additional experiments involving external injections of methanol and ethanol were performed to understand the reaction pathways involved during higher alcohol synthesis. It was observed that, at least part of the hydrocarbons is formed from alcohol decomposition and the higher alcohols are formed via aldehyde route. The steady-state power-law and Langmuir-hinshelwood type kinetic models were developed based on

these observations to demonstrate the effect of reaction temperature, pressure, gas hourly space velocity, and hydrogen to carbon monoxide feed ratio on product yields. The power-law and Langmuir-hinshelwood model requires seven reactions. The singular value decomposition was applied for the first time to a higher alcohol synthesis system. Only two empirical forward reactions are sufficient to describe the catalytic behavior under higher alcohol synthesis conditions. An empirical kinetic model based on these empirical reactions was developed. A genetic algorithm minimization tool was employed to estimate the kinetic parameters associated with the power-law, Langmuir-hinshelwood, and empirical kinetic models. Finally, a non-isothermal reactor model was developed based on the two reaction empirical kinetic model and further extended to incorporate the recycle of un-converted syngas from out let of the reactor.

Chapter 1

Introduction

1.1. Alcohols as Alternative Fuels and Additives

For decades, alcohols have long been used as renewable fuels and fuel additives such as, for example, octane boosters in gasoline formulated fuels. A blended fuel E85 (85% ethanol fuel and 15% gasoline) is used by flexible-fuel vehicles (FFVs) in the United States. The government has been promoting the development of this blend and several motor vehicle manufacturers, such as Ford, Chrysler, and General Motors have increased the production of FFVs [1]. In 2011, world ethanol production for fuels reached 22.36 billion US gallons with the United States as the top producer at 13.9 billion US gallons [2]. Alcohol-based additives including methanol (derived from natural gas), and ethanol (derived from bio-mass sources) offer relatively high blending octane numbers, competitive pricing and ample availability.

Energy-volume densities of alcohols are generally much lower than gasoline. For example, the energy-volume density of methanol is about 18.6 *MJ/L*, while gasoline is about 34 *MJ/L*. Although methanol's energy-volume density is relatively low, the energy-volume density of alcohols increases with increasing molecular weight of the particular alcohol. Higher alcohols such as, for example, ethanol and butanol have energy-volume densities of about 24 *MJ/L* and 29.2 *MJ/L*, respectively. If adequate supplies of ethanol, as well as mixtures of higher alcohols, can be made available, such higher alcohols can

be utilized extensively on a wider scale, particularly as an alternative fuel, as well as booster additives for both octane and cetane fuels.

1.2. Background of Higher Alcohol Synthesis from Synthesis Gas

Since the early 20th century, catalysts have been formulated to produce mixtures of methanol and higher alcohols from synthesis gas or syngas (a gas mixture composed of hydrogen and carbon monoxide) [3]. Certain catalysts formulated for synthesizing hydrocarbons from syngas were later discovered by Fischer and Tropsch (FT) to produce linear alcohols as by-products when impregnated with alkali impurities [4]. This discovery eventually led to the development of other FT catalysts and alkali-doped zinc oxide/chromium (III) oxide catalysts capable of higher alcohol synthesis (HAS) [5, 6]. During the late 1940's, the discovery of high yield oil fields diminished commercial interest in synthesis of alcohol from syngas [6, 7]. The oil embargos of the 1970's promoted interest in the use of syngas to produce higher alcohols for blending with gasoline. A large number of patents were filed in 1980's for HAS; most notably by the DOW Chemical Company [8-13] and the Union Carbide Corporation [14, 15] based alkali or alkaline earth metal doped molybdenum disulfide (MoS_2) catalysts for HAS. Interest in HAS from syngas again declined after oil prices began to decline after 1985.

Recently, in the face of rising crude oil costs and the nation's increasing reliance on foreign sources of oil, the Energy Independence and Security Act of 2007 was passed requiring the total amount of renewable fuels added to gasoline formulations be raised to 36 billion US gallons by 2022 [16]. It was further stipulated that corn-based ethanol production will be capped at 15 billion gallons per year and that ethanol or other fuels

derived from non-food sources will be gradually increase to 21 billion gallons per year by 2022 [2]. These considerations have resulted in renewed interest and research in the synthesis of higher alcohols including ethanol.

1.3. Higher Alcohol Synthesis Process

Thermochemical conversion of biomass to ethanol and higher alcohols seems to offer an attractive and promising source of renewable energy [17-20]. This process includes converting biomass into syngas, and then catalytically converting syngas to ethanol and other higher alcohols (Fig.1.1).

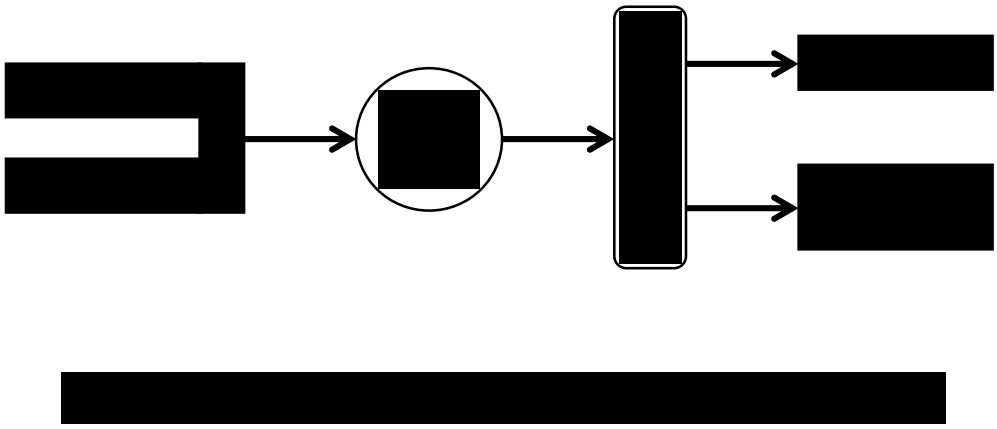

Plentiful biomass, particularly agricultural and forest refuse, municipal solid waste, landfill gas, and the like, represent a potential source of syngas. Such biomass-based sources of renewable energy are expected to play an increasingly important role in the synthesis of clean, sustainable fuels and fuel additives.

Commercial production of higher alcohols from syngas has been hampered by poor alcohol selectivity and low yields [5]. Currently, no commercial plant exists, largely due to the lack of appropriate catalysts for HAS from syngas.

1.4. Catalysts for Higher Alcohol Synthesis

Addition of alkali metals to the formulation is common to all HAS catalysts. Basic sites provided by alkali metal activate the surface adsorbed CO and enhance the formation of the surface intermediates responsible for HAS. The HAS catalysts can be broadly classified into four different groups, based on their composition and include:

- Modified methanol synthesis catalysts – alkali-doped ZnO/Cr_2O_3, $Cu/ZnO/Cr_2O_3$, Cu/ZnO, and $Cu/ZnO/Al_2O_3$ [21-25],
- Modified FT catalysts – alkali-doped $CuO/CoO/Al_2O_3$, $CuO/CoO/Cr_2O_3$, and $CuO/CoO/ZnO/Al_2O_3$ [26-29],
- Molybdenum based catalysts – alkali-doped MoS_2, CoS/MoS_2, and Mo_2C [8-15, 30-36], and
- Rhodium based catalysts – Rh/SiO_2 [37-40].

These catalysts require to be operated at relatively high reaction temperature, e.g. 530 – 610 *°K* or higher and operating pressure of 40 – 280 *bar* with a H_2/CO ratio of 1 – 2 *v/v*. In addition to the alcohols formed over the catalysts, the product mixture contains 15 – 20 *mol %* or higher amounts of hydrocarbons, principally consisting of methane [41].

The distribution of the product depends upon the type of catalyst used. For example, modified methanol catalysts can selectively produce methanol from syngas with low selectivity toward ethanol and higher alcohols. Modified FT and rhodium (Rh) based

catalysts have high selectivity for ethanol, as well as for hydrocarbons. The carbide based catalysts (Mo_2C) also exhibit high selectivity for hydrocarbons. The associated high selectivity for hydrocarbons makes the modified FT, Rh, and Mo_2C based catalysts unattractive, if the ethanol product is desired. Furthermore, Rh based catalysts are expensive to produce both because of cost and limited supply of Rh. On the other hand, the MoS_2 based catalysts have shown high selectivity to mixed alcohols. The activity and product distribution of MoS_2 catalyst can be significantly improved by impregnating it with selected transition metals such as Co. Additionally, unlike modified methanol and FT catalysts, MoS_2 based catalysts are sulfur resistant.

The alkali metal impregnated MoS_2 catalyst for the synthesis of higher alcohols from syngas was first patented by the DOW Chemical Company [8-13] and the Union Carbide Corporation [14, 15]. The un-impregnated MoS_2 catalyst produces only hydrocarbons, primarily methane; however, the selectivity of the catalyst dramatically shifts towards alcohols upon alkali impregnation. The role of alkali metal is two-fold; to suppress activity for the formation of hydrocarbons and to promote alcohol formation, including higher alcohols. Following advantages, makes MoS_2 based catalysts one of the most promising catalyst candidates at present for HAS from syngas:

- The MoS_2 based catalysts are sulfur resistant, unlike the modified methanol catalysts deactivates by sulfur impurities present in the syngas feed [42].
- Less sensitive to the presence of carbon dioxide in the syngas feed compared to other HAS catalysts [41].
- Favors the production of linear alcohols [14].

- Excellent water-gas-shift (WGS) catalysts [30, 43, 44].

A variety of alkalis have been reported in the literature for impregnation of MoS_2 catalysts, however most of the efforts have centered on using potassium (K). To further improve the catalyst performance, several concepts have been reported without much success. For example:

- Addition of cobalt to the catalyst [8, 10, 13].
- Addition of H_2S in the syngas feed to make up for the loss of sulfur [9, 45].

Addition of cobalt in the catalyst appeared to confirm the improvement of the selectivity to ethanol and other higher alcohols [34]. However, it was found that the distribution of alcohols in the product after 25 *hrs* on stream was largely independent of the cobalt content in the catalyst. This was attributed to the loss of sulfur from the catalyst causing cobalt to convert from its active form, CoS_2 into the inactive Co_9S_8 form [34, 45, 46]. To overcome this, a source of sulfur (e.g. H_2S) was added to the syngas feed to maintain the sulfidity of the catalyst. This however led to an undesirable incorporation of sulfur species into the ethanol and higher alcohol product.

Other possible approaches to improve the catalyst performance reported in the literature are:

- Catalyst activation at a preferred environment and conditions [47, 48].
- Uniform distribution and mixing of alkali and active materials [46, 49-51].

Our work, primarily focused on alkali promoted MoS_2 catalysts for HAS from syngas.

1.5. Reaction Mechanism

The MoS_2 has layered structure with single layers of Mo atoms are sandwiched between two layers of S atoms. The catalytically active sites are located at the edge planes of MoS_2 and not at ordered basal planes and these active sites are related to sulfur vacancies [30]. A Density Functional Theory (DFT) calculations on S-reconstructed surfaces to represent a realistic MoS_2 catalyst surface on hydrogen rich atmosphere show the following favorable sequence of reaction path involving C_1 species for the formation of hydrocarbon [52]:

$$CO \rightarrow CHO \rightarrow CH_2O \rightarrow CH_2OH \rightarrow CH_2 \rightarrow CH_3 \rightarrow CH_4 \quad (1.1)$$

$$CH_2OH \rightarrow OH \rightarrow H_2O \quad (1.2)$$

The hydrocarbon formation reaction on MoS_2 is always accompanied with the WGS reaction. A DFT calculation shows the following favorable reaction paths for WGS reaction [53]:

$$CO + H_2O \rightarrow CO + OH + H \rightarrow CO + O + 2H \rightarrow CO_2 + H_2 \quad (1.3)$$

Similar approach has been made to investigate ethanol synthesis from methanol [54, 55]. The DFT calculations show the following sequence of reactions for ethanol formation from methanol:

$$CH_3OH \rightarrow CH_3 + H_2O \rightarrow CH_3CO \rightarrow CH_3CHO \rightarrow CH_3CHOH \rightarrow CH_3CH_2OH \quad (1.4)$$

The surface CH_3* species and H_2O were formed by hydrogenolysis of methanol. The surface CH_3* species reacts with adsorbed CO* and form CH_3CO* (acyl) species. The subsequent hydrogenation of acyl species form ethanol *via* aldehyde route. On un-promoted catalysts (absence of alkali), formation of acyl species by CO insertion is not

competitive compared to the formation of methane by hydrogenation of CH_3* species. The most favorable products of CO hydrogenation over MoS_2 are hydrocarbons (primarily methane), carbon dioxide, and water.

The addition of alkali metal on MoS_2 catalysts shifts the product selectivity towards alcohols. The DFT studies on sulfur modified edge show that, the K^+ ions preferred to locate at an interstitial position between the Mo and S edge [55, 56]. Increase in alcohol selectivity is attributed to the increase in surface basicity due to the surface electron charge donated by alkali doping.

The overall reaction steps for alkali promoted MoS_2 catalysts are shown in Fig. 1.2 [34]. The CO insertion to a surface alkyl (RCH_2*) species forms an acyl (RCH_2CO*) species, that can be hydrogenated to the corresponding alcohol or to a longer alkyl species. The hydrocarbons are formed by hydrogenation of the corresponding alkyl species.

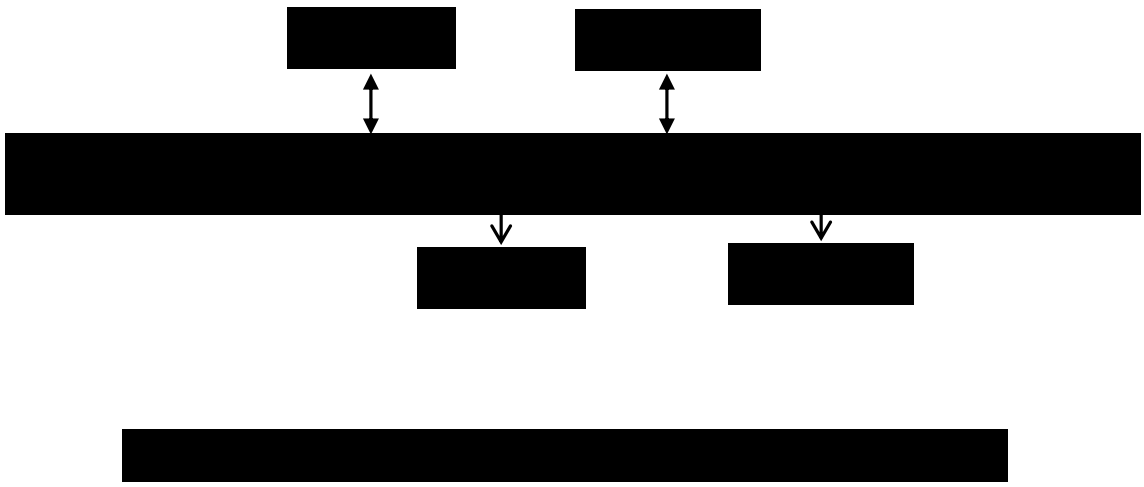

1.6. Kinetics of Higher Alcohol Synthesis

The HAS over alkali promoted MoS_2 catalysts is a complex reaction and it involves, many series, parallel, alcohol and hydrocarbon formation reactions, and WGS reaction [57]. The published data on kinetics of these reactions are somewhat limited. The apparent activation energy of 68 *KJ/mol*, 94.9 *KJ/mol*, and 98.5 *KJ/mol* respectively for methanol, ethanol, and propanol formation reactions, based on cesium promoted MoS_2 bulk catalysts was first reported by Santiesteban [30]. The rate expressions for HAS over MoS_2 catalysts are generally represented by using either the power-law [58-61] or Langmuir-Hinshelwood (LH) [57, 59, 60] type models. The kinetic models can be developed either by considering a set of independent parallel reactions (formation of alcohols and hydrocarbons directly from carbon monoxide and hydrogen) or series reactions (formation of higher alcohols from corresponding lower alcohols by carbon monoxide addition and formation of hydrocarbons by dehydration of corresponding alcohols). Some of these model formulations are too complex and require to consider at-least five or more reactions. The predicted values from these models are often compared with the experimental values by parity plots [59-61] or compared only with few experimental values [62]. Each of the operating variables, such as, reactor temperature, pressure, feed hydrogen to carbon monoxide ratio, and feed flow rate has significant effect on the production and selectivity of each individual product. It is difficult to apprehend these effects from the parity plots.

Improvement on kinetic model development for HAS over MoS_2 catalysts may include:

- Experimental data collection: The MoS_2 based catalysts may take hundreds of hours to reach steady-state [59, 60]. The experimental data must be collected after the catalyst reaches a steady-state for steady-state kinetic analysis.
- Development of simplified reaction schemes and rate expressions.
- Comparison with experimental values by pictorial representations, depicting the effect of each of the operating variables, such as, temperature, pressure, feed flow rate, and hydrogen to carbon monoxide ratio on productivity and selectivity of each of the products.

1.7. Challenges for Higher Alcohol Synthesis

It is clear that the prior art catalysts do not provide a commercially attractive catalysts. In addition, development of reliable and simplified HAS reaction kinetics and reactor models are another areas needs to be improved for the commercialization of the HAS process. In order to make the catalytic HAS process more feasible for commercial applications; improvement should be made on catalytic properties, such as, stability, selectivity, and activity of the catalyst, catalysts preparation and testing process, and HAS process developments, such as kinetics and reactor models, HAS process simulations, cost and process optimizations:

1.7.1. Catalyst Properties

- Stability of the catalyst under syngas reaction conditions and its tolerance to typical syngas and recycle impurities, such as hydrogen sulfide, carbon dioxide, methane, nitrogen, water, and methanol needs to be evaluated. Presence of water, produced during HAS reactions and/or present as an impurity in the feed, can permanently deactivate the catalyst [34]. It should also be noted that, the cobalt based MoS_2 catalysts deactivates due to the loss of sulfur from cobalt species [34, 46, 50]. It is required to minimize the formation of water and sulfur loss during HAS for long-tern stability of the catalyst.
- Selectivity of alcohols should be improved to minimize the quantity of side products formed, e.g. hydrocarbons. In addition to overall selectivity of alcohols, it is also required to improve the selectivity of higher alcohols, e.g. ethanol and higher.
- Improved activity of the catalyst could minimize the amount of un-reacted syngas to be recycled and increase throughput of the alcohols.

1.7.2. Catalyst Preparation and Testing Process

- Reduce the formation of catalytically inactive species for HAS, such as, formations of sulfates and oxides in the presence of water and/or oxygen [30, 34, 63-65]. The source of water could be the ambient moisture, water formed during HAS reactions, and/or present in the syngas and recycle feed streams.

- Improve uniform distribution and intimate mixing between the catalytically active species, such as, alkali and MoS_2 on an optional support to improve the catalyst activity and selectivity for alcohols [49, 50].
- The catalyst should be relatively easy to make at a cheaper cost and the catalyst preparation process should be scalable for mass productions and industrial use for HAS.
- Catalyst activation process prior to syngas exposure, to increase catalyst activity and selectivity [30, 47, 66].

1.7.3. Higher Alcohol Synthesis Process Developments

- Kinetic models for HAS over MoS_2 catalysts are limited and some of them require complex formulations [57, 62]. It is required to develop simplified reaction schemes and rate expressions to represent the catalyst behavior under the influence of reactor temperature, pressure, feed flow rate, and feed compositions.
- Literatures based on reactor design for HAS from syngas are very limited. It is required to develop simplified reactor models. The reactor model can further be extended for biomass to HAS process simulation, process optimization, and cost optimization. Different process configurations, such as, syngas recycle and purge recycle etc can be considered for optimization of the HAS process.
- Techno-economic analysis must be performed to evaluate the catalyst and HAS process performance. The HAS process can be simulated in a commercial simulator, such as, Aspen plus and Hysys, and required information regarding

viability of the process can be acquired. Economic evaluation is necessary to commercialize the technology.

1.8. Research Objective

It is clear from the prior art that the selectivity of MoS_2 catalysts for ethanol and higher alcohols is greatly enhanced by impregnating the catalyst with an alkali. It was also clear from the prior art that K and Co either alone or in combination cannot provide the performance to make these catalyst commercially attractive. The research objectives must be focused on:

- Catalyst composition and preparation process developments to enhance the catalyst stability, activity, and selectivity. It should also accompany with the catalyst characterization after each stages of catalyst preparation process.
- Catalyst preparation and testing process developments to ensure scalability of the process for industrial use.
- Development of simplified and accurate reaction schemes and rate expressions.
- Development of reactor models based on simplified governing equations and kinetic models.
- Application of the efficient optimization tools, such as, Genetic Algorithm (GA) for the minimization problems, such as, to calculate kinetic parameters, and commercial simulators, such as, Aspen plus and Hysys for the HAS process simulation, optimization, and techno-economic evaluation.

1.9. Thesis Organization

With reference to the points outlined in the previous sections, the thesis is organized into the following chapters.

- Chapter 2: A catalyst composition and the preparation method has been developed for the HAS from syngas. The catalytically active material includes, molybdenum sulfide complexes promoted with an effective amount of cesium, carried on an inert support. This section also involves, optimization of the cesium loading, obtaining information about stabilization time (time to reach steady-state) and stability of the catalyst at HAS conditions, optimization of HAS process variables, such as, reactor temperature, pressure, feed flow rate, and feed compositions, effect of feed impurities, such as, methanol, ethanol, methane, and carbon dioxide on product yield and selectivity, obtaining information about scalability of the catalyst preparation process, and x-ray diffraction (XRD) and x-ray photoelectron spectroscopy (XPS) analyses of the catalyst pellets after each preparation and testing stages.
- Chapter 3: The catalyst preparation method developed in Chapter 2 has been improved. It relates the effect of sufidation temperature on catalyst phase composition, and its effect on catalyst activity and selectivity towards alcohols. In another attempt, the catalyst preparation method has been simplified to a fewer steps. It also involves, determination of stabilization time, long-term stability of the catalyst at HAS conditions, optimization of HAS process variables, generation of steady-state experimental results for kinetic analysis, and XRD analyses of the

catalyst pellets after each preparation and testing stages. Similar catalyst preparation method was also applied for the preparation of cobalt containing oxide catalysts supported on activated carbon.

- Chapter 4: The steady-state power-law and LH type kinetic models based on seven reactions (one reaction each for methanol, ethanol, propanol^{+}, methane, ethane, propane, and carbon dioxide production) were developed; describing the effect of HAS process variables, such as, reactor temperature, pressure, feed flow rate, and feed compositions on product yield and selectivity. A two reaction empirical (EMP) model was developed by employing singular value decomposition (SVD) to the steady-state experimental results. The LH type rate expressions were used for the empirical model. The GA optimization tool was used to estimate the apparent activation energies and other kinetic parameters featured in the rate expressions of the power-law, LH, and empirical model.
- Chapter 5: A non-isothermal reactor model has been developed based on simplified governing equations and the two reaction empirical model developed in chapter 4. The reactor diameter and feed flow rates have significant effect on reactor temperature profile along the catalyst bed. Effect of reactor diameter and feed flow rates were examined on catalyst performance and reactor behavior. A runaway situation could be possible at lower feed rate and larger reactor diameter scenarios. The reactor model was also simulated in Aspen plus, a commercial simulator for process design and optimization, and effect of syngas recycle (from outlet of the reactor) on reactor performance, product yield, and product

selectivity was examined. The HAS process model developed in Aspen plus can further be extended for process and cost optimization.

- Chapter 6: This chapter concludes the important findings and results of the present work. It also includes the unfinished work and future directions to the current work.

1.10. References

1. RFA, *Falling Walls and Rising Tides: ethanol industry outlook.* 2014, Renewable Fuels Association.
2. RFA, *Accelerating industry innovation: ethanol industry outlook*. 2012, Renewable Fuels Association.
3. Forzatti, P., E. Tronconi, and I. Pasquon, *Higher alcohol synthesis.* Catalysis Reviews, 1991. **33**(1-2): p. 109-168.
4. Fischer, F. and H. Tropsch, *The synthesis of petroleum at atmospheric pressures from the gasification products of coal.* Brennstoff-Chemie., 1926. **7**: p. 97-104.
5. Herman, R., *Advances in catalytic synthesis and utilization of higher alcohols.* Catalysis Today, 2000. **55**(3): p. 233-245.
6. Subramani, V. and S.K. Gangwal, *A Review of Recent Literature to Search for an Efficient Catalytic Process for the Conversion of Syngas to Ethanol.* Energy & Fuels, 2008. **22**: p. 814-839.
7. Feng, M., *Review of Molybdenum Catalysts for Direct Synthesis of Mixed Alcohols from Synthesis Gas.* Recent Patents on Catalysis, 2012. **1**: p. 13-26.

8. Cochran, G.A., et al., *Preparation of ethanol and higher alcohols from lower carbon number alcohols*. 1989, Patent US4825013.

9. Conway, M.M., C.B. Murchison, and R.R. Stevens, *Method for adjusting methanol to higher alcohol ratios*. 1987, Patent US4675344.

10. Conway, M.M. and R.R. Stevens, *Mixed alcohols production from syngas*. 1988, Patent US4752623.

11. Quarderer, G. and K. Cochran, *Catalytic process for producing mixed alcohols from hydrogen and carbon monoxide*, in *European Patent 0,119,609*. 1984, WO 84/03696.

12. Quarderer, G.J. and G.A. Cochran, *Process for Producing Alcohols from Synthesis Gas*. 1988, Patent US4749724.

13. Stevens, R.R., *Process for producing alcohols from synthesis gas*. 1988, Patent US4752622.

14. Kinkade, N., *Process for producing alcohols from carbon monoxide and hydrogen using an alkali-molybdenum sulfide catalyst*, in *PCT Int. Pat. Publication No. WO*. 1985, Patent WO 85/03073. p. 03073.

15. Kinkade, N.E., *Catalytic process for the production of alcohols from carbon monoxide, hydrogen and olefins*. 1986, Patent US4590314.

16. EISA, *Energy Independence and Security Act of 2007*. 2007.

17. Dutta, A., R.L. Bain, and M.J. Biddy, *Techno-economics of the production of mixed alcohols from lignocellulosic biomass via high-temperature gasification.* Environmental Progress & Sustainable Energy, 2010. **29**(2): p. 163-174.

18. Dutta, A., et al., *Techno-economics for conversion of lignocellulosic biomass to ethanol by indirect gasification and mixed alcohol synthesis.* Environmental Progress & Sustainable Energy, 2012. **31**(2): p. 182-190.

19. Dutta, A., et al., *Process Design and Economics for Conversion of Lignocellulosic Biomass to Ethanol: Thermochemical Pathway by Indirect Gasification and Mixed Alcohol Synthesis*. 2011, National Renewable Energy Laboratory.

20. Phillips, S.D., *Technoeconomic Analysis of a Lignocellulosic Biomass Indirect Gasification Process to Make Ethanol via Mixed Alcohols Synthesis.* Ind. Eng. Chem. Res., 2007. **46**: p. 8887-8897.

21. Di Pietro, R. and A. Paggini, *Process for the production of a mixture of methanol and higher alcohols of" fuel grade"*. 1984, Patent US4481012.

22. Bock, O., K. Kochloefl, and M. Schneider, *Catalyst for the synthesis of methanol and alcohol mixtures containing higher alcohols and method of making the catalyst*. 1986, Patent US4598061.

23. Fattore, V., et al., *Catalytic system for producing mixtures of methanol and higher alcohols*. 1985, Patent US4513100.

24. Heracleous, E., et al., *Investigation of K-promoted Cu-Zn-Al, Cu-X-Al and Cu-Zn-X (X= Cr, Mn) catalysts for carbon monoxide hydrogenation to higher alcohols.* Applied Catalysis A: General, 2013. **455**: p. 145-154.

25. Tronconi, E., et al., *Higher alcohol synthesis over alkali metal-promoted high-temperature methanol catalysts.* Applied Catalysis, 1989. **47**(2): p. 317-333.

26. Freund, E. and A. Sugier, *Process for manufacturing alcohols, particularly linear saturated primary alcohols, from synthesis gas*. 1978, Patent US4122110.

27. Freund, E. and A. Sugier, *Process for manufacturing alcohols and more particularly saturated linear primary alcohols from synthesis gas*. 1981, Patent US4291126.

28. Courty, P., et al., *Process for manufacturing a mixture of methanol and higher alcohols from synthesis gas*. 1987, Patent US4659742.

29. Chaumette, P., et al., *Process for synthesizing a mixture of primary alcohols from a synthesis gas in the presence of a catalyst containing copper, cobalt, zinc and aluminum*. 1988, Patent US4791141.

30. Santiesteban, J.G., *Alcohol Synthesis from Carbon Monoxide and Hydrogen over MoS_2-based Catalysts*, in *Chemistry*. 1989, Lehigh University.

31. Okatsu, H., et al., *Supported K/MoS_2 and K/Mo_2C Catalysts for Higher Alcohol Synthesis from Synthesis Gas: Impact of Molybdenum Precursor and Metal Oxide Support on Activity and Selectivity.* Catalysis Letters, 2014. **144**(5): p. 825-830.

32. Xiang, M., et al., *Performances of mixed alcohols synthesis over potassium promoted molybdenum carbides.* Fuel, 2006. **85**(17): p. 2662-2665.

33. Xiang, M., et al., *Mixed alcohols synthesis from carbon monoxide hydrogenation over potassium promoted β-Mo_2C catalysts.* Fuel, 2007. **86**(9): p. 1298-1303.

34. Christensen, J.M., *Catalytic synthesis of long-chained alcohols from syngas*, in *Department of Chemical and Biochemical Engineering*. 2011, Technical University of Denmark.

35. Kharas, K., *Cobalt-molybdenum sulfide catalyst materials and methods for stable alcohol production from syngas*. 2013, Patent US8586801B2.

36. Durand, J.P. and K. Kharas, *Cobalt-molybdenum sulfide catalyst materials and methods for ethanol production from syngas*. 2011, Patent US7923405B2.

37. Atkins, M.P., *Process for the conversion of synthesis gas to oxygenate*. 2011, Patent US7939571B2.

38. Gerber, M.A., et al., *Evaluation of Promoters for Rhodium-Based Catalysts for Mixed Alcohol Synthesis*. 2008, U. S. Department of Energy.

39. Gao, J., *Catalysis of Ethanol Synthesis from Syngas*, in *Chemical Engineering*. 2010, Clemson University.

40. Zaman, S.F. and K.J. Smith, *Synthesis gas conversion over a Rh–K–MoP/SiO_2 catalyst.* Catalysis Today, 2011. **171**(1): p. 266-274.

41. Herman, R.G. *Classical and non-classical routes for alcohol synthesis*. in *Studies in Surface Science and Catalysis, New Trends in CO Activation*. 1991. Elsevier.

42. Wood, B.J., W.E. Isakson, and H. Wise, *Kinetic Studies of Catalyst Poisoning during Methanol Synthesis at High Pressures.* Ind. Eng. Chem. Prod. Res. Dev., 1980. **19**(2): p. 197-204.

43. Hou, P., D. Meeker, and H. Wise, *Kinetic studies with a sulfur-tolerant water gas shift catalyst.* Journal of Catalysis, 1983. **80**(2): p. 280-285.

44. Overstreet, A.D., *A screening study of a new water gas shift catalyst*. 1974, Virginia Polytechnic Institute and State University: Blacksburg, Virginia.

45. Hensley, J.E., S. Pylypenko, and D.A. Ruddy, *Deactivation and stability of K-$CoMoS_x$ mixed alcohol synthesis catalysts.* Journal of Catalysis, 2014. **309**: p. 199-208.

46. Iranmahboob, J. and D.O. Hill, *Alcohol synthesis from syngas over $K_2CO_3/CoS/MoS_2$ on activated carbon.* Catalysis Letters, 2002. **78**(1-4): p. 49-55.

47. Alsum, P.J., et al., *Methods for improving syngas-to-alcohol catalyst activity and selectivity*. 2012, Patent US8318986B2.

48. Kharas, K., H.J. Robota, and E.M. Wilcox, *Methods for improving syngas-to-ethanol catalyst selectivity*. 2009, Patent US20100152498A1.

49. Stites, R.C., *Methods for promoting syngas-to-alcohol catalysis*. 2013, Patent US8344184B2.

50. Iranmahboob, J., *Formation of Ethanol and Higher Alcohols from Syngas*, in *Chemical Engineering*. 1999, Mississippi State University.

51. Iranmahboob, J., et al., *The influence of clay on $K_2CO_3/Co–MoS_2$ catalyst in the production of higher alcohol fuel.* Fuel processing technology, 2002. **79**(1): p. 71-75.

52. Shi, X.-R., et al., *CO hydrogenation reaction on sulfided molybdenum catalysts.* Journal of Molecular Catalysis A: Chemical, 2009. **312**(1): p. 7-17.

53. Shi, X.-R., et al., *Density functional theory study on water–gas-shift reaction over molybdenum disulfide.* Applied Catalysis A: General, 2009. **365**(1): p. 62-70.

54. Chen, Y.-Y., et al., *Mechanistic aspect of ethanol synthesis from methanol under CO hydrogenation condition on MoS< sub> x</sub> cluster model catalysts.* Journal of Molecular Catalysis A: Chemical, 2010. **329**(1): p. 77-85.

55. Zaman, S. and K.J. Smith, *A Review of Molybdenum Catalysts for Synthesis Gas Conversion to Alcohols: Catalysts, Mechanisms and Kinetics.* Catalysis Reviews, 2012. **54**(1): p. 41-132.

56. Andersen, A., et al., *Adsorption of potassium on MoS_2 (100) surface: A first-principles investigation.* The Journal of Physical Chemistry Chemistry, 2011. **115**(18): p. 9025-9040.

57. Park, T.Y., I.-S. Nam, and Y.G. Kim, *Kinetic analysis of mixed alcohol synthesis from syngas over K/MoS_2 catalyst.* Industrial & engineering chemistry research, 1997. **36**(12): p. 5246-5257.

58. Christensen, J.M., et al., *Effects of H_2S and process conditions in the synthesis of mixed alcohols from syngas over alkali promoted cobalt-molybdenum sulfide.* Applied Catalysis A: General, 2009. **366**(1): p. 29-43.

59. Gunturu, A.K., et al., *A kinetic model for the synthesis of high-molecular-weight alcohols over a sulfided Co-K-Mo/C catalyst.* Industrial & engineering chemistry research, 1998. **37**(6): p. 2107-2115.

60. Gunturu, A.K., et al., *The Economical Production of Alcohol Fuels from Coal-Derived Synthesis Gas: Chapter 5 A Kinetic Model for the Synthesis of High-Molecular-Weight Alcohols over a Sulfided Co-K-Mo/C Catalyst*. 1999, West Virginia University Research Corporation. p. 87-117.

61. Surisetty, V.R., A.K. Dalai, and J. Kozinski, *Intrinsic Reaction Kinetics of Higher Alcohol Synthesis from Synthesis Gas over a Sulfided Alkali-Promoted Co− Rh− Mo Trimetallic Catalyst Supported on Multiwalled Carbon Nanotubes (MWCNTs).* Energy & fuels, 2010. **24**(8): p. 4130-4137.

62. Smith, K.J., R.G. Herman, and K. Klier, *Kinetic modelling of higher alcohol synthesis over alkali-promoted Cu/ZnO and MoS_2 catalysts.* Chemical Engineering Science, 1990. **45**(8): p. 2639-2646.

63. Ross, S. and A. Sussman, *Surface Oxidation of Molybdenum Disulfide.* J. Phys. Chem., 1955. **59**(9): p. 889-892.

64. Woo, H.C., et al., *Surface species on the oxidized K_2CO_3/MoS_2 and their effects on catalytic carbon monoxide hydrogenation.* Applied Catalysis A: General, 1993. **104**: p. 199-214.

65. Woo, H.C., et al., *Room-Temperature Oxidation of K_2CO_3/MoS_2 Catalysts and Its Effects on Alcohol Synthesis from CO and H_2*. Journal of Catalysis, 1992. **138**: p. 525-535.

66. Kharas, K. and G. MEITZNER, *Methods for promoting syngas-to-alcohol catalysts*. 2012, Patent US20100075837A1.

Chapter 2

Activated Carbon Supported Cesium-Promoted Molybdenum Sulfide Catalysts for Higher Alcohol Synthesis from Syngas

The catalyst composition, preparation and testing method described in this chapter has been published as "Catalyst composition formulated for synthesis of alcohols and method of preparing the same" by Hugo S. Caram, Ranjan K. Sahoo, Richard G. Herman, and Divyanshu R. Acharya, US patent 8815963 B1, published on Aug 26, 2014

The work described in this chapter has been titled "Activated Carbon Supported Cesium-Promoted Molybdenum Sulfide Catalysts for Higher Alcohol Synthesis from Syngas" by Ranjan K. Sahoo, Hugo S. Caram, Divyanshu R. Acharya, and Richard G. Herman, *manuscript in preparation.*

Abstract

A catalyst preparation method has been developed for the preparation of cesium promoted molybdenum based supported catalysts for higher alcohol synthesis from syngas. The basic steps involved are formation of crystalline molybdenum dioxide upon thermal decomposition of highly dispersed ammonium molybdate tetrahydrate on activated carbon support, followed by transformation to sulfide complexes upon sulfidation, and cesium promotion being the last step. The cesium to molybdenum molar ratio was varied from 0.03 to 2.72, and its effect on catalyst performance in-terms of product yields, carbon monoxide conversion, and alcohols selectivity was studied. The optimum cesium to molybdenum ratio of 0.7-0.8 was observed for this catalyst; however

a value between 0.23-1.57 can be used without appreciable loss of alcohol yields. The catalyst preparation method was reproducible and scalable for mass productions.

The catalyst was tested extensively under higher alcohol synthesis conditions to; determine the stabilization time, optimize the reaction conditions, such as, temperature, pressure, gas hourly space velocity, and hydrogen to carbon monoxide ratio, and study the long-term stability of the catalyst. The catalyst requires a stabilization time of at least 10-25 hours or more to reach a steady-state. The optimum reaction temperature range for the catalyst is 570-610 °K; further increase in temperature decreases the alcohol yields and selectivity. The yield of hydrocarbons and alcohols increases with increase in reaction pressure, additionally, the yield of hydrocarbons increases at a faster rate than alcohols. The optimum reaction temperature shifts towards a lower value with increase in reaction pressure. The alcohol yields and selectivity increases with increase in gas hourly space velocity. Increase in hydrogen to carbon monoxide ratio favors the yield of methanol and methane, probably due to increase in hydrogen partial pressure. Optimum hydrogen to carbon monoxide ratio of 0.5 to 1.0 can be used for higher alcohol yields. The alcohol yield, carbon monoxide conversion, alcohol selectivity, and C_2^+ to methanol weight ratio of 576-942 g/kg metals/hr, 7-22 %, 53-65 mol%, and 0.39-0.74 respectively was achieved at higher alcohol synthesis conditions of 588 °K, 100 bar, 3300-6600 hr^{-1} gas hourly space velocity, and hydrogen to carbon monoxide ratio of 1-2. The catalyst maintains its activity for more than 500 hours. The water and sulfur compounds were not detected in the products during this period.

The external injections of methanol and ethanol into the reactor along with syngas and in an inert atmosphere (absence of syngas) were performed to; study its effect on

catalyst performance, and to understand the reaction mechanism. Following observations were made; at least part of the hydrocarbons are formed from decomposition of the alcohols, additional butanol are produced by coupling of ethanol, alcohols are formed via aldehyde route, methanol formation reaction is a reversible reaction, higher alcohols and hydrocarbon formation reactions are forward reactions, and the catalyst regains its activity once the presence of external methanol or ethanol was removed. A reaction network was proposed from these observations.

The x-ray diffraction (XRD) and x-ray photoelectron spectroscopy (XPS) analyses were performed after each stage of catalyst preparation and testing process. The molybdenum dioxide is the only phase present after calcination of the ammonium molybdate tetrahydrate promoted on activated carbon. The XRD and XPS analyses of the sulfidized sample revels that, the sulfidized sample retains the bulk characteristic of molybdenum dioxide, whereas the surface is covered with poorly crystalline or amorphous molybdenum disulfide. The S^{2-} to Mo^{4+} oxidation state ratio of 1.36-1.56 was observed at the surface of a randomly selected cesium promoted catalyst pellet stored in an inert atmosphere. The catalytically inactive sulfate species were formed upon exposure of cesium promoted catalyst pellets to ambient atmosphere. The hygroscopic nature of the cesium compound accelerates the oxidation reaction and form undesirable sulfate species. The exposure of catalysts to ambient conditions must be avoided after its being promoted with cesium. The sulfate species were not present for the tested catalyst stored in an inert atmosphere.

2.1. Objective

The objective of this chapter is:

- To develop a catalyst composition and catalyst preparation method for the same, for higher alcohol synthesis.
- Optimize the catalyst composition; specifically the ratio of alkali to molybdenum ratio.
- Optimize the higher alcohol synthesis reaction conditions for catalyst activity, alcohol selectivity, and alcohol yields.
- Determine the stabilization time, the time required reach a steady-state upon exposure to syngas.
- Study the long-term stability of the catalyst under higher alcohol synthesis conditions.
- Study the effect of external injections of methanol and ethanol into the syngas at inlet of the reactor on catalyst performance.
- Understand the reaction mechanism.
- Check the reproducibility and scalability of the process for mass production of alcohols.
- Surface and bulk characterization of the catalyst sample after each catalyst preparation and testing steps.

2.2. Design of Experiments and Catalyst Preparations

2.2.1. Selection of the Alkali Promoter

Generally it is reported that the heavier alkalis are preferable. Their order of promotion for alcohol synthesis increases with increase in basicity. Kinkade [1] ranks these alkali metals for a fixed doping of 0.616 *mol* alkali per mole of molybdenum as:

$$Cs > Rb > K > Na > Li \tag{2.1}$$

Santiesteban [2] also found that Cs is better promoter than K, for an alkali doping of 0.22 *mol* alkali per mole of MoS_2 un-supported catalysts, in-terms of higher alcohol yields and selectivity. Contrary to this, Iranmahboob et al [3, 4] reported that K is better promoter than Cs, with respect to higher alcohol yield and ethanol selectivity for cobalt modified MoS_2 catalysts supported on clay. The study conducted by Iranmahboob et al was based on same mass loading of Cs_2CO_3 and K_2CO_3 rather than mole basis. On mole basis, the K loading was more than twice that of the Cs, so a direct comparison of these two catalysts on the basis of promoter basicity alone is not possible. We therefore decided to focus our efforts on impregnating the MoS_2 catalyst with Cs metal, since Cs has significantly greater basicity compared to K and as a result, it is expected to be the more effective alkali promoter [2].

2.2.2. Selection of the Support

Recognizing that effective dispersion of active catalyst components on an inert support will not only enhance the activity and selectivity of the catalyst but it will also

help to avoid hot spots in the reactor by diluting the catalytically active materials on an inert support, we decided to support the active Cs-MoS_2 on an inert support. The main requirement of the support material is that it should be neutral or basic, or may be rendered neutral or basic by addition of the alkali promoters to avoid acid catalyzed reactions such as ether formation [5, 6]. Because of the absence of acidic surfaces on activated carbon and its larger surface area, we selected activated carbon (AC) as a support for Cs-promoted MoS_2 catalyst over activated alumina support [7, 8].

2.2.3. Preparation of the Catalyst

The steps involved in preparation of the catalyst are formation of crystalline MoO_2 upon thermal decomposition of highly dispersed ammonium molybdate tetrahydrate (AMT) on AC support, followed by transformation to sulfide complexes upon sulfidation [9, 10] and cesium promotion being the last step. The basic catalyst preparation steps are shown in Fig. 2.1.

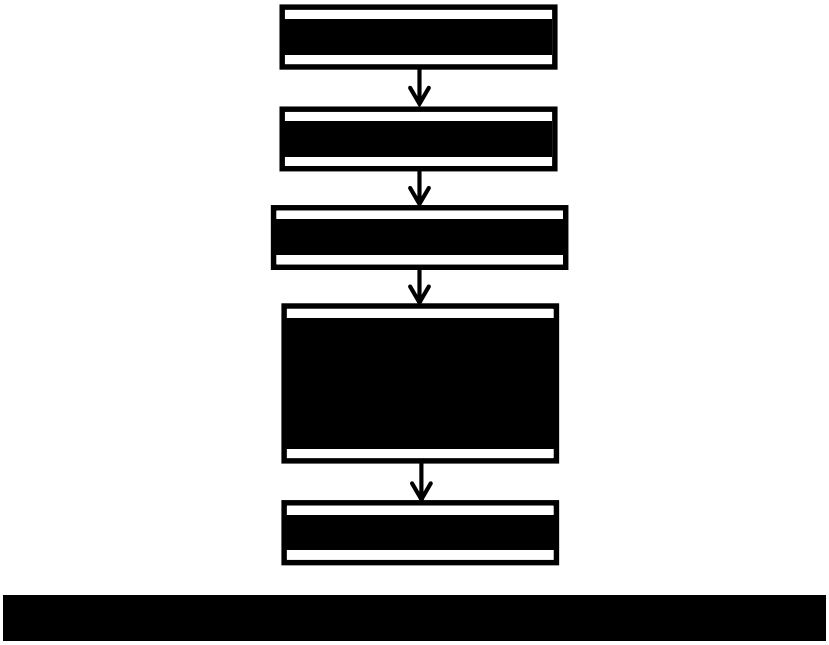

2.2.3.1. Support Preparation

The extruded AC (General Carbon, 3 *mm*, surface area 1000 m^2/g) was cut and sieved between 2.36 *mm* and 4 *mm*. The resulting cylindrical AC pellets had an aspect ratio (length to diameter) of approximately one. The cut, sieved AC was washed by soaking in an aqueous 1.0 *M* HNO_3 (70 % HNO_3 from Sigma-Aldrich, CAS Number 7697-37-2, mixed with deionized water) solution for ten minutes then filtering through a Buchner funnel connected to an aspirator [7]. This process was repeated three times. Each step is followed by washing with boiling deionized (DI) water to remove any acid left in the AC pellets. After the final washing step, the AC was rinsed with an excess of boiling DI water. The washing procedure is designed to remove metal impurities that could affect the performance of the catalyst for mixed alcohol synthesis. The AC was vacuum dried at 343.15 °*K* and 20-25 *in. Hg* vacuum for 24 *hr*.

2.2.3.2. AMT Promotion

The cut, cleaned, dried AC pellets were promoted with an aqueous solution of AMT (Sigma-Aldrich, CAS Number 12054-85-2), using a solution feed rate of 7 – 20 *ml/hr* in a Rotovap (Rotavapor from Buchi Corp., Model RE 111), simulating spray drying technique under vacuum. The AMT solution was prepared by dissolving *x g* of AMT in 2*x*/solubility *ml* of deionized water. The solubility of AMT at room temperature is 43 *g* per 100 ml water [11]. Different size of rotovap vessels were selected, depending on the amount of AC being used for promotion. The volume of AC is always kept between 10 – 25 % of the vessel volume. Water bath temperature was maintained at 353.15 °*K*. The mass of AMT was selected to achieve Mo loading of 10 –

18 *wt%* [12]. The AMT solution is highly unstable at high temperature, so pre-heating of the AMT solution must be avoided [11]. Following AMT promotion the catalyst was vacuum dried at 343.15 °*K* and 20-25 *in Hg* vacuum for 24 *hr*.

2.2.3.3. Calcination

The dried, AMT promoted AC pellets were calcined at an elevated temperature of 723.15 – 773.15 °*K* and at atmospheric pressure [13] in a quartz tube reactor for 3 – 20 *hr*, depending on the size of the calcining batch and inert gas flow rate. The pellets were positioned at the center of the reactor using quartz wools. Inert atmosphere was maintained by flowing N_2 through the reactor during calcination. Heating was accomplished with a 5 – 10 °*K/min* ramp and the catalyst was allowed to cool naturally after calcination was completed. The representative x-ray diffraction (XRD) pattern of AMT promoted AC pellets, calcined at 723.15 °*K* is shown in Fig. 2.2. When compared with the literature it is found that, it was a crystalline MoO_2 [13]. Following calcination, pellets were stored in N_2 purged bottles/vials to avoid moisture uptake from ambient atmosphere.

2.2.3.4. Sulfidation

A quartz tube reactor was used for the sulfidation. The MoO_2/AC (calcined AMT promoted AC) pellets were heated to 673.15 °*K* or 723.15 °*K* with 1 or 2 *hr* temperature ramp, under flowing 2 or 5 *vol%* H_2S in H_2 at 100 *ml/min* (Praxair, Inc., part no. HY HS5C-A3). The maximum temperature of 673.15 °*K* or 723.15 °*K* was maintained at atmospheric pressure with 2 or 5 *vol%* H_2S in H_2 still flowing through the reactor at 100 *ml/min* [13-15].

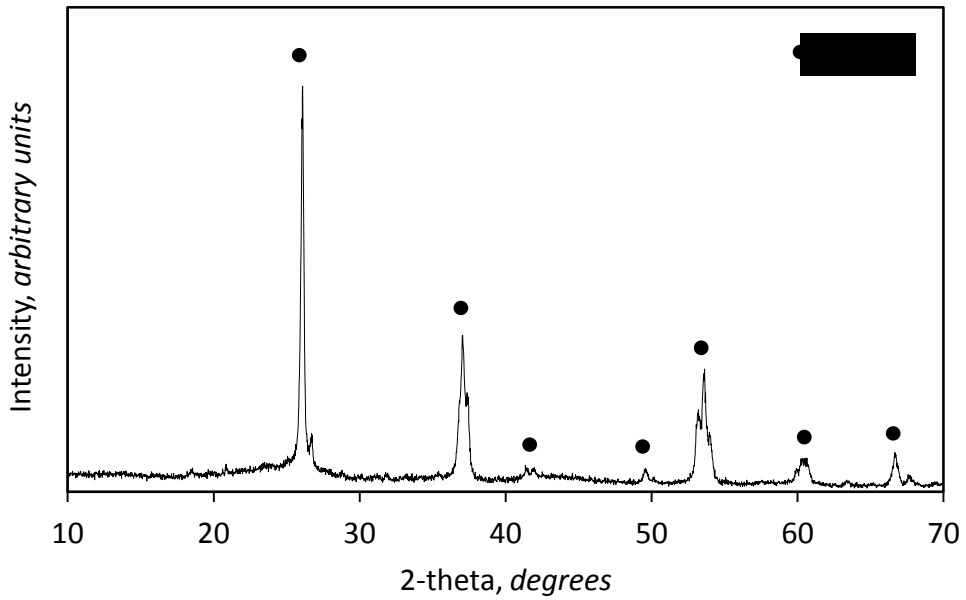

[redacted]

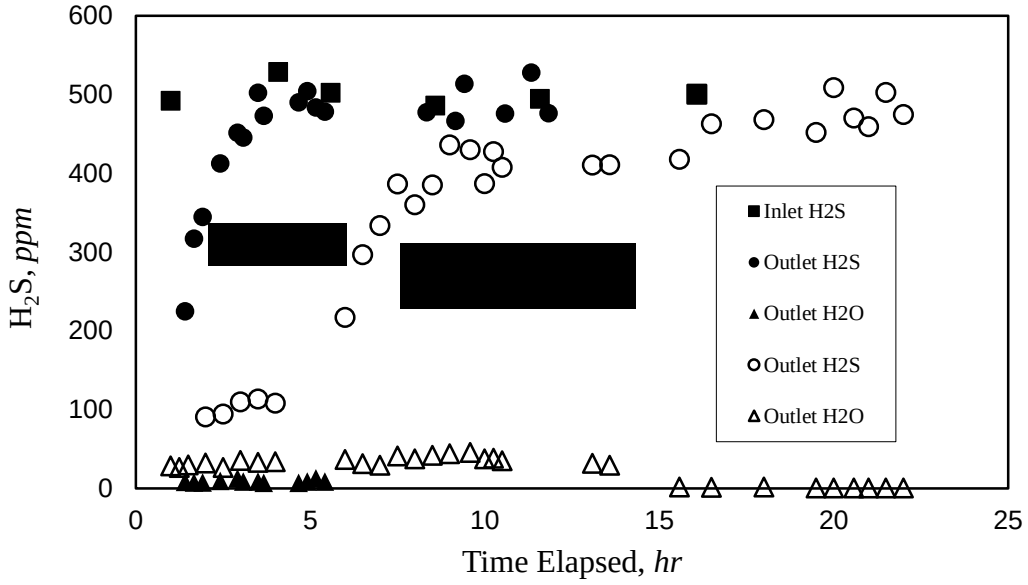

[redacted]

The sulfidation process was followed by monitoring the water content of exit gas by a gas chromatography (GC). The sulfidation of MoO_2 generates H_2O vapors [10, 16], which should exit at outlet of the reactor along with balance H_2S and H_2. The exit stream from the reactor was bubbled through a NaOH solution before venting it through the hood. The NaOH solution was used to capture H_2S from exit of the reactor. The sulfidation time was determined by disappearance of H_2O at outlet of the reactor. Fig. 2.3 shows sulfidation breakthrough curves at a sulfidation temperature of 673.15 *°K*, using 5 *vol%* H_2S in H_2 as the sulfidizing agent for two different batches of 8 *g* and 45 *g* calcined pellets. Rapid consumption of H_2S was observed during initial period of sulfidation and later it slowly stabilizes to a plateau. It can be seen from the plot that, it takes 5 *hr* and 20 *hr* to reach steady-state for 8 *g* and 45 *g* of calcined pellets respectively. Following sulfidation, the catalyst was allowed to cool down naturally to about 473.15 - 523.15 *°K* with 5 *vol%* H_2S in H_2 flowing through the reactor. Finally, the sulfidized pellets were purged with N_2 at 100 *ml/min* for 0.5 *hr* to remove any physically adsorbed H_2S and allowed to cool down to room temperature under N_2 atmosphere. The sulfidized pellets were stored in an inert atmosphere to prevent any moisture uptake from the air.

2.2.3.5. Cesium Promotion

The sulfidized catalyst pellets were promoted with 0.15 *M* solution of Cs formate (Sigma-Aldrich, CAS Number 3495-36-1), using a solution feed rate of 3 – 12 *ml/hr* in a Rotovap, simulating spray drying system under vacuum, similar to the AMT promotion process. The mass of Cs formate was selected to achieve a Cs/Mo mass ratio of 1 (molar Cs/Mo ratio of 0.7) [17]. The Brunauer-Emmett-Teller (BET) surface area of

475±8 m^2/g was measured for one of the cesium promoted catalyst sample. The catalyst was vacuum-dried at 343.15 °*K* and 20-25 *in Hg* vacuum for 24 *hr* and stored in an inert atmosphere. Care must be taken in performing this step in an inert atmosphere. The MoS_2 is a highly inert component, whereas Cs can readily absorb oxygen from ambient and form undesirable oxide, carbonate, and sulfate species [2, 15, 18-21]. This can cause segregation of Cs in bulk phases on the catalyst and reduce catalyst activity for alcohols. The finished catalyst must be stored in an inert atmosphere; nitrogen purged bottles or drums, vacuum sealed borosilicate glass ampoules, or hermetically sealed stainless steel containers.

The catalyst preparation process parameters, such as the batch size, promotion rates, temperature, ramp time or temperature rate, and time of each preparation steps were summarized in Table 2.1. The Mo content of the calcined pellets reported in Table 2.1 was calculated by performing mass balance of the catalyst preparation process (weight difference, before and after each step). In the calculation of Mo *wt %*, it was assumed that, the AC weight does not change by high temperature applications and only MoO_2/AC was present after the calcination step.

An example catalyst composition calculation for the catalyst number 7 is given in Appendix 2A. The pictures of rotovap (used for AMT and Cs promotion), sulfidation and calcination unit, final catalyst, and catalyst testing unit are shown in Appendix 2B.

Cat. No.	AMT Promotion		Calcination					Sulfidation				Cesium Promotion		
	Batch, *g*	Rate, *ml/h*	Batch, *g*	Max. T, *°K*	Ramp, *°K/min*	Time, *hr*	Mo, *wt %*	Batch, *g*	Max. T, *°K*	Ramp, *hr*	Time, *hr*	Batch, *g*	Rate, *ml/hr*	Cs/Mo, *mol/mol*
1	30.0	10.0	10	773.15	5	16	15.5	16.0	723.15	1	17.0	16.0	5.0	0.03
2	30.0	10.0	10	773.15	5	16	15.5	16.0	723.15	1	17.0	12.2	7.5	0.23
3	30.0	10.0	10	773.15	5	16	15.5	16.0	723.15	1	17.0	8.7	12.0	0.79
4	30.0	10.0	10	773.15	5	16	15.5	16.0	723.15	1	17.0	7.8	8.0	1.58
5	30.0	10.0	10	773.15	5	16	15.5	16.0	723.15	1	17.0	5.1	8.0	2.72
6	50.0	7.0	20	773.15	10	3	14.3	10.0	673.15	1	17.3	5.0	3.5	0.59
7	15.0	12.0	9	773.15	5	15	11.8	8.0	673.15	1	12.0	8.0	7.5	0.71
8	51.0	12.5	50	773.15	8	20	13.1	44.3	673.15	1	26.0	14.0	12.0	0.64
9	50.0	7.0	20	773.15	10	3	14.3	10.0	673.15	1	21.0	5.0	3.8	0.66
10	40.0	Drop-wise*	10	673.15	6	3	16.7	9.7	673.15	1	19.0	4.5	Drop-wise*	0.48

*Drop-wise impregnation using a funnel

Table 2.1. Cesium-promoted MoS_2/AC catalysts preparation process parameters.

2.3. Catalyst Testing and Analytical Procedures

2.3.1. Catalyst Testing Unit

A schematic diagram of the catalyst testing unit is shown in Fig. 2.4. The Plug Flow Reactor (PFR) is a single pass fixed-bed tubular reactor. It consisted of 1.27 *cm* ID (1/2" ID & 3/4" OD), schedule 40, 316 stainless steel tubing. It was fitted with a 0.32 *cm* OD thermo-well of the same material to measure axial catalyst bed temperature. The reactor was heated using a split tube furnace (Applied Test Systems, Inc.). The reactor furnace had three separate heat zones individually controlled by Omega temperature controllers (CN 9000A), which allowed control of the catalyst bed temperature usually within ± 1 ^{o}K. The locations of the monitoring thermocouples were the following: reactor inlet (top), outside of the reactor tube at middle (middle), reactor outlet (bottom), internal axial reactor temperature, back-pressure regulator, line between back-pressure regulator and a 3-way valve, and GC loop temperature. The PFR system was designed for a usual maximum operating pressure of 100 *atm* (1500 *psig*), although it could optionally be utilized at up to about 125 *atm* (1800 *psig*). The desired pressure in the system was regulated by a Mity Mite back-pressure regulator having a Teflon disk diaphragm and obtained from pressurized cylinders of the reactant gases; hydrogen and carbon monoxide (Praxair, Inc., part no. CO 2.5-T for CO and HY 4.5Z-T for H_2). Mordenite and activated carbon were used in the purifying traps to purify the feed gases from moisture and iron carbonyls respectively. The back-pressure regulator reduced the downstream pressure to atmospheric while maintaining the upstream pressure at the desired level.

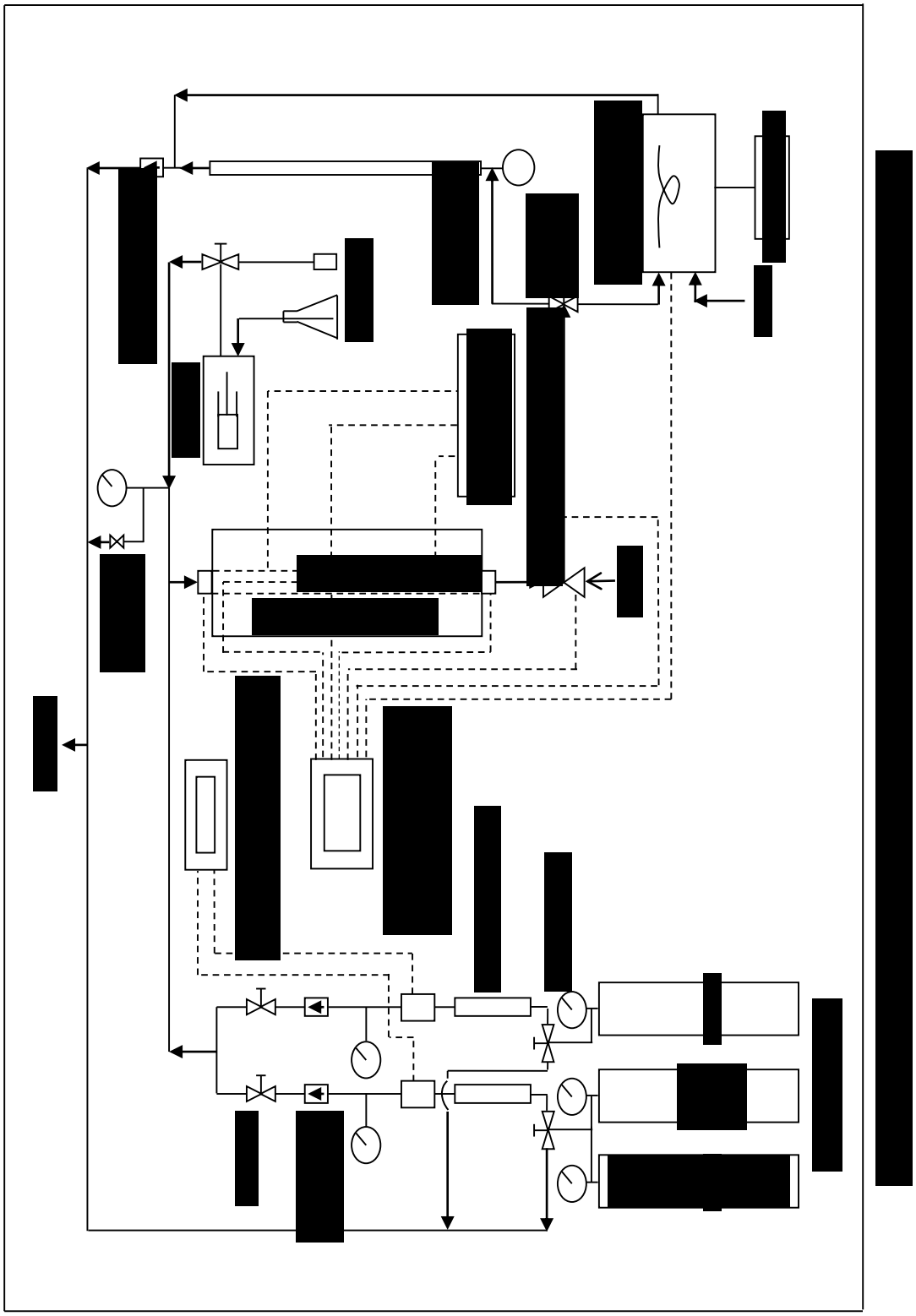

The unit is provided with mass flow controllers (Brooks Instruments) integrated with a 4-channel controller capable of operating at high pressures and regulating the H_2 and CO flows separately, as well as the 2% H_2/balance N_2 reduction/activation gas and N_2 gas at atmospheric pressure. Heating and insulating tapes were wrapped around the stainless steel inlet and outlet lines to maintain temperatures around 400-475 $°K$ to avoid condensation of the reaction product components. The product stream from the PFR can be directed to a bubble meter for the measurements of gas flow, or to the gas chromatograph (Hewlett Packard, Model 5890 Series II) for the analysis of the reaction products. The gas chromatograph was coupled to a HP integrator/printer. Analyses were achieved with a 10.0 *m* Poroplot Q capillary column (Agilent Technologies, Part no. CP7550) using a 6-way valve for injection of a portion of the heated outlet gas stream. Provisions were made to inject liquid reactants into the reactor inlet line and test gases into the gas chromatograph. A high pressure liquid pump (Model 1LM from Eldex Lab., Inc.) was used to inject methanol or ethanol into the reactor through inlet line. For safety purposes, two CO alarms (Model HIC-203 from Industrial Test Equipment Co., Inc. Port Washington, NY) and a H_2 (Model HIC-821 from Industrial Test Equipment Co., Inc. Port Washington, NY) alarm were in continual use.

2.3.2. Catalyst Loading and Activation

In each test, a 3 *g* (4 *ml*) of catalyst was centered in the PFR using clean 2 – 3 *mm* pyrex glass beads. A glass wool plug was used between catalyst bed and clean glass beads on exit side of the reactor, to assist in keeping the catalyst in place. A small piece of glass wool was also used at exit end of the reactor to prevent the beads from blocking

the reactor exit. Activation of the catalyst was carried out at 623.15 or 673.15 °*K* by flowing 60 *ml/min* of 2 % H_2/balance N_2 at atmospheric pressure through the catalyst in the PFR [2]. In each case, the temperature was gradually increased to the reduction temperature over a period of about 2 *hr*. The activation process was followed by monitoring the water content of the exit gas by gas chromatography, and it was terminated when a sudden drop in the production of water was observed. The desired higher alcohol synthesis reaction conditions were attainted by decreasing the reactor temperature with flowing 2 % H_2/balance N_2 at atmospheric pressure and then increasing the reactor pressure to a desired value using H_2 and CO feed.

2.3.3. Analytical Procedure

The gas chromatograph utilized a thermal conductivity detector (TCD) for analysis of the products, and the integrator/printer produced the chromatogram with uncorrected integrated areas, peak widths, and % area composition. The parameters for an analysis were injection of the sample at 306.15 °*K* and maintaining this temperature for one min and then heating to 473.15 °*K* using a heating rate of 25 °*K/min*. The 473.15 °*K* temperature was then maintained for 7 *min* before cooling the GC oven back to 306.15 °*K*. The GC operating parameters used during the catalyst testing is given in Table 2.2.

Identification of the peaks was achieved by injection of known components and correlating the retention times. The retention times of the components obtained using the GC parameters given in Table 2.2 are listed in Appendix 2C.

GC	Hewlett Packard, Model 5890 Series II
GC Column	CP-PoraPLOT Q, CP 7550
Carrier Gas	Helium
Injection	Split
Detector	TCD
Sensitivity	High
Column Head upstream pressure, *psig*	60-70
Column Head Pressure, *psi*	15-16
Total Flow, *ml/min*	90 – 100
Septum Purge, *ml/min*	2.5 – 3
Carrier Gas, *ml/min*	2 – 2.5
Auxiliary Gas, *ml/min*	12 – 14
Reference Gas, *ml/min*	25 – 27
Injector Temperature, *°K*	473.15
Detector Temperature, *°K*	498.15
Oven Temperature, *°K*	306.15 – 473.15
Temperature Program	306.15 *°K* – 1 *min*,
	25 *°K/min*,
	473.15 *°K* – 7 *min*

Table 2.2. Gas chromatograph (GC) operating parameters of GC-HP 5890 II.

Since hydrogen has a higher thermal conductivity than the helium carrier gas, a negative signal was obtained. This signal was not integrated, and hence excluded from the analysis. A sample chromatograph of reactor (higher alcohol synthesis) product is shown in Appendix 2D. The relative molar concentration of compounds in the exit stream (excluding hydrogen) was determined from the integrated areas under the peaks in the gas chromatogram. The integrated areas were corrected for the sensitivities of each component by dividing the integrated areas by the respective thermal response factors (TRFs) and then normalizing these results to give the percent molar concentrations.

The literature TRFs [22-27] were checked by the injection of pure and diluted mixtures into the GC using a syringe or by using the mass flow controllers, e.g. a mixture of liquid methanol, ethanol, and propanol dissolved in DI water, a mixture of CO_2 diluted in CO using the mass flow controllers, etc. It was found that the experimental TRFs are constant and matched the literature values at higher area counts of the chromatographs. However, it was also observed that, the TRFs for alcohols and hydrocarbons at lower gas chromatograph area counts are not constant, and it increases with increase in area counts. In order to estimate the TRFs for alcohols (methanol, ethanol and propanol) at lower GC area counts, a series of syringe liquid injections of different volumes (0.1 - 0.5 μl) were made from diluted samples of methanol, ethanol and propanol in deionized water at different concentrations. The TRFs increases with increase in GC area counts and reaches a plateau at higher GC area counts; TRF of 47 for methanol, and 83 for propanol at higher GC area counts was estimated with reference to a literature TRF value of 72 for ethanol. The reported TRFs for methanol and propanol are respectively 55 and 83 in the literature [22]. A lower value of TRF was also reported for methanol. Santiesteban used a TRF value of 40 for methanol [2]. The TRF of a component *i*, can be calculated from the TRF of a reference component *r*, for a given mole or volume fractions by [24]:

$$TRF_i = \frac{\left(GC\ Area / mole\ or\ volume\ fraction\right)_i}{\left(GC\ Area / mole\ or\ volume\ fraction\right)_r} \times TRF_r \qquad (2.2)$$

Similarly, a series of pure and mixture of gases at different concentrations were injected into the GC to calculate the TRFs for hydrocarbons, CO_2 and CO. The calculated TRFs obtained from the syringe injections of pure gases are 42.0 and 54.0 for CO and CO_2

respectively with reference to a literature TRF value of 35.7 for methane. The literature TRF values for CO and CO_2 are 42 and 48 respectively [22]. Similar to alcohols, non-liner TRF values for methane were observed at lower GC area counts. Since the concentration of CO in the product is always more than 70 *mol %*, a constant TRF for CO was expected at such a high concentration values, however, the integrated CO area was affected by the presence of hydrogen in the product, and thereby, the CO TRF values were calibrated with respect to hydrogen to CO ratio (H_2/CO), instead of GC area counts. Calculation of TRFs for alcohols, hydrocarbons, CO and CO_2 are explained in Appendix 2E. The TRF values or the TRF co-relations used for our calculations are given in Appendix 2E, Table 2E (8). The literature TRFs were used for other components [22-27]. Once the molar percentages of outlet components were calculated by using the respective TRFs, the molar percentages were then combined with the overall carbon balance to determine the molar flows of each of the species.

CO conversion and alcohols selectivity were then calculated by,

$$CO_{conversion} = \frac{CO_{in} - CO_{out}}{CO_{in}} \times 100 \quad (2.3)$$

$$Alcohol_{Selectivity} = \frac{\sum \left(\frac{mol}{kg\ cat.hr}\right)_{alcohols}}{\sum \left(\frac{mol}{kg\ cat.hr}\right)_{alcohols} + \sum \left(\frac{mol}{kg\ cat.hr}\right)_{Hydrocarbons}} \times 100 \quad (2.4)$$

2.4. Catalyst Characterization

The bulk and surface analyses of the catalysts were performed using X-ray diffraction (XRD) and X-ray photoelectron spectroscopy (XPS) respectively. The XRD patterns were collected using a Rigaku MiniFlex II diffractometer with a Cu-Kα X-ray source (λ = 1.54056 *Å*) operated at 30 *kV* and 15 *mA*, 2θ angles from 10° to 70° at a scanning speed of 1 or 2 *°/min*. The pellets were crushed to powder using a mortar and pestle for XRD analysis. The XPS measurements were performed on a Scienta ESCA 300 with a monochromatic Al Kα X-ray source. A randomly selected single pellet was used for the XPS.

2.4.1. Calcined Sample

The representative XRD patterns of acid washed AC and calcined sample are displayed in Fig. 2.5. The XRD pattern of calcined sample is compared with the reference pattern of MoO_2 obtained from the PDF card number 01-073-1249 [28]. The calcined sample has the bulk characteristics of crystalline MoO_2.

$$3(NH_4)_6Mo_7O_{24} \xrightarrow{>773.15\,°K,\,N_2} 21MoO_2 + 30H_2O \uparrow + 7N_2 \uparrow + 4NH_3 \uparrow \qquad (2.5)$$

The representative survey XPS spectrum of calcined sample is shown in Fig. 2.6. Fig. 2.7-9 shows the high-resolution XPS spectra and peak fitting of Mo 3d, O 1s, and C 1s respectively.

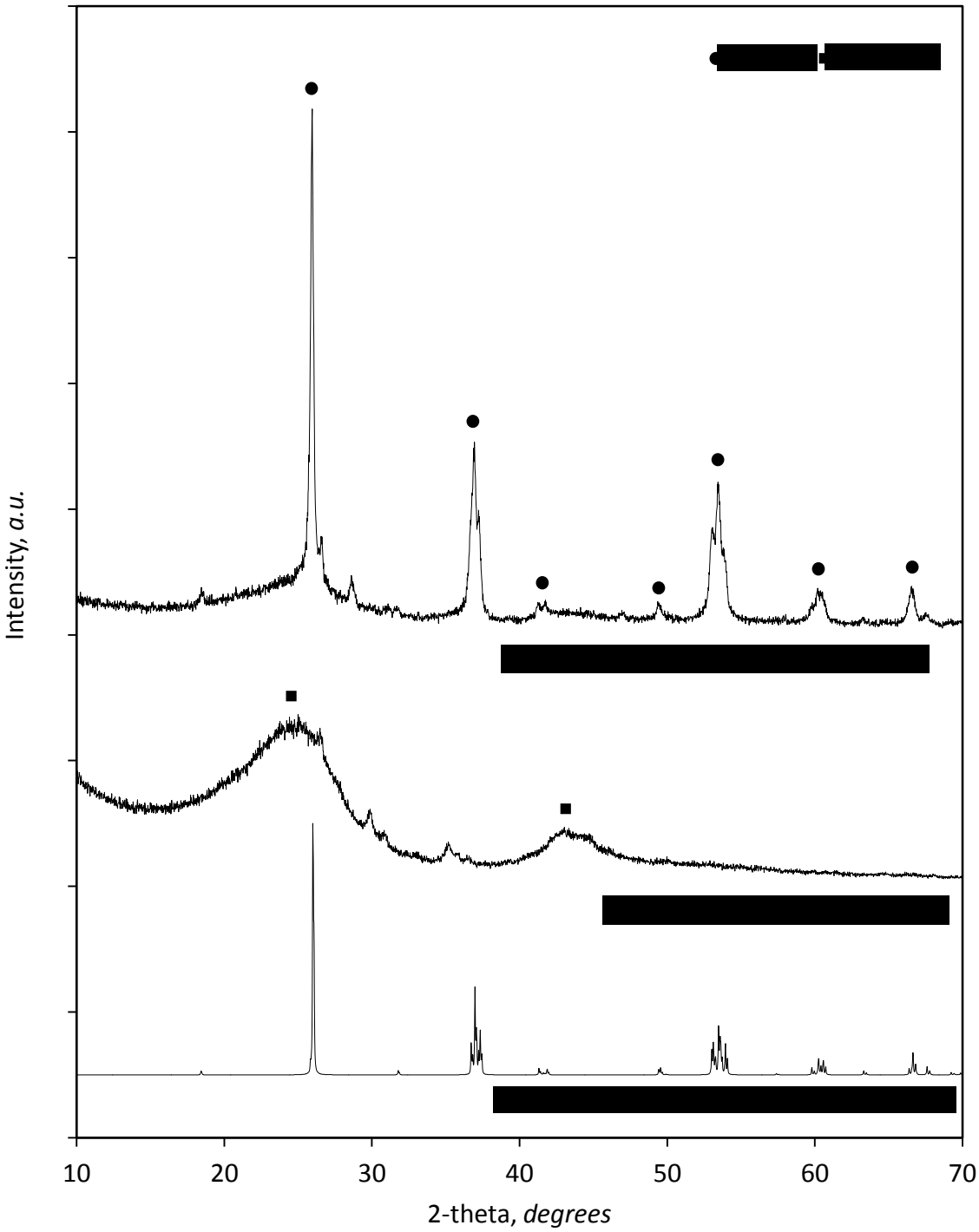

[redacted]

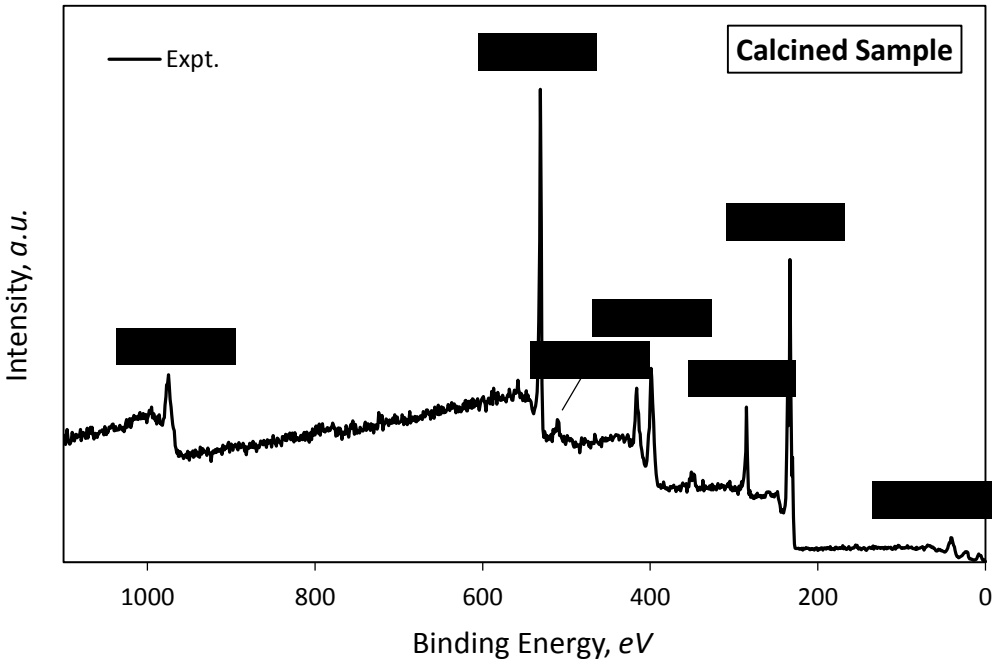

[redacted]

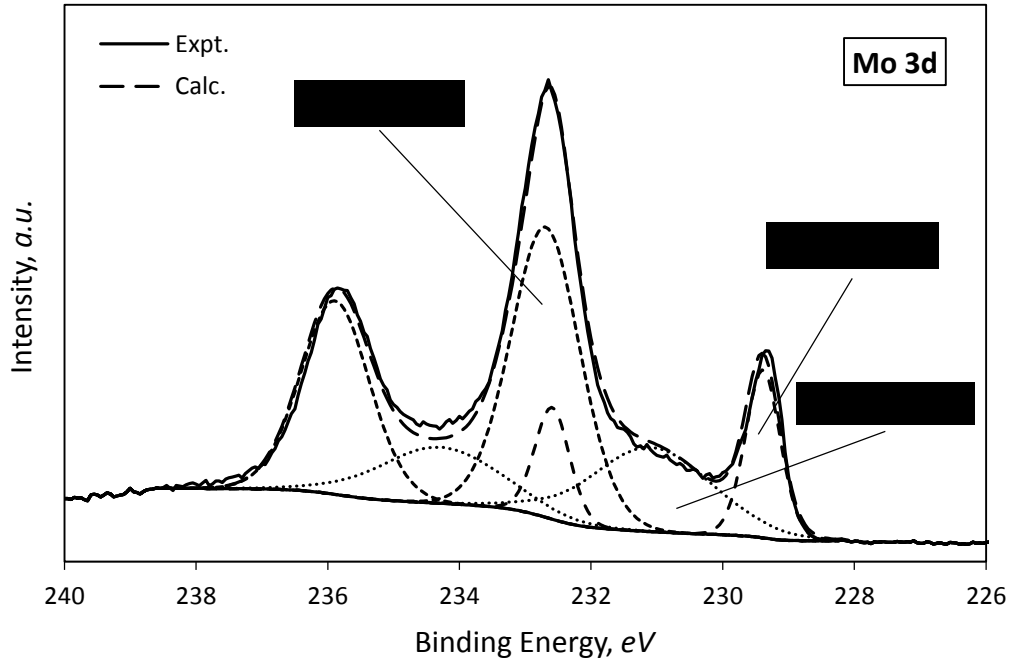

[redacted]

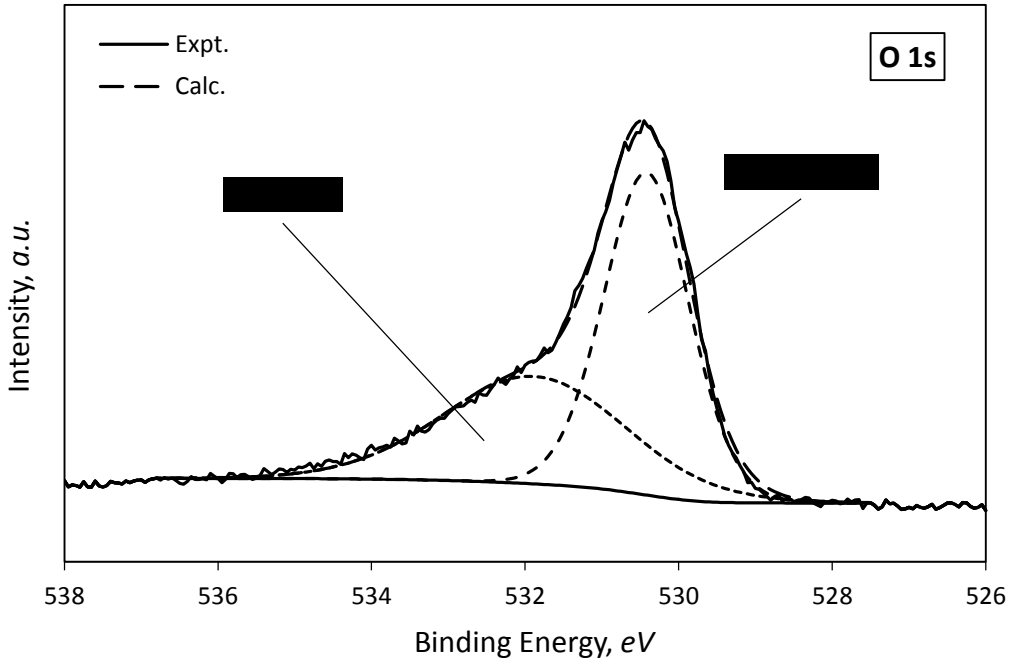

[redacted]

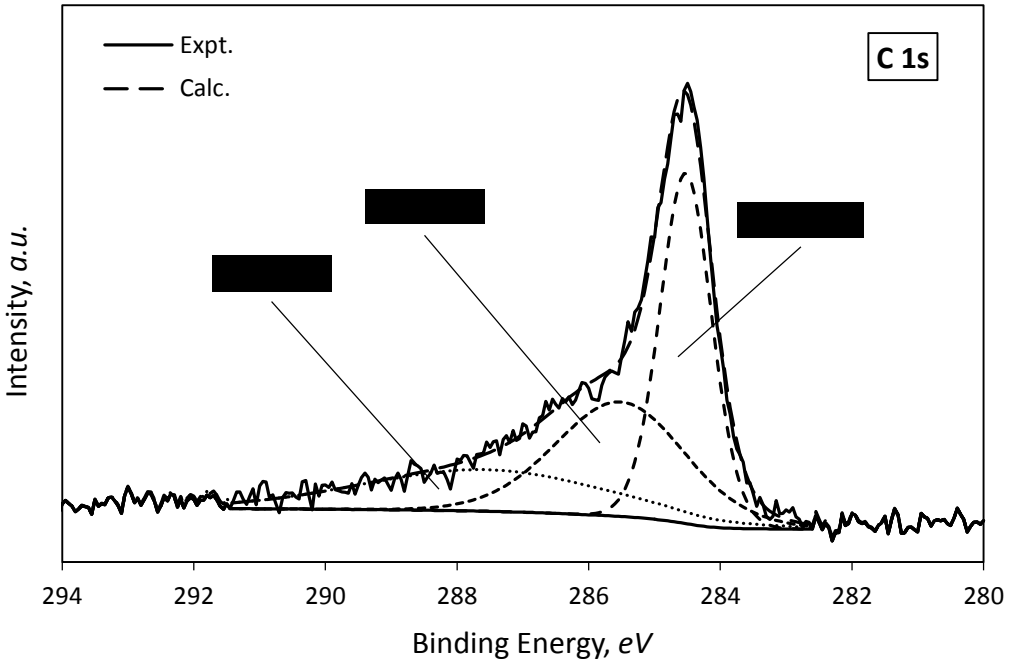

[redacted]

The peaks of Mo 3d and O 1s in the survey spectrum can be assigned to the characteristics of molybdenum oxides [29]. The peak C 1s is assigned to the characteristics of carbon matrix of the AC support. Different oxidation states of Mo were observed at the surface of MoO_2. The reason of higher oxidation states at the surface could be due to the oxidation of unstable MoO_2 with oxygen from air [30, 31]. The peak fitting of high-resolution XPS spectra of Mo 3d, O 1s, and C 1s was performed using CasaXPS software [32]. A fixed separation of 3.2 *eV*, fixed area ratio of 1.5 (3d 5/2 to 3d 3/2), and same full width at half the maximum height (FWHM) was used for Mo doublets, Mo 3d 5/2 and 3d 3/2. The Mo 3d spectra can be well fitted into three doublets. The position of 3d 5/2 peaks measured at 229.39, 231.09, and 232.69 *eV* corresponds to Mo^{4+}, Mo^{5+}, and Mo^{6+} oxidation states respectively. Only molybdenum oxides were expected after calcination of AMT promoted AC pellets, hence, the Mo^{4+}, Mo^{5+}, and Mo^{6+} oxidation states can be attributed to MoO_2, Mo_2O_5, and MoO_3 respectively. The composition of Mo^{4+}, Mo^{5+}, and Mo^{6+} oxidation states were calculated to be 16.22, 28.16, and 55.63 *%* respectively. The presence of Mo_2O_5 and MoO_3 at the surface could be due to the progressive reaction of MoO_2 with ambient oxygen (from air) during handling and storage of the calcined pellets. The threshold partial pressure of oxygen calculated from the Ellingham diagram for the oxidation of MoO_2 to MoO_3 at room temperature is 1.317×10^{-48} *bar*, much lower than the atmospheric oxygen partial pressure. The MoO_3 is more stable than MoO_2 at room temperature.

$$2MoO_2 + \frac{1}{2}O_2 \xrightarrow{298.15\,°K} Mo_2O_5 + \frac{1}{2}O_2 \xrightarrow{298.15\,°K} 2MoO_3 \qquad (2.6)$$

The C1s spectra can be fitted with three peaks. The strong peak at 284.53 *eV* can be assigned to the C – C bonds in the AC. The small peaks of C 1s at 285.52, and 287.57, and the peak of O 1s at 531.89 *eV*, indicates the adsorption of oxygen in the AC.

2.4.2. Sulfidized Sample

The representative XRD pattern of sulfidized sample is shown in Fig. 2.10. The XRD pattern is compared with the reference pattern of MoS_2 obtained from PDF card number 01-073-1249 [28]. Several new peaks with broad intensities were appeared upon sulfidation of the calcined sample at 672.15 °*K*. These broad peaks can be attributed to the amorphous or poorly crystalline MoS_2 phase. The presence of molybdenum sulfides is further evident by XPS analysis of the sulfidized pellets. The XPS was performed at the outside surface of a randomly selected pellet. The representative survey XPS spectrum of the sulfidized sample is shown in Fig. 2.11. Fig. 2.12-14 shows the high-resolution XPS spectra and peak fitting of Mo 3d, S 2p, and O 1s respectively. The XPS was also performed at inside of the pellet. The pellet was cut into half on the axial direction for the XPS analysis at inside of the pellet. The XPS analysis result for inside of the pellet is presented in Appendix 2F. The peaks of Mo 3d, S 2s, and S 2p in the survey spectrum can be assigned to the characteristics of molybdenum sulfides [29]. The O 1s peak signifies the presence of molybdenum oxides as well. The Mo 3d spectra are well fitted into two doublets. The position of 3d 5/2 peaks measured at 229.40 and 231.10 *eV* corresponds to Mo^{4+} and Mo^{5+} oxidation states respectively. The S 2s peak is located at 226.70 *eV*.

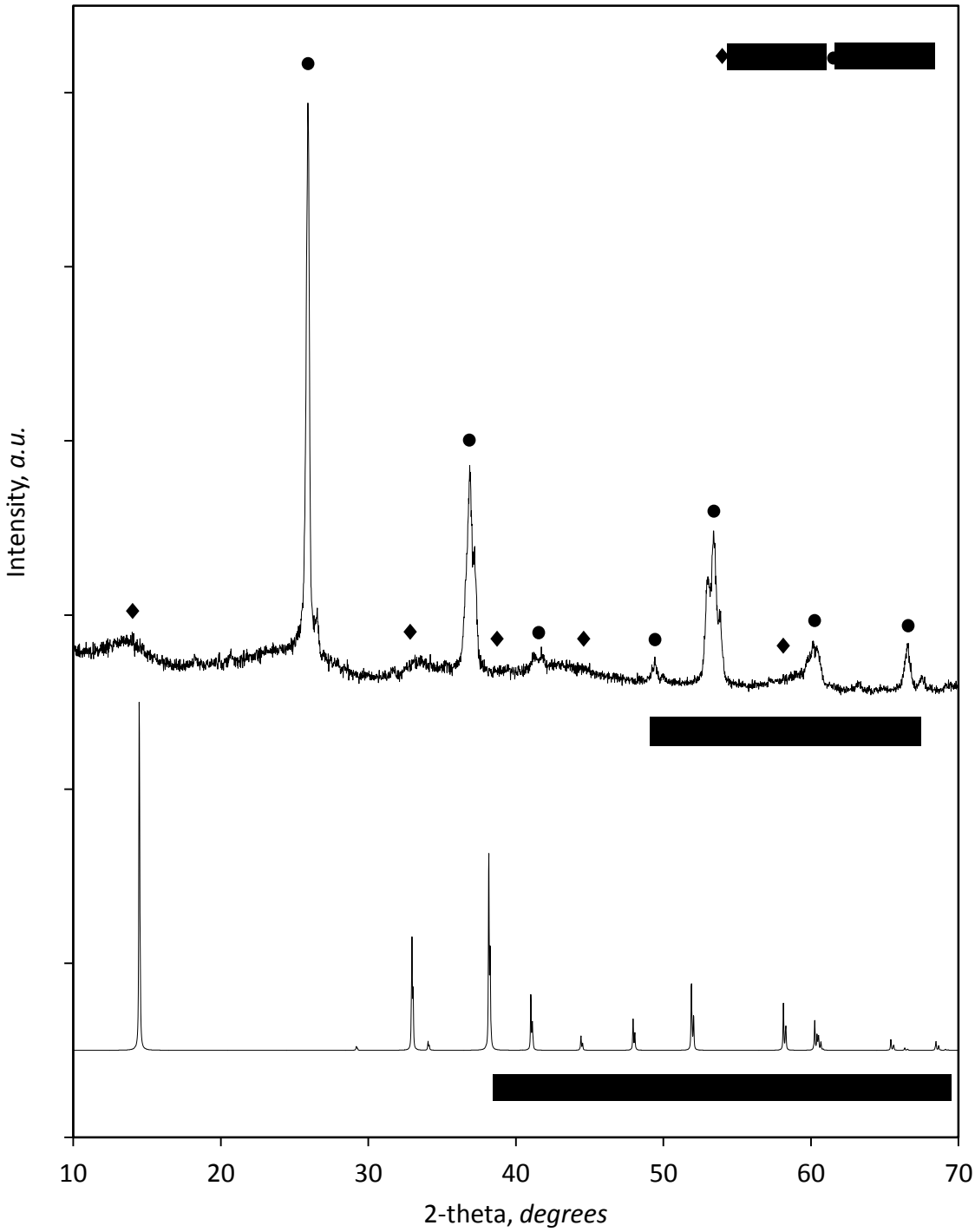

[redacted]

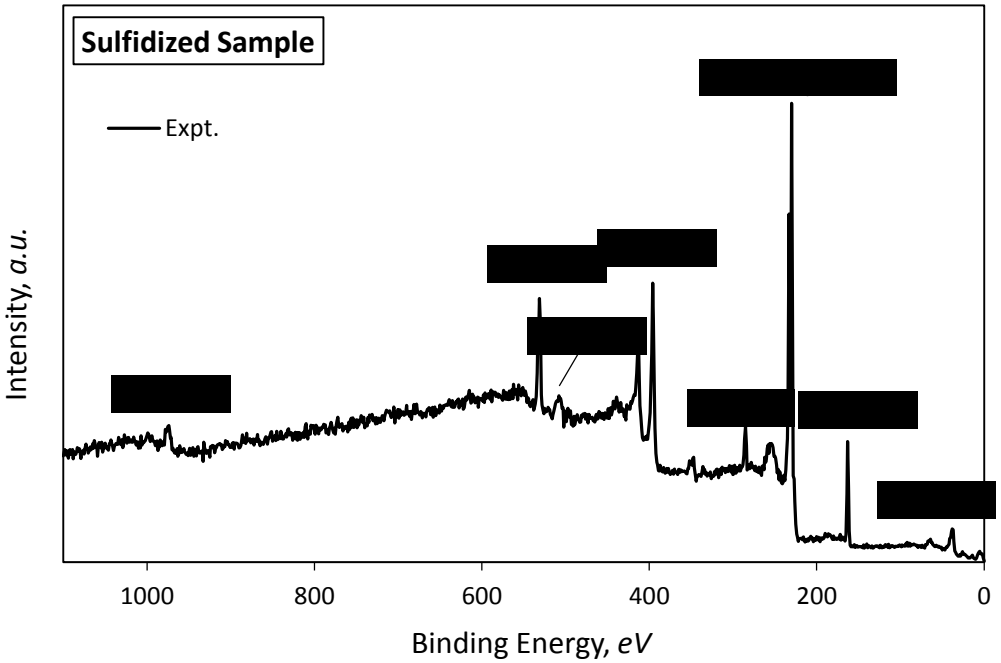

[redacted]

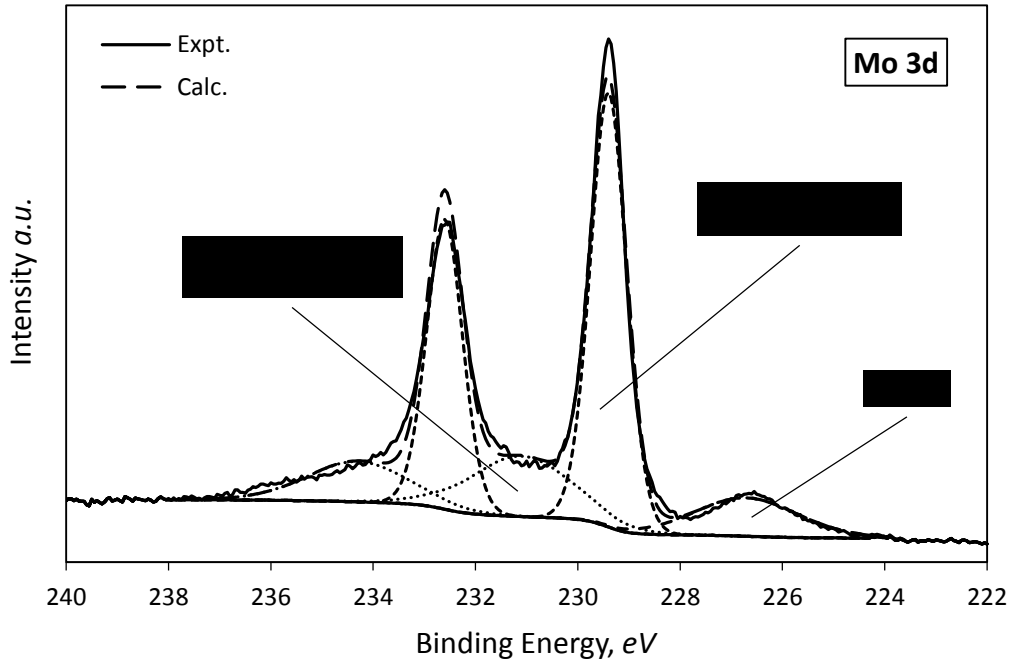

[redacted]

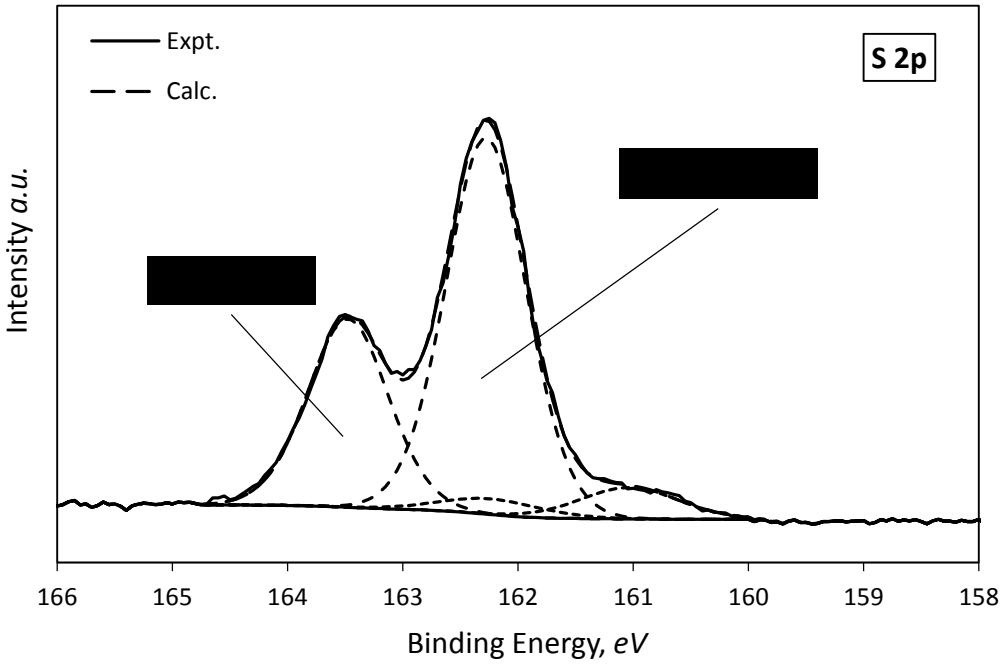

[redacted]

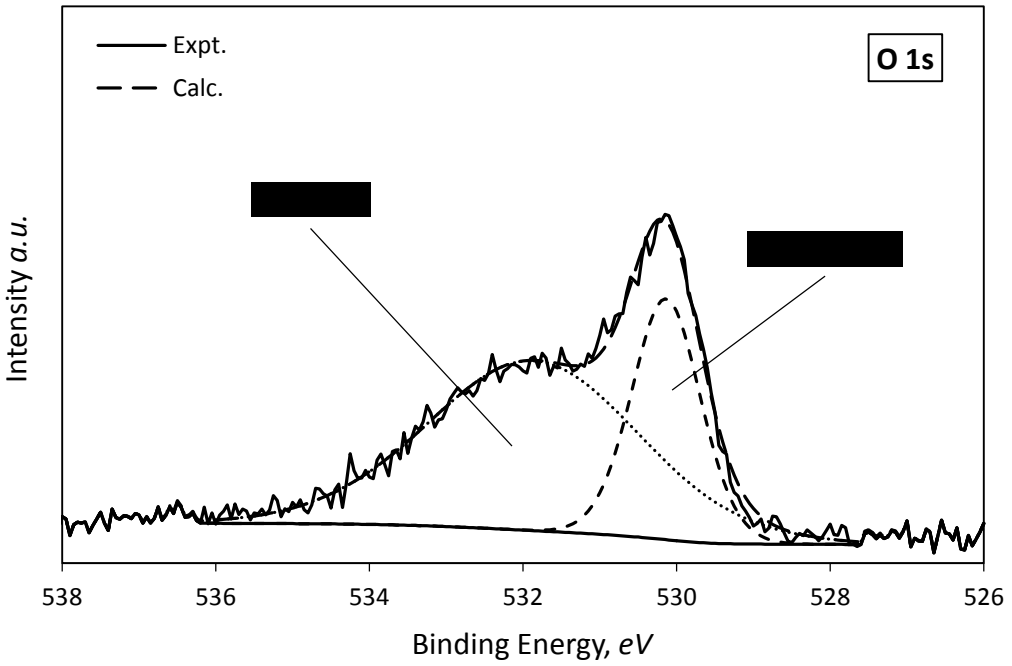

[redacted]

The composition of Mo^{4+} and Mo^{5+} oxidation states were calculated to be 71.91 and 28.09 *%* respectively. The Mo^{6+} oxidation state, attributed to MoO_3 in the calcined sample, is completely reduced to Mo^{4+} and Mo^{5+} species due to the reducing atmosphere provided by 5% H_2S in H_2 flow during sulfidation. Since the Mo oxidation states of MoO_2 and Mo_2O_5 is the same as the oxidation states of MoS_2 and Mo_2S_5 respectively, the presence of MoO_2 and Mo_2O_5 can't be neglected [33, 34]. The reduction of O 1s peak at 530.14 *eV* also confirms the presence of both oxide and sulfide species. The surface S to Mo ratio can be calculated from the high-resolution XPS spectra of Mo 3d and S 2p [35]. A fixed separation of 1.2 *eV*, fixed area ratio of 2 (2p 3/2 to 2p 1/2), and same FWHM was used for S doublets, S 2p 3/2 and 2p 1/2. The overall S/Mo ratio (S 2p to Mo 3d) was calculated to be **1.08**. The S 2p doublet, with S 2p 3/2 peak located at 162.28 *eV* is the characteristic S^{2-} peak of MoS_2. The S^{2-} to Mo^{4+} ratio (mixture of MoS_2 and MoO_2) is calculated to be **1.36**. The overall S/Mo and S^{2-}/Mo^{4+} ratio at center (inside) of the pellet are **0.88** and **1.56** respectively. The XPS spectra at inside of the pellet and the peak fittings are shown in Appendix 2F. Irrespective of the spatial positions in the pellet, the mixed oxides and sulfides species were always present at the surface, the predominant Mo^{4+} species and small amount of Mo^{5+} species, with overall S/Mo and S^{2-}/Mo^{4+} ratio of approximately **0.88-1.08** and **1.36-1.56** respectively. As we have seen, it is difficult to sulfidize MoO_2 at 673.15 *°K*. The length of sulfidation reaction does not have any effect on S/Mo ratio; even a 55 *hr* sulfidation time is not enough to produce MoS_2 from MoO_2. Compared to MoO_2, MoO_3 can be completely converted to MoS_2 at a lower sulfidation temperature, e.g. 673.15 *°K* [34, 36]. It is probably the surface MoO_3 of the calcined MoO_2/AC pellets is completely converted to MoS_2 and the partial sulfidation of MoO_2 to

MoS_2 forms MoS_2 layers only at the surface of the catalyst, while the bulk is still the un-sulfided MoO_2.

$$MoO_3 + H_2 + 2H_2S \xrightarrow{673.15\ ^\circ K} MoS_2 + 3H_2O \quad (2.7)$$

$$MoO_2 + 2H_2S \xrightarrow{>673.15\ ^\circ K} MoS_2 + 2H_2O \quad (2.8)$$

Reaction 2.8 is not favorable at 673.15 °*K*; it requires a higher sulfidation temperature. The sulfidation temperature of MoO_2 is unknown at this point for AC supported MoO_2 pellets. The amount of MoS_2 can further be increased by promoting the reaction 2.7 by employing a higher sulfidation temperature, above 673.15 °*K*. Further reduction of Mo^{4+} to Mo^{2+}, or Mo^0, or carbide formation was not observed. Since the alcohol synthesis reactions occur only at the surface of the catalyst, the catalyst is still very active for alcohol synthesis despite having bulk MoO_2 structure. The MoS_2 is stable in air and protects oxidation of bulk molybdenum oxides to MoO_3, as the bulk molybdenum oxides were covered by MoS_2 layers at the surface and thereby reducing its exposure to ambient oxygen.

2.4.3. Cesium Promoted Sample

The representative XRD patterns of fresh and tested catalyst samples were shown in Fig. 2.15. The XRD patterns are compared with the reference pattern of Cs_2SO_4 (PDF cad number 00-043-0306) [28].

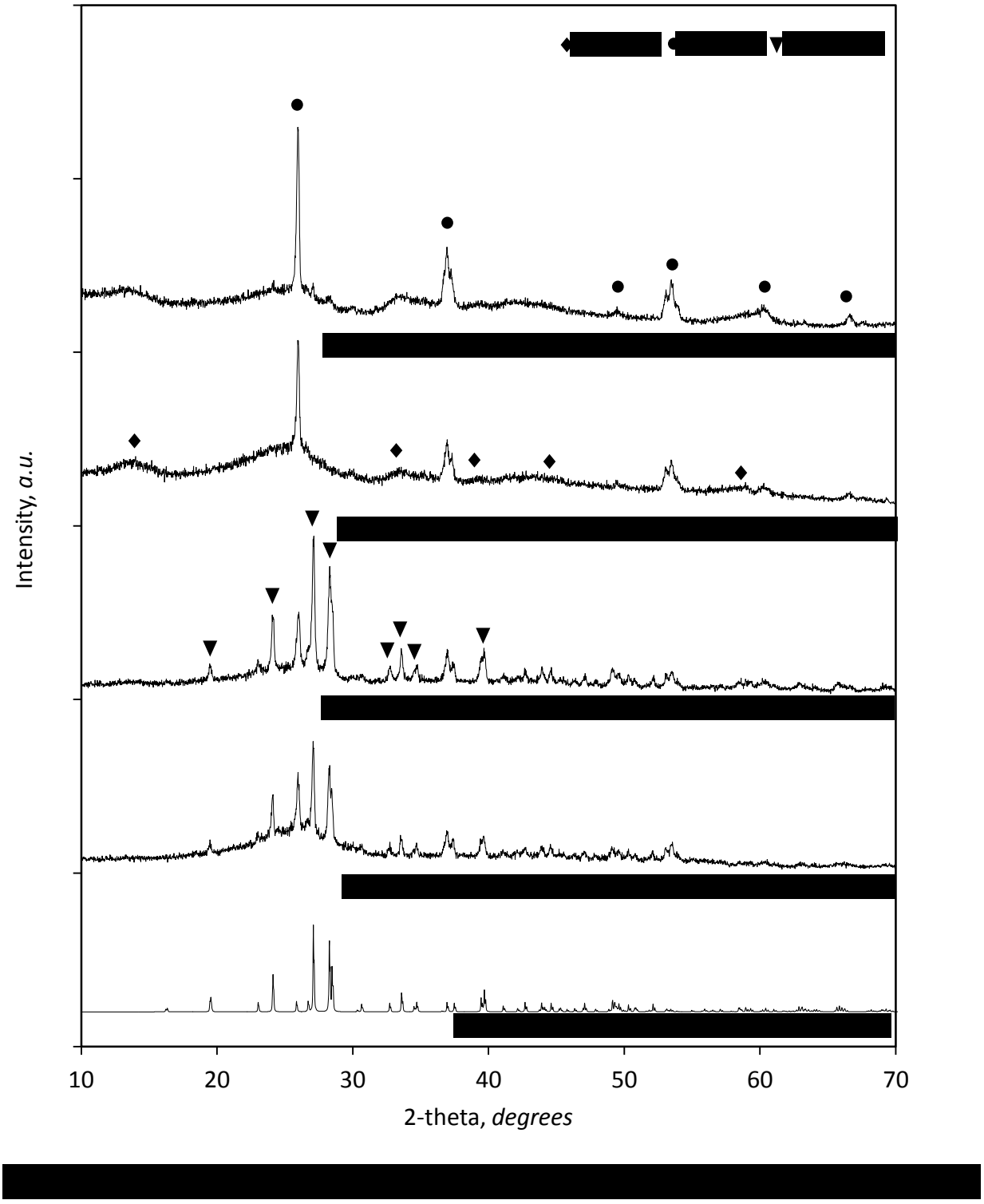
Intensity, *a.u.*
10
20
30
40
50
60
70
2-theta, *degrees*

The catalysts retain the bulk MoO_2 and amorphous or poorly crystalline MoS_2 structure after CsCOOH promotion and exposure to syngas for a Cs loading of Cs to Mo ratio of 0.23 *mol/mol*. Traces of sulfate species of the Cs_2SO_4 type was observed on the spent catalyst. The Cs_2SO_4 species are more prominent for the catalyst with higher Cs loading. The representative survey XPS spectrum of a CsCOOH promoted catalyst exposed to atmosphere for weeks and a tested catalyst stored in N_2 atmosphere after testing are shown in Fig. 2.16 and Fig. 2.17 respectively. Fig. 2.18-23 shows the high-resolution XPS spectra and peak fitting of Mo 3d, S 2p, and Cs 3d respectively for both fresh and spent catalysts. It is difficult to detect Mo and/or S at outside surface of the fresh catalyst, due to large amount of cesium present at the surface after it was exposed to atmosphere for weeks. The XPS performed at inside of a randomly selected CsCOOH promoted catalyst pellet is presented. The pellet was cut into half on the axial direction for the XPS analysis. The representative survey XPS spectrum taken at outside of a freshly prepared catalyst stored in N_2 purged vial and the corresponding high-resolution Mo3d spectra are shown in Appendix 2G. All these catalysts were exposed to atmosphere for brief period of time while handling; transferring from rotovap to vacuum oven for drying, catalyst loading and un-loading to the alcohol synthesis reactor, vacuum oven or alcohol synthesis reactor to N_2 purged bottle or vial till used for XPS or XRD analysis. Moreover, the catalyst pellets were crushed to powder using a mortar and pestle in ambient atmosphere for powder XRD analysis. While MoS_2 is stable in air, upon CsCOOH promotion, it can oxidize to molybdenum (Mo^{6+}) and sulfur (S^{6+}) oxides by reacting with absorbed oxygen and moisture from atmosphere due to the hygroscopic nature of CsCOOH [15, 19, 20].

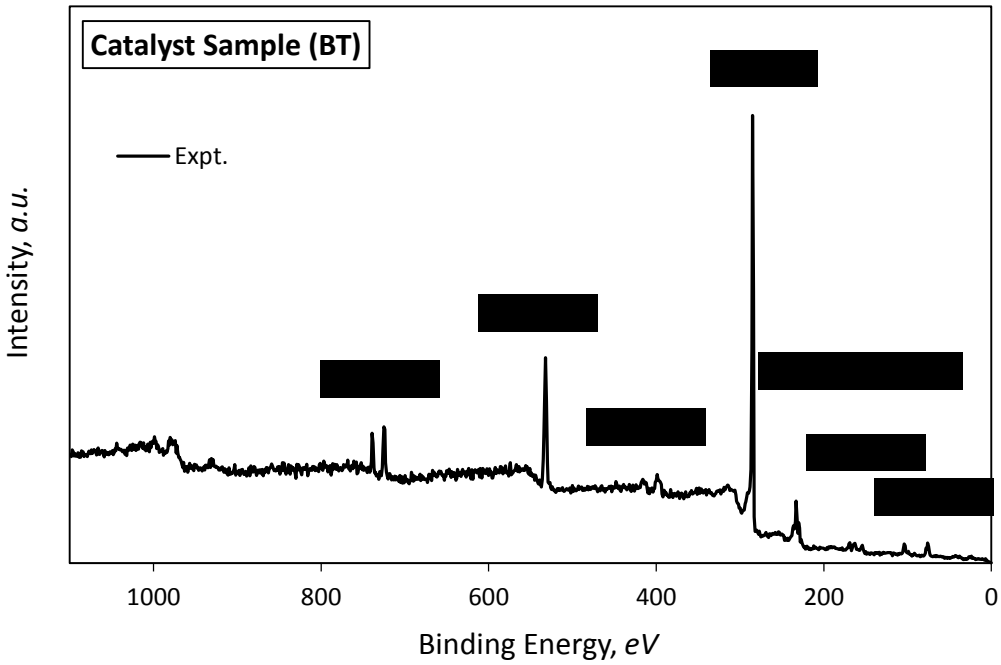

[redacted]

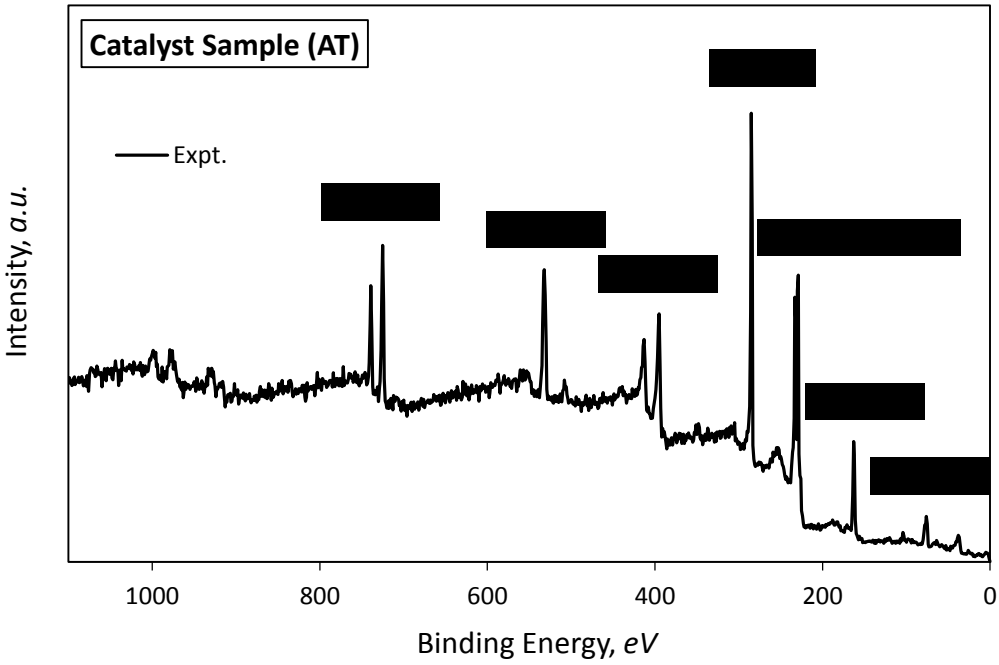

[redacted]

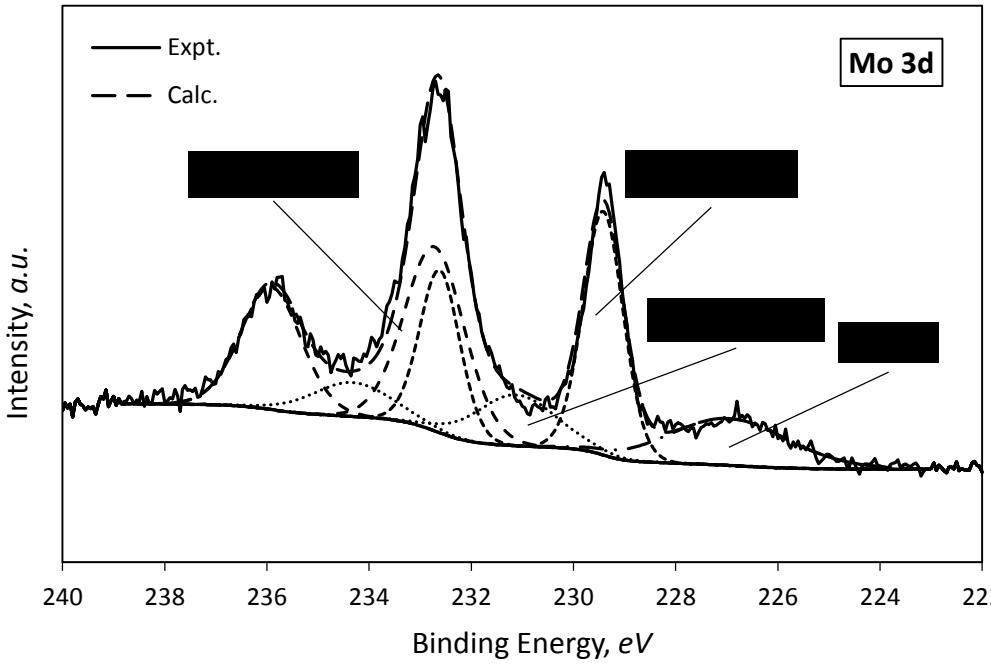

[redacted]

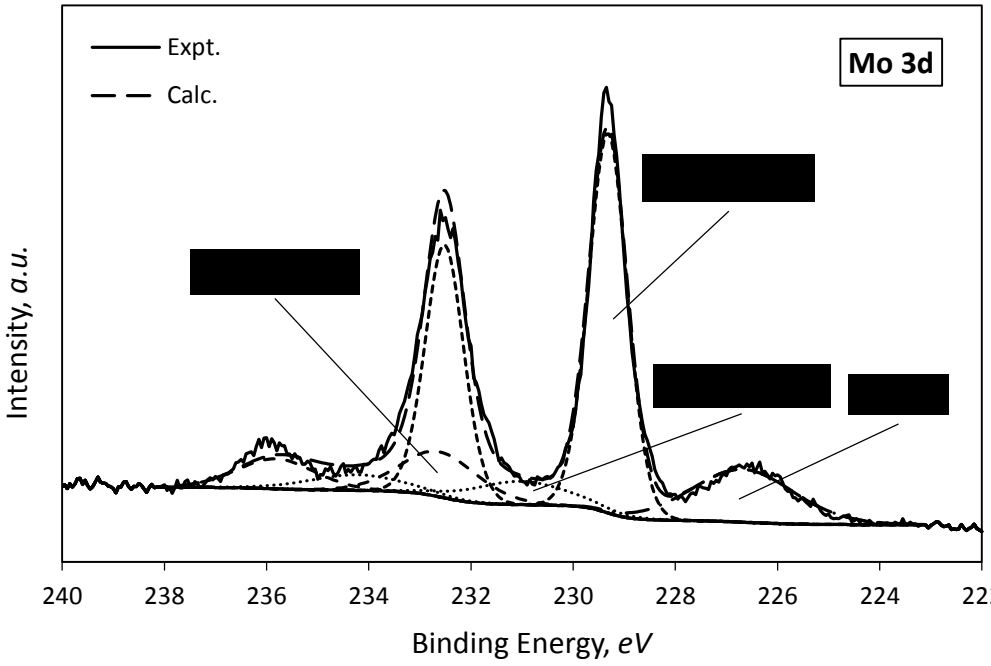

[redacted]

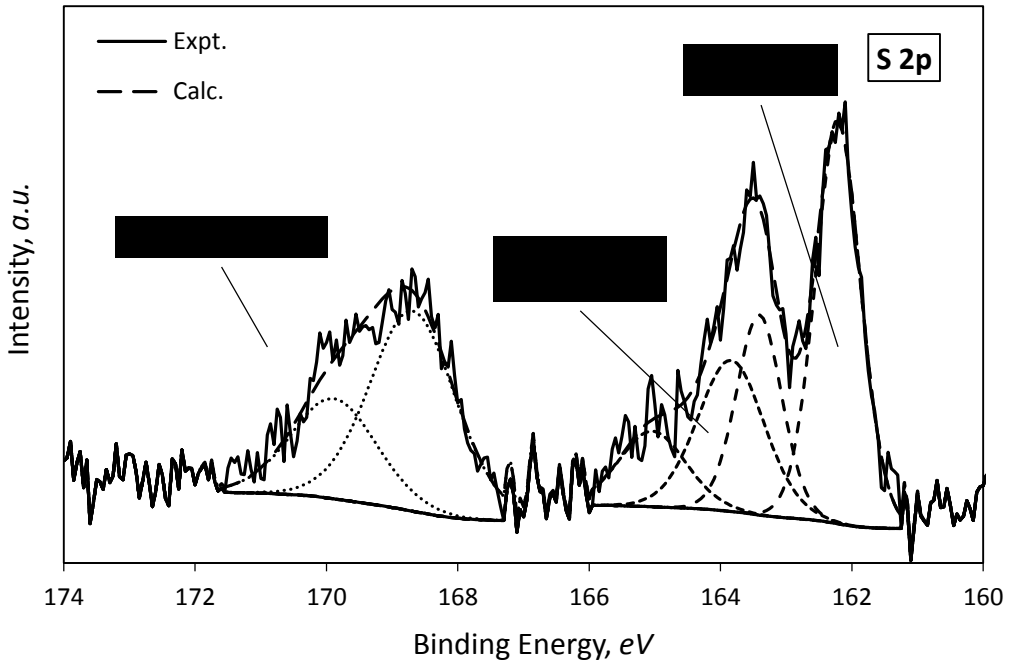

[redacted]

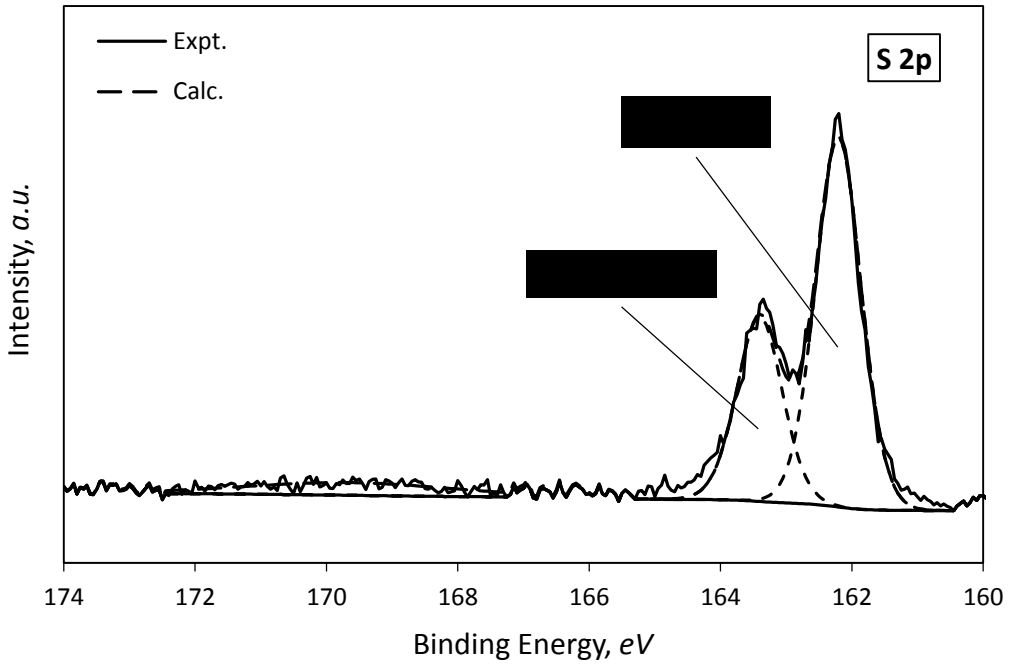

[redacted]

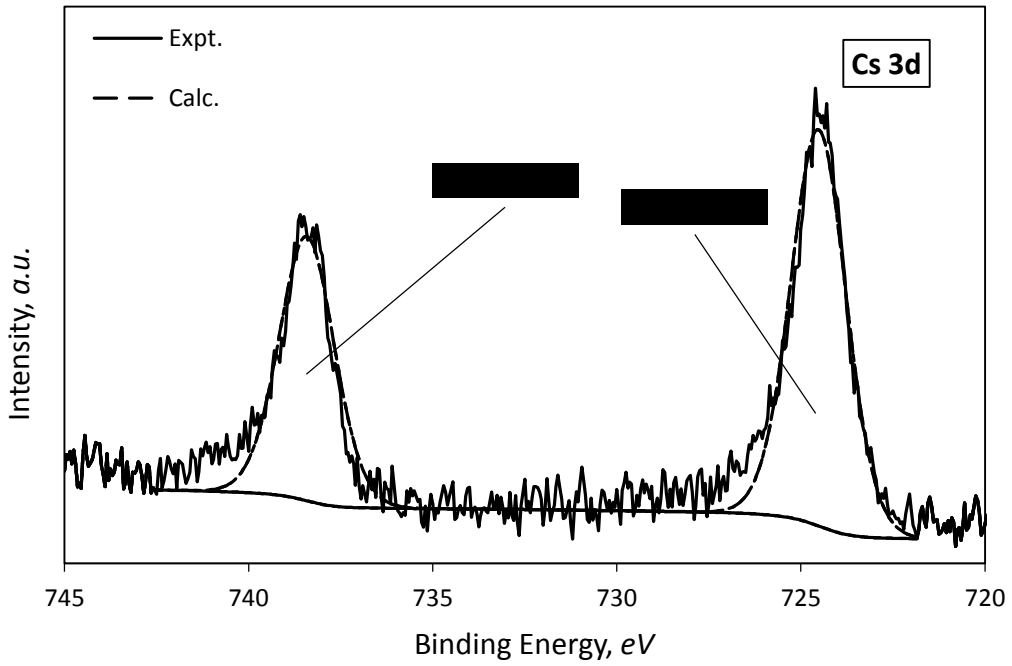

[redacted]

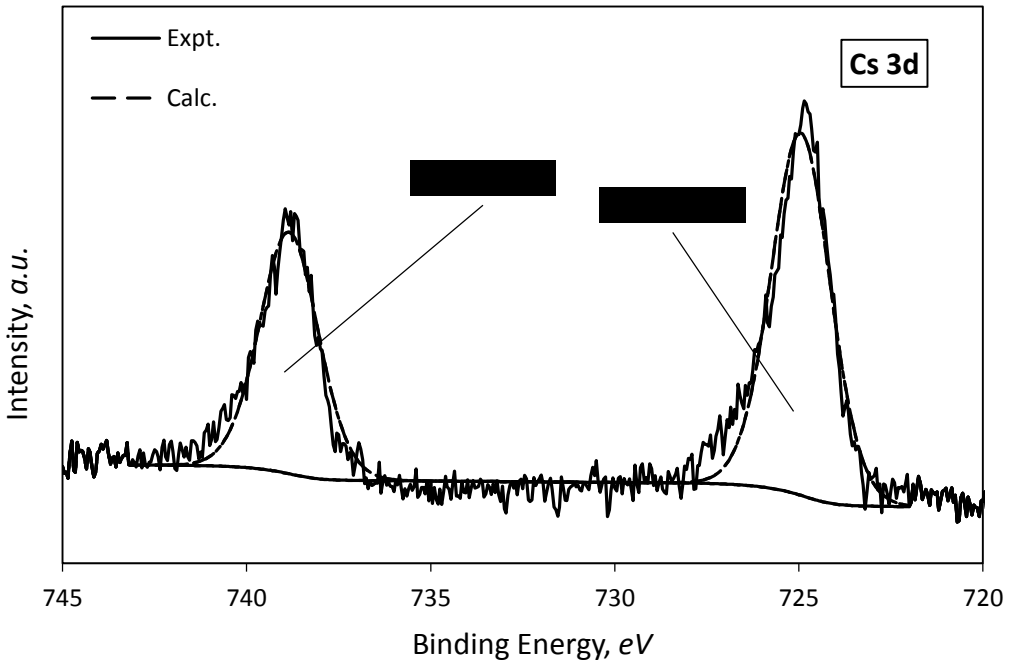

[redacted]

The Mo^{6+} oxidation state appears for the CsCOOH promoted un-tested catalyst exposed to atmosphere for weeks (Fig. 2.18). Even a short term exposure can oxidize both un-tested and tested catalyst (Fig. 2H (2) and Fig. 2.19). The composition of Mo^{6+} oxidation state was increased to 20.34 % and 62.32 % for un-tested catalyst by short-term and prolonged exposure to air respectively. The composition of Mo^{4+}, Mo^{5+}, and Mo^{6+} oxidation states were calculated to be 71.89, 11.02, and 17.09 % respectively for the tested catalyst sample. The increase in Mo^{4+} oxidation state is due to the reducing atmosphere provide by H_2 during pre-treatment of the catalyst by 2% H_2/balance N_2 flow and H_2 from syngas during alcohol synthesis reaction. Additional sulfur doublets, S_2^{2-} and S^{6+} were observed at 163.84 and 168.69 *eV* respectively for the catalyst exposed to air for weeks (Fig. 2.20). The S^{6+} peak is the characteristic peak of sulfate (SO_4^{2-}) species. The S^{6+} peak is not present for the tested catalyst stored in N_2 atmosphere (Fig. 2.21). Small amount sulfate species might have been formed during short term exposure of freshly prepared catalyst was reduced by pre-treatment of the catalyst by 2% H_2/balance N_2 at 623.15 °*K*. The sulfate species do not form during higher alcohol synthesis reaction conditions used for the present study. These results are consistent with the results reported for CsCOOH/MoS_2 powder catalyst [2]. The S 2p/Mo 3d (overall) and S^{2-}/Mo^{4+} ($Mo^{4+}S_x$) ratio is calculated to be **1.41** and **1.94** respectively. The Cs 3d 5/2 peak is located at around 724.95 *eV*. The oxidation state of Cs was unchanged after higher alcohol synthesis reactions. The Cs_2SO_4 species observed by XRD patterns are possibly formed by the reaction of CsCOOH with MoS_2 in air during catalyst handling and preparation of power sample for XRD analysis (crushing to power in ambient conditions). Furthermore, agglomeration and crystallization of Cs species took place

upon exposure to air. Increased Cs_2SO_4 intensity of the tested catalysts are probably the byproduct of more intimately mixed Cs precursor and MoS_2 during pre-treatment and higher alcohol synthesis reactions and its reaction with oxygen and moisture upon subsequent exposure to air after testing; during handling and sample preparation for XRD analysis. The active species for alcohol synthesis reactions are alkali-Mo-S, $(alkali)_2S$, and MoS_2 species [37, 38]. The Cs_2SO_4 is not considered as the active species involved for alcohol synthesis [20, 39]. The presence of molybdenum oxides increases the production of hydrocarbons and furthermore it increases the production of higher hydrocarbons. Formation of Cs_2SO_4 and MoO_x should be avoided by keeping the catalyst away from air at any point of time after CsCOOH promotion. The remaining MoO_2 in the catalyst should be converted to MoS_2 by employing higher sufidation temperature.

2.5. Testing Results and Discussions

The catalyst testing results obtained from each of the catalyst listed in Table 2.1 is presented in a systematic manner. The catalyst number 3, number 7, and number 9 were tested extensively,

- To determine the stabilization time.
- Effect of HAS process parameters, such as, reaction temperature, pressure, gas hourly space velocity (GHSV), and H_2/CO ratio on product yields, CO conversion and alcohol selectivity.
- Stability of the catalyst at steady-state.
- Effect of external injections of methanol and ethanol on product yields, CO conversion and alcohol selectivity.

- Decomposition of methanol and ethanol in an inert atmosphere, i.e. helium.

The catalysts number 1 to number 5 were prepared with varying Cs/Mo molar ratio from 0.03 to 2.72 to optimize the Cs/Mo ratio.

The catalysts number 6 – 8, and number 10 were prepared using different batch sizes for each of the catalyst preparation steps (Table 1) to check the reproducibility and scalability of the catalyst preparation process.

The testing results of all the catalysts are given in Appendix 2H. In this section, only selected results are presented.

Only linear alcohols, hydrocarbons and carbon dioxide along with un-reacted carbon monoxide and hydrogen were observed in the product. The major alcohols and hydrocarbons in the products are: methanol, ethanol, propanol and methane. Small amount of butanol observed in the products are lumped together with propanol, and termed as propanol^{+}. Methane is the major product among hydrocarbons. The water formed during higher alcohol and hydrocarbon synthesis reactions is consumed by simultaneous water-gas shift reaction. For this catalyst, all the water formed are consumed and converted to CO_2, on the other way, one can relate the amount of CO_2 to the amount of higher alcohols and hydrocarbons formed [2]. Methanol, ethanol, propanol^{+}, and methane yields were used for the comparison of different catalyst testing results. The alcohol selectivity is calculated by considering all the alcohols and hydrocarbons, including ethane and propane, and excluding CO_2, as defined by equation *2.4*.

2.5.1. Stabilization Time of the Catalyst

The stabilization time is the time period required for the catalyst under reaction conditions to reach its steady-state level of activity and selectivity. Initial transient behavior of product yields and the corresponding CO conversion and alcohol selectivity are respectively sown in Fig. 2.24 and Fig. 2.25 for the catalyst number 3 and number 7. The operating conditions maintained for catalyst number 3 are: 590 *°K*, 85.3 *bar*, 2992.9 *L/kg cat/hr* GHSV, and H_2/CO = 0.993 *v/v*, and the operating conditions for catalyst number 7 are: 606 *°K*, 97.0 *bar*, 3350.0 *L/kg cat/hr* GHSV, and H_2/CO = 1.962 *v/v*. In both the cases, high amount of hydrocarbon forms during initial period of reaction and gradually decreases with reaction proceeds and stabilizes to a lower value. In the contrary, alcohols increases gradually with reaction time and stabilizes at a higher value. Lower selectivity of catalyst number 7 is due to high temperature and high pressure reaction. The catalyst number 7 operating at a higher temperature, pressure, GHSV and H_2/CO ratio took **10 *hrs*** to reach steady-state, compared to the catalyst number 3 took at-least 25 *hrs* to reach steady-state. Very small, but gradual improvement on alcohol selectivity was observed for the catalyst number 3, even after 25 *hrs* of reaction. Quicker stabilization time for the catalyst number 7 is probably due to the effective dispersion of active materials, specifically the cesium compounds at high temperature and pressure conditions.

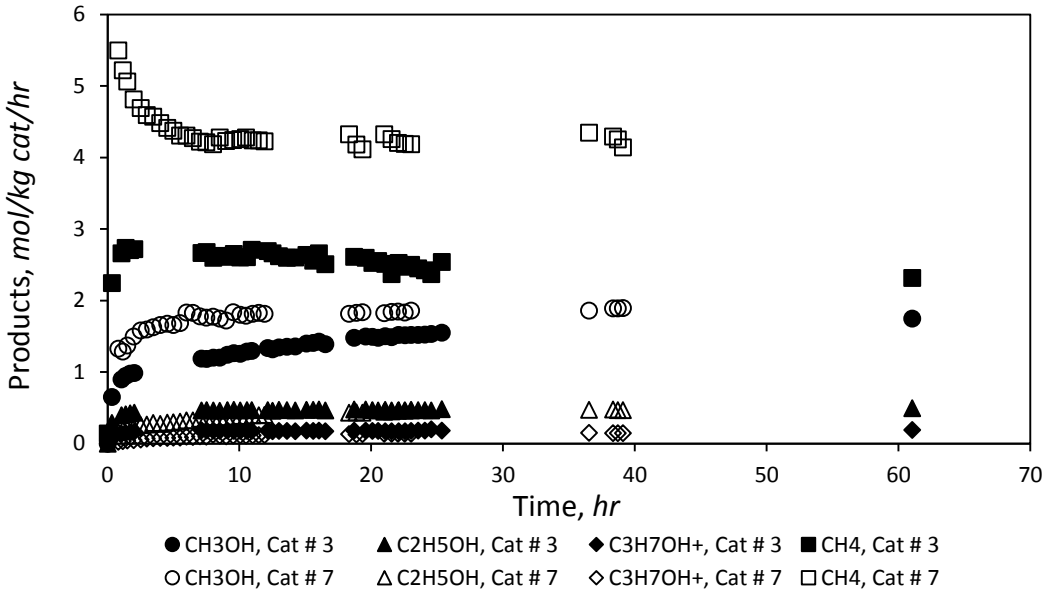

[redacted]

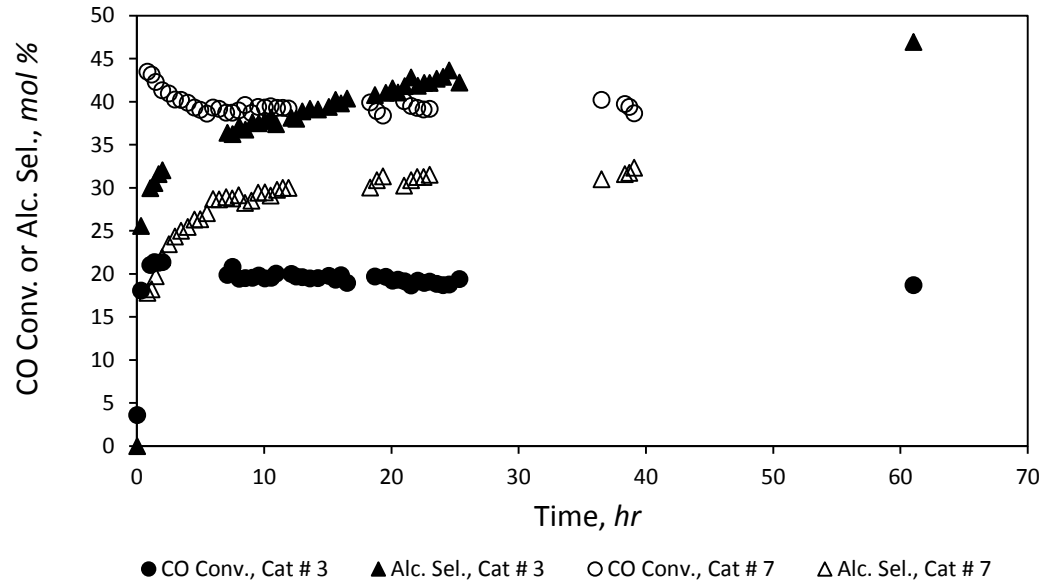

[redacted]

2.5.2. Effect of Reaction Temperature, Pressure, GHSV, and H_2/CO

Fig. 2.26 – 33 respectively shows the effect of reaction temperature, pressure, GHSV, and H_2/CO on product yields, CO conversion and alcohol selectivity.

The reaction temperature was varied from 520 °*K* to 610 °*K* for the catalyst number 3, operating at a fixed pressure, GHSV, and H_2/CO ratio of 86 or 53 *bar*, 2992.9 *L/kg cat/hr*, and 0.993 *v/v*, respectively. The reaction temperature was varied from 520 °*K* to as high as 670 °*K* for the catalyst number 7. Most of the cases, catalyst exposure to a high temperature was avoided, which is otherwise, may deactivate the catalyst due to excessive formation of carbon dioxide and/or water at a very high temperature. Fig. 2.26 shows the effect of temperature on the product yields and Fig. 2.27 shows the corresponding CO conversion and alcohol selectivity. It can be seen that, the hydrocarbon increases monotonically with increase in reaction temperature, whereas the alcohols gradually increases to a maximum value before it decreases again at high temperatures. Similar behaviors of product yields were observed irrespective of the reaction pressure employed. The optimum temperature is defined as the temperature at which the catalyst produces maximum amount of alcohols. In all of the cases, the methane yield surpasses the methanol yield at the optimum temperature. It can also be seen that, the optimum temperature shifts slightly towards higher temperature with decrease in reaction pressure. The optimum temperature for catalyst number 3 increases from 590 °*K* to 600 °*K* with decrease in pressure from 86 *bar* to 53 *bar*. The optimum temperature is 590 °*K* for both the catalyst number 3 and number 7 operating under similar operating conditions. It can be noted from the Table 2.1, that the catalyst number 7 was sulfidized at a lower

temperature of 673.15 °*K*, compared to 723.15 °*K* for the catalyst number 3. The sulfidation temperature does have effect on activity of the catalyst. The CO conversion and the alcohol selectivity follow the similar trend irrespective of the pressure employed. Improved alcohol selectivity was observed at lower reaction pressure with an expense of decreased CO conversion and alcohol productivity. The optimum temperature range for this catalyst is: **570 °*K* to 610 °*K*.**

The effect of reaction pressure from 60 *bar* to 100 *bar* at a fixed temperature, GHSV, and H_2/CO ratio of 590 °*K*, 2992.9 *L/kg cat/hr*, and 0.993 *v/v* respectively on product yields for catalyst number 3 is shown in Fig. 2.28 and the corresponding CO conversion and alcohol selectivity is shown in Fig. 2.29. High pressure favors production of alcohols as well as hydrocarbons. The methanol, ethanol, propanol$^+$ and methane yields are increases monotonically with increase in pressure. The methane yield increases at a faster rate than alcohols, as a result CO conversion increases but alcohol selectivity decreases with increase in reaction pressure. It can be seen from Fig. 2.26 that, the methane yield increases at a higher rate with increase in reaction pressure. In order to get the optimum performance from this catalyst, the reaction temperature should be lowered at high pressure reactions, as the optimum temperature increases with increase in reaction pressure and vice versa.

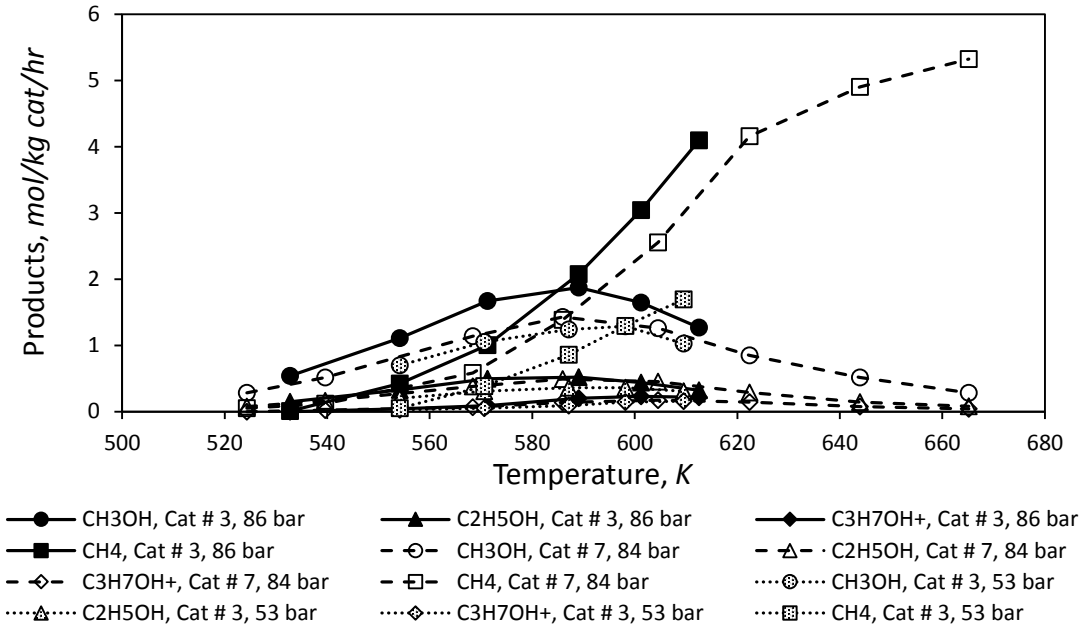

[redacted]

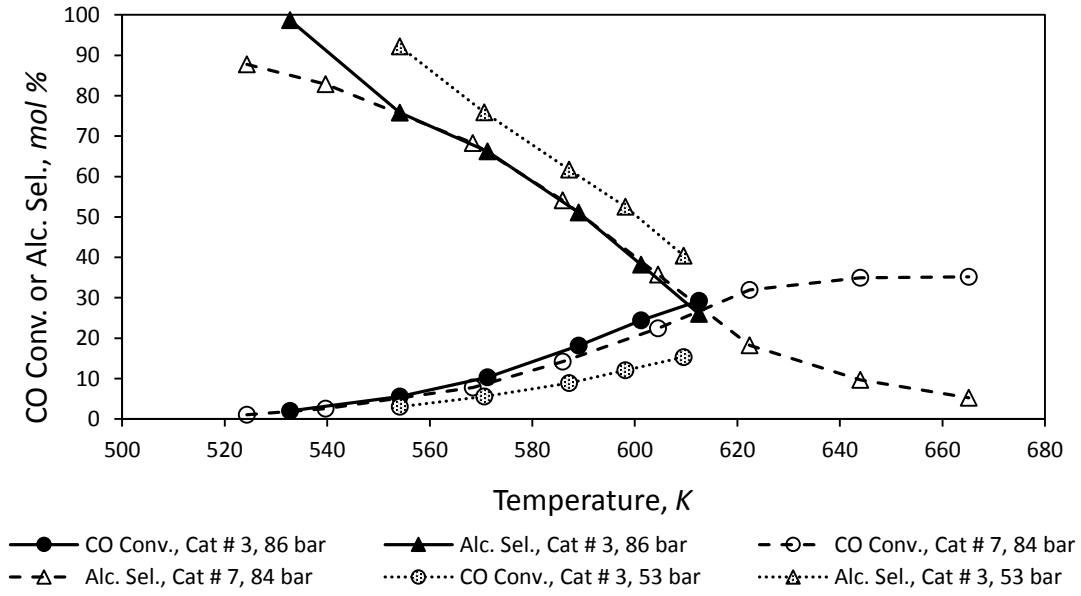

[redacted]

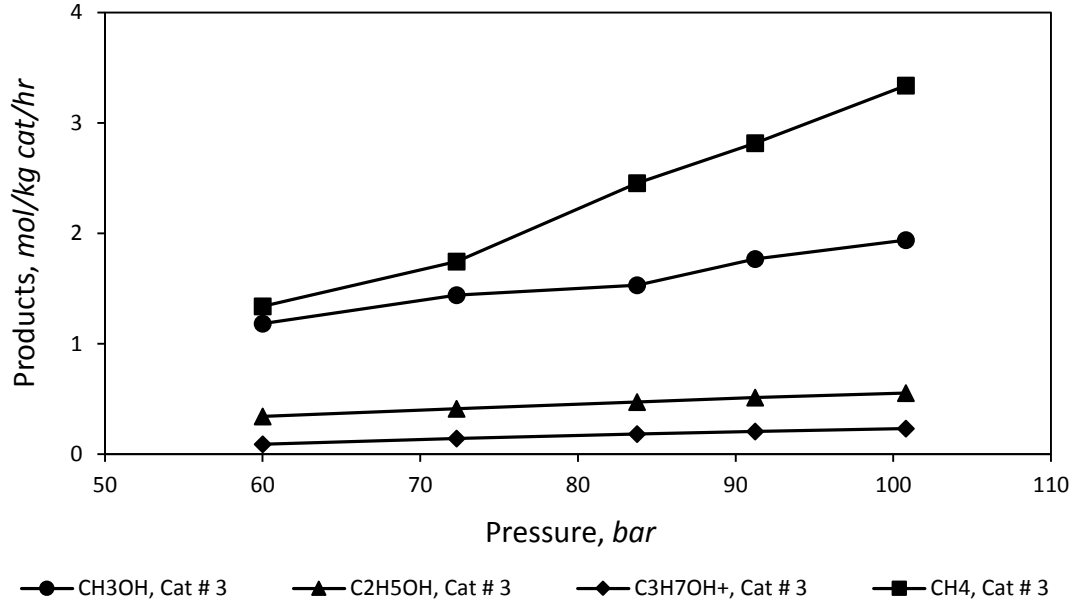

[redacted]

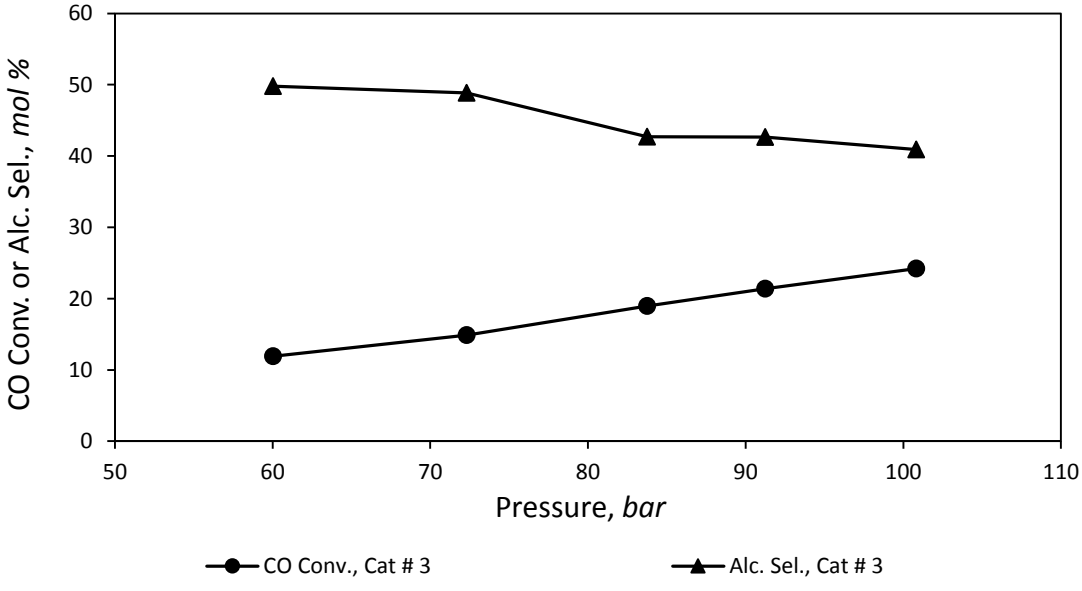

[redacted]

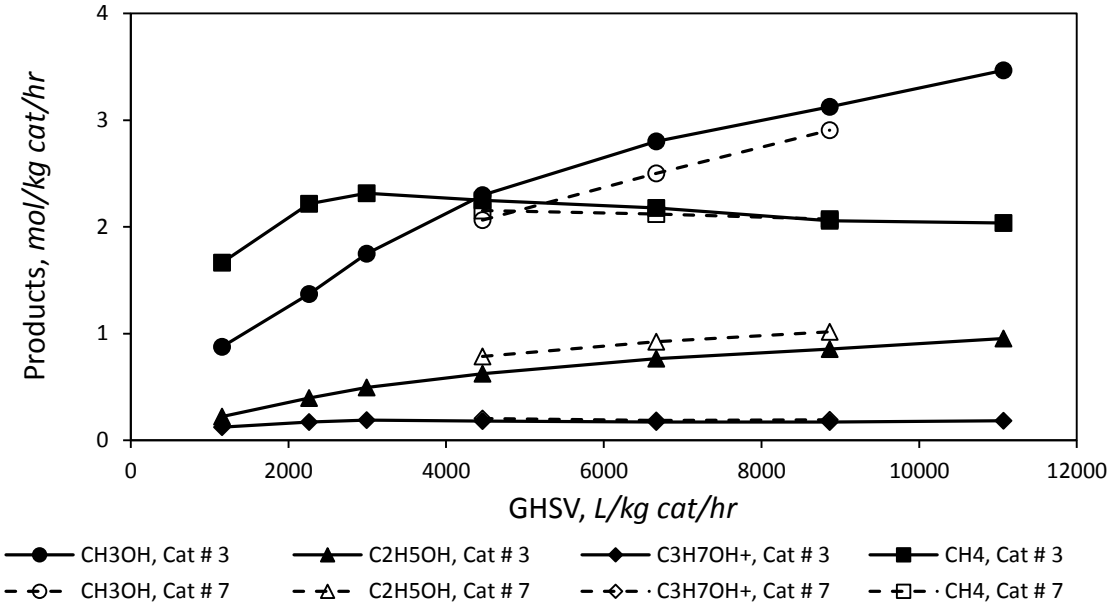

[redacted]

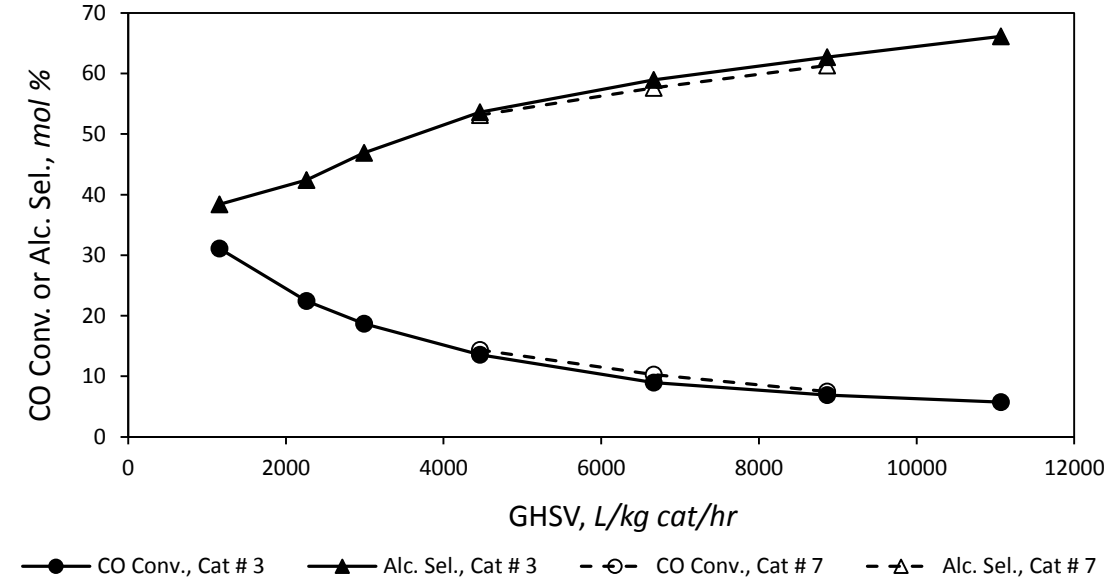

[redacted]

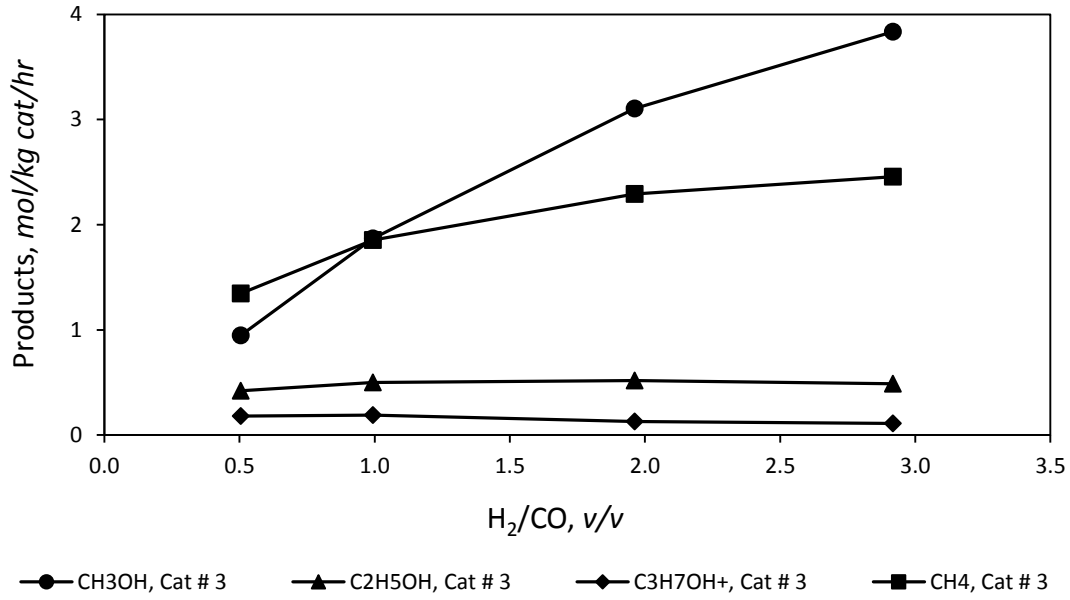

[redacted]

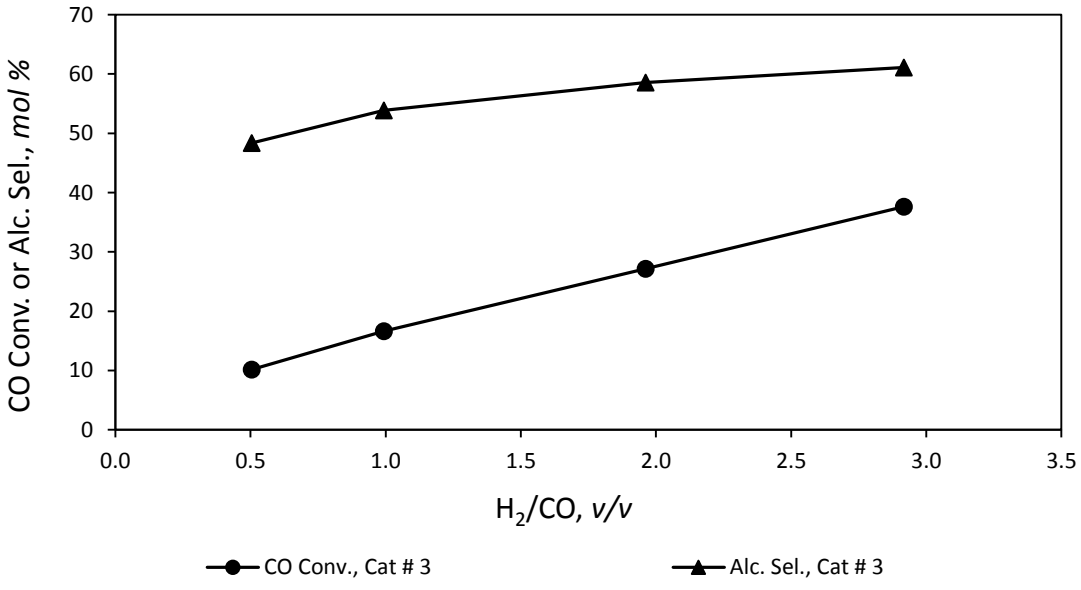

[redacted]

The effect of GHSV on product yields and the corresponding CO conversion and alcohol selectivity are shown respectively in Fig. 2.30 and Fig. 2.31. The alcohol yields increases with increase in GHSV from 1000 to 11000 *L/kg cat/hr*, whereas the methane yield increases with increase in GHSV until 3000 *L/kg cat/hr* and then decreases with further increase in GHSV to 11000 *L/kg cat/hr*. The H_2/CO ratio was varied from 0.5 to 3.0 *v/v* at a constant reaction condition of 589 *°K*, 86 *bar*, and 2990 *L/kg cat/hr* (Fig. 2.32 and Fig. 2.33). The methane and methanol yield increases with increase in H_2/CO ratio, probably due to increase in hydrogen partial pressure and it favors the production of methanol and methane. The higher alcohols, such as ethanol and propanol possesses a maximum value at a certain H_2/CO ratio (H_2/CO ratio of 2 and 1 for ethanol and propanol respectively) and decreases with further increase in H_2/CO ratio, as a consequence the C_2^+ alcohols/methanol ratio decreases with increase in H_2/CO ratio. The C_2^+ alcohols refer to the combined production of ethanol, propanol and butanol. The C_2^+ alcohols/methanol ratio of 1.02 and 0.58 *w/w* was observed at H_2/CO ratio of 0.5 and 1.0 *v/v* respectively.

2.5.3. Stability of the Catalyst

Stability time is the time period under which the present catalyst was tested to verify that the catalyst did not undergo deactivation during HAS operation. The catalyst number 9 was tested for an extended period of 500 *hrs* (Fig. 2.34 and Fig. 2.35). The catalyst exhibited long term stability during this period of continuous operation. The alcohol and hydrocarbon yields were observed to remain stable throughout the entire period of operation. No sulfur products were observed during this period.

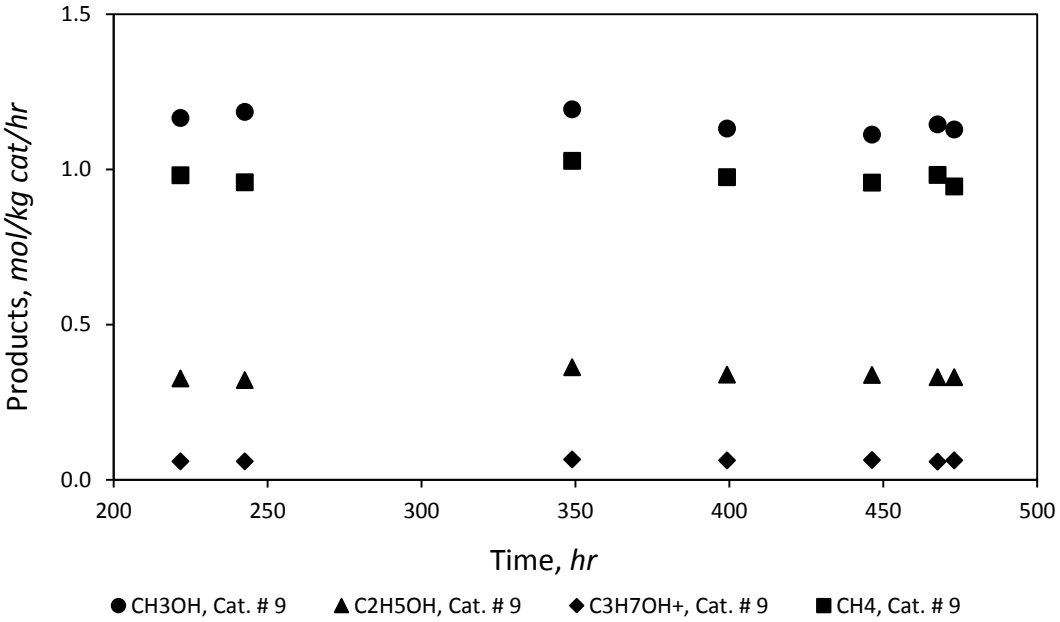

[redacted]

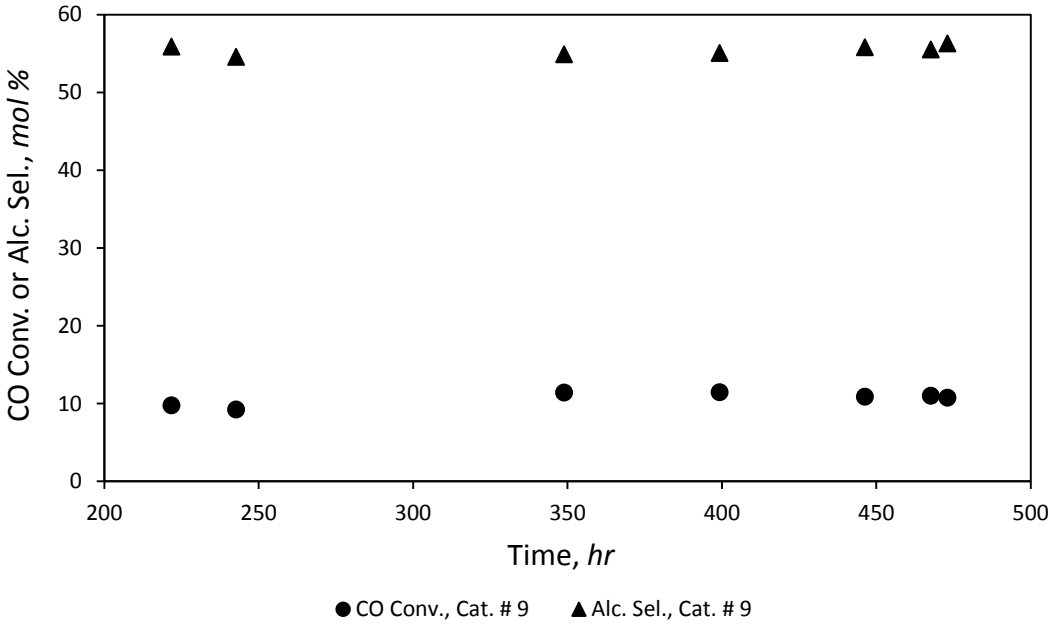

[redacted]

It should be noted that, the catalyst may take up to 200 *hrs* or more to reach steady-state. The results obtained from the testing of catalyst number 3 to demonstrate the effect of temperature, pressure, GHSV and H_2/CO ratio, while the catalyst is still in the transient stage or close to reaching steady-state.

2.5.4. Effect of Cesium Loading

A series of catalysts, catalyst number 1 to number 5, with different CsCOOH loadings were prepared to optimize the Cs/Mo ratio for the alcohol productions. The Cs/Mo molar ratio was varied from 0.03 to 2.72 with a constant Mo loading of 15.5 *wt%* (based on MoO_2/AC after calcination). The detailed catalyst preparation process parameters are presented in Table 2.1. The effects of Cs/Mo ratio on product yields are shown in Fig. 2.36. The corresponding CO conversion and alcohol selectivity are shown in Fig. 2.37. The results obtained between 37 to 62 *hrs* of reaction were used for the comparison. The operating conditions maintained during this period are: 585 – 590 °*K*, 84 – 86 *bar*, 2992.9 *L/kg cat/h*r GHSV, and H_2/CO ratio of 0.993 *v/v*. It should be noted that, the water was not observed in the product from the catalysts with Cs/Mo ratio varying from 0.23 to 2.71 and only traces of water was observed from the catalyst with Cs/Mo ratio of 0.03. All or most of the water formed from higher alcohols and hydrocarbon reactions are converted to CO_2 through water-gas shift reaction. The formation of alcohols goes through a maximum value with increase in Cs/Mo ratio, while the formation methane or more specifically the hydrocarbons were progressively suppressed.

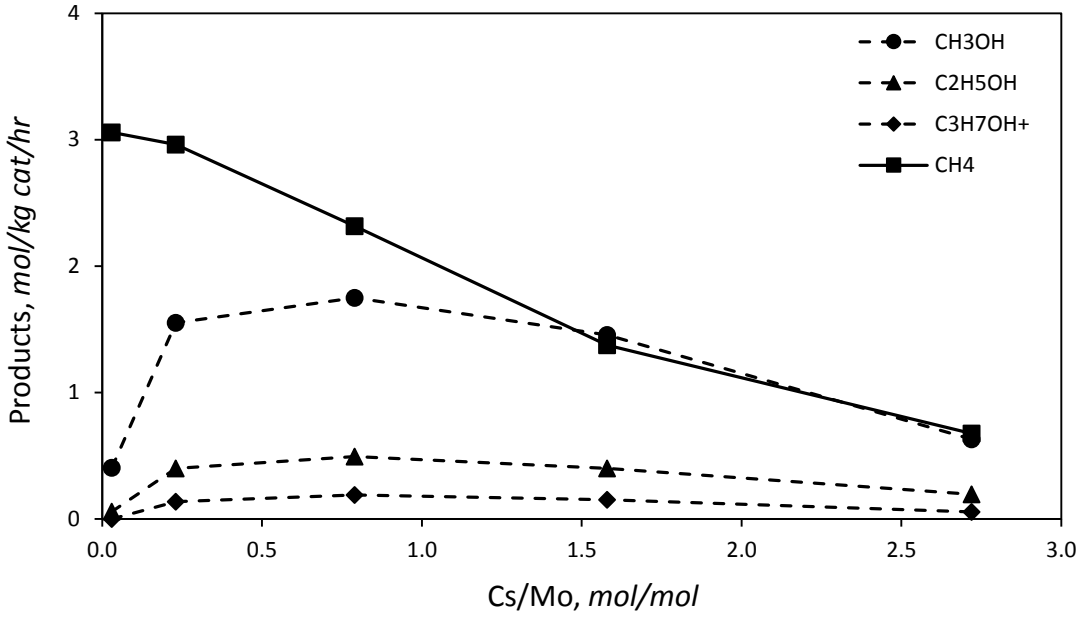

[redacted]

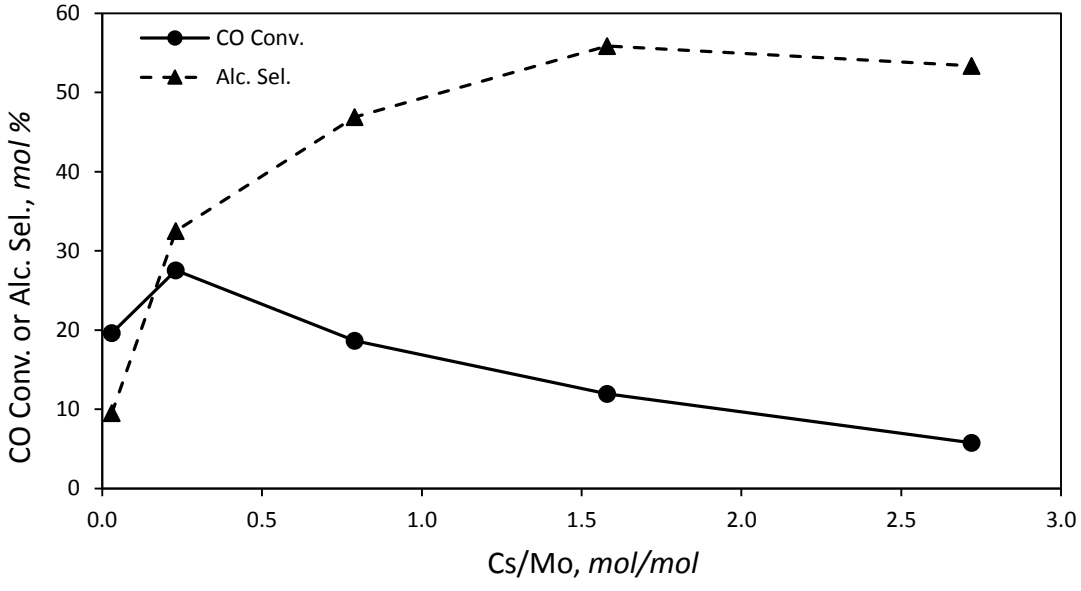

[redacted]

The Cs/Mo ratio for the maximum alcohol production is around **0.79**. A broader range of Cs/Mo ratio from 0.23 to 1.58 can be selected without appreciable loss of alcohol productions. The hydrogen active sites are produced by dissociative adsorption of hydrogen on MoS_2. The MoS_2 itself can activate CO, which leads to production of hydrocarbons. The introduction of Cs like basic component activates CO in such a way that a new reaction pathway for the alcohol production was introduced. The increase in the total product yield is due to the increase of CO active sites introduced by Cs. The balance between hydrogen and CO active components; MoS_2 and Cs^+, are responsible for the maximum activity of the catalyst [2]. The decreases in hydrocarbon yields are due to the decreased availability of active hydrogen in the presence of Cs. Excess Cs doping leads to the blockage of hydrogen active sites and thereby the activity of the catalyst decreased due to the lack of available active hydrogens.

2.5.5. Reproducibility and Scalability of the Catalyst Preparation Process

The catalyst number 6 – 8, number 10 were prepared by using different batch sizes (AMT promotion, calcination, sulfidation and Cs promotion batch size) and promotion rates (AMT and Cs promotion rate). The details of batch sizes for each catalyst preparation stages and promotion rates are given in Table 2.1. The sulfidation temperature of 673.15 *°K* was used for all the catalysts. These catalysts were tested under similar operating conditions of 577 – 601 *°K*, 83 – 94 *bar*, 2992.9 *L/kg cat/hr* GHSV, and H_2/CO ratio of 0.993. All these catalysts give similar results, in terms of alcohol yields (Fig. 2.38).

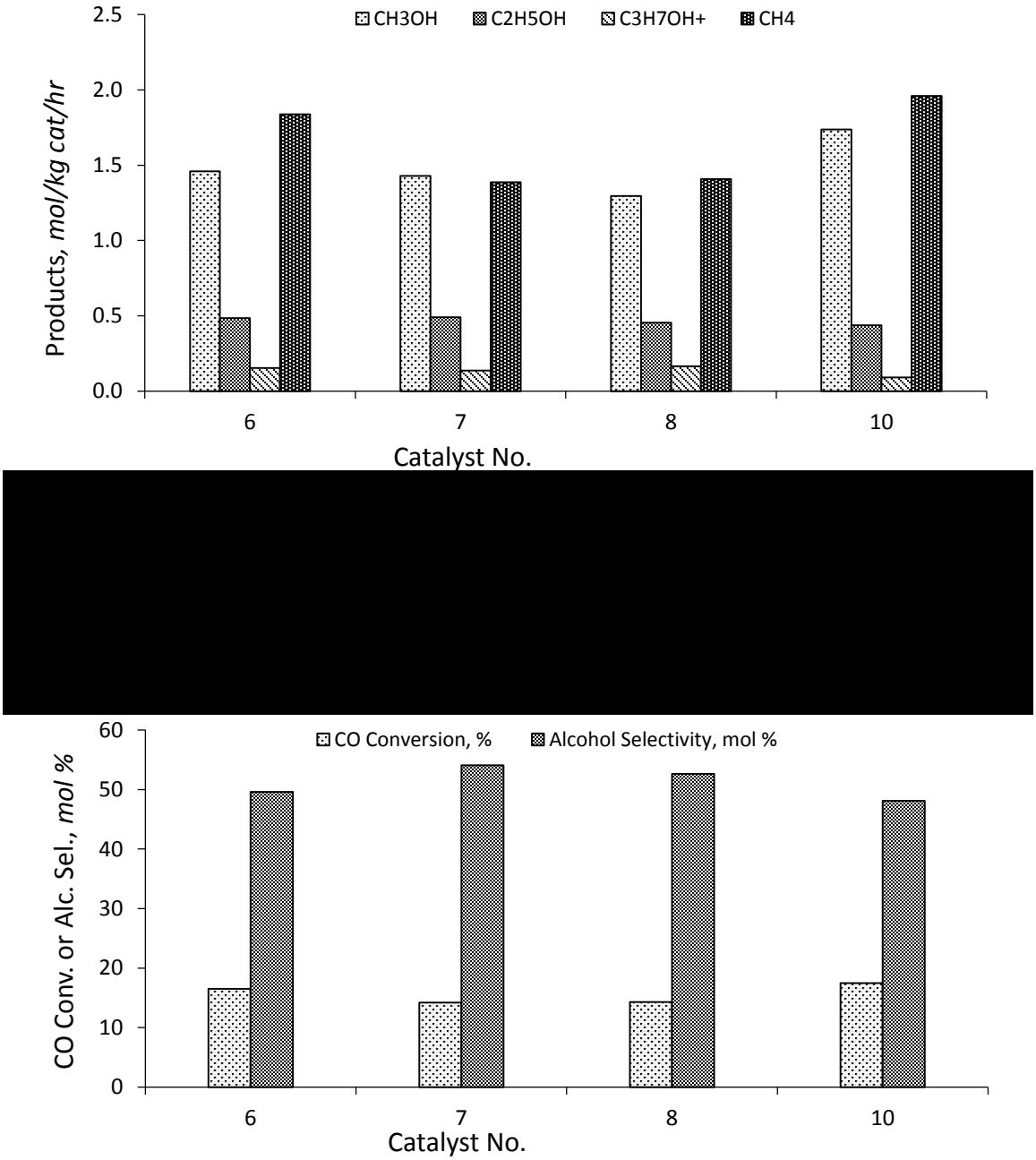

Fig. 2.39. Reproducibility and scalability of the catalyst, CO conversion and alcohol selectivity for cat # 6 to cat # 8, cat # 10. The operating conditions for cat # 6 are: 585 °K, 83 bar, 2992.9 L/kg cat/hr GHSV, H_2/CO = 0.993 v/v, and 88 hr of reaction, the operating conditions for cat # 7 are: 586 °K, 83 bar, 2992.9 L/kg cat/hr GHSV, H_2/CO = 0.993 v/v, and 209 hr of reaction, the operating conditions for cat # 8 are: 601 °K, 90 bar, 2992.9 L/kg cat/hr GHSV, H_2/CO = 0.993 v/v, and 199 hr of reaction, and the operating conditions for cat # 10 are: 577 °K, 94 bar, 2992.9 L/kg cat/hr GHSV, H_2/CO = 0.993 v/v, and 276 hr of reaction.

The results taken from the catalyst number 6 was after 88 *hrs* of reaction, whereas the results taken from catalyst number 7, number 8, and number 10 were at 199, 209, and 296 *hrs* of reaction respectively. We have seen earlier that these catalysts may take up to 200 *hrs* or more reaction time to reach steady state. The higher yield of methane for catalyst number 6 is due to the fact that this catalyst is still undergoing the transient phase. The alcohols reach steady-state, whereas the methane is still decreasing and it will stabilize to a lower value. The catalyst number 10 was operating relatively at a higher pressure of 94 *bar* and a lower temperature of 577 °*K*. Higher pressure reaction can increase the production of alcohols and hydrocarbons.

Irrespective of batch sizes, we can able to prepare these catalysts, which can give similar results under similar operating conditions. The AMT and Cs promotion rates can be adjusted based on the batch size used. A calcination temperature of 773.15 °*K* is sufficient to decompose AMT on AC support and produce crystalline MoO_2. The sulfidation time should be determined by disappearance of water at the exit of the sulfidation reactor and the exit H_2S concentration should equal the inlet H_2S concentration.

2.5.6. Comparison with the Results Reported in the Literature

A comparison of the results obtained from the testing of catalyst number 7 with MoS_2 based catalysts reported recently in the literature is provided in Table 2.3. The present catalyst composition exhibits improved catalyst performance over those observed in the literature.

Catalysts	Composition, *wt %* (Mo/Co/Alkali)	Reaction time, *hr*	Pressure, *bar*	Temp., °K	GHSV, hr^{-1}	H_2/CO, *v/v*	CO Conversion, *%*	Alcohol Selectivity, *mol %*	Total Alcohols[$], *g/kg metals*/hr*	C_2^+/Methanol, *w/w*
Catalyst # 7 (present work)	10.51/0/10.15	87.6	97.5	587.2	3345.9	0.99	14.36	53.12	576.62	0.74
		93.8	97.8	587.8	4997.9	0.99	10.31	57.64	672.05	0.67
		116.3	98.0	588.4	6649.9	0.99	7.47	61.35	760.36	0.63
		110.5	97.5	587.7	3336.0	1.96	22.12	57.48	712.84	0.40
		134.7	97.7	588.5	4982.9	1.96	17.62	62.34	845.31	0.39
		139.9	98.2	588.8	6629.9	1.96	11.94	65.11	942.20	0.39
Mo/K/CNT (catalyst A, [14])	15/0/9	n.a.	96.5	593.0	3600.0[#]	2.00	32.90	28.00	458.33	0.93
K_2CO_3/CoS/MoS_2 (catalyst B, [3, 40])	30.81/9.46/5.66	n.a.	165.5	603.2	4032.0	1.10	11.68**	67.76	696.71	0.55
KCoMo (catalyst C1, [41])	13.6/2.71/9.0	24.0	100.0	623.2	4263.4	1.00	18.00	65.00[##]	1090.48	0.90
		27.5	100.0	598.2	4352.0	1.00	8.00	79.00[##]	766.50	0.65
KCoMo (catalyst C2, [41])	4.23/2.30/9.3	30.0	100.0	600.2	4265.9	1.00	3.00	90.00[##]	536.96	0.57

[$] calculated based on catalyst composition

* "kg metal" is the total weight of elemental Mo, alkali (Cs or K) and/or Co present in the catalyst.

CNT = Multiwalled Carbon Nanotubes

[#] L/kg cat/hr

** exclusive CO_2

[##] C based selectivity

Table 2.3. Catalyst performance compared with the recent carbon supported molybdenum sulfide based catalysts reported in the literature.

Although catalyst A is reported to exhibit high CO conversion, it possesses a low value of alcohol production, indicating undesirable formation of high amounts of hydrocarbons. Cobalt containing catalysts B, C1, and C2 have been reported to lose sulfur very quickly. The loss of sulfur adversely affects performance. For example, it has been reported that the production of total alcohols and C_2^+ alcohols to methanol ratio of catalyst C1 decreases respectively from initial 1090.48 *g/kg metals/hr* and 0.9 *w/w* to 766.50 *g/kg metals/hr* and 0.65 *w/w* with increase in time on syngas stream from 24 *hr* to 27.5 *hr* [41]. Such catalysts typically require continuous replenishment of sulfur to maintain performance levels. This is generally accomplished by sustaining continuous sulfidation through addition of hydrogen sulfide in the syngas feedstock to make-up for the sulfur loss [37]. Unlike Catalysts B and C, the present catalyst maintains its activity for more than 500 *hrs* without the addition of hydrogen sulfide.

Catalyst B has also been observed to produce over 5 *wt%* water [3], while the present catalyst composition produces little or no water as a by-product. Production of water increases the energy consumption of the process as it necessitates energy intensive alcohols-water separation.

2.5.7. Bench-scale Catalyst Testing

A 100 *g* of Cs/MoS_2/AC catalyst was tested in a scaled-up catalyst testing unit. The unit was constructed with a 0.834" ID × 42" long stainless steel tube reactor heated by series of band heaters controlled by multiple temperature controllers. The description of the unit and the testing results are provided in the US patent US8815963 B1.

2.5.8. Effect of Feed and Recycle Impurities

The objective of this study is to examine the effect of alcohols, CO_2, and methane in the syngas feed, that might be present in the recycle or syngas feed stream to the alcohol reactor. Methanol and Ethanol were injected into the syngas feed at different flow rates and its effect on other alcohols, and hydrocarbons were studied.

2.5.8.1. External Injections of Methanol and Ethanol with Syngas

Methanol was injected into the reactor, along with H_2 and CO at higher alcohol reaction conditions. The effect of methanol injections at different flow rates on ethanol, propanol, butanol, methane, ethane, and water are shown in Fig. 2.40 and Fig. 2.41. The increase in methanol injections significantly increases the methane yields. Traces of water were also observed at higher methanol injection rates. The additional methane yield and traces of water by methanol injections were contributed by methanol decomposition,

$$CH_3OH + H_2 \rightarrow CH_4 + H_2O \tag{2.9}$$

Since this catalyst is an excellent water-gas shift catalyst, most of the water formed is converted to carbon dioxide.

$$H_2O + CO \rightarrow CO_2 + H_2 \tag{2.10}$$

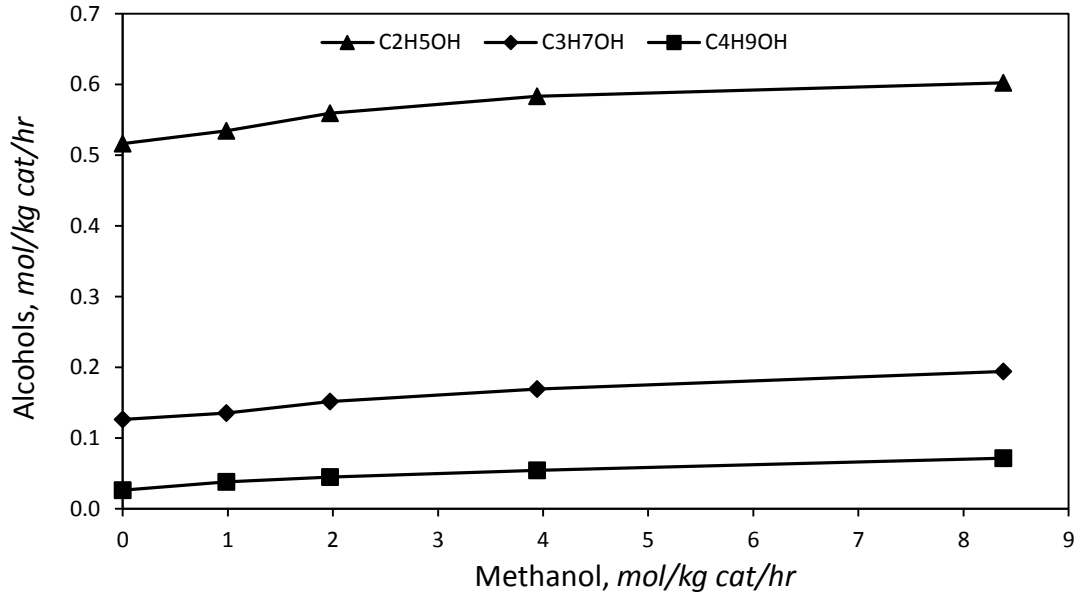

[redacted]

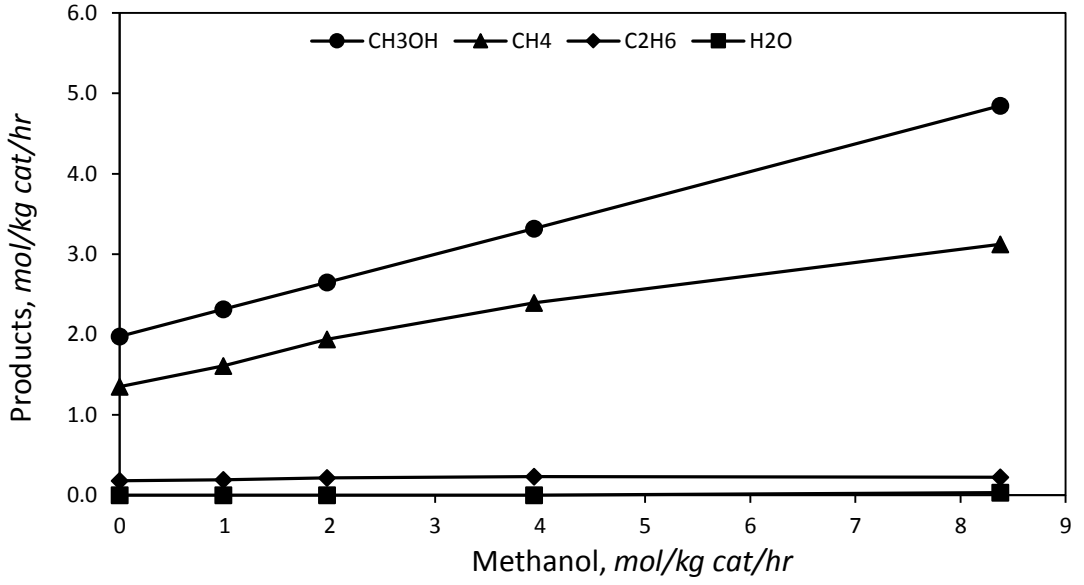

[redacted]

Increase in methanol in the syngas feed is also increases the yield of ethanol, propanol, and butanol. The higher alcohols are formed by addition of CO from syngas to the immediate lower alcohols, e.g. Ethanol is formed from methanol by CO addition from syngas, and so on.

$$CH_3OH + CO + 2H_2 \rightarrow C_2H_5OH + H_2O \quad (2.11)$$

$$C_2H_5OH + CO + 2H_2 \rightarrow C_3H_7OH + H_2O \quad (2.12)$$

$$C_3H_7OH + CO + 2H_2 \rightarrow C_4H_9OH + H_2O \quad (2.13)$$

Similar to methanol injection experiments, the effect of ethanol injections into the syngas on different products was studied. The effect of ethanol injections on methanol, propanol, butanol, methane, ethane, and water are shown in Fig. 2.42 and Fig. 2.43. Ethane is most significantly affected by the ethanol injections. Similar to methane formation from methanol, additional ethane is coming from the decomposition of ethanol,

$$C_2H_5OH + H_2 \rightarrow C_2H_6 + H_2O \quad (2.14)$$

As we have seen in the methanol injection experiments, higher alcohols in the product are also increases with increase in ethanol injections. With higher alcohol productions from CO addition to the corresponding lower alcohols, eq. 2.12 and 2.13, we should expect a gradual decrease in the higher alcohol production rates with increase in carbon number, e.g. increase in the rate of production of butanol should be lower than the rate of propanol production with increase in ethanol in the feed. Contradicting to this phenomenon, Fig. 42 shows that the increase in rate of production of butanol is higher than that of propanol and it approaches the propanol yield at higher ethanol injection rates.

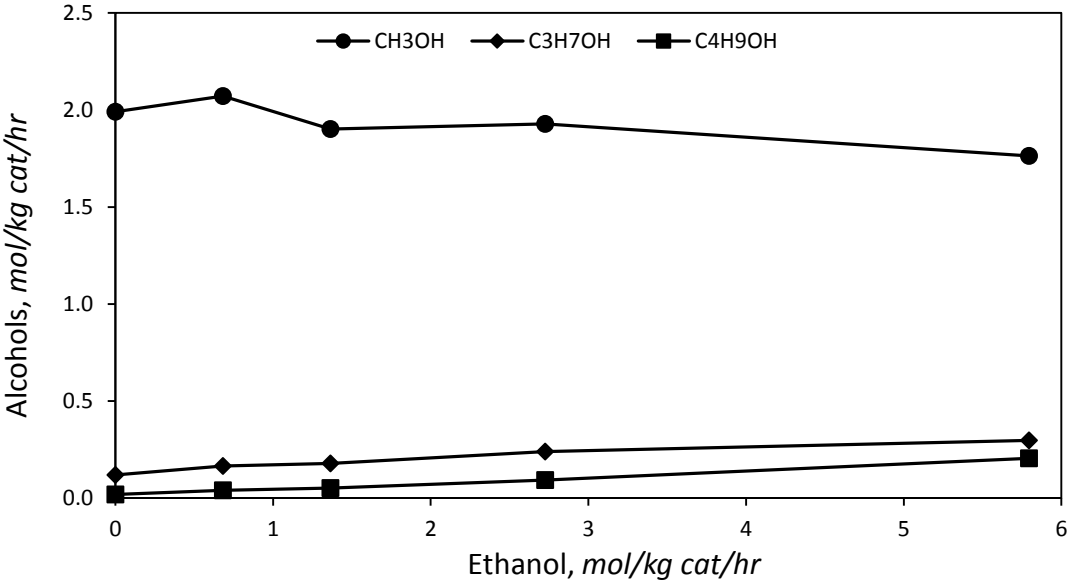

[redacted]

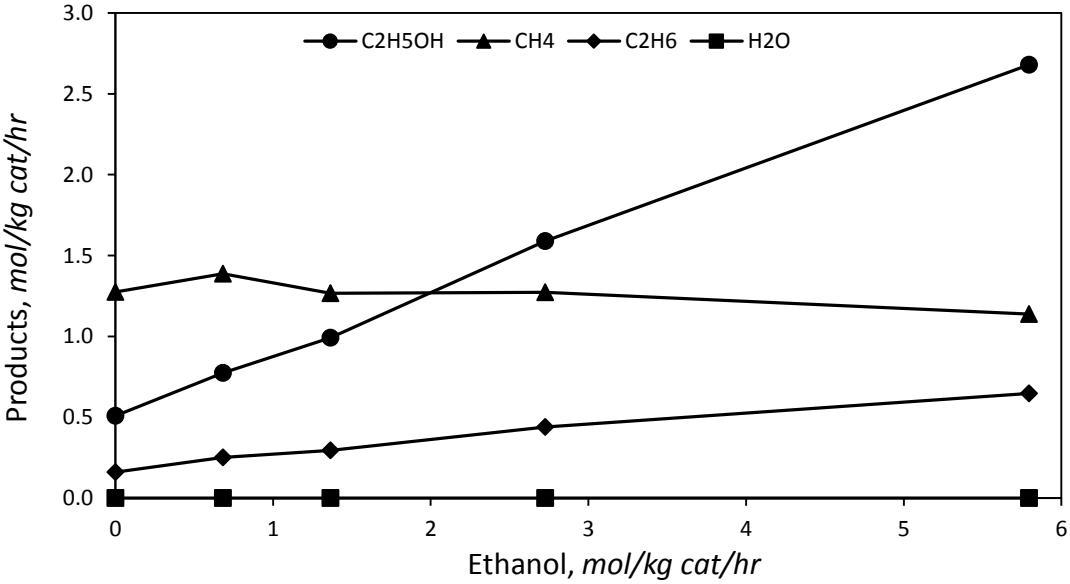

[redacted]

The enhanced butanol yield could be due to the coupling of ethanol or ethanol derived species into butanol [15].

$$2C_2H_5OH \rightarrow C_4H_9OH + H_2O \quad (2.15)$$

Water was not observed in any of these ethanol injection experiments, confirming the excellent water-gas shift properties of the catalyst.

Production of methanol and methane decreases with increase in ethanol injection rate in the syngas feed. The decrease in methanol and methane is probably due to the increased rate of productions of higher carbon number products, which consumes CO and H_2, which could otherwise be used by methanol and methane formation reactions.

2.5.8.2. Decomposition of Methanol and Ethanol in the Absence of Syngas

In order to check the reversible nature of the higher alcohol reactions, methanol and ethanol were injected into the reactor along with helium instead of syngas at higher alcohol synthesis operating conditions. Methanol and ethanol decomposition product distributions are shown in Fig. 2.44 and Fig. 2.45 respectively. The only products from methanol decomposition are CO, H_2, CH_4 and CO_2. Methanol can decompose into methane and water even without the presence of syngas as shown by eq. 2.9. The hydrogen required for methanol decomposition to methane is probably coming from the decomposition of methanol to CO and H_2.

$$CH_3OH \rightarrow CO + 2H_2 \quad (2.16)$$

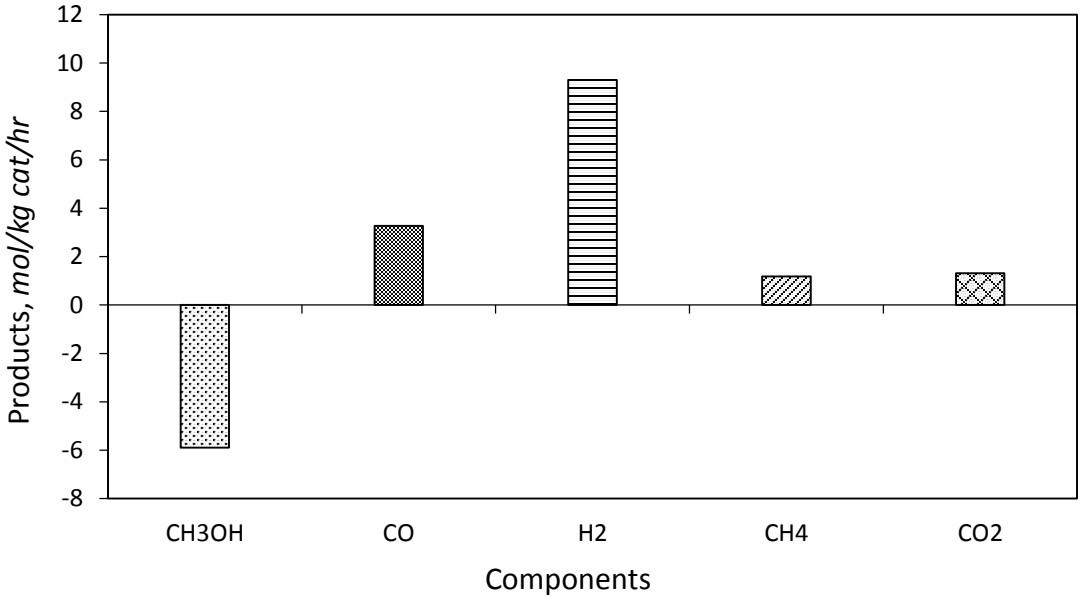

[redacted]

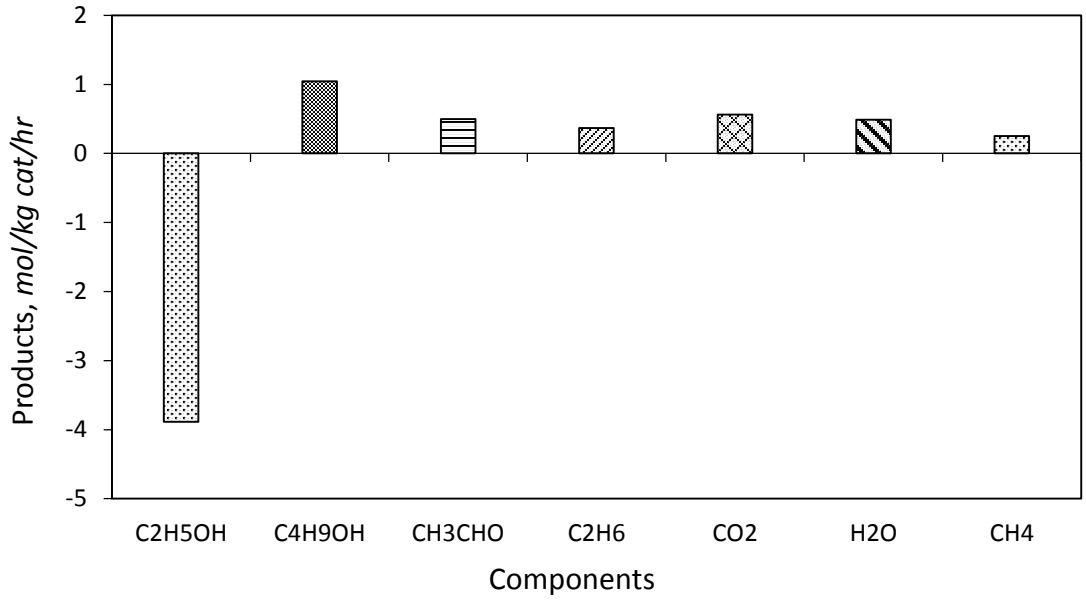

[redacted]

Methane, CO, H_2, and CO_2 formations from decomposition of methanol by eq. 2.9, 2.10, and 2.16 are stoichiometrically consistent with the product distributions shown in Fig. 2.44. Higher alcohols and higher hydrocarbons were not observed in the product.

The major products from decomposition of ethanol in helium at higher alcohol synthesis reactions are butanol, acetaldehyde, ethane, carbon dioxide, and water. A trace of methane is also observed. Butanol and ethane are formed by ethanol coupling (equation 2.15) and decomposition (equation 2.14) reaction respectively. Acetaldehyde might have been formed by dehydrogenation of ethanol,

$$C_2H_5OH \rightarrow CH_3CHO + H_2 \tag{2.17}$$

Formations of higher alcohol from corresponding lower alcohol by CO insertion mechanism are forward reactions (equation 2.11-13). The acetaldehyde formed by ethanol decomposition might be one of the stable intermediate which is otherwise be reacted with CO and formed propanol. The presence of acetaldehyde is due to the lack of CO partial pressure present during ethanol decomposition in helium. Due to the similarities of these reactions, we can generalize the formation of higher alcohols through the aldehyde intermediates, e.g. formaldehyde, acetaldehyde, propionaldehyde, and butanaldehyde are one of the intermediates involved during formation of alcohols.

$$CO \overset{+H_2}{\longleftrightarrow} CH_2O \overset{+H_2}{\longleftrightarrow} CH_3OH \tag{2.18}$$

$$CH_3OH \overset{-H_2}{\longleftrightarrow} CH_2O \xrightarrow{+CO,+2H_2} CH_3CHO \overset{+H_2}{\longleftrightarrow} C_2H_5OH \tag{2.11}$$

$$C_2H_5OH \overset{-H_2}{\longleftrightarrow} CH_3CHO \xrightarrow{+CO,+2H_2} C_2H_5CHO \overset{+H_2}{\longleftrightarrow} C_3H_7OH \tag{2.12}$$

$$C_3H_7OH \overset{-H_2}{\longleftrightarrow} C_2H_5CHO \xrightarrow{+CO,+2H_2} C_3H_7CHO \overset{+H_2}{\longleftrightarrow} C_4H_9OH \tag{2.13}$$

However, aldehydes are not the stable products during alcohol synthesis reactions.

Traces of methane observed is formed by decomposition of acetaldehyde,

$$CH_3CHO \rightarrow CH_4 + CO \qquad (2.19)$$

The CO formed by decomposition of acetaldehyde, equation 2.19 is reacted with the water formed from equation 2.14 and 2.15 and form CO_2 and H_2 by shift reaction shown by equation 2.10 and the reaction is not complete probably due to the lack of CO partial pressure. The stoichiometry of these reactions may not be consistent with the amount of products calculated from the mass balance due to the uncertainties involved with thermal response factors (TRFs) used for such low concentrations. The TRF for acetaldehyde is directly taken from the literature.

Effect of ethanol feed rate on butanol, acetaldehyde, ethane, CO_2, and water is shown in Fig. 2.46. Production of butanol, and acetaldehyde are increases linearly, whereas increase in rate of production of water is higher than that of butanol and acetaldehyde, with increase in ethanol feed rate. Decrease in production rate of CO_2 and ethane was observed with increase in ethanol feed rate. Different rates of reactions 2.10, 2.14, 2.15, 2.17, and 2.19 controls the final product distributions. Production of butanol and acetaldehyde are dependent only on ethanol partial pressure, whereas production of CO_2 and ethane are affected by CO and H_2 partial pressure. Production of water is dependent on ethanol, CO, and H_2 partial pressure. Complete conversion of water to CO_2 is hindered by lack of CO partial pressure; otherwise it would have been converted completely to CO_2.

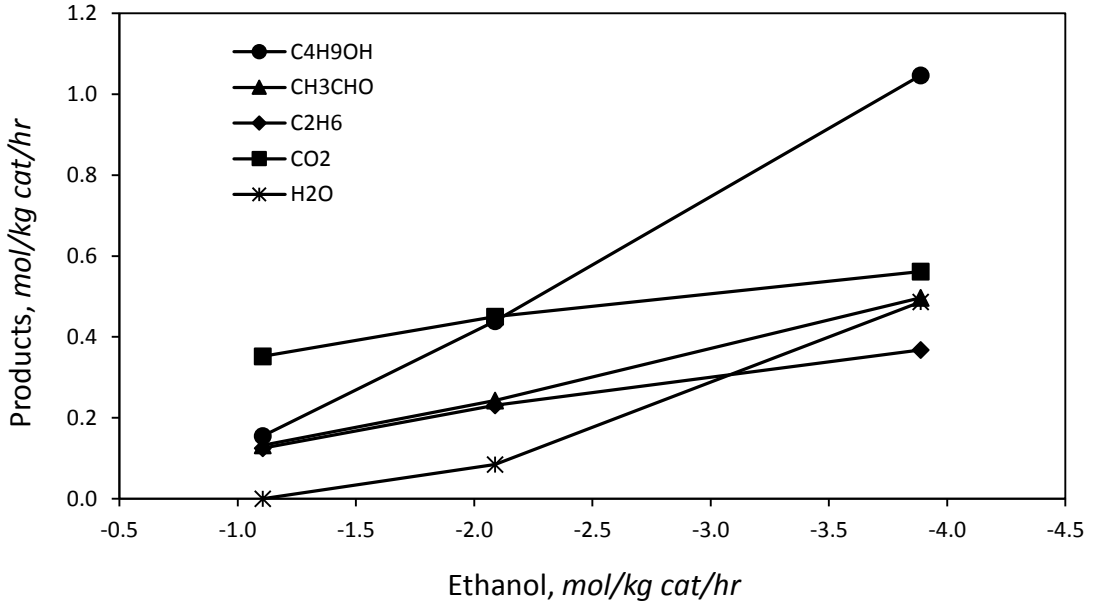

[redacted]

Effect of CO_2 and methane in the syngas feed were also studied. The results were presented in Table 2H (3) of Appendix 2H. Concentration of CO_2 was increased up to 12.5 *vol %* in the syngas. Water was not detected till CO_2 concentration increased to 7.98 *vol %*, further increase in CO_2 to 12.52 *vol %* produces small amount of water. It confirms the reversible nature of water gas shift reaction at higher CO_2 concentrations.

$$CO_2 + H_2 \rightarrow H_2O + CO \qquad (2.20)$$

Presence of methane in the syngas feed only increases additional methane in the product. Decrease in alcohol productions are due to the decrease in H_2 and CO partial pressure caused by the presence of CO_2 or CH_4. Catalyst regains its original activity once the presence of methanol, ethanol, CO_2, or CH_4 are removed from the syngas feed.

2.5.8.3. Reaction Pathways

Higher alcohol synthesis reactions over alkali promoted MoS_2 based catalysts can be summarized into four groups,

- *Series reactions*: Higher alcohols and hydrocarbons synthesized from syngas with alcohols [42].

$$C_nH_{2n+1}OH + (i-n)CO + 2(i-n)H_2 \rightarrow C_iH_{2i+1}OH + (i-n)H_2O$$

$$n = 1, 2, \ldots., \qquad i = n+1, n+2, \ldots., \qquad n_1 \tag{2.21}$$

$$C_nH_{2n+1}OH + (i-n)CO + [2(i-n)+1]H_2 \rightarrow C_iH_{2i+2} + (i-n+1)H_2O$$

$$n = 1, 2, \ldots., \qquad i = n, n+1, \ldots., \qquad n_2 \tag{2.22}$$

- *Parallel reactions*: Formation of alcohols and hydrocarbons directly from syngas [42], and

$$iCO + 2iH_2 \rightarrow C_iH_{2i+1}OH + (i-1)H_2O; \quad i = 1, 2, 3, \ldots., \qquad n_1 \tag{2.23}$$

$$iCO + (2i+1)H_2 \rightarrow C_iH_{2i+2} + iH_2O; \qquad i = 1, 2, 3, \ldots., \qquad n_2 \tag{2.24}$$

- *Ethanol coupling*: Formation of butanol by ethanol coupling reaction,

$$2C_2H_5OH \rightarrow C_4H_9OH + H_2O \tag{2.15}$$

- *Water*-gas-shift reaction: Formation of CO_2 from water formed during higher alcohol and hydrocarbon reactions.

$$H_2O + CO \leftrightarrow CO_2 + H_2 \quad (2.25)$$

Total number of reactions can be calculated by,

$$j = n_1 + n_2 + \frac{n_1(n_1 - 1)}{2} + \frac{n_2(n_2 + 1)}{2} \quad (2.26)$$

Alcohols and hydrocarbons above butanol and propane respectively are negligible in the product. The total number of reactions involved for number of alcohol products, $n_1 = 4$ (methanol, ethanol, propanol, and butanol), and number of hydrocarbon products, $n_2 = 4$ (methane, ethane, propane, and butane) is calculated to be 26 (16 series, 8 parallel, 1 ethanol coupling, and 1 water-gas-shift reaction). The series, coupling, and parallel reactions are not independent reactions. The minimum number of independent reactions required to describe the reaction network is equal to the number of parallel reactions and water-gas-shift reaction 2.25, i.e., 9 for $n_1 = n_2 = 4$. The selection of independent reactions can be any combinations of series and parallel reactions which involves one reaction per product. For example the combination of reactions 2.18, 2.11 – 13, 2.9, 2.14, 2.25, 2.27, and 2.28 as given by,

$$C_3H_7OH + H_2 \rightarrow C_3H_8 + H_2O \quad (2.27)$$

$$C_4H_9OH + H_2 \rightarrow C_4H_{10} + H_2O \quad (2.28)$$

Combining equations 2.9 – 2.28, overall reaction network and reaction pathways can be drawn as shown in Fig. 2.47 and Fig. 2.48 respectively.

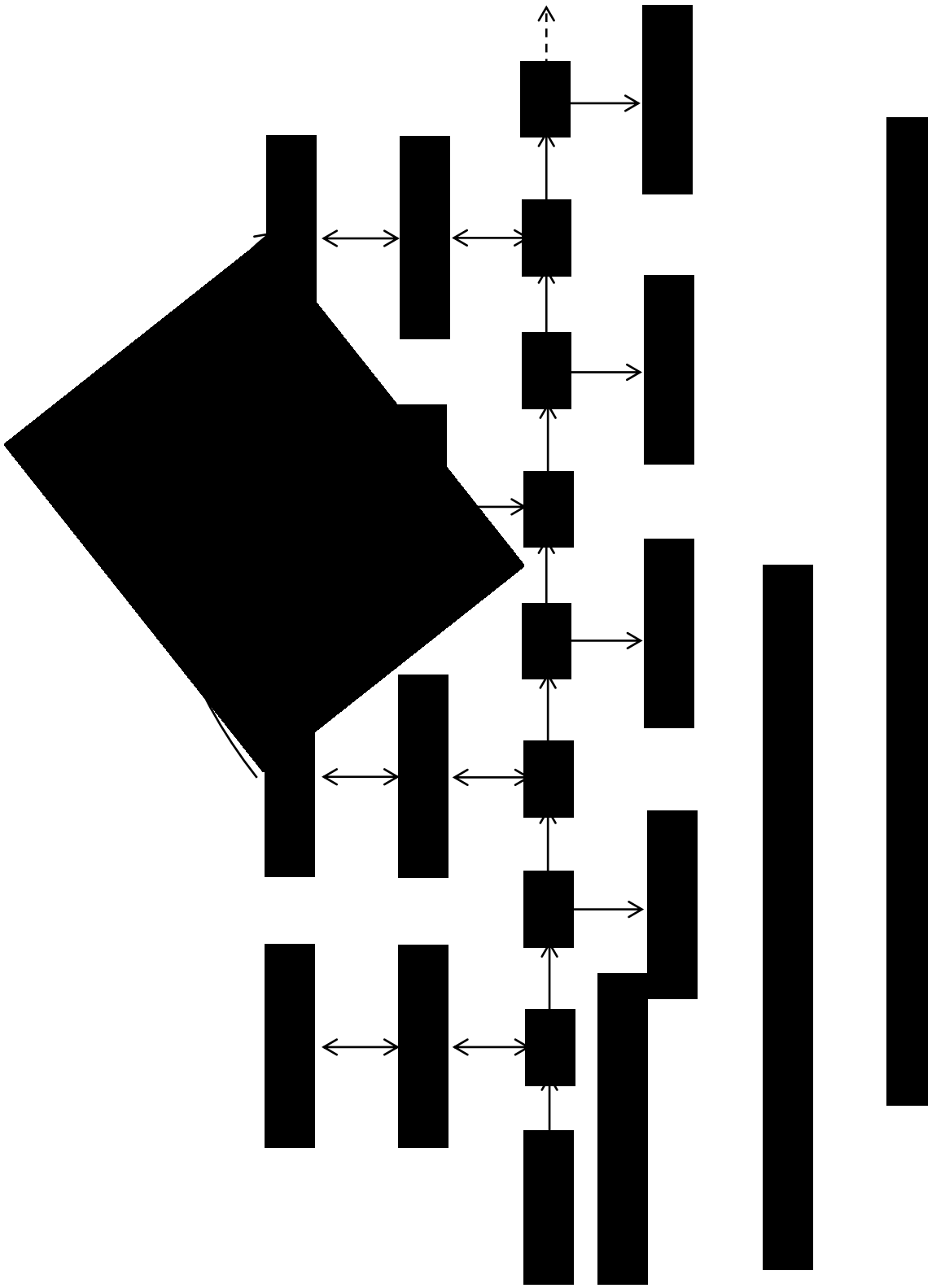

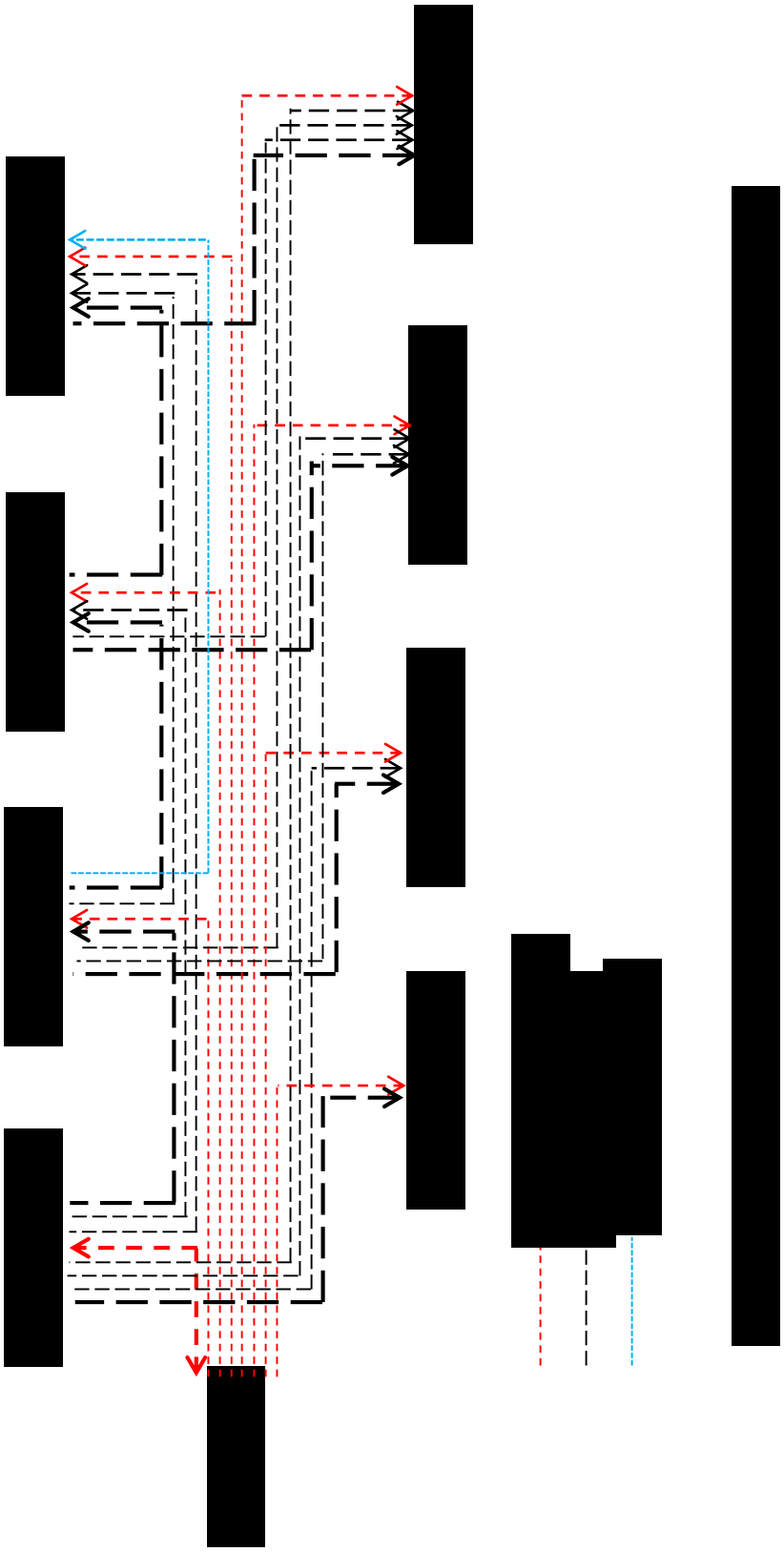

The A's and H's are surface species for alcohol and hydrocarbon formation reactions respectively. The reaction pathways shown by long dashed (black), short dashed (red), and dotted (blue) lines are respectively representing series, parallel, and ethanol coupling reactions. Bold lines are one of the possible combinations of independent reactions describing the reaction network. The ethanol coupling reaction is represented by a dotted line (blue). The rate of water-gas-shift reaction is dependent on the amount of water formed by higher alcohol and hydrocarbon reactions.

2.6. Conclusions

The cesium promoted molybdenum based supported catalysts were prepared and tested for higher alcohol synthesis. The catalyst composition and alcohol synthesis reaction conditions were optimized for alcohol yields, alcohol selectivity, and CO conversion. The catalyst maintains its activity for more than 500 *hrs* at higher alcohol synthesis conditions. The loss of sulfur and production of water was not observed during this period. The XRD and XPS analyses were performed after each stage of catalyst preparation and testing process to determine the bulk and surface characteristics of the catalyst. The external injections of methanol and ethanol experiments were conducted to study its effect on catalyst performance. Additional, methanol and ethanol decomposition experiments were performed to understand the reaction mechanism involved during higher alcohol synthesis.

2.7. Acknowledgement

The financial support from AMCS Corporation is gratefully acknowledged.

2.8. Appendix

Appendix 2A: Example Catalyst Composition Calculation

Mass balance of catalyst preparation process for catalyst number 7

Step: AMT Impregnation

Clean AC pellets used (AC) = 15.0 *g*

AMT used = 6.06 *g*

Vacuum dried AMT promoted AC pellets (AMT/AC) = 19.56 *g*

Step: Calcination

AMT promoted AC pellets used (AMT/AC) = 9.02 *g*

Calcined pellets (MoO_2/AC) = 8.21 *g*

Calculation of Mo content of the calcined pellets

C in MoO_2/AC calcined pellets = 15/19.56×9.02 = 6.9172 *g*

MoO_2 in MoO_2/AC calcined pellets = 8.21 – 6.917 = 1.293 *g*

Mo in MoO_2/AC calcined pellets = 1.293/127.939×95.94 = 0.9695 *g*

Composition of Mo in MoO_2/AC calcined pellets = 0.9695/8.21×100 = **11.81** ***wt%***

Composition of C in MoO_2/AC calcined pellets = 6.9172/8.21×100 = 84.25 *wt%*

Composition of O in MoO_2/AC calcined pellets = (8.21 – 6.9172 – 0.9695)/8.21×100 = 3.94 *wt%*

Step: Sulfidation

MoO_2/AC calcined pellets used = 8.02 *g*

Sulfidized pellets (MoS_2/AC) = 8.20 *g*

C in sulfidized pellets = 6.9172/8.21×8.02 = 6.7571 *g*

Moles of Mo in sulfidized pellets = 0.9695/95.94 = 0.009871

Moles of MoS_2 in sulfidized pellets = (8.20 – 8.02)/(160.07 –127.939) = 0.005602

Moles of MoO_2 in sulfidized pellets = moles of Mo – moles of MoS_2 = 0.004269

Composition of C in sulfidized pellets = 6.7571/8.20×100 = 82.40 *wt%*

Composition of Mo in sulfidized pellets = (0.009871×95.94)/8.20×100 = 11.55 *wt%*

Composition of S in sulfidized pellets = (moles of MoS_2×2×32.065)/8.20×100 = 4.38 *wt%*

Composition of O in sulfidized pellets = 100 – 82.40 – 11.55 – 4.38 = 1.67 *wt%*

Calculated sulfur to molybdenum ratio, S/Mo = (4.38/32.065)/(11.55/95.94) = **1.135**

Step: CsCOOH Impregnation

Sulfidized pellets used = 8.01 *g*

CsCOOH (98%) used = 1.25 *g*

Final weight of the catalyst = 9.24 *g*

Amount of Cs in the final catalyst = 1.25×0.98/177.9229×132.905 = 0.9151 *g*

Amount of formate (-COOH) = 1.25×0.98 – 0.9151 = 0.3099 *g*

Amount of Mo in the final catalyst = 8.01×11.55/100 = 0.9251 *g*

Amount of S in the final catalyst = 8.01×4.38/100 = 0.3509 *g*

Amount of C in the final catalyst = 8.01×82.40/100 + 0.3099/45.017×12.011= 6.6832 *g*

Amount of O in the final catalyst = 8.01×1.67/100 + 0.3099/45.017×2×15.999 = 0.3538 *g*

Amount of H in the final catalyst = 0.3099/45.017×1.008 = 0.00694 *g*

Calculated total weight of the catalyst = 9.235 *g*

Calculated cesium to molybdenum ratio, Cs/Mo = (0.9151/132.905)/(0.9251/95.94) = **0.71**

Final Catalyst Composition

Composition of catalyst number 12 calculated from mass balance is given in Table 2A.

Elements	**C**	**Mo**	**S**	**O**	**Cs**	**H**	**S/Mo**	**Cs/Mo**
Catalyct # 7	72.37	10.02	3.80	3.83	9.91	0.08	1.135	0.714

Table 2A. Elemental composition of catalyst number 12 calculated from mass balance.

Appendix 2B: Catalyst Preparation and Testing Apparatus, and the Final Catalyst

2B.1. Rotovap (Buchi Corp., Model RE 111) for AMT, CsCOOH, $MoO_2(acac)_2$, and cobalt acetate tetrahydrate promotion.

It is equipped with a syringe pump to control the promotion rate.

Fig. 2B (1). Rotovap for AMT/CsCOOH promotion.

2B.2. Calcination and Sulfidation Reactor.

Sanitary fittings were used at both ends of the reactor for easy handling of sulfidized pellets.

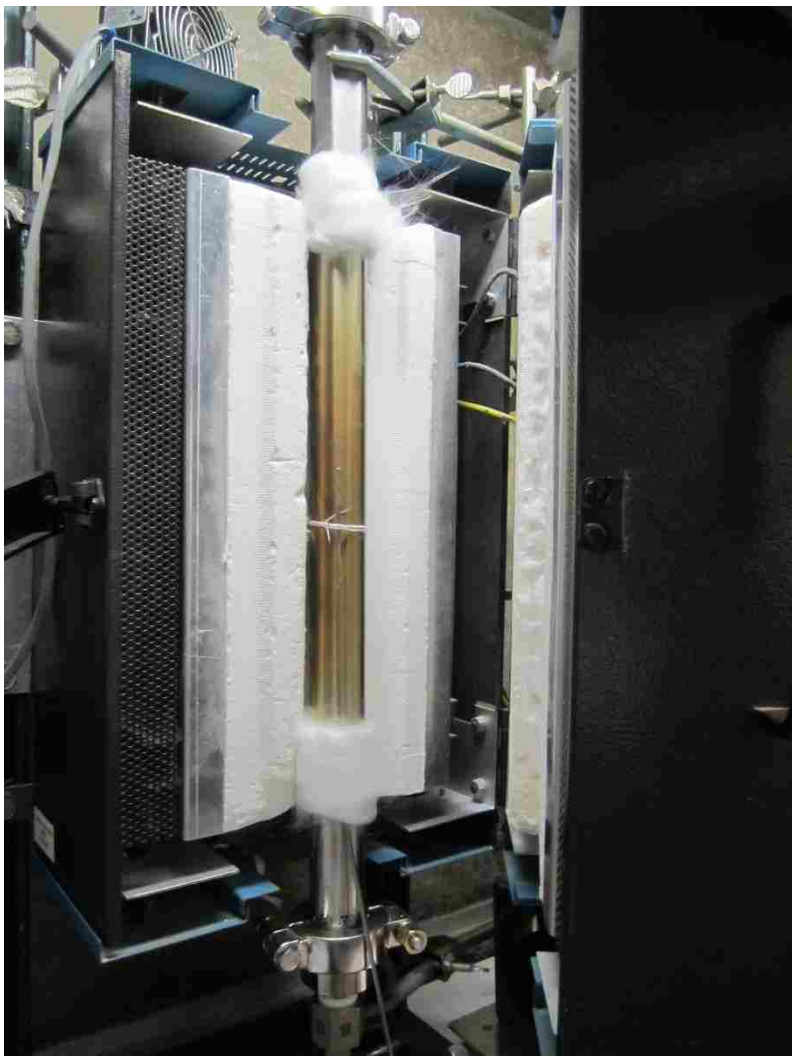

Fig. 2B (2). Calcination and sulfidation unit.

2B.3. Final Catalyst Pellets ready for Testing

Fig. 2B (3). Final catalyst pellets.

2B.4. Catalyst Testing Unit

Lab-scale catalyst testing unit

Fig. 2B (4). Lab-scale testing unit.

Appendix 2C: Retention Time of the Components obtained using the GC-HP 5890 II (GC parameters are given in Table 2.2)

Product	Formula	Retention Time, *min*
Nitrogen	N_2	0.729
Carbon Monoxide	CO	0.756 - 0.784
Methane	CH_4	0.803 - 0.867
Carbon Dioxide	CO_2	1.07 - 1.11
Ethane	C_2H_6	1.899 - 1.979
Hydrogen Sulfide	H_2S	2.098-2.150
Water	H_2O	2.842 - 2.901
Formaldehyde/Methanal	CH_2O	3.605 - 3.62 (Broad)
Propane	C_3H_8	3.905 - 4.012
Methanol	CH_4O	4.000 - 4.474
Dimethyl Ether	C_2H_6O	4.376
Acetaldehyde/Ethanal	C_2H_4O	4.924 – 5.016
Methyl Formate	$C_2H_4O_2$	5.459 - 5.547
Butane	C_4H_{10}	5.70 - 5.86
Ethanol	C_2H_6O	5.590 - 5.965
Propionaldehyde/Propanal	C_3H_6O	6.700
2-Propanol/Propyl Alcohol	C_3H_8O	6.786 - 6.829
Ethyl Formate	$C_3H_6O_2$	7.005 - 7.096
Methyl Acetate	$C_3H_6O_2$	7.00 - 7.17
Diethyl Ether	$C_4H_{10}O$	7.161 - 7.258
Pentane	C_5H_{12}	7.297 - 7.362
Propanol	C_3H_8O	7.140 - 7.444
Acetic Acid	$C_2H_4O_2$	7.475 – 7.504
Propyl Acetate	$C_5H_{10}O_2$	7.367 - 7.415
2-Butanone/MEK	C_4H_8O	8.087 – 8.111
Ethyl Acetate	$C_4H_8O_2$	8.184 - 8.279
Isobutanol	$C_4H_{10}O$	8.376 - 8.407
Hexane	C_6H_{14}	8.585 - 8.76
Butanol	$C_4H_{10}O$	8.560 - 8.846
Iso-Propyl Acetate	$C_5H_{10}O_2$	9.27 - 9.335
Propyl Acetate	$C_5H_{10}O_2$	9.640
Heptane	C_7H_{16}	10.714 - 10.785
Pentanol	$C_5H_{12}O$	10.748 - 10.901
Iso-Butyl Acetate	$C_6H_{12}O_2$	12.083 - 12.193
Butyl Acetate	$C_6H_{12}O_2$	12.891 - 13.004

Table 2C. Retention time of the components obtained from GC-HP 5890 II.

A sample calibration mixture chromatograph of hydrocarbons

Calibration mixture was obtained from *SUPELCO*

C_1-C_6 n-paraffins in helium calibration mixture; 1000 ppm methane, and 1010 ppm each of C_2-C_6 n-paraffins.

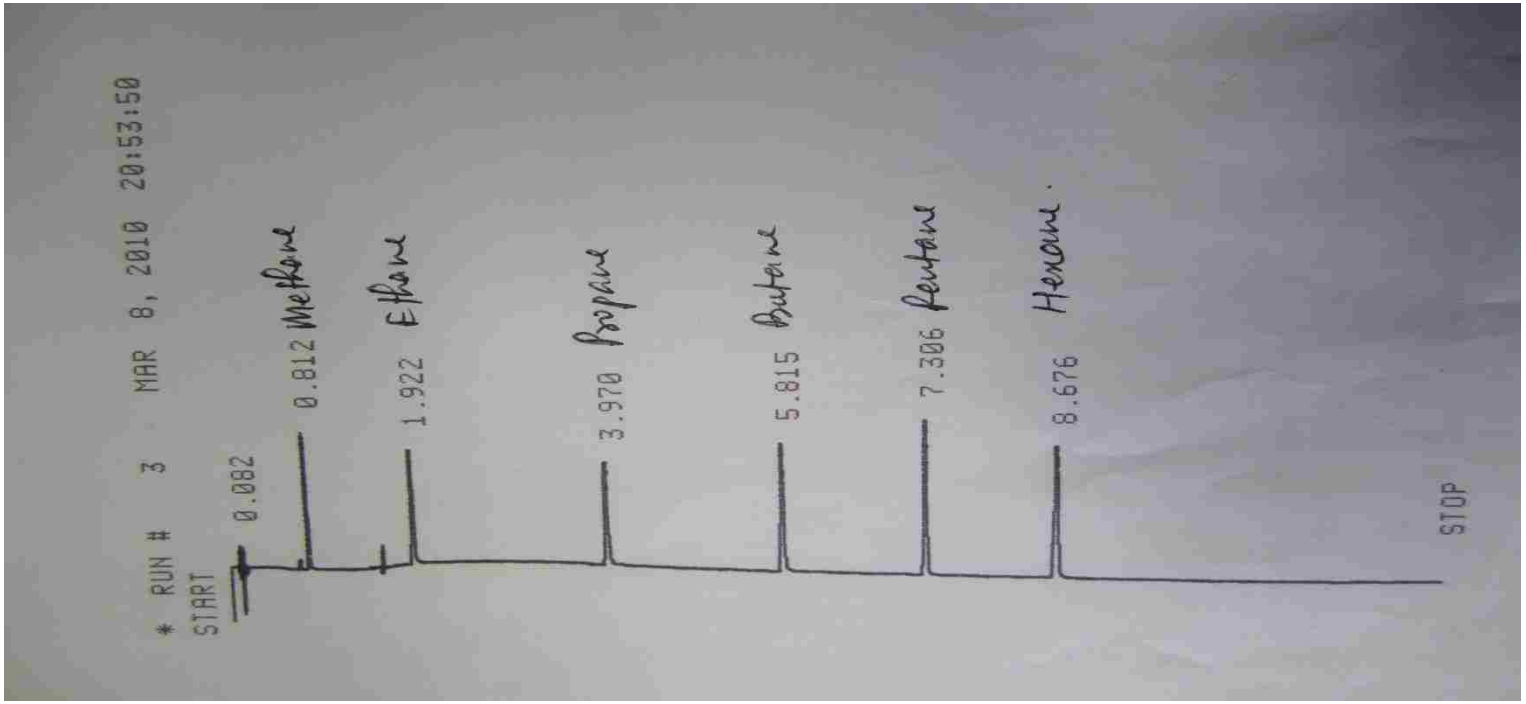

Appendix 2D: Sample Reactor Outlet Chromatograph obtained from the GC-HP 5890 II

RUN# 48 MAR 28, 2012 18:11:33

AREA%

RT	AREA TYPE	WIDTH	AREA%	
.784	357838 PB	.023	76.76950	– CO
.867	17532 PB	.016	3.76126	– Methane
1.086	52726 PB	.020	11.31168	– CO_2
1.899	3424 PB	.026	.73457	– Ethane
3.985	1473 BV	.035	.31601	– Propane
4.007	20366 VV	.067	4.36926	– Methanol
5.593	9253 BV	.050	1.98511	– Ethanol
5.735	751 VB	.039	.16112	– Butane
7.141	2388 VV	.037	.51231	– Propanol
8.563	369 FB	.045	.07916	– Butanol

TOTAL AREA= 466120
MUL FACTOR=1.0000E+00

Appendix 2E: Calibration of the GC-HP II (Calculation of the TRFs)

2E.1. TRFs for Alcohols (liquid injections)

Eight different diluted alcohol mixtures in deionized water were prepared and 0.1 – 0.5 μl volumes were injected from each mixture. The list of liquid mixtures and the calculation of TRFs for alcohols are demonstrated in Table 2E (1). The reference component for the calculation of TRFs is Ethanol. Average GC area from at least two injections was reported. Non-linear behavior of TRFs at lower GC area counts can be easily observed from Fig. 2E (1).

Mixture	Comp.	wt, *g*	Expt. m*ol%*	*mol%*, water free	GC Area (0.1 μl)	TRF	Pred. *mol%*	GC Area (0.2 μl)	TRF	Pred. *mol%*	GC Area (0.3 μl)	TRF	Pred. *mol%*	GC Area (0.4 μl)	TRF	Pred. *mol%*	GC Area (0.5 μl)	TRF	Pred. *mol%*
1	H_2O	6.14	86.07																
	CH_3OH	0.31	2.41	17.31				4672.0	27.0	17.38	7444.0	28.0	17.42	10789.5	30.0	17.35	14252.0	32.0	17.22
	C_2H_5OH	2.07	11.30	81.16				58142.5	72.0	81.09	89054.5	72.0	81.05	121054.0	72.0	81.12	151363.5	72.0	81.26
	C_3H_7OH	0.05	0.21	1.53				1131.5	74.0	1.54	1750.0	75.0	1.53	2461.5	78.0	1.52	3116.0	79.0	1.52
2	H_2O	5.52	77.67																
	CH_3OH	0.76	5.97	26.73	4693.5	27.0	26.85	11728.5	31.0	26.72	20318.5	33.0	26.89	29474.5	35.0	26.81	37753.5	37.0	26.79
	C_2H_5OH	2.92	15.98	71.57	32847.5	71.0	71.46	72997.0	72.0	71.59	117713.0	72.0	71.41	161664.0	72.0	71.49	196099.0	72.0	71.51
	C_3H_7OH	0.09	0.38	1.70	768.0	70.0	1.69	1819.5	76.0	1.69	3064.5	79.0	1.69	4266.0	80.0	1.70	5323.5	82.0	1.70
3	H_2O	4.05	63.68																
	CH_3OH	2.07	18.28	50.33	15828.5	32.0	50.43	40955.5	37.0	50.44	68690.5	39.5	50.36	101970.0	40.5	50.30	125563.5	42.0	50.33
	C_2H_5OH	2.84	17.41	47.94	33097.5	70.5	47.86	75527.0	72.0	47.80	119083.5	72.0	47.90	172871.0	72.0	47.96	205024.1	72.0	47.93
	C_3H_7OH	0.13	0.63	1.74	1195.0	71.0	1.72	3042.5	79.0	1.76	4938.5	82.0	1.74	7236.0	83.0	1.74	8573.5	83.0	1.74

Contd.

Contd.

4	H_2O	5.80	74.18																
	CH_3OH	3.53	25.33	98.11				76930.5	40.0	98.10	127486.5	42.0	98.11	182658.0	47.0	98.10	228376.0	47.0	98.10
	C_2H_5OH	0.08	0.38	1.47				1433.0	49.5	1.48	2250.0	49.5	1.47	3181.0	54.5	1.47	4093.0	56.0	1.48
	C_3H_7OH	0.03	0.11	0.42				539.0	65.0	0.42	934.0	71.0	0.43	1298.5	77.0	0.43	1610.0	77.0	0.42
5	H_2O	5.58	72.95																
	CH_3OH	3.50	25.66	94.85	30801.0	35.0	94.87	78321.5	40.0	94.88	128603.0	42.0	94.84	179260.5	47.0	94.84	226363.5	47.0	94.88
	C_2H_5OH	0.21	1.05	3.90	1779.5	49.5	3.88	4473.0	56.0	3.87	7262.0	57.5	3.91	10061.0	64.0	3.91	12775.0	65.0	3.87
	C_3H_7OH	0.09	0.34	1.25	757.0	65.0	1.26	1899.5	73.5	1.25	3028.5	75.0	1.25	4184.5	83.0	1.25	5319.5	84.0	1.25
6	H_2O	5.15	70.03																
	CH_3OH	3.52	26.87	89.65	29686.5	35.0	89.65	76607.5	40.0	89.67	129308.0	42.0	89.67	179645.5	47.0	89.63	225359.5	47.0	89.73
	C_2H_5OH	0.51	2.72	9.09	5115.0	59.5	9.09	12305.5	63.5	9.07	20019.0	62.5	9.07	27367.5	70.5	9.10	33922.0	70.5	9.00
	C_3H_7OH	0.09	0.38	1.26	804.5	67.5	1.26	1962.5	73.0	1.26	3240.5	74.0	1.26	4476.0	83.0	1.26	5557.5	82.5	1.26
7	H_2O	3.87	59.92																
	CH_3OH	3.57	31.02	77.40	31285.0	35.0	77.38	83032.5	42.5	77.46	131865.0	45.0	77.41	188546.0	46.5	77.44	243718.5	47.5	77.35
	C_2H_5OH	1.40	8.45	21.08	15479.5	63.5	21.10	37623.0	71.0	21.01	57413.0	72.0	21.07	79312.0	72.0	21.04	100892.0	72.0	21.13
	C_3H_7OH	0.13	0.61	1.52	1155.5	66.0	1.52	3039.0	79.0	1.53	4718.0	82.0	1.52	6571.5	82.5	1.52	8438.0	83.5	1.52
8	H_2O	5.57	78.06																
	CH_3OH	0.74	5.85	26.64				11380.5	32.0	26.72	18670.0	34.0	26.76	27963.5	36.5	26.64	38110.5	38.0	26.70
	C_2H_5OH	2.88	15.71	71.60				68544.0	72.0	71.53	105593.5	72.0	71.47	148221.5	72.0	71.59	193453.0	72.0	71.54
	C_3H_7OH	0.09	0.38	1.75				1688.5	72.5	1.75	2662.0	73.5	1.77	3944.0	77.5	1.77	5300.5	80.5	1.75

Table 2E (1). Calculation of TRFs for alcohols.

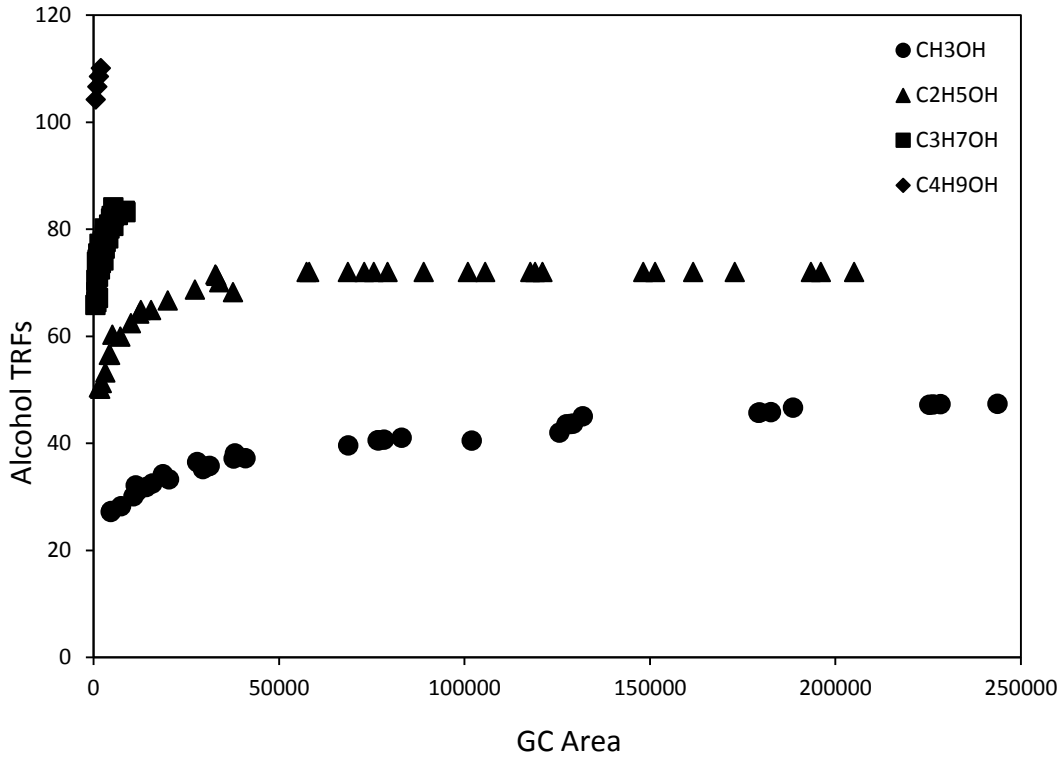
120
100
80
60
40
20
0
Alcohol TRFs
0
50000
100000
150000
200000
250000
GC Area
CH3OH
C2H5OH
C3H7OH
C4H9OH

2E.2. TRFs for Hydrocarbons, pure CO and pure CO_2 (Gaseous Product Injections)

A series of pure and mixture of gaseous components were injected using a syringe (0.1 to 1 *ml*) for the calculation of TRFs. Table 2E (2-3) shows the calculation of TRFs for hydrocarbons, pure CO and pure CO_2, with reference to a TRF value of 35.7 for methane.

Vol., *ml*	CH_4 GC Area	TRF	CO GC Area	TRF	CO_2 GC Area	TRF
0.08	118203.7	35.7	139893.0	42.3	172177.7	52.0
0.13	173967.3	35.7	203730.0	41.8	269377.5	55.3
0.23	274445.3	35.7			412618.3	53.7
0.33	357260.0	35.7			551835.3	55.1
Average		**35.7**		**42.0**		**54.0**

Table 2E (2). Calculation of TRFs for pure CO and CO_2.

Volume, *ml*[#]	CH_4 GC Area	C_2H_6 GC Area	C_3H_8 GC Area	C_4H_{10} GC Area	C_5H_{12} GC Area	C_6H_{14} GC Area	TRF, CH_4	TRF, C_2H_6	TRF, C_3H_8	TRF, C_4H_{10}	TRF, C_5H_{12}	TRF, C_6H_{14}
0.33	367.5	573.0	763.5	903.5	1086.0	1246.0	11.7	18.1	24.1	28.6	34.3	39.4
0.53	514.0	798.5	1058.0	1306.5	1532.5	1770.0	16.4	25.2	33.5	41.3	48.5	56.0
0.73	625.0	979.3	1290.3	1577.7	1863.7	2131.7	20.0	31.0	40.8	49.9	58.9	67.4
1.03	827.3	1276.0	1690.0	2075.7	2431.0	2795.0	26.4	40.3	53.4	65.6	76.9	88.4

[#] *SUPELCO C_1-C_6 n-paraffins in helium calibration mixture; 1000 ppm methane, 1010 ppm each for C_2-C_6 n-paraffins.*

Table 2E (3). Calculation of TRFs for hydrocarbons.

In order to complete the methane calibration curve, few more injections at different concentration of methane in hydrogen were injected into the GC. The Brooks mass flow controllers were used to mix methane and hydrogen and flow rates of methane was varied to get different concentrations. Similar method was employed for the calculation of TRFs for CO in the presence of H_2. The TRFs of CO_2 was also checked with this method. CO_2 was mixed with a 49.7 *vol %* H_2/balance CO pre-mixture to simulate the higher alcohol synthesis reaction product composition. A TRF of 55.4 for CO_2 was calculated using this method as compared to a TRF of 54.0 calculated from the syringe injections.

Fig. 2E (2-6) shows the mass flow controller calibration lines for CO, H_2, methane, CO_2 and 49.7 *vol %* H_2 in CO pre-mixture at room temperature and pressure.

Table 2E (4-6) shows the calculation of TRFs for CO_2, CH_4 (Hydrocarbons) and CO (in the presence of H_2).

Fig. 2E (7) shows the TRFs for hydrocarbons and CO_2.

Fig. 2E (8) shows the TRFs for CO as the function of H_2/CO ratio.

Table 2E (7) compares the calculated TRFs at high GC area counts with the literature TRFs.

Table 2E (8) listed the TRFs or the TRF co-relations used for the calculations.

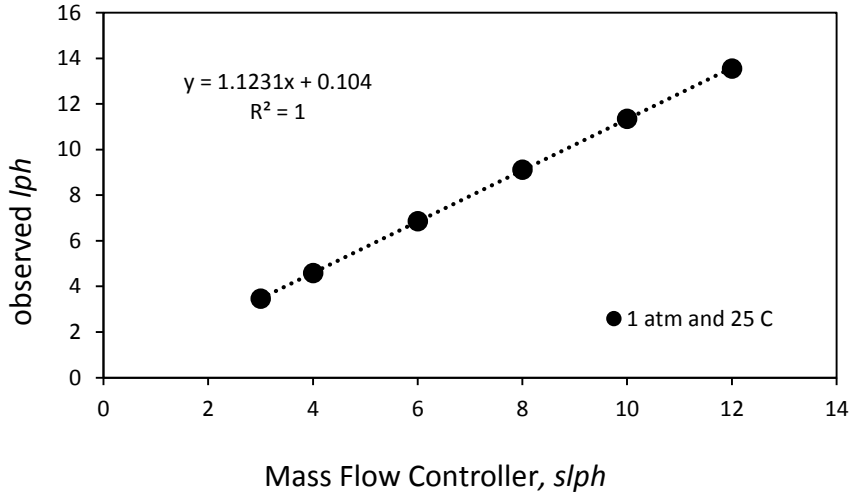

[redacted]

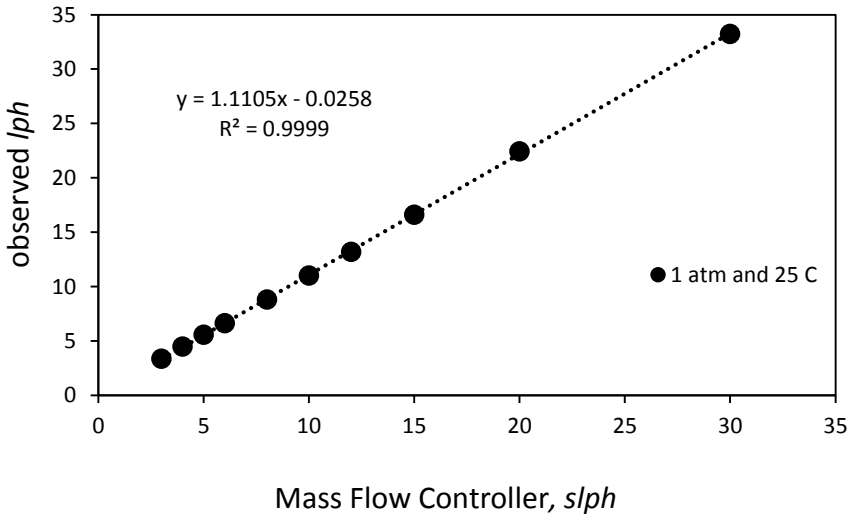

[redacted]

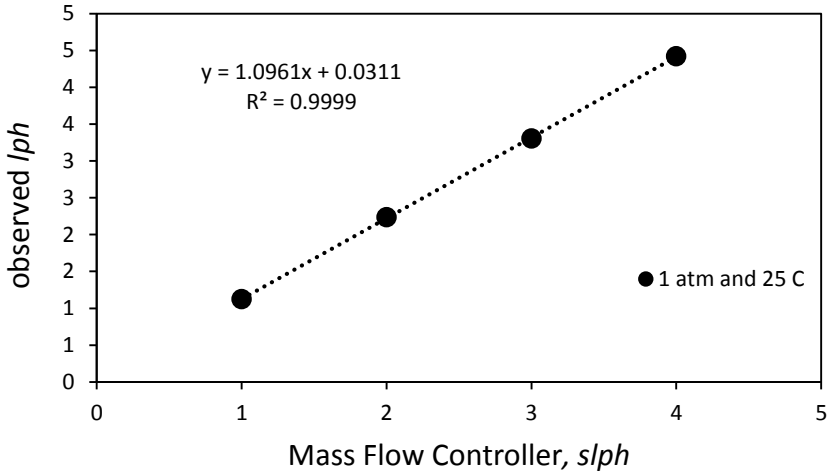

[redacted]

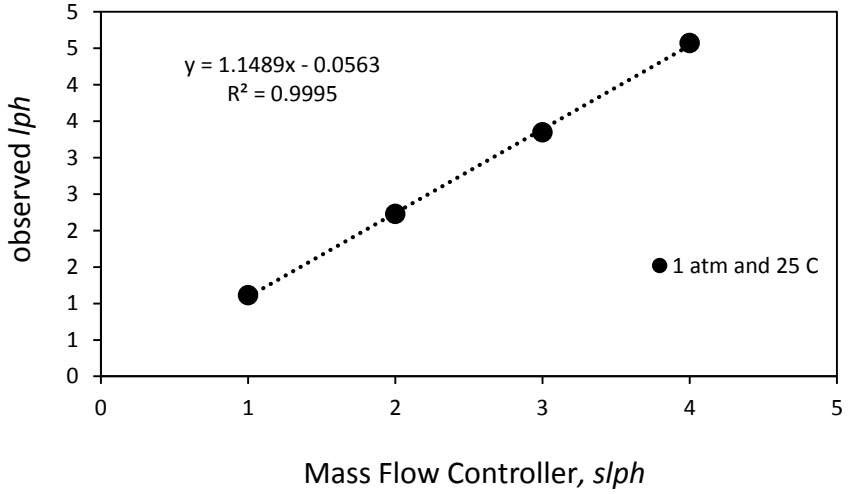

[redacted]

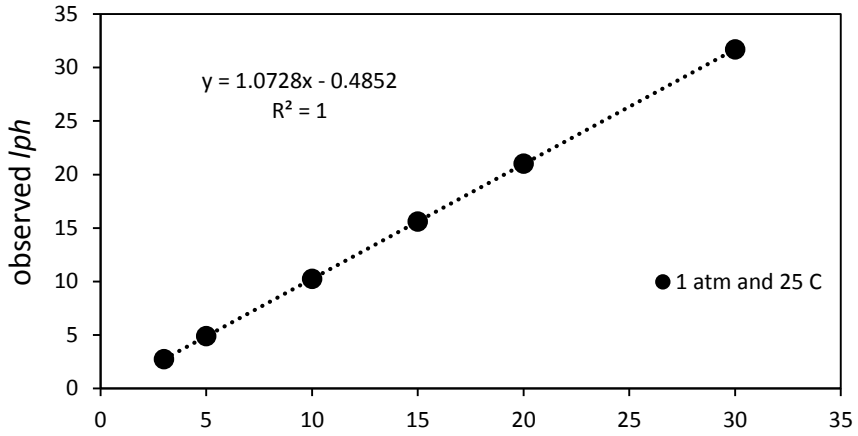

[redacted]

CO_2, *slph*	$H_2/CO^{\#}$, *slph*	CO_2, *lph*	CO, *lph*	H_2, *lph*	CO_2, *mol fract.*	CO, *mol fract.*	CO_2 GC Area	CO GC Area	TRF, CO_2	TRF, CO
0.5	30.0	0.7	15.9	15.8	0.020	0.493	37354.8	502133.8	58.4	32.5
0.5	20.0	0.7	10.5	10.4	0.031	0.488	50655.3	485663.0	52.9	31.8
1.0	20.0	1.4	10.5	10.4	0.062	0.472	109360.5	487501.8	56.0	33.0
2.0	20.0	2.9	10.5	10.4	0.120	0.443	203297.7	470929.3	54.1	34.0
Average									**55.4**	**32.8**

[#] 49.7 % H_2/balance CO pre-mixture

Table 2E (4). Calculation of TRFs for CO_2.

CH_4, *slph*	H_2, *slph*	CH_4, *lph*	H_2, lph	CH_4, *mol fract.*	CH_4 GC Area	TRF, CH_4	TRF, C_2H_6	TRF, C_3H_8	TRF, C_4H_{10}	TRF, C_5H_{12}	TRF, C_6H_{14}
0.5	30.0	0.6	33.3	0.017	17596.5	32.9	50.6	67.0	81.6	96.4	110.8
1.0	30.0	1.1	33.3	0.033	35818.5	34.9	53.8	71.3	86.7	102.5	117.8
2.0	30.0	2.2	33.3	0.063	69935.0	35.7	54.9	72.8	88.6	104.7	120.3
3.0	30.0	3.3	33.3	0.091	101369.1	**35.7**	**55.0**	**72.8**	**88.7**	**104.8**	**120.4**

Table 2E (5). Calculation of TRFs for CH_4 and predicted TRFs for C_2-C_6 n-paraffins.

CO2, *slph*	H_2, *slph*	CO, *lph*	H_2, *lph*	CO, *mol fract.*	CO GC Area	H_2/CO	TRF, CO
2.0	6.0	2.4	6.6	0.261	388313.3	2.8	47.4
2.4	5.6	2.8	6.2	0.311	399441.5	2.2	41.0
2.8	5.2	3.2	5.7	0.361	416472.7	1.8	36.8
3.2	4.8	3.7	5.3	0.411	445892.0	1.4	34.7
3.6	4.4	4.1	4.9	0.460	466689.0	1.2	32.4
4.0	4.0	4.6	4.4	0.510	484673.5	1.0	30.3
4.4	3.6	5.0	4.0	0.560	508403.0	0.8	29.0
4.8	3.2	5.5	3.5	0.609	522202.8	0.6	27.4
5.2	2.8	5.9	3.1	0.658	531237.3	0.5	25.8
5.6	2.4	6.4	2.6	0.708	543528.3	0.4	24.5
6.0	2.0	6.8	2.2	0.757	556807.3	0.3	23.5

Table 2E (6). Calculation of TRFs for CO at different H_2/CO ratio.

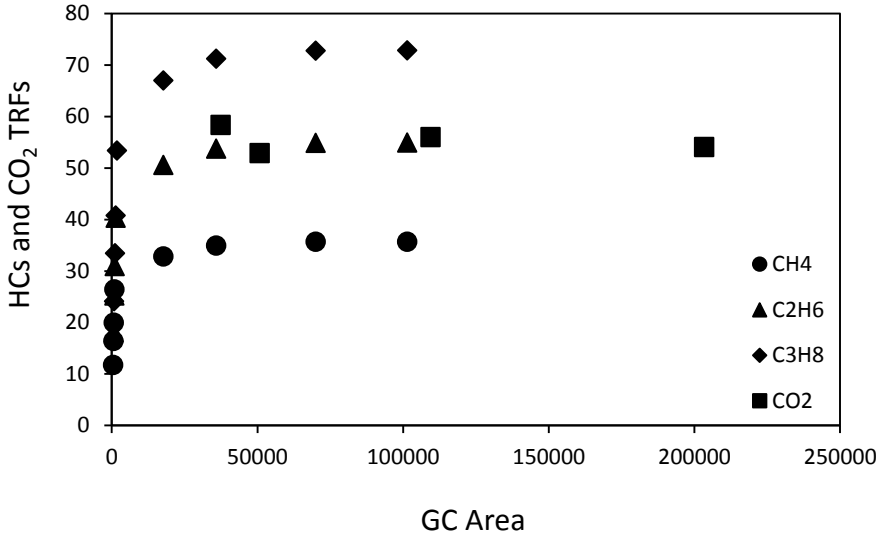

[redacted]

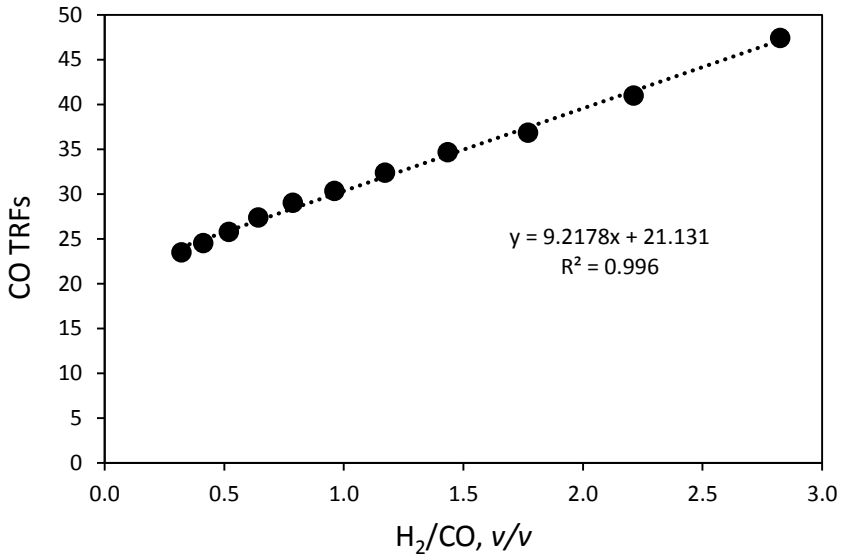

[redacted]

Components	TRFs, calculated	TRFs, Literature [22-27]
CO	42.0	42.0
CO_2	54.0	48.0
CH_3OH	47.4	40, 55
C_2H_5OH	72.0	72.0
C_3H_7OH	83.2	83.0
C_4H_9OH	110.1	95.0
CH_4	35.7	35.7
C_2H_6	55.0	51.2
C_3H_8	72.8	64.5
C_4H_{10}	88.7	85.0
C_5H_{12}	104.8	105.0
C_6H_{14}	120.4	123.0

Table 2E (7). Comparison of the calculated TRFs at high GC area counts and the reported TRFs in the literature.

Components	Area Range		TRFs or TRF correlations
CO	388313.3	556807.3	$9.2178 \times (H_2/CO)_{out} + 21.131$
CO[#]	0.321[#]	2.824[#]	
CO_2	37354.8	203297.7	55.3749
CH_3OH	4672	40955.5	$7.4983 \times (\text{GC area})^{0.1518}$
C_2H_5OH	1779.5	20019	$20.314 \times (\text{GC area})^{0.1218}$
C_3H_7OH	539	8573.5	$39.315 \times (\text{GC area})^{0.0853}$
C_4H_9OH	631.5	1931.5	$76.089 \times (\text{GC area})^{0.0488}$
CH_4	827.33	69935	$16.562 \times (\text{GC area})^{0.0699}$
C_2H_6	1276	35818.5	$21.769 \times (\text{GC area})^{0.0863}$
C_3H_8	1290.33	35818.5	$16.678 \times (\text{GC area})^{0.1418}$
C_4H_{10}	903.5	2075.7	$0.0316 \times (\text{GC area})$
C_5H_{12}	1086	2431	$0.0316 \times (\text{GC area})$
C_6H_{14}	1246	2795	$0.0316 \times (\text{GC area})$

[#] $(H_2/CO)_{out} = 0.9806 \times (H_2/CO)_{in}^{1.1688}$ is the approximate co-relation between outlet and inlet H_2/CO for $Cs/MoS_2/AC$ catalyst during reaction

Table 2E (8). The TRFs or the TRF correlations used for the calculations.

Appendix 2F: Representative XPS Spectra taken at Center (Inside) of the Sulfidized Pellet

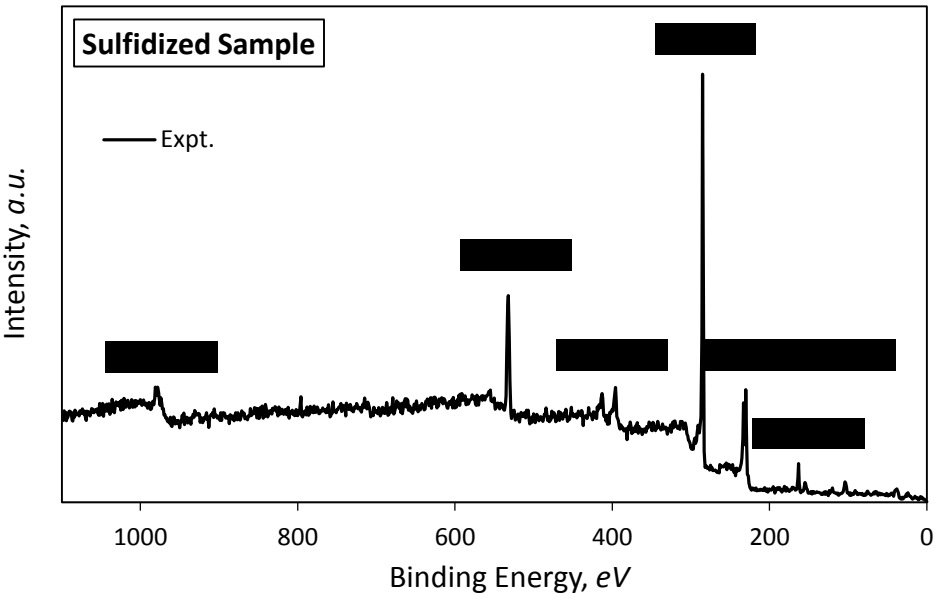

[redacted]

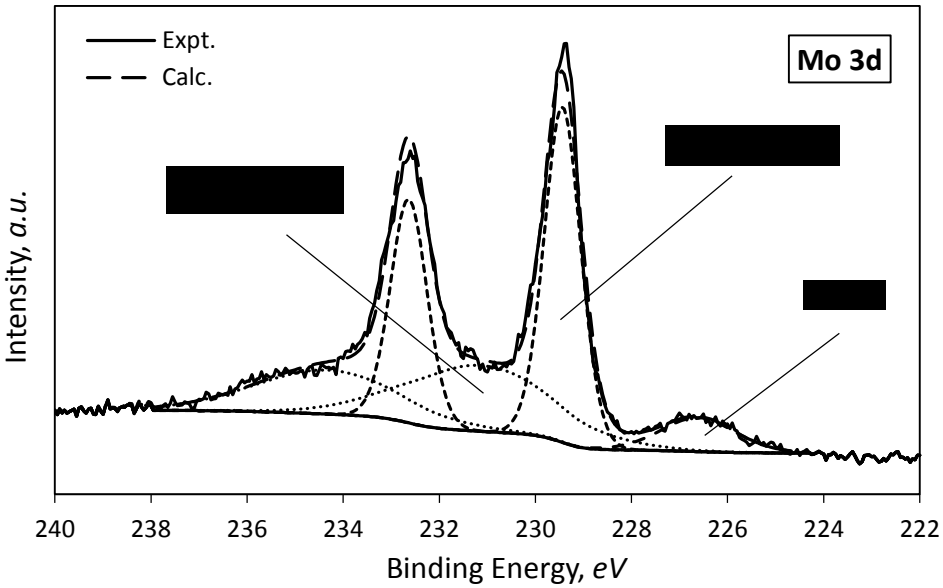

[redacted]

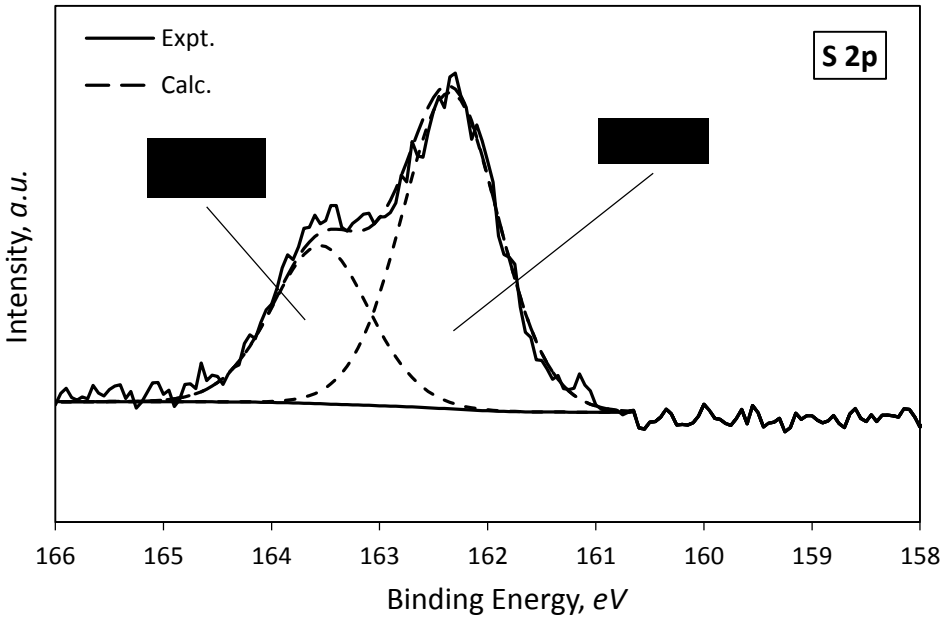

[redacted]

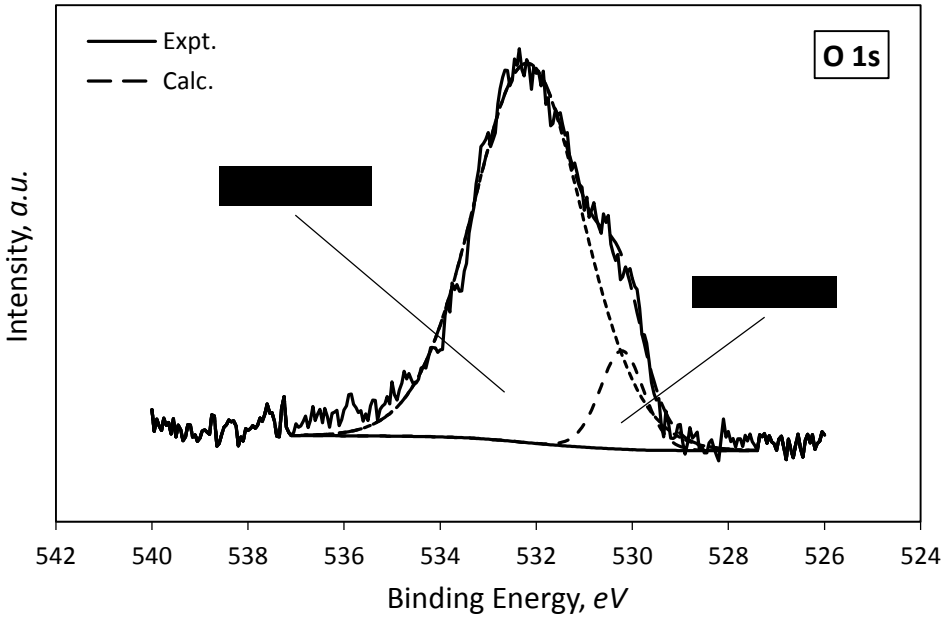

[redacted]

Appendix 2G: Representative XPS Spectra (at outside of the pellet) of the Cesium Promoted Catalyst Stored in Nitrogen Purged Vial, but Briefly Exposed to Atmosphere while Handling.

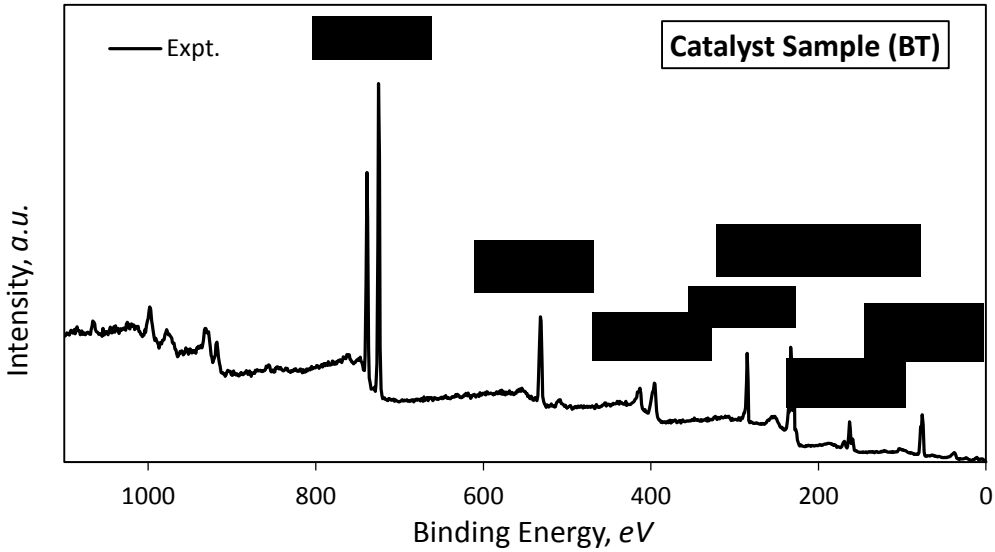

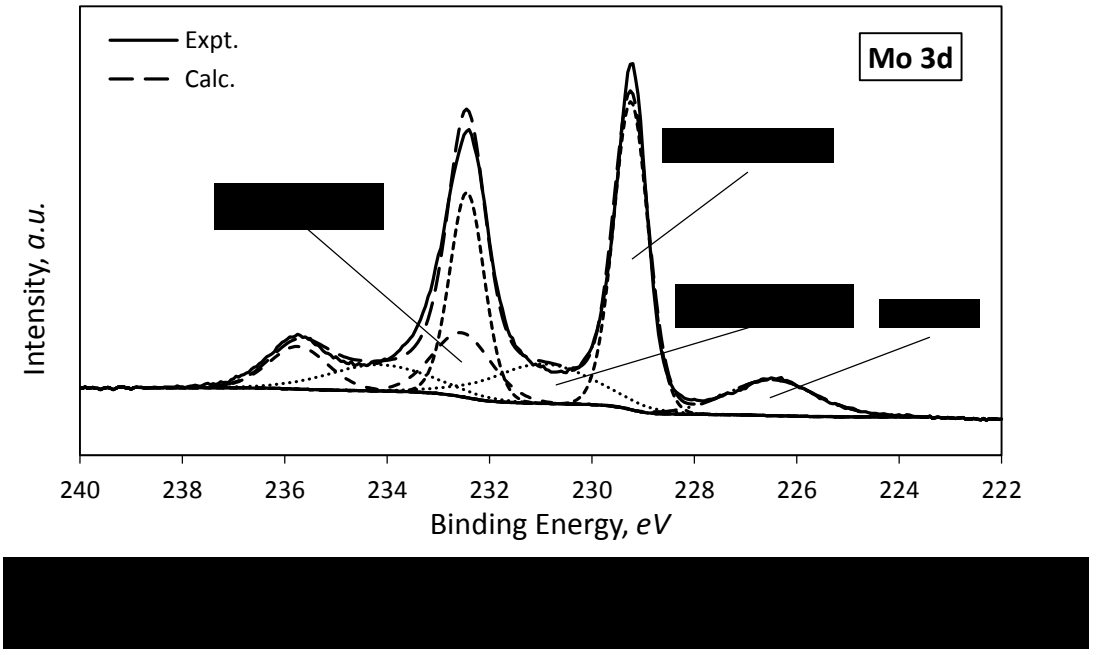

Appendix 2H: Testing Results of the Catalysts

2H.1. Catalyst # 1 results

Time, *hr*	*P*, *bar*	*T*, *°K*	H_2/CO, *v/v*	GHSV, *L/kg cat/hr*	Products, *mol/kg cat/hr*												CO Conv., *%*	Alc. Sel., *mol %*
					CO	H_2	CH_3OH	C_2H_5OH	C_3H_7OH	CH_4	C_2H_6	C_3H_8	CO_2	H_2O	Tot. Alc.	Tot. HCs		
43.1	85	590	0.99	2993	49.32	48.20	0.41	0.06	0.00	3.06	0.94	0.40	4.47	0.09	0.46	4.40	19.6	9.5

Table 2H (1). Operating conditions and testing results of catalyst # 1.

2H.2. Catalyst # 2 results

Time, *hr*	*P*, *bar*	*T*, *°K*	H_2/CO, *v/v*	GHSV, *L/kg cat/hr*	Products, *mol/kg cat/hr*												CO Conv., *%*	Alc. Sel., *mol %*
					CO	H_2	CH_3OH	C_2H_5OH	C_3H_7OH	CH_4	C_2H_6	C_3H_8	CO_2	H_2O	Tot. Alc.	Tot. HCs		
23.5	84	589	0.99	2993	44.47	44.49	1.55	0.40	0.11	2.96	0.92	0.45	7.07	0.00	2.09	4.33	27.5	32.5
41.2	84	588	0.99	2993	45.25	44.92	1.59	0.45	0.12	2.81	0.83	0.40	6.55	0.00	2.20	4.04	26.3	35.2
50.3	84	578	0.99	2993	50.13	48.67	1.68	0.48	0.11	1.75	0.45	0.21	3.90	0.00	2.29	2.41	18.3	48.7
63.1	84	571	0.99	2993	53.52	51.89	1.57	0.44	0.08	1.19	0.28	0.11	2.60	0.00	2.10	1.59	12.8	56.9

Table 2H (2). Operating conditions and testing results of catalyst # 2.

2H.3. Catalyst # 3 results

Time, *hr*	*P*, *bar*	*T*, °*K*	H_2/CO, *v/v*	GHSV, *L/kg cat/hr*	Ext. Feed, mol*/kg cat/hr*	Products, *mol/kg cat/hr*												CO Conv., *%*	Alc. Sel., *mol %*
						CO	H_2	CH_3OH	C_2H_5OH	C_3H_7OH	CH_4	C_2H_6	C_3H_8	CO_2	H_2O	Tot. Alc.	Tot. HCs		
0.0	87	588	0.99	2993	0.00	59.16	62.48	0.00	0.00	0.00	0.14	0.04	0.00	2.00	0.00	0.00	0.18	3.6	0.0
0.3	87	590	0.99	2993	0.00	50.29	53.18	0.65	0.29	0.07	2.25	0.50	0.19	5.44	0.00	1.01	2.94	18.1	25.6
1.1	87	590	0.99	2993	0.00	48.46	50.55	0.90	0.40	0.12	2.66	0.49	0.20	5.59	0.00	1.43	3.36	21.0	29.9
1.4	87	591	0.99	2993	0.00	48.26	50.20	0.95	0.41	0.12	2.74	0.49	0.20	5.59	0.00	1.50	3.42	21.4	30.5
1.7	87	591	0.99	2993	0.00	48.32	50.11	0.98	0.43	0.12	2.71	0.48	0.19	5.52	0.06	1.56	3.37	21.3	31.6
2.0	87	590	0.99	2993	0.00	48.27	50.06	0.99	0.43	0.13	2.72	0.47	0.19	5.48	0.00	1.59	3.37	21.3	32.0
7.1	86	590	0.99	2993	0.00	49.16	50.62	1.19	0.47	0.13	2.67	0.40	0.15	5.12	0.00	1.84	3.22	19.9	36.4
7.5	87	590	0.99	2993	0.00	48.59	49.91	1.18	0.47	0.13	2.68	0.40	0.15	5.11	0.00	1.83	3.23	20.8	36.2
8.0	86	590	0.99	2993	0.00	49.46	50.79	1.20	0.46	0.14	2.60	0.39	0.15	4.93	0.00	1.85	3.13	19.4	37.2
8.5	86	590	0.99	2993	0.00	49.40	50.76	1.20	0.46	0.13	2.62	0.39	0.15	4.99	0.00	1.84	3.16	19.5	36.8
9.1	86	590	0.99	2993	0.00	49.38	50.68	1.24	0.47	0.13	2.61	0.39	0.15	4.95	0.00	1.89	3.14	19.5	37.6
9.6	86	590	0.99	2993	0.00	49.23	50.52	1.26	0.47	0.14	2.65	0.39	0.15	5.02	0.00	1.92	3.19	19.8	37.5
10.1	86	590	0.99	2993	0.00	49.43	50.70	1.25	0.47	0.13	2.60	0.38	0.15	4.92	0.00	1.90	3.13	19.5	37.8
10.6	86	590	0.99	2993	0.00	49.38	50.60	1.29	0.47	0.13	2.61	0.38	0.14	4.92	0.00	1.93	3.13	19.6	38.2
10.9	85	590	0.99	2993	0.00	49.08	50.33	1.30	0.47	0.14	2.71	0.39	0.15	5.07	0.00	1.94	3.25	20.0	37.4
12.2	85	590	0.99	2993	0.00	49.10	50.32	1.34	0.47	0.14	2.69	0.39	0.14	5.06	0.00	1.99	3.23	20.0	38.1
12.5	86	590	0.99	2993	0.00	49.28	50.48	1.32	0.46	0.13	2.66	0.39	0.14	4.96	0.00	1.95	3.19	19.7	38.0
13.0	85	590	0.99	2993	0.00	49.34	50.49	1.35	0.47	0.13	2.62	0.38	0.14	4.91	0.00	2.00	3.14	19.6	38.9
13.6	85	590	0.99	2993	0.00	49.43	50.56	1.35	0.47	0.13	2.60	0.37	0.14	4.86	0.00	2.00	3.11	19.5	39.2
14.2	85	590	0.99	2993	0.00	49.41	50.56	1.36	0.47	0.13	2.60	0.38	0.14	4.88	0.00	2.00	3.12	19.5	39.1
15.1	85	590	0.99	2993	0.00	49.24	50.33	1.40	0.47	0.14	2.64	0.38	0.14	4.93	0.00	2.05	3.16	19.8	39.4
15.6	85	590	0.99	2993	0.00	49.52	50.56	1.41	0.47	0.13	2.56	0.37	0.13	4.77	0.00	2.06	3.06	19.3	40.2
16.0	84	590	0.99	2993	0.00	49.19	50.26	1.43	0.48	0.14	2.66	0.35	0.14	4.94	0.00	2.09	3.16	19.9	39.8
16.5	84	590	0.99	2993	0.00	49.75	50.75	1.39	0.46	0.13	2.51	0.36	0.13	4.66	0.00	2.03	3.00	19.0	40.3
18.7	84	590	0.99	2993	0.00	49.30	50.27	1.48	0.48	0.14	2.61	0.37	0.13	4.84	0.00	2.14	3.11	19.7	40.8
19.6	84	590	0.99	2993	0.00	49.31	50.26	1.50	0.48	0.14	2.60	0.37	0.13	4.84	0.00	2.16	3.10	19.7	41.0

Contd.

20.1	84	590	0.99	2993	0.00	49.59	50.50	1.49	0.47	0.13	2.53	0.36	0.13	4.68	0.00	2.14	3.01	19.2	41.5
20.5	84	590	0.99	2993	0.00	49.52	50.45	1.48	0.46	0.13	2.56	0.36	0.13	4.73	0.00	2.12	3.05	19.3	41.1
21.1	84	590	0.99	2993	0.00	49.63	50.51	1.50	0.47	0.13	2.51	0.36	0.13	4.66	0.00	2.15	3.00	19.1	41.8
21.6	84	590	0.99	2993	0.00	49.93	50.85	1.49	0.47	0.13	2.37	0.35	0.12	4.52	0.00	2.13	2.85	18.6	42.8
22.1	84	590	0.99	2993	0.00	49.58	50.43	1.52	0.47	0.13	2.53	0.36	0.13	4.66	0.00	2.17	3.01	19.2	41.8
22.6	84	590	0.99	2993	0.00	49.75	50.61	1.51	0.46	0.13	2.47	0.36	0.12	4.59	0.00	2.15	2.95	18.9	42.2
23.0	84	590	0.99	2993	0.00	49.65	50.50	1.52	0.47	0.13	2.50	0.35	0.13	4.62	0.00	2.17	2.98	19.1	42.2
23.6	84	590	0.99	2993	0.00	49.80	50.62	1.52	0.47	0.13	2.45	0.35	0.12	4.53	0.00	2.17	2.92	18.9	42.7
24.1	84	590	0.99	2993	0.00	49.90	50.66	1.52	0.47	0.13	2.43	0.35	0.12	4.46	0.00	2.17	2.89	18.7	42.9
24.6	84	590	0.99	2993	0.00	49.86	50.66	1.53	0.47	0.13	2.37	0.35	0.12	4.46	0.00	2.20	2.84	18.8	43.6
25.4	84	590	0.99	2993	0.00	49.47	50.31	1.55	0.48	0.13	2.54	0.36	0.13	4.70	0.00	2.21	3.03	19.4	42.2
61.0	86	589	0.99	2993	0.00	49.91	50.43	1.75	0.49	0.14	2.32	0.33	0.11	4.33	0.00	2.43	2.75	18.7	46.9
88.4	86	589	0.99	2993	0.00	50.25	50.66	1.81	0.50	0.14	2.15	0.31	0.10	4.11	0.00	2.51	2.55	18.1	49.6
135.4	86	589	0.99	2993	0.00	50.90	51.24	1.85	0.50	0.14	1.91	0.28	0.08	3.79	0.00	2.54	2.27	17.1	52.8
179.9	86	589	0.99	2993	0.00	51.71	51.93	1.84	0.49	0.13	1.69	0.24	0.07	3.37	0.00	2.51	2.00	15.8	55.6
228.6	85	588	0.99	2993	0.00	51.55	51.66	2.15	0.55	0.15	1.74	0.23	0.07	3.55	0.00	2.90	2.04	16.0	58.8
47.1	60	588	0.99	2993	0.00	54.07	54.86	1.18	0.34	0.09	1.34	0.22	0.07	2.67	0.00	1.61	1.63	11.9	49.8
55.8	72	588	0.99	2993	0.00	52.24	52.88	1.44	0.41	0.11	1.75	0.26	0.09	3.36	0.00	2.00	2.09	14.9	48.8
24.1	84	590	0.99	2993	0.00	49.74	50.55	1.53	0.47	0.13	2.46	0.35	0.12	4.55	0.00	2.19	2.93	19.0	42.7
37.3	91	590	0.99	2993	0.00	48.25	48.96	1.77	0.51	0.15	2.82	0.40	0.13	5.17	0.00	2.49	3.35	21.4	42.6
42.3	101	591	0.99	2993	0.00	46.52	47.05	1.94	0.55	0.17	3.34	0.45	0.15	5.89	0.07	2.73	3.94	24.2	40.9
163.4	85	588	1.01	1157	0.00	16.20	16.97	0.88	0.22	0.08	1.67	0.23	0.07	3.04	0.04	1.22	1.97	31.1	38.4
62.6	85	589	1.00	2259	0.00	35.87	36.61	1.37	0.40	0.12	2.22	0.31	0.10	4.11	0.01	1.94	2.63	22.4	42.4
61.0	86	589	0.99	2993	0.00	49.91	50.43	1.75	0.49	0.14	2.32	0.33	0.11	4.33	0.00	2.43	2.75	18.7	46.9
66.0	85	590	0.99	4461	0.00	79.23	79.49	2.30	0.63	0.16	2.25	0.33	0.10	4.35	0.00	3.10	2.68	13.6	53.6
69.3	84	591	0.99	6664	0.00	124.77	125.25	2.80	0.77	0.17	2.18	0.33	0.10	4.35	0.00	3.74	2.60	9.0	59.0
72.6	84	591	0.99	8867	0.00	169.87	170.64	3.13	0.85	0.17	2.06	0.32	0.10	4.33	0.00	4.15	2.47	6.9	62.7
76.1	84	591	0.99	11069	0.00	214.88	216.03	3.47	0.95	0.18	2.04	0.32	0.00	4.46	0.00	4.61	2.36	5.7	66.1
93.1	85	533	0.99	2993	0.00	60.14	61.35	0.54	0.15	0.00	0.01	0.00	0.00	0.40	0.00	0.68	0.01	2.0	98.7
107.4	86	554	0.99	2993	0.00	57.93	58.53	1.11	0.33	0.04	0.42	0.05	0.00	1.05	0.00	1.48	0.47	5.6	75.8
110.8	86	571	0.99	2993	0.00	55.02	55.23	1.67	0.50	0.09	1.00	0.13	0.02	2.12	0.00	2.26	1.15	10.4	66.2
114.4	85	589	0.99	2993	0.00	50.22	50.61	1.87	0.52	0.15	2.08	0.31	0.09	4.10	0.00	2.59	2.48	18.2	51.1
117.4	86	601	0.99	2993	0.00	46.40	47.45	1.65	0.44	0.16	3.04	0.52	0.19	5.94	0.09	2.32	3.74	24.4	38.2
120.7	87	613	0.99	2993	0.00	43.41	45.37	1.27	0.32	0.14	4.10	0.73	0.30	7.77	0.12	1.81	5.13	29.3	26.0

Contd.

138.9	85	589	0.50	3002	0.00	73.28	34.15	0.95	0.42	0.13	1.35	0.23	0.08	3.35	0.00	1.55	1.65	10.2	48.4
142.2	86	589	0.99	2993	0.00	51.15	51.40	1.87	0.50	0.14	1.85	0.26	0.08	3.62	0.00	2.56	2.19	16.7	53.9
157.0	86	588	1.96	2984	0.00	30.00	69.21	3.11	0.52	0.13	2.29	0.28	0.08	3.58	0.10	3.75	2.65	27.2	58.6
160.3	86	588	2.92	2980	0.00	19.39	77.76	3.83	0.49	0.11	2.46	0.28	0.08	3.31	0.15	4.43	2.82	37.6	61.1
189.0	54	554	0.99	2993	0.00	59.53	60.59	0.70	0.20	0.03	0.05	0.03	0.00	0.57	0.00	0.92	0.08	3.0	92.2
193.2	54	571	0.99	2993	0.00	57.93	58.69	1.05	0.31	0.05	0.38	0.07	0.00	1.11	0.00	1.41	0.45	5.6	75.8
203.8	53	587	0.99	2993	0.00	55.90	56.63	1.24	0.36	0.09	0.86	0.14	0.05	1.98	0.00	1.69	1.05	8.9	61.7
210.1	53	598	0.99	2993	0.00	53.97	54.97	1.29	0.36	0.11	1.29	0.24	0.08	2.91	0.00	1.79	1.62	12.1	52.5
213.4	53	610	0.99	2993	0.00	51.97	53.50	1.03	0.31	0.11	1.69	0.37	0.14	3.86	0.00	1.49	2.20	15.3	40.4
228.6	85	588	0.99	2993	0.00	51.55	51.66	2.15	0.55	0.15	1.74	0.23	0.07	3.55	0.00	2.90	2.04	16.0	58.8
277.1	84	588	0.99	2993	0.99#	52.99	53.89	2.31	0.53	0.14	1.61	0.19	0.05	3.29	0.00	3.02	1.85	13.7	62.0
257.3	85	588	0.99	2993	1.97#	52.58	54.25	2.65	0.56	0.15	1.94	0.22	0.06	3.82	0.00	3.40	2.21	14.3	60.6
246.7	86	588	0.99	2993	3.94#	52.54	55.71	3.32	0.58	0.17	2.39	0.23	0.06	4.53	0.00	4.12	2.69	14.4	60.5
235.8	84	588	0.99	2993	8.38#	53.58	59.79	4.84	0.60	0.19	3.12	0.22	0.07	5.50	0.03	5.71	3.41	12.7	62.6
284.5	84	588	0.99	2993	0.00	53.18	53.31	1.98	0.52	0.13	1.35	0.18	0.05	2.86	0.00	2.65	1.58	13.4	62.7
295.0	87	587	0.99	2993	0.68*	53.33	53.85	2.07	0.77	0.16	1.39	0.25	0.05	3.08	0.00	3.05	1.69	13.1	64.3
299.9	86	587	0.99	2993	1.36*	54.54	55.59	1.90	0.99	0.18	1.27	0.29	0.05	2.92	0.00	3.12	1.62	11.1	65.9
304.8	84	588	0.99	2993	2.73*	54.94	56.89	1.93	1.59	0.24	1.27	0.44	0.07	3.35	0.00	3.85	1.78	10.5	68.4
307.9	84	588	0.99	2993	5.79*	57.75	61.99	1.76	2.68	0.30	1.14	0.65	0.07	3.75	0.00	4.94	1.85	5.9	72.7
325.6	85	588	0.99	2993	0.00	53.56	53.62	1.99	0.51	0.12	1.27	0.16	0.04	2.68	0.00	2.64	1.47	12.7	64.2
331.5	85	588	0.99	2699	0.00	47.93	47.21	2.21	0.48	0.10	1.21	0.15	0.04	2.41	0.00	2.80	1.40	13.6	66.7
383.0	85	588	0.99	2699	15.92$	48.92	49.43	1.58	0.47	0.10	16.67	0.15	0.03	2.55	0.00	2.17	16.85	11.9	11.4
399.5	85	587	0.99	2699	19.04$	48.34	48.03	1.53	0.45	0.10	20.61	0.13	0.03	2.45	0.00	2.09	20.77	12.9	9.2
404.0	84	588	0.99	2699	22.30$	48.18	47.29	1.43	0.42	0.10	24.41	0.12	0.03	2.27	0.00	1.96	24.56	13.2	7.4
407.7	84	587	0.99	2699	29.35$	49.44	49.51	1.37	0.41	0.09	30.45	0.12	0.03	2.13	0.00	1.88	30.60	10.9	5.8
414.8	86	588	0.99	2699	0.00	47.71	47.61	1.83	0.50	0.12	1.33	0.15	0.03	2.81	0.00	2.46	1.51	14.0	62.1
421.2	48	586	0.99	2699	0.00	51.43	51.98	0.86	0.30	0.06	0.66	0.08	0.04	1.49	0.00	1.23	0.77	7.3	61.4
482.8	49	586	0.99	2699	1.85+	52.74	53.05	0.86	0.24	0.05	0.36	0.05	0.00	2.66	0.00	1.15	0.42	5.0	73.2
460.9	48	586	0.99	2699	4.22+	52.40	53.58	0.74	0.17	0.03	0.38	0.04	0.00	5.69	0.00	0.94	0.41	5.6	69.4
454.4	48	586	0.99	2699	6.85+	52.29	53.82	0.69	0.15	0.03	0.36	0.03	0.00	8.57	0.00	0.86	0.40	5.8	68.5
435.8	48	586	0.99	2699	9.56+	52.56	53.83	0.63	0.13	0.02	0.46	0.03	0.00	11.03	0.00	0.78	0.49	5.3	61.5
430.9	48	586	0.99	2699	15.79+	52.87	54.08	0.51	0.10	0.02	0.49	0.02	0.00	17.14	0.05	0.62	0.51	4.7	55.0
489.5	49	587	0.99	2993	0.00	57.12	58.15	1.01	0.33	0.07	0.52	0.08	0.04	1.58	0.00	1.41	0.64	6.9	68.7
554.2	86	587	0.99	2993	0.00	53.72	54.35	1.83	0.49	0.11	1.19	0.13	0.03	2.93	0.00	2.44	1.36	12.5	64.3

Contd.

580.8	88	585	1.00	2930[##]	8.38[#]	3.28	9.31	2.48	0.00	0.00	1.19	0.00	0.00	1.32	0.00	2.48	1.19	70.4	67.6
649.5	85	585	1.00	2930[##]	1.36*	0.15	1.16	0.13**	0.26	0.00	0.18	0.13	0.13[$$]	0.35	0.00	0.41	0.30	81.2	57.8
616.4	86	585	1.00	2930[##]	2.73*	0.18	1.72	0.24**	0.64	0.04	0.24	0.23	0.16[$$]	0.45	0.08	1.12	0.47	76.6	70.3
602.7	88	585	1.00	2930[##]	5.79*	0.21	2.67	0.50**	1.91	0.10	0.25	0.37	0.18[$$]	0.56	0.49	3.06	0.62	67.1	83.2

[#] External methanol injection in syngas; * External ethanol injection in syngas; [$] External methane injection in syngas; [+] External carbon dioxide injection in syngas
[##] Helium flow; ** Acetaldehyde; [$$] Propionaldehyde

Table 2H (3). Operating conditions and testing results of catalyst # 3.

2H.4. Catalyst # 4 results

Time, *hr*	*P*, *bar*	*T*, *°K*	H_2/CO, *v/v*	GHSV, *L/kg cat/hr*	Products, *mol/kg cat/hr*												CO Conv., *%*	Alc. Sel., *mol %*
					CO	H_2	CH_3OH	C_2H_5OH	C_3H_7OH	CH_4	C_2H_6	C_3H_8	CO_2	H_2O	Tot. Alc.	Tot. HCs		
20.1	84	589	0.99	2993	53.94	52.65	1.45	0.39	0.10	1.46	0.17	0.05	2.79	0.00	1.98	1.68	12.1	54.1
38.3	84	589	0.99	2993	54.04	52.78	1.46	0.40	0.11	1.37	0.16	0.05	2.75	0.00	2.01	1.58	11.9	55.9

Table 2H (4). Operating conditions and testing results of catalyst # 4.

2H.5. Catalyst # 5 results

Time, *hr*	*P*, *bar*	*T*, *°K*	H_2/CO, *v/v*	GHSV, *L/kg cat/hr*	Products, *mol/kg cat/hr*												CO Conv., *%*	Alc. Sel., *mol %*
					CO	H_2	CH_3OH	C_2H_5OH	C_3H_7OH	CH_4	C_2H_6	C_3H_8	CO_2	H_2O	Tot. Alc.	Tot. HCs		
37.8	85	585	0.99	2993	57.84	57.25	0.63	0.20	0.06	0.68	0.08	0.01	1.49	0.00	0.88	0.77	5.8	53.4

Table 2H (5). Operating conditions and testing results of catalyst # 5.

2H.6. Catalyst # 6 results

Time, *hr*	*P*, *bar*	*T*, *°K*	H_2/CO, *v/v*	GHSV, *L/kg cat/hr*	Products, *mol/kg cat/hr*												CO Conv., *%*	Alc. Sel., *mol %*
					CO	H_2	CH_3OH	C_2H_5OH	C_3H_7OH	CH_4	C_2H_6	C_3H_8	CO_2	H_2O	Tot. Alc.	Tot. HCs		
42.3	84	586	0.99	2993	50.95	52.08	1.41	0.48	0.14	1.89	0.25	0.07	4.10	0.00	2.05	2.21	17.0	48.1
64.8	84	572	0.99	2993	55.15	56.28	1.29	0.41	0.00	1.12	0.13	0.04	2.61	0.00	1.69	1.29	10.1	56.7
70.1	83	560	0.99	2993	57.48	58.69	0.91	0.30	0.01	0.59	0.07	0.01	1.60	0.00	1.22	0.67	6.4	64.5
77.4	84	600	0.99	2993	47.33	49.19	1.39	0.48	0.19	2.93	0.42	0.14	6.10	0.00	2.06	3.49	22.9	37.2
87.6	83	585	0.99	2993	51.24	52.17	1.46	0.48	0.14	1.84	0.23	0.06	3.86	0.00	2.10	2.13	16.5	49.6
92.3	84	587	0.99	4461	81.32	82.40	1.88	0.59	0.15	2.02	0.24	0.07	4.14	0.00	2.62	2.33	11.3	53.0
111.1	85	586	0.99	2993	51.48	52.30	1.45	0.47	0.13	1.84	0.21	0.06	3.70	0.00	2.07	2.11	16.1	49.5
117.0	83	584	0.99	2993	51.98	52.78	1.42	0.47	0.12	1.68	0.20	0.05	3.46	0.00	2.03	1.93	15.3	51.2
208.3	83	583	0.99	2993	54.34	55.43	1.37	0.41	0.10	1.23	0.15	0.04	2.92	0.00	1.88	1.42	11.5	57.0
235.5	84	584	0.99	2993	54.31	55.46	1.36	0.40	0.10	1.23	0.15	0.04	2.98	0.00	1.86	1.41	11.5	56.8

Table 2H (6). Operating conditions and testing results of catalyst # 6.

2H.7. Catalyst # 7 results

Time, *hr*	*P*, *bar*	*T*, *°K*	H_2/CO, *v/v*	GHSV, *L/kg cat/hr*	Products, *mol/kg cat/hr*												CO Conv., *%*	Alc. Sel., *mol %*
					CO	H_2	CH_3OH	C_2H_5OH	C_3H_7OH	CH_4	C_2H_6	C_3H_8	CO_2	H_2O	Tot. Alc.	Tot. HCs		
0.5	97	605	1.96	3350	23.35	66.65	0.92	0.08	0.00	8.08	1.28	0.32	9.75	0.12	1.00	9.67	49.5	9.4
0.8	97	607	1.96	3350	26.13	70.37	1.33	0.16	0.03	5.50	1.12	0.40	8.56	0.05	1.52	7.02	43.5	17.8
1.2	97	607	1.96	3350	26.28	70.72	1.29	0.19	0.03	5.22	1.14	0.45	8.50	0.00	1.52	6.80	43.2	18.2
1.5	97	606	1.96	3350	26.68	70.87	1.37	0.21	0.04	5.06	1.10	0.44	8.17	0.00	1.63	6.61	42.3	19.7
2.0	97	606	1.96	3350	27.14	71.11	1.50	0.23	0.05	4.81	1.09	0.43	7.83	0.00	1.78	6.33	41.3	21.9
2.5	97	606	1.96	3350	27.31	71.11	1.58	0.26	0.06	4.69	1.06	0.44	7.64	0.00	1.90	6.20	40.9	23.5
3.0	97	606	1.96	3350	27.62	71.44	1.60	0.27	0.06	4.59	0.99	0.43	7.51	0.00	1.94	6.01	40.3	24.4
3.5	97	606	1.96	3350	27.65	71.39	1.63	0.29	0.06	4.57	0.99	0.41	7.45	0.00	1.99	5.97	40.2	25.0
4.0	97	606	1.96	3350	27.80	71.53	1.66	0.28	0.06	4.48	1.00	0.41	7.38	0.00	2.01	5.89	39.9	25.5
4.5	97	606	1.96	3350	28.05	71.74	1.68	0.30	0.07	4.42	0.93	0.40	7.25	0.00	2.05	5.75	39.3	26.3
5.0	97	606	1.96	3350	28.18	71.90	1.66	0.30	0.07	4.37	0.93	0.39	7.20	0.00	2.04	5.69	39.0	26.4
5.5	97	606	1.96	3350	28.38	72.03	1.69	0.31	0.07	4.31	0.91	0.39	7.08	0.00	2.08	5.60	38.6	27.1
6.0	97	606	1.96	3350	28.05	71.56	1.83	0.33	0.08	4.31	0.90	0.40	7.13	0.00	2.26	5.61	39.3	28.7
6.5	97	605	1.96	3350	28.13	71.59	1.83	0.33	0.08	4.27	0.90	0.42	7.06	0.00	2.25	5.59	39.2	28.6
7.0	97	605	1.96	3350	28.34	71.88	1.78	0.35	0.08	4.22	0.85	0.41	7.01	0.00	2.23	5.48	38.7	28.9
7.5	96	605	1.96	3350	28.33	71.89	1.76	0.36	0.08	4.21	0.89	0.39	7.03	0.00	2.21	5.49	38.7	28.7
8.0	97	605	1.96	3350	28.21	71.56	1.78	0.37	0.11	4.18	0.94	0.41	6.91	0.00	2.27	5.53	39.0	29.1
8.5	98	605	1.96	3350	27.91	71.42	1.75	0.36	0.09	4.28	0.97	0.40	7.14	0.00	2.22	5.65	39.6	28.2
9.0	98	605	1.96	3350	28.35	71.87	1.72	0.37	0.09	4.23	0.88	0.39	6.98	0.00	2.19	5.50	38.7	28.5
9.5	98	605	1.96	3350	28.02	71.33	1.84	0.38	0.09	4.24	0.90	0.44	6.98	0.00	2.33	5.58	39.4	29.4
10.1	98	605	1.96	3350	28.06	71.62	1.80	0.39	0.10	4.26	0.87	0.39	7.15	0.00	2.30	5.51	39.3	29.5

Contd.

10.5	98	605	1.96	3350	28.00	71.59	1.79	0.38	0.10	4.28	0.88	0.39	7.18	0.00	2.28	5.55	39.4	29.1
11.0	98	605	1.96	3350	28.08	71.61	1.81	0.40	0.10	4.24	0.86	0.39	7.11	0.00	2.33	5.49	39.3	29.8
11.5	98	605	1.96	3350	28.08	71.60	1.83	0.40	0.10	4.24	0.85	0.39	7.11	0.00	2.34	5.48	39.3	30.0
11.9	98	605	1.96	3350	28.11	71.62	1.82	0.40	0.10	4.23	0.86	0.38	7.08	0.00	2.34	5.47	39.2	30.0
18.3	98	606	1.96	3350	27.79	71.39	1.82	0.43	0.11	4.33	0.85	0.38	7.28	0.00	2.38	5.55	39.9	30.0
18.9	98	605	1.96	3350	28.24	71.77	1.83	0.44	0.11	4.18	0.81	0.36	7.05	0.00	2.40	5.36	38.9	30.9
19.3	97	605	1.96	3350	28.50	71.96	1.84	0.43	0.11	4.12	0.80	0.36	6.90	0.00	2.40	5.27	38.4	31.3
21.0	97	606	1.96	3350	27.71	71.32	1.82	0.45	0.12	4.33	0.85	0.38	7.32	0.00	2.41	5.55	40.1	30.2
21.6	97	605	1.96	3350	27.97	71.49	1.84	0.45	0.12	4.26	0.82	0.37	7.16	0.00	2.43	5.44	39.5	30.9
22.0	97	605	1.96	3350	28.08	71.56	1.84	0.46	0.12	4.20	0.81	0.37	7.07	0.00	2.44	5.38	39.3	31.2
22.5	97	605	1.96	3350	28.16	71.65	1.83	0.46	0.12	4.19	0.81	0.36	7.04	0.00	2.44	5.36	39.1	31.3
23.0	97	605	1.96	3350	28.12	71.58	1.86	0.46	0.12	4.19	0.81	0.36	7.04	0.00	2.46	5.36	39.2	31.5
36.5	97	606	1.96	3350	27.65	71.22	1.86	0.47	0.13	4.35	0.82	0.36	7.33	0.00	2.48	5.53	40.2	31.0
38.3	97	606	1.96	3350	27.86	71.33	1.89	0.48	0.13	4.29	0.80	0.35	7.19	0.00	2.52	5.45	39.7	31.6
38.7	97	605	1.96	3350	28.03	71.44	1.89	0.47	0.12	4.25	0.79	0.35	7.08	0.00	2.51	5.39	39.4	31.7
39.1	97	605	1.96	3350	28.37	71.75	1.90	0.47	0.13	4.14	0.77	0.34	6.91	0.00	2.51	5.26	38.6	32.3
38.2	97	606	1.96	3350	27.98	71.44	1.88	0.47	0.13	4.26	0.79	0.35	7.13	0.00	2.50	5.41	39.5	31.7
41.6	97	586	1.96	3350	33.04	75.41	2.35	0.60	0.13	2.54	0.39	0.16	4.34	0.00	3.10	3.08	28.5	50.1
46.2	97	572	1.96	3350	37.93	80.87	2.33	0.58	0.10	1.04	0.22	0.07	2.83	0.00	3.01	1.34	18.0	69.2
69.9	97	572	0.99	3360	61.07	59.88	1.42	0.60	0.11	0.94	0.20	0.07	2.85	0.00	2.14	1.20	11.4	64.0
63.8	97	587	0.99	3360	55.58	54.32	1.66	0.69	0.17	2.30	0.42	0.16	4.99	0.00	2.55	2.88	19.4	46.9
66.8	97	607	0.99	3360	46.54	46.60	1.35	0.56	0.19	5.22	1.00	0.46	9.66	0.00	2.14	6.67	32.5	24.3
231.0	84	524	0.99	2993	60.70	60.07	0.28	0.07	0.00	0.05	0.00	0.00	0.21	0.00	0.36	0.05	1.1	87.7
186.5	84	540	0.99	2993	59.79	59.02	0.52	0.16	0.02	0.12	0.02	0.00	0.51	0.00	0.70	0.15	2.6	82.9
206.6	84	568	0.99	2993	56.59	55.63	1.14	0.38	0.07	0.58	0.12	0.03	1.78	0.00	1.58	0.74	7.8	68.3

Contd.

209.3	83	586	0.99	2993	52.67	51.54	1.43	0.49	0.12	1.39	0.26	0.10	3.22	0.00	2.06	1.75	14.2	54.1
213.9	84	605	0.99	2993	47.59	47.37	1.26	0.45	0.15	2.56	0.58	0.25	5.68	0.00	1.88	3.38	22.5	35.8
233.9	84	622	0.99	2993	41.79	43.23	0.85	0.29	0.11	4.16	1.07	0.49	9.06	0.00	1.28	5.72	31.9	18.3
238.4	84	644	0.99	2993	39.91	41.83	0.52	0.14	0.05	4.91	1.32	0.63	10.13	0.00	0.73	6.85	35.0	9.7
261.7	85	665	0.99	2993	39.77	41.54	0.28	0.08	0.03	5.33	1.43	0.61	10.16	0.00	0.41	7.37	35.2	5.2
256.3	84	585	1.00	2259	38.28	37.53	1.10	0.40	0.11	1.32	0.24	0.09	2.85	0.00	1.63	1.64	17.2	49.8
161.8	84	586	0.99	3360	59.60	58.30	1.50	0.54	0.13	1.46	0.29	0.11	3.44	0.00	2.18	1.86	13.6	54.0
166.3	84	586	0.99	4461	81.78	79.72	1.74	0.61	0.13	1.51	0.28	0.10	3.46	0.00	2.49	1.88	10.8	56.9
87.6	98	587	0.99	4461	78.49	76.46	2.06	0.79	0.18	2.15	0.40	0.14	4.86	0.00	3.05	2.69	14.4	53.1
93.8	98	588	0.99	6664	122.95	119.54	2.50	0.92	0.19	2.12	0.39	0.14	4.91	0.00	3.61	2.65	10.3	57.6
116.3	98	588	0.99	8867	168.87	164.42	2.91	1.02	0.19	2.07	0.39	0.13	4.89	0.00	4.12	2.59	7.5	61.3
159.2	83	586	1.96	3350	36.45	78.99	2.17	0.49	0.10	1.76	0.29	0.11	3.14	0.00	2.77	2.15	21.2	56.2
110.5	98	588	1.96	4448	47.80	104.04	3.16	0.70	0.14	2.44	0.38	0.14	4.32	0.00	4.00	2.96	22.1	57.5
182.0	84	586	1.96	4448	51.32	108.07	2.47	0.54	0.10	1.65	0.27	0.10	3.02	0.00	3.12	2.02	16.4	60.7
134.7	98	588	1.96	6644	75.51	160.06	3.77	0.85	0.14	2.35	0.39	0.14	4.46	0.00	4.76	2.88	17.6	62.3
139.9	98	589	1.96	8840	107.38	221.15	4.20	0.94	0.16	2.31	0.40	0.13	4.49	0.00	5.31	2.84	11.9	65.1

Table 2H (7). Operating conditions and testing results of catalyst # 7.

2H.8. Catalyst # 8 results

Time, *hr*	*P*, *bar*	*T*, *°K*	H_2/CO, *v/v*	GHSV, *L/kg cat/hr*	Products, *mol/kg cat/hr*												CO Conv., *%*	Alc. Sel., *mol %*
					CO	H_2	CH_3OH	C_2H_5OH	C_3H_7OH	CH_4	C_2H_6	C_3H_8	CO_2	H_2O	Tot. Alc.	Tot. HCs		
60.5	84	589	0.99	2993	57.38	56.43	0.82	0.24	0.05	0.73	0.12	0.04	1.47	0.00	1.11	0.89	6.5	55.6
65.4	83	601	0.99	2993	55.43	54.48	0.86	0.26	0.07	1.10	0.18	0.07	2.15	0.00	1.19	1.35	9.7	46.9
111.5	97	590	0.99	3360	61.59	60.65	1.13	0.43	0.10	1.10	0.19	0.06	2.80	0.00	1.69	1.35	10.7	55.5
109.2	97	602	0.99	3360	58.25	57.41	1.19	0.48	0.14	1.82	0.31	0.11	4.07	0.00	1.85	2.23	15.5	45.3
113.5	97	613	0.99	3360	54.48	54.01	1.20	0.50	0.18	2.94	0.49	0.19	5.90	0.00	1.95	3.62	21.0	35.0
66.3	97	602	1.96	3350	36.95	79.37	1.96	0.40	0.11	1.81	0.26	0.10	2.81	0.00	2.47	2.17	20.1	53.2
86.0	96	602	1.96	3350	36.35	79.78	1.57	0.41	0.11	2.00	0.31	0.11	3.64	0.00	2.11	2.43	21.4	46.5
90.0	96	613	1.96	3350	33.52	76.98	1.56	0.39	0.13	2.71	0.43	0.17	4.68	0.00	2.12	3.32	27.5	39.0
93.0	96	624	1.96	3350	31.56	75.33	1.37	0.34	0.13	3.44	0.57	0.25	5.70	0.00	1.90	4.26	31.7	30.8
159.2	87	599	1.04	607	7.59	8.46	0.24	0.11	0.05	1.03	0.17	0.07	2.14	0.00	0.43	1.27	37.7	25.2
157.4	87	600	1.01	1157	16.64	17.26	0.51	0.22	0.09	1.41	0.23	0.09	3.03	0.00	0.86	1.73	29.3	33.1
227.8	86	600	1.01	1157	16.97	17.43	0.56	0.23	0.09	1.34	0.21	0.08	2.81	0.00	0.91	1.62	27.9	36.1
155.3	87	600	1.00	2259	37.48	37.30	0.96	0.37	0.12	1.51	0.25	0.09	3.49	0.00	1.49	1.86	18.9	44.5
198.6	90	601	0.99	2993	52.61	51.90	1.30	0.46	0.13	1.41	0.24	0.08	3.47	0.00	1.92	1.72	14.3	52.7
133.8	86	601	0.99	3360	60.67	59.87	1.07	0.41	0.12	1.43	0.24	0.08	3.27	0.00	1.62	1.76	12.0	48.0
161.7	88	601	0.99	4461	82.09	80.60	1.53	0.53	0.14	1.43	0.24	0.08	3.63	0.00	2.22	1.76	10.4	55.8
206.0	86	601	0.99	4461	82.88	81.28	1.53	0.50	0.13	1.24	0.21	0.07	3.25	0.00	2.18	1.52	9.6	59.0
164.6	88	601	0.99	5563	104.51	102.14	1.69	0.58	0.15	1.43	0.24	0.10	3.44	0.00	2.44	1.77	8.6	57.9
208.5	85	602	0.99	6664	128.73	126.20	1.80	0.58	0.13	1.19	0.20	0.06	3.24	0.00	2.51	1.45	6.1	63.3
211.0	86	602	0.99	8867	174.42	170.99	1.95	0.61	0.12	1.08	0.19	0.00	3.13	0.00	2.68	1.27	4.4	67.9
216.0	86	602	0.99	11069	219.53	215.05	2.11	0.65	0.13	1.11	0.19	0.00	3.15	0.00	2.88	1.30	3.7	68.9
178.8	88	600	1.96	1154	9.82	24.73	0.76	0.19	0.07	1.35	0.20	0.07	2.39	0.00	1.05	1.62	38.4	39.2
178.1	88	601	1.96	2252	22.71	51.66	1.39	0.33	0.10	1.54	0.24	0.08	2.96	0.00	1.85	1.86	27.0	49.8
203.8	90	601	1.96	3350	37.24	80.36	1.91	0.43	0.11	1.52	0.24	0.08	3.10	0.00	2.47	1.84	19.5	57.4

Contd.

182.3	89	601	1.96	4448	51.66	109.18	2.16	0.49	0.12	1.47	0.25	0.08	3.25	0.00	2.79	1.80	15.8	60.8
184.4	89	602	1.96	5546	67.00	139.01	2.43	0.54	0.13	1.47	0.25	0.09	3.30	0.00	3.12	1.81	12.4	63.3
180.6	89	602	1.96	6644	81.34	167.60	2.61	0.60	0.13	1.80	0.27	0.09	3.53	0.00	3.34	2.15	11.3	60.8
213.5	86	602	1.96	8840	113.13	228.65	2.65	0.58	0.11	1.31	0.21	0.00	2.96	0.00	3.34	1.51	7.2	68.8
218.4	86	602	1.96	11036	143.11	287.63	2.83	0.61	0.12	1.31	0.21	0.00	2.99	0.00	3.56	1.52	6.0	70.0
229.8	86	491	1.01	1157	22.97	23.12	0.18	0.05	0.01	0.05	0.00	0.00	0.19	0.00	0.24	0.05	2.4	82.1

Table 2H (8). Operating conditions and testing results of catalyst # 8.

2H.10. Catalyst # 10 results

Time, *hr*	***P*, *bar***	***T*, °K**	**H_2/CO, *v/v***	**GHSV, *L/kg cat/hr***	**Products, *mol/kg cat/hr***												**CO Conv., *%***	**Alc. Sel., *mol %***
					CO	**H_2**	**CH_3OH**	**C_2H_5OH**	**C_3H_7OH**	**CH_4**	**C_2H_6**	**C_3H_8**	**CO_2**	**H_2O**	**Tot. Alc.**	**Tot. HCs**		
259.0	94	577	0.99	2993	50.90	50.41	2.17	0.31	0.05	2.09	0.36	0.13	3.43	0.10	2.53	2.59	17.1	49.5
266.1	95	577	0.99	2993	50.53	50.42	2.06	0.37	0.07	2.08	0.36	0.13	3.72	0.04	2.50	2.57	17.7	49.3
276.3	94	577	0.99	2993	50.64	51.06	1.74	0.44	0.09	1.96	0.36	0.13	3.88	0.05	2.27	2.44	17.5	48.1

Table 2H (10). Operating conditions and testing results of catalyst # 10.

2H.9. Catalyst # 9 results

Time, *hr*	*P*, *bar*	*T*, *°K*	H_2/CO, *v/v*	GHSV, *L/kg cat/hr*	Products, *mol/kg cat/hr*												CO Conv., *%*	Alc. Sel., *mol %*
					CO	H_2	CH_3OH	C_2H_5OH	C_3H_7OH	CH_4	C_2H_6	C_3H_8	CO_2	H_2O	Tot. Alc.	Tot. HCs		
208.6	85	603	0.99	2993	51.81	50.94	1.08	0.36	0.09	1.68	0.39	0.17	3.55	0.00	1.52	2.25	15.6	40.4
221.8	85	585	0.99	2993	55.39	54.05	1.17	0.33	0.06	0.98	0.18	0.07	1.99	0.00	1.55	1.23	9.8	55.9
225.9	84	566	0.99	2993	58.53	57.44	0.88	0.21	0.00	0.45	0.07	0.00	0.96	0.00	1.10	0.52	4.6	67.9
230.8	85	618	0.99	2993	47.86	47.85	1.00	0.27	0.08	2.68	0.69	0.33	5.69	0.00	1.36	3.70	22.0	26.8
242.7	85	584	0.99	2993	55.71	54.35	1.19	0.32	0.06	0.96	0.28	0.07	1.94	0.00	1.57	1.31	9.2	54.6
303.1	84	583	1.01	1157	18.86	18.89	0.58	0.19	0.04	0.89	0.16	0.06	1.78	0.00	0.81	1.11	19.8	42.3
314.4	84	582	0.99	4461	83.96	82.48	1.24	0.44	0.00	1.27	0.24	0.08	2.93	0.00	1.68	1.59	8.4	51.4
325.1	85	583	0.99	6664	130.08	127.89	1.24	0.45	0.00	1.26	0.24	0.08	2.89	0.00	1.69	1.59	5.1	51.5
328.8	84	584	0.99	8867	175.37	172.45	1.28	0.49	0.00	1.33	0.25	0.00	3.06	0.00	1.77	1.58	3.9	52.8
330.8	84	585	0.99	11069	220.50	216.69	1.44	0.49	0.00	1.34	0.26	0.00	3.17	0.00	1.93	1.60	3.3	54.6
348.9	85	581	0.99	2993	54.36	53.62	1.19	0.36	0.07	1.03	0.23	0.08	2.75	0.00	1.62	1.33	11.4	54.9
399.3	84	582	0.99	2993	54.35	53.43	1.13	0.34	0.06	0.98	0.21	0.07	2.51	0.00	1.54	1.25	11.4	55.0
446.3	84	581	0.99	2993	54.70	53.65	1.11	0.34	0.06	0.96	0.18	0.06	2.29	0.00	1.52	1.20	10.9	55.8
467.7	85	581	0.99	2993	54.62	53.57	1.15	0.33	0.06	0.98	0.19	0.06	2.34	0.00	1.53	1.23	11.0	55.5
473.1	84	581	0.99	2993	54.77	53.70	1.13	0.33	0.06	0.95	0.18	0.06	2.26	0.00	1.52	1.18	10.8	56.3
493.8	84	581	0.99	2993	55.08	53.94	1.16	0.31	0.06	0.88	0.17	0.06	2.11	0.00	1.53	1.10	10.3	58.1
497.2	85	582	0.99	2993	55.10	53.86	1.21	0.32	0.06	0.85	0.16	0.05	2.04	0.00	1.59	1.07	10.2	59.8
517.2	84	583	0.99	2993	55.15	53.85	1.25	0.31	0.06	0.84	0.16	0.05	1.99	0.00	1.62	1.05	10.1	60.6
542.0	85	581	0.99	2993	56.18	54.95	1.31	0.32	0.06	0.79	0.14	0.05	1.86	0.00	1.69	0.98	8.5	63.3
545.1	84	581	0.99	2993	55.70	54.26	1.37	0.33	0.06	0.75	0.14	0.05	1.79	0.00	1.76	0.93	9.3	65.4
564.0	84	582	0.99	2993	56.24	54.86	1.35	0.34	0.06	0.77	0.14	0.04	1.76	0.00	1.74	0.96	8.4	64.6

Table 2H (9). Operating conditions and testing results of catalyst # 9.

2.9. References

1. Kinkade, N., *Process for producing alcohols from carbon monoxide and hydrogen using an alkali-molybdenum sulfide catalyst*, in *PCT Int. Pat. Publication No. WO*. 1985, Patent WO 85/03073. p. 03073.
2. Santiesteban, J.G., *Alcohol Synthesis from Carbon Monoxide and Hydrogen over MoS_2-based Catalysts*, in *Chemistry*. 1989, Lehigh University.
3. Iranmahboob, J., *Formation of Ethanol and Higher Alcohols from Syngas*, in *Chemical Engineering*. 1999, Mississippi State University.
4. Iranmahboob, J., H. Toghiani, and D.O. Hill, *Dispersion of alkali on the surface of Co-MoS_2/clay catalyst: a comparison of K and Cs as a promoter for synthesis of alcohol.* Applied Catalysis A: General, 2003. **247**(2): p. 207-218.
5. Cochran, G.A., et al., *Preparation of ethanol and higher alcohols from lower carbon number alcohols*. 1989, Patent US4825013.
6. Quarderer, G. and K. Cochran, *Catalytic process for producing mixed alcohols from hydrogen and carbon monoxide*, in *European Patent 0,119,609*. 1984, WO 84/03696.
7. Li, Z.-r., et al., *Active carbon supported Mo–K catalysts used for alcohol synthesis.* Journal of Catalysis, 2001. **199**(2): p. 155-161.
8. Bian, G.-z., et al., *High temperature calcined K–MoO_3/γ-Al_2O_3 catalysts for mixed alcohols synthesis from syngas: Effects of Mo loadings.* Applied Catalysis A: General, 1998. **170**(2): p. 255-268.

9. Voorhies, J.D., *Process for improved carbon-supported hydrodesulfurization catalysts*. 1978, Patent US4082652.

10. Afanasiev, P., *Synthetic approaches to the molybdenum sulfide materials.* Comptes Rendus Chimie, 2008. **11**(1-2): p. 159-182.

11. Tslgdinos, G.A., H.Y. Chen, and B.J. Streusand, *Molybdate Solutions for Catalyst Preparation. Stability, Adsorption Properties, and Characterization.* Ind. Eng. Chem. Prod. Res. Dev., 1981. **20**: p. 619-623.

12. Li, X., et al., *Higher Alcohols from Synthesis Gas using Carbon-Supported Doped Molybdenum-based Catalysts.* Ind. Eng. Chem. Res., 1998. **37**: p. 3853-3863.

13. Thomazeau, C., V. Martin, and P. Afanasiev, *Effect of support on the thermal decomposition of $(NH_4)_6Mo_7O_{24}{\cdot}4H_2O$ in the inert gas atmosphere.* Applied Catalysis A: General, 2000. **199**(1): p. 61-72.

14. Surisetty, V.R., A. Tavasoli, and A.K. Dalai, *Synthesis of higher alcohols from syngas over alkali promoted MoS_2 catalysts supported on multi-walled carbon nanotubes.* Applied Catalysis A: General, 2009. **365**(2): p. 243-251.

15. Christensen, J.M., *Catalytic synthesis of long-chained alcohols from syngas*, in *Department of Chemical and Biochemical Engineering*. 2011, Technical University of Denmark.

16. Jong, A.M.d., et al., *Sulfidation Mechanism of Molybdenum Catalysts Supported on a SiO_2/Si(100) Model Support Studied by Surface Spectroscopy.* J. Phys. Chem., 1993. **97**: p. 6477-6483.

17. Liu, Z., et al., *Screening of alkali-promoted vapor-phase-synthesized molybdenum sulfide catalysts for the production of alcohols from synthesis gas.* Industrial & engineering chemistry research, 1997. **36**(8): p. 3085-3093.

18. Papageorgopoulos, C., *Adsorption of Cs and O_2 on MoS_2.* Surface Science, 1978. **75**(1): p. 17-28.

19. Woo, H.C., et al., *Surface species on the oxidized K_2CO_3/MoS_2 and their effects on catalytic carbon monoxide hydrogenation.* Applied Catalysis A: General, 1993. **104**: p. 199-214.

20. Woo, H.C., et al., *Room-Temperature Oxidation of K_2CO_3/MoS_2 Catalysts and Its Effects on Alcohol Synthesis from CO and H_2.* Journal of Catalysis, 1992. **138**: p. 525-535.

21. Ross, S. and A. Sussman, *Surface Oxidation of Molybdenum Disulfide.* J. Phys. Chem., 1955. **59**(9): p. 889-892.

22. Dietz, W.A., *Response Factors for Gas Chromatographic Analysis.* J Chromatogr Sci, 1967. **5**(2): p. 68-71.

23. Rosie, D.M. and R.L. Grob, *Thermal conductivity behavior. Importance in quantitative gas chromatography.* Analytical Chemistry, 1957. **29**(9): p. 1263-1264.

24. Gislason, J. and S.M. Wharry, *Relative Molar Response Factors for Thermal Conductivity Detectors.* Journal of Chromatographic Science, 2000. **38**: p. 129-132.

25. Hoffmann, E., *Calculation of Relative Molar Response Factors of Thermal Conductivity Detectors in Gas Chromatography.* Analytical Chemistry, 1962. **34**(10): p. 1216-1222.

26. Jalali-Heravi, M. and M.H. Fatemi, *Prediction of thermal conductivity detection response factors using an artificial neural network.* Journal of Chromatography A, 2000. **897**: p. 227-235.

27. Katritzky, A.R., et al., *Prediction of Gas Chromatographic Retention Times and Response Factors Using a General Qualitative Structure-Property Relationships Treatment.* Anal. Chem., 1994. **66**(11): p. 1799-1807.

28. *JCPDS - International Centre for Diffraction Data, Powder Diffraction File - 4, 2014, 2015*. Newtown Square, PA 19073-3273, USA.

29. Wagner, C.D., et al., *Handbook of X-Ray Photoelectron Spectroscopy*. Perkin-Elmer Corporation.

30. Castle, J.E., *The Composition of Metal Surfaces After Atmospheric Exposure: An Historical Perspective.* The Journal of Adhesion, 2008. **84**(4): p. 368-388.

31. Irfan, F. So, and Y. Gao, *Photoemission Spectroscopy Characterization of Attempts to Deposit MoO_2 Thin Film.* International Journal of Photoenergy, 2011. **2011**: p. 1-6.

32. Fairley, N., *CasaXPS, Casa Software Ltd., Teighnmouth, Devon, UK 2003*.

33. Spevack, P.A., *Reaction and Oxidation Chemistry of Molybdenum Oxide and Sulfide Surfaces*, in *Department of Chemistry*. 1993, The University of Western Ontario.

34. Weber, T., et al., *Basic Reaction Steps in the Sulfidation of Crystalline MoO_3 to MoS_2, As Studies by X-ray Photoelectron and Infrared Emission Spectroscopy.* J. Phys. Chem., 1996. **100**: p. 14144-14150.

35. Baker, M.A., et al., *XPS investigation of preferential sputtering of S from MoS_2 and determination of MoS_x stoichiometry from Mo and S peak positions.* Applied Surface Science, 1999. **150**: p. 255-262.

36. Arnoldy, P., et al., *Temperature-Programmed Sulfiding of MoO_3/Al_2O_3 Catalysts.* Journal of Catalysis, 1985. **92**: p. 35-55.

37. Hensley, J.E., S. Pylypenko, and D.A. Ruddy, *Deactivation and stability of K-$CoMoS_x$ mixed alcohol synthesis catalysts.* Journal of Catalysis, 2014. **309**: p. 199-208.

38. Surisetty, V.R., A.K. Dalai, and J. Kozinski, *Synthesis of higher alcohols from synthesis gas over Co-promoted alkali-modified MoS_2 catalysts supported on MWCNTs.* Applied Catalysis A: General, 2010. **385**(1): p. 153-162.

39. Woo, H., et al., *Structure and Distribution of Alkali Promoter in K/MoS_2 Catalysts and Their Effects on Alcohol Synthesis from Syngas.* Journal of Catalysis, 1993. **142**(2): p. 672-690.

40. Iranmahboob, J. and D.O. Hill, *Alcohol synthesis from syngas over $K_2CO_3/CoS/MoS_2$ on activated carbon.* Catalysis Letters, 2002. **78**(1-4): p. 49-55.

41. Christensen, J.M., et al., *Effects of H_2S and process conditions in the synthesis of mixed alcohols from syngas over alkali promoted cobalt-molybdenum sulfide.* Applied Catalysis A: General, 2009. **366**(1): p. 29-43.

42. Park, T.Y., I.-S. Nam, and Y.G. Kim, *Kinetic analysis of mixed alcohol synthesis from syngas over K/MoS_2 catalyst.* Industrial & engineering chemistry research, 1997. **36**(12): p. 5246-5257.

Chapter 3

Effect of Sulfidation Temperature on Activated Carbon Supported Cesium-Promoted Molybdenum Sulfide Catalysts for Higher Alcohol Synthesis from Syngas

The direct sulfidation of AMT promoted AC pellets and the effect of sulfidation temperature on catalyst performance described in this chapter has been titled "An Improved Method for the Preparation of Novel Catalyst for Ethanol and Higher Alcohols Synthesis" by Ranjan K. Sahoo, Hugo S. Caram, Divyanshu R. Acharya, and Richard G. Herman, *manuscript in preparation for US patent.*

The work described in this chapter has been titled "Effect of Sulfidation Temperature on Activated Carbon Supported Cesium-Promoted Molybdenum Sulfide Catalysts for Higher Alcohol Synthesis from Syngas" by Ranjan K. Sahoo, Hugo S. Caram, Divyanshu R. Acharya, and Richard G. Herman, *manuscript in preparation.*

Abstract

The cesium promoted molybdenum based supported catalysts were prepared and tested for higher alcohol synthesis. The basic steps involved are formation of crystalline molybdenum dioxide upon thermal decomposition of highly dispersed ammonium molybdate tetrahydrate on activated carbon support, followed by transformation to sulfide complexes upon sulfidation, and cesium promotion being the last step. The effect of sulfidation temperature on catalyst performance in-terms of alcohol yields, alcohol selectivity, and carbon monoxide conversion was studied. Increase in alcohol yields, alcohol selectivity, and catalyst activity was observed with increase in sulfidation

temperature. The XRD analysis reveals that, a sulfidation temperature of 723.15 °K was not enough for complete sulfidation of molybdenum dioxide to molybdenum disulfide. The complete conversion to molybdenum disulfide was achieved at an elevated temperature of 923.15 °K. The increase in alcohol yields, alcohol selectivity, and catalyst activity with increase in sulfidation temperature was attributed to the increase in molybdenum disulfide phase and decrease in molybdenum dioxide phase.

Another attempt was made to prepare the catalyst by direct sulfidation of ammonium molybdate tetrahydrate dispersed on activated carbon support. A sulfidation temperature of 923.15 °K was used for this process. The catalyst was tested extensively at higher alcohol synthesis conditions to; determine the stabilization time, collect steady-state experimental results for kinetic analysis, and study the long-term stability of the catalyst. The formation of alcohols was observed immediately upon syngas exposure. The steady-state results were collected after 385 hrs of reactions for kinetic analysis. The catalyst maintains its activity for more than 600 hours of syngas exposure. The presence of water and sulfur compounds was not observed in the product at any time. The alcohol selectivity was improved to 46 mol% and 56 mol% respectively by high temperature sulfidation of calcined pellets at 923.15 °K and direct sulfidation of ammonium molybdate tetrahydrate promoted pellets at 923.15 °K from an alcohol selectivity of 43 mol% for the catalyst sulfidized at 723.15 °K.

Similar preparation method was also applied to prepare the molybdenum sulfide based supported catalyst using molybdenum dioxydiacetylacetonate as the molybdenum precursor and cobalt containing molybdenum oxide based supported catalyst. An alcohol selectivity of 53 mol% was observed for the catalyst prepared from molybdenum

dioxydiacetylacetonate. The C_2^+ to methanol weight ratio of 3.21 was achieved with an expense of alcohol selectivity to 18 mol% for the cobalt based molybdenum oxide catalyst.

3.1. Objective

It was observed from the previous chapter that, the complete sulfidation of molybdenum dioxide to molybdenum disulfide was not achieved at 723.15 °*K*. This chapter primarily focused on high temperature sulfidation and its effect on catalyst performance. The objective of this chapter is:

- To study the effect of high temperature sulfidation of calcined pellets on catalyst composition and its effect on catalyst performance.
- Direct sulfidation of ammonium molybdate tetrahydrate promoted activated carbon pellets at high temperature and its effect on catalyst performance.
- To study the long-term stability of the catalyst prepared from direct sulfidation of ammonium molybdate tetrahydrate promoted activated carbon pellets.
- Collection of steady-state experimental data for kinetic analysis.
- Use of molybdenum dioxydiacetylacetonate as an alternative molybdenum precursor.
- Preparation and testing of the cobalt containing molybdenum based oxide catalyst supported on activated carbon.

3.2. Catalyst Preparation

The catalyst preparation process parameters, such as the batch size, promotion rates, temperature, ramp time or temperature rate, and time of each preparation steps were summarized in Table 3.1. Following attempts were made on the catalyst preparation process described in chapter 2 to improve the catalyst performance in terms of catalyst activity and alcohol selectivity:

- High temperature sulfidation of the calcined pellets (MoO_2/AC).
- Direct sulfidation of the AMT promoted AC pellets at a high temperature (eliminating the calcination step).
- Addition of Cobalt, Co: Cobalt containing oxide catalyst, Cs/CoO/MoO_2/AC was prepared and tested.
- Different Mo precursor: Molybdenum dioxydiacetylacetonate ($MoO_2(acac)_2$) was used as the Mo precursor instead of AMT [1].

3.2.1. High Temperature Sulfidation

The catalyst number 11 and number 12 were prepared by employing a high temperature sufidation of 923.15 °*K* [1]. The detailed catalyst preparation procedure is given in section 2.2.3 of chapter 2. The testing results from the catalyst number 3 (723.15 °*K* sulfidation, chapter 2), number 11 (923.15 °*K* sulfidation) and number 13 (no sulfidation) were compared to access the effect of sulfidation temperature on catalyst performance. Catalyst number 13 was prepared without sulfidizing the pellets.

Cat. No.	AMT Promotion		Calcination					Sulfidation				CsCOOH Promotion		
	Batch, *g*	Rate, *ml/h*	Batch, *g*	Max. T, *°K*	Ramp, *°K/min*	Time, *hr*	Mo, *wt %*	Batch, *g*	Max. T, *°K*	Ramp, *hr*	Time, *hr*	Batch, *g*	Rate, *ml/hr*	Cs/Mo, *mol/mol*
11	30.0	10.0	14	773.15	5	20	15.5	4.0	923.15	1	8.5	3.9	8.0	0.82
12	42.0**	20.0	13.5	773.15	5	18	14.5	12.0	923.15	2	17.0	12.0	7.0	0.78
13	30.0	10.0	14	773.15	5	20	15.5	n.a.	n.a.	n.a.	n.a.	4.0	7.5	0.84
14	42.0**	20.0	n.a.	n.a.	n.a.	n.a.	14.5	13.5	923.15	2	20.0	12.5	7.0	0.76
15	30.0	10.0	n.a.	n.a.	n.a.	n.a.	15.5	5.0	723.15^{S} /923.15	1	8.7^{S} /7.5	4.0	8.0	0.82
16	30.0	10.0	14	773.15	5	20	15.5	n.a.	n.a.	n.a.	n.a.	n.a.	n.a.	n.a.
	8.0$^{\#}$	12.0$^{\#}$	10$^{\#\#}$	923.15	5	20	0.57^{+}					4.0	7.0	0.81
17	20.0*	20.0	9	773.15	5	20	12.3	4.8	723.15	1	8.0	3.8	7.0	0.89

* $MoO_2(acac)_2$ was used as Mo precursor

$^{\#}$ MoO_2/AC was for cobalt acetate tetrahydrate promotion

$^{\#\#}$ Cobalt acetate tetrahydrate promoted MoO_2/AC used for high temperature calcination; $^{+}$ Co/Mo molar ratio

^{S} Step-wise sulfidation, 723.15 °*K* for 8.7 *hr* and 923.15 °*K* for 7.5 *hr*

** Acid washed activated carbon (3 *mm*) from Prominent Systems, Inc.

Table 3.1. Catalyst preparation process parameters (modification of the process).

3.2.2. Direct Sulfidation of AMT Promoted Pellets

The basic catalyst preparation steps are shown in Fig. 3.1. The catalyst number 14 and number 15 were prepared by direct sulfidation and step-wise sulfidation of AMT promoted AC pellets respectively. All other steps, such as, support preparation, AMT promotion, and cesium promotion was similar to the process described in section 2.2.3 of chapter 2.

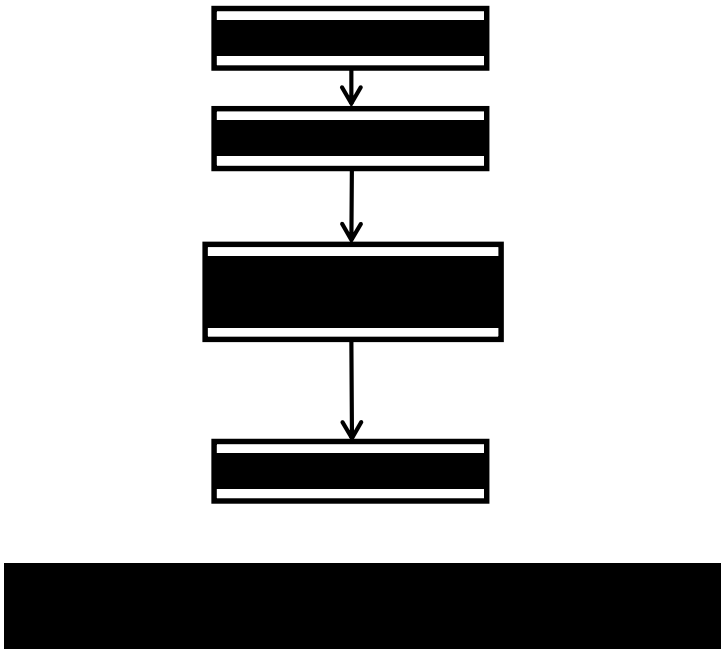

3.3.3. Cobalt Containing Oxide Catalyst

The MoO_2/AC (calcined) pellets were promoted with an aqueous solution of cobalt acetate tetrahydrate (Sigma-Aldrich, CAS Number 6147-53-1), using a solution feed rate of 12 *ml/hr* in a Rotovap, as described in the AMT promotion, section 2.2.3.2 of

chapter 2. The Co solution was prepared by dissolving 3.75 *g* of cobalt acetate tetrahydrate in 75 *ml* of DI water. The target Co/Mo molar ratio was 0.6. The Co promoted MoO_2/AC was calcined at an elevated temperature of 923.15 °*K*, under flowing N_2 in a quartz tube reactor. The calcined pellets were promoted with cesium formate as described in chapter 2 (section 2.3.3.5). The catalyst preparation process parameters are given in Table 3.1 (catalyst number 16).

3.3.4. $MoO_2(acac)_2$ as the Mo Precursor

The acid washed AC pellets were promoted with a solution of $MoO_2(acac)_2$ (Sigma-Aldrich, CAS Number 17524-05-9), using a solution feed rate of 20 *ml/hr* in a Rotovap, as described in the AMT promotion, section 2.2.3.2 of chapter 2. The $MoO_2(acac)_2$ solution, prepared by dissolving 14.95 *g* of $MoO_2(acac)_2$ in 300 *ml* of 95 *%* ethanol (Sigma-Aldrich, CAS Number 64-17-5) [2], was used to promote 20.02 *g* of acid washed AC. The $MoO_2(acac)_2$ promoted AC was calcined, sulfidized and promoted with cesium formate, as described in chapter 2 (section 2.2.3). The preparation process parameters are given in Table 3.1 (catalyst number 17).

The Mo content of the catalysts was also reported in Table 3.1. In calculation of Mo *wt %*, it was assumed that, the AC weight does not change by high temperature application and only MoO_2/AC was present after the calcination step. The CoO was assumed to be present after calcination of Co containing catalyst for the calculation of Co composition [3]. Example catalyst composition calculations for catalyst number 14 (direct sulfidation) is given in Appendix 3A.

3.3. Catalyst Testing Results and Discussions

In each test, a 3 *g* (4 *ml*) of catalyst was tested under HAS reaction conditions. The detailed description of catalyst testing and analytical procedures is given in section 2.3 of chapter 2. An example mass balance calculation is given in Appendix 3B. The testing results of all the catalysts are given in Appendix 3C. In this section, only selected results are presented.

3.3.1. Effect of Sulfidation Temperature

The performance of catalyst number 13, number 3, and number 11 were compared at similar HAS reaction conditions. The product yields, CO conversion, and alcohol selectivity are listed in Table 3.2. The graphical representation of catalyst performance is also shown in Fig. 3.2 and Fig. 3.3. The product yields, CO conversion and alcohol selectivity were progressively improved upon high temperature sulfidation from no sufidation to a sulfidation temperature of 923.15 °*K*. The ethanol yield, CO conversion, and alcohol selectivity for the catalyst number 11, sulfidized at 923.15 °*K*, is 0.651 *mol/kg cat/hr*, 22.75 *%*, and 46.15 *mol %*, respectively compared to 0.201, 9.82, and 35.08 respectively for an un-sulfidied catalyst, number 13.

Cat. #	Sulfidation Temp., °*K*	Testing (HAS) Conditions			Products, *mol/kg cat/hr*				CO Conv, *%*	Alc. Sel., m*ol %*
		T, °*K*	Pressure, *bar*	Time, *hr*	CH_3OH	C_2H_5OH	$C_3H_7OH^+$	CH_4		
13	n.a.	589	84.3	16.5	0.617	0.201	0.032	1.173	9.82	35.08
3	723.15	590	83.8	24.1	1.530	0.472	0.183	2.456	18.97	42.71
11	923.15	585	83.8	25.0	1.965	0.651	0.251	2.804	22.75	46.15
15	723.15/ 923.15*	582	85.1	20.0	1.883	0.537	0.193	2.234	19.31	48.98

* Direct Sulfidation of AMT/AC, 723.15 °*K* for 8.7 *hr* and at 923.15 °*K* for 7.5 *hr*
GHSV of 2992.9 *L/kg cat/hr*, and H_2/CO ratio of 0.993 *v/v* was used for all the cases.

Table 3.2. Effect of sulfidation temperature on catalyst performance.

The X-ray diffraction (XRD) patterns of these catalysts are shown in Fig. 3.4. The XRD was measured with a Rigaku MiniFlex II diffractometer with a Cu-Kα X-ray source operated at 30 *kV* and 15 *mA*, 2θ angles from 10° to 70° at a scanning speed of 1°/*min*. The General Structure Analysis System (GSAS) software using EXPGUI interface [4, 5] and Rigaku PDXL software were used for the analysis of the XRD data [6]. An example quantitative analysis using GSAS and PDXL is given in Appendix 3D. The calculated phase compositions are given in Table 3.3. The MoS_2 weight percent increases with increase in sulfidation temperature. Increase in MoS_2 and decrease in MoO_2 phase is also evident from the XRD patterns (Fig. 3.4). A complete conversion of MoO_2 to MoS_2 can be achieved by sulfidizing the calcined pellets at a higher temperature of 923.15 °*K*. The improved performance of the catalyst can be attributed to increased percentage of MoS_2 in the catalyst.

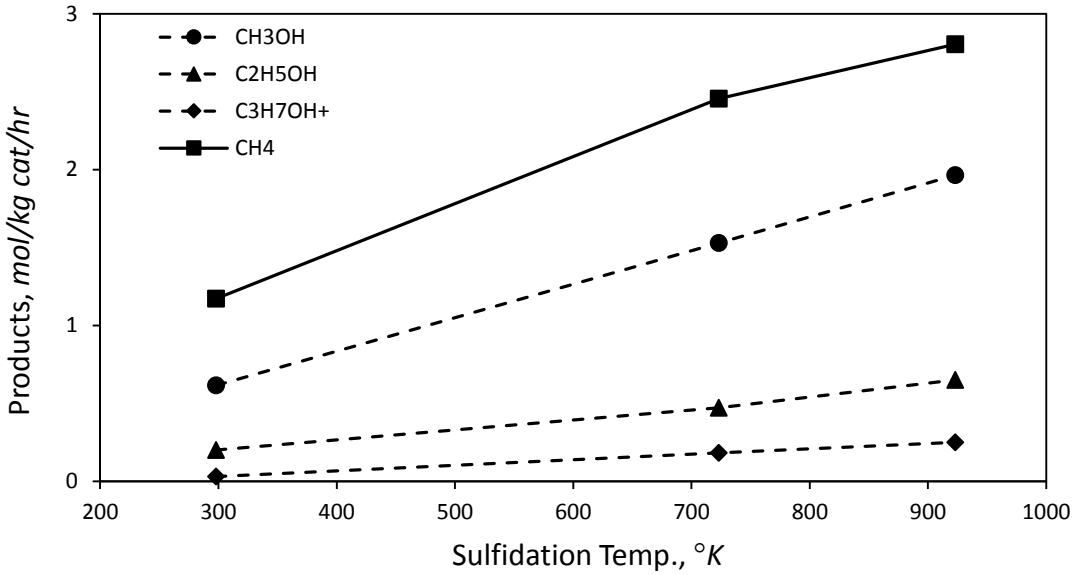

[redacted]

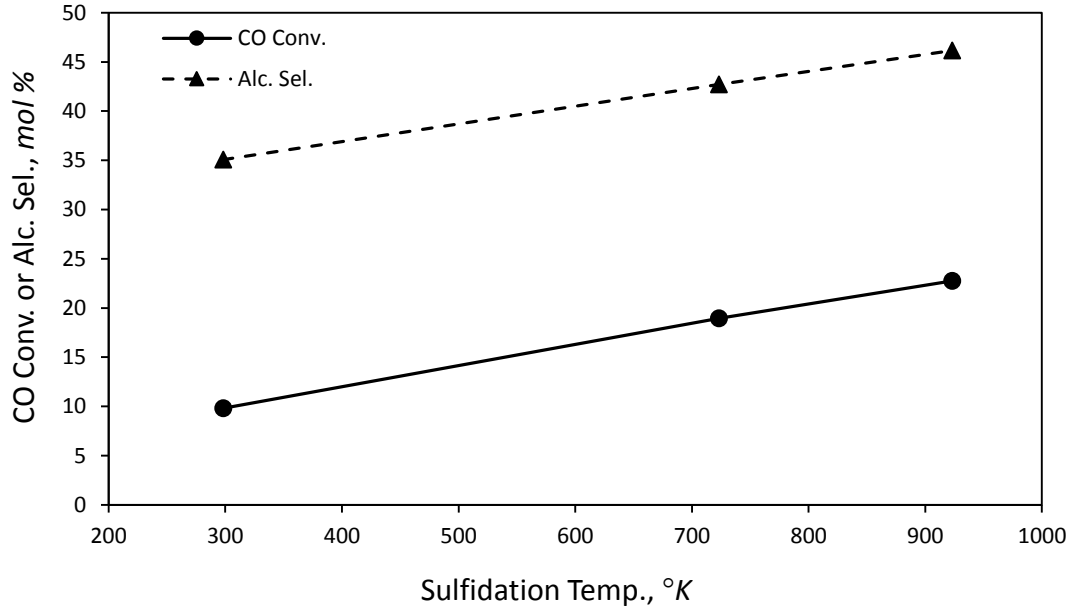

[redacted]

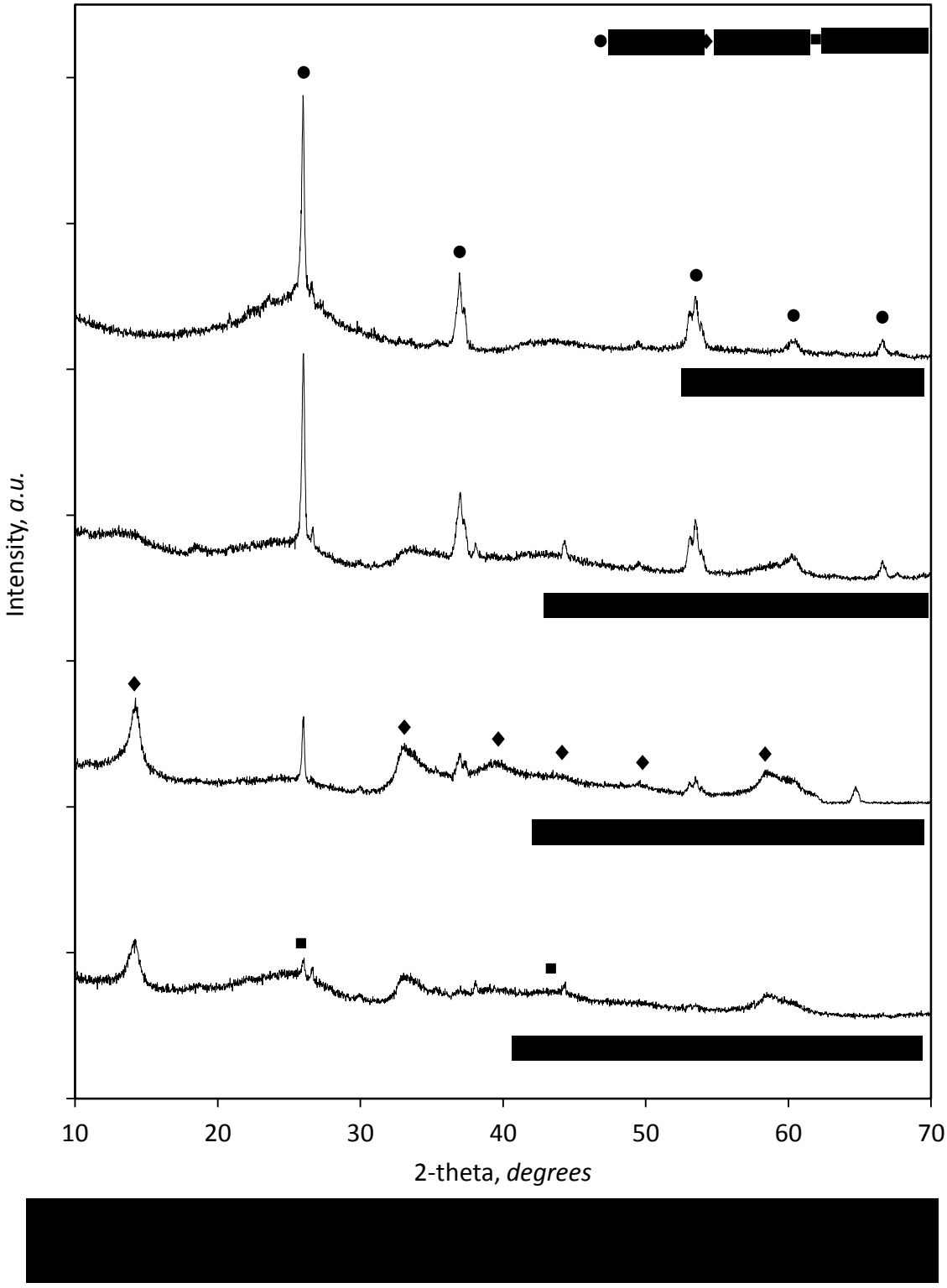
Intensity, a.u.
10
20
30
40
50
60
70
2-theta, degrees

Phase, *wt %*	**Cata # 13**		**Cat # 3**		**Cat # 11**		**Cat # 15**	
	GSAS	PDXL	GSAS	PDXL	GSAS	PDXL	GSAS	PDXL
MoO_2	100.0	100.0	n.a.	38.0	24.7	26.0	2.7	0.0
MoS_2	0.0	0.0	n.a.	62.0	75.3	74.0	97.3	100.0

Table 3.3. MoO_2 and MoS_2 relative composition determined from GSAS (Quantitative phase analysis) and PDXL (Reference Intensity Ratio, RIR method).

As we have seen, a complete conversion of MoO_2 to MoS_2 requires a high temperature sulfidation. An attempt was made to sulfidize the AMT promoted pellets directly, instead of sulfidizing the calcined pellets. The catalyst number 15 was prepared by direct sulfidation of AMT promoted AC pellets. Initially we have tried to sulfidize it at a lower temperature of 723.15 °*K*, but it was unsuccessful, hence sulfidation temperature was further increased to 923.15 °*K*. A complete conversion to MoS_2 was achieved at 923.15 °*K* sulfidation temperature. Improved catalytic activity and alcohol selectivity was also observed for this catalyst.

3.3.2. Direct Sulfidation of AMT Promoted Pellets

The catalyst number 14 was prepared by direct sulfidation of AMT promoted AC pellets at a high temperature, and tested extensively at alcohol synthesis conditions to determine stabilization time, effect of operating parameters (reaction temperature, pressure, GHSV, and H_2/CO) at steady-state, and stability of the catalyst for an extended period of run. Another objective was to collect steady-state testing results for kinetic model developments. The catalyst number 12 was prepared by high temperature sulfidation of calcined pellets. The catalyst preparation process parameters were given in

Table 3.1. The XRD patterns after each catalyst preparation steps are shown in Fig. 3.5. A complete conversion to MoS_2 was achieved by high temperature sulfidation. The average MoS_2 crystal size of 6.3 *nm* and 4.5 *nm* were determined by Halder Wagner method using PDXL software for high temperature sulfidation of calcined pellets (catalyst 12) and direct sulfidation of AMT impregnated AC pellets (catalyst 14) respectively. The MoS_2 crystal size is reduced to 5.2 and 2.3 *nm* upon CsCOOH promotion for catalyst number 12 and number 14 respectively. The presence of CsCOOH improves the dispersion of active materials in the catalyst. Improved alcohol selectivity of 56.05 *mol%* was observed for catalyst number 14 compared to 46.46 *mol%* for catalyst 12, after approximately 50 *hrs* of reactions.

3.3.2.1. Stabilization Time and Stability of the Catalyst

The initial stabilization and stability profile of the product yields, CO conversion, and alcohol selectivity at steady-state are shown in Fig 3.6 to 3.9. The alcohol yields can be seen immediately upon exposure to syngas. The catalyst was stable for more than 600 *hrs* of continuous run under alcohol synthesis reaction conditions. No loss of catalyst activity was observed during this period.

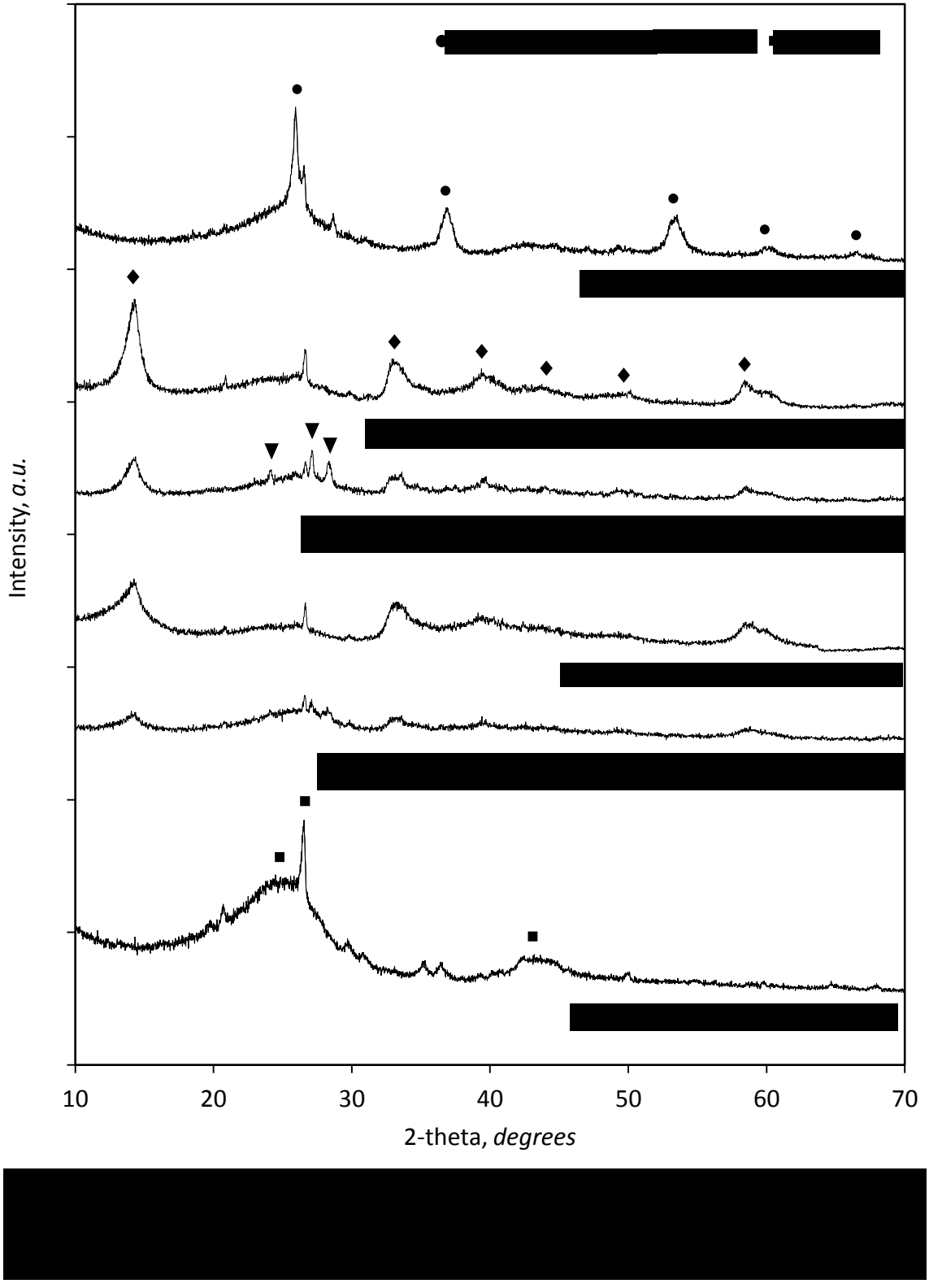
Intensity, a.u.
10
20
30
40
50
60
70
2-theta, degrees

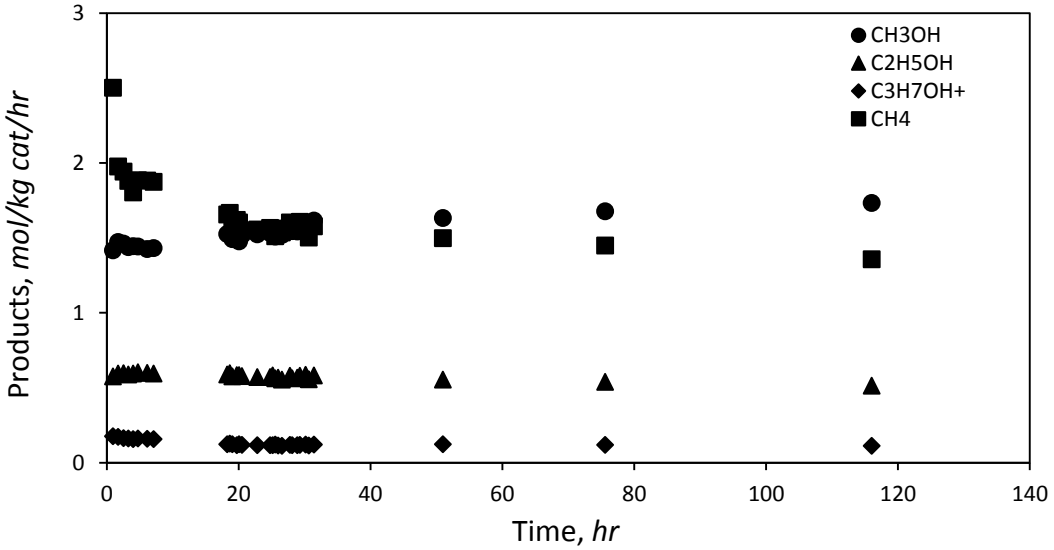

[redacted]

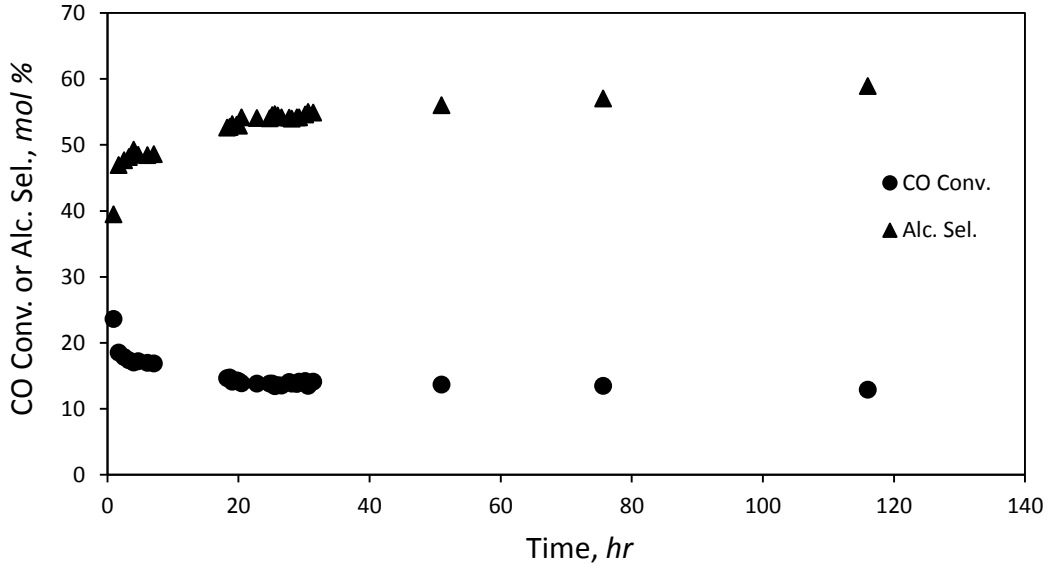

[redacted]

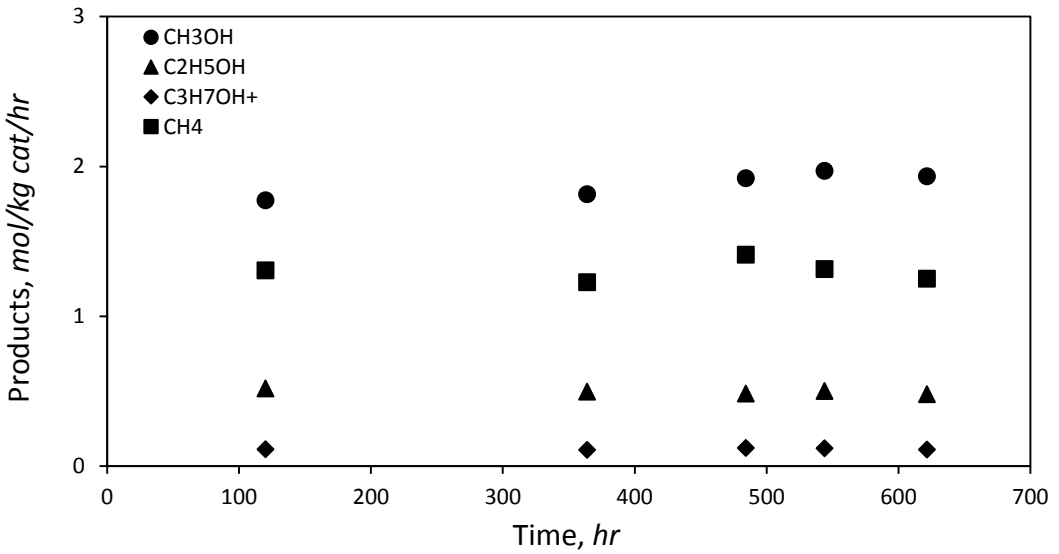

[redacted]

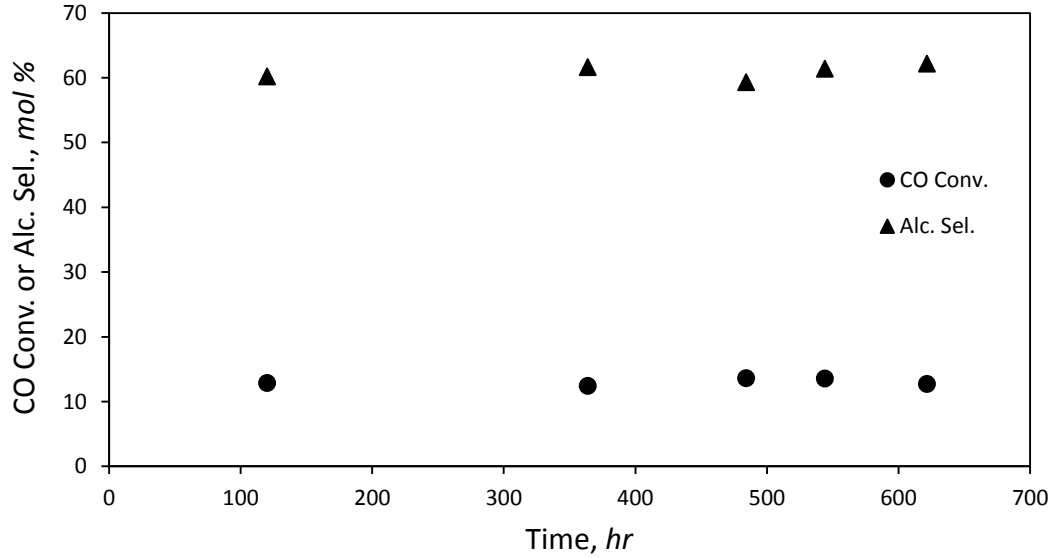

[redacted]

3.3.2.2. Effect of Temperature, Pressure, GHSV, and H_2/CO at Steady-State

The objective of this exercise is to obtain steady-state testing results for kinetic analysis. The catalyst was tested extensively for different variations in operating conditions at steady-state. Effect of temperature, pressure, GHSV, and H_2/CO ratio on product yields, CO conversion, and alcohol selectivity are shown in Fig. 3.10 to 3.17. The following additional observations were made at steady-state:

- The catalyst maintains constant alcohol selectivity with increase in reaction pressure.
- The hydrocarbon yield decreases with increase in GHSV.

3.3.3.3. $MoO_2(acac)_2$ as the Mo precursor and Co Containing Oxide Catalyst

Effect of different molybdenum precursor, $MoO_2(acac)_2$ (catalyst number 17) and addition of cobalt (catalyst number 16) on CO conversion, alcohol selectivity, and product yields were evaluated at similar operating conditions of 582 – 589 *°K*, 84.3 – 85.9 *bar*, 2992.9 *L/kg cat/hr*, and H_2/CO ratio of 0.993 *v/v*. Testing results are compared with the results of catalyst number 3 (calcination followed by sulfidation at 723.15 *°K*), catalyst number 14 (direct sulfidation at 923.15 *°K*), and catalyst number 13. The lab-scale testing results are shown in Table 3.4. Pictorial representation of product yields, CO conversion, and alcohol selectivity are shown in Fig. 3.18 and Fig. 3.19. Catalyst number 3, number 17, and number 14 are sulfide based catalysts, whereas catalyst number 13 and number 16 are oxide based catalysts.

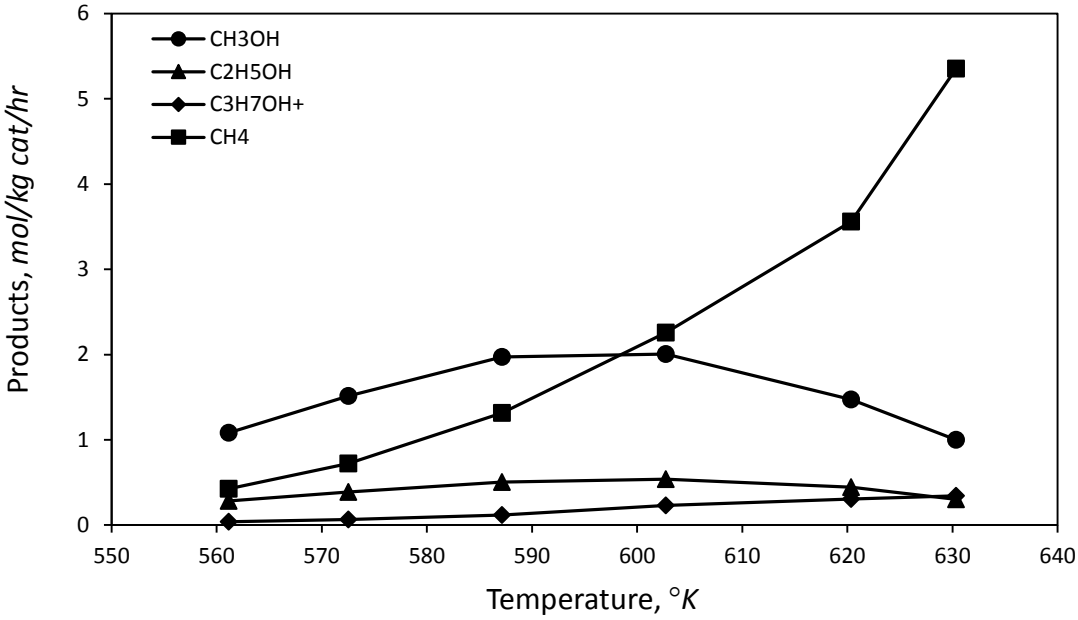
CH3OH
C2H5OH
C3H7OH+
CH4
Products, mol/kg cat/hr
Temperature, °K

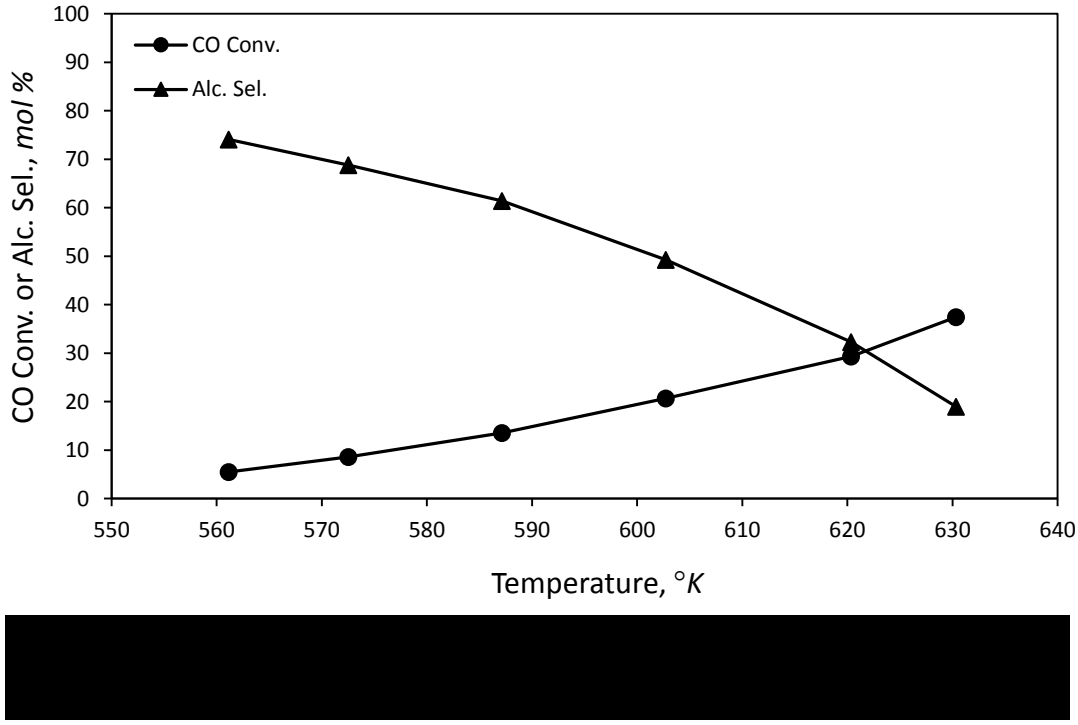
CO Conv.
Alc. Sel.
CO Conv. or Alc. Sel., mol %
Temperature, °K

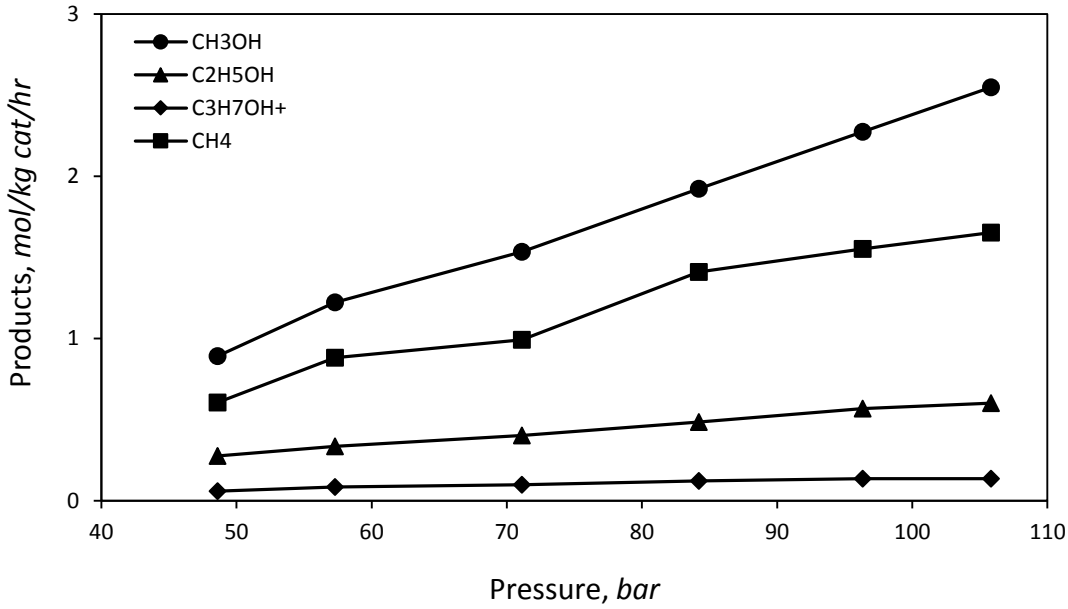
CH3OH
C2H5OH
C3H7OH+
CH4
Products, *mol/kg cat/hr*
Pressure, *bar*
0
1
2
3
40
50
60
70
80
90
100
110

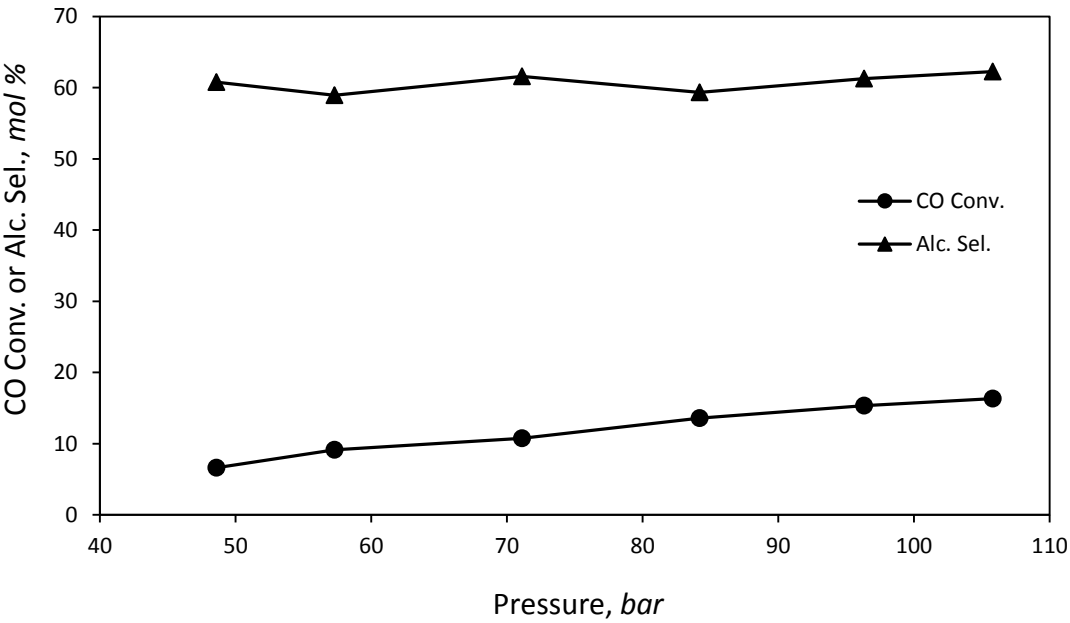
CO Conv.
Alc. Sel.
CO Conv. or Alc. Sel., *mol %*
Pressure, *bar*
0
10
20
30
40
50
60
70
40
50
60
70
80
90
100
110

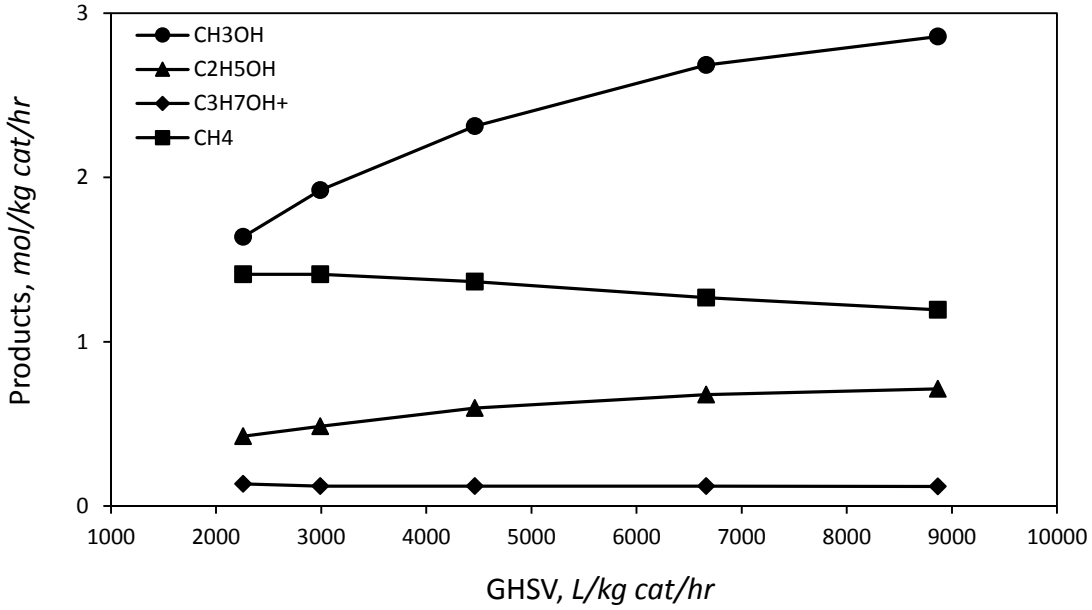

[redacted]

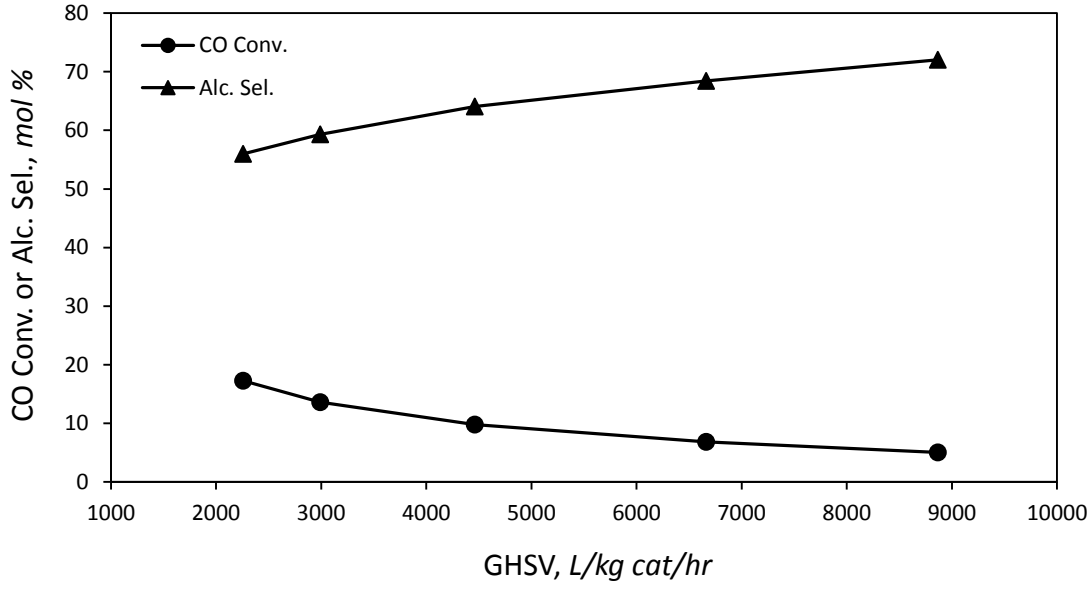

[redacted]

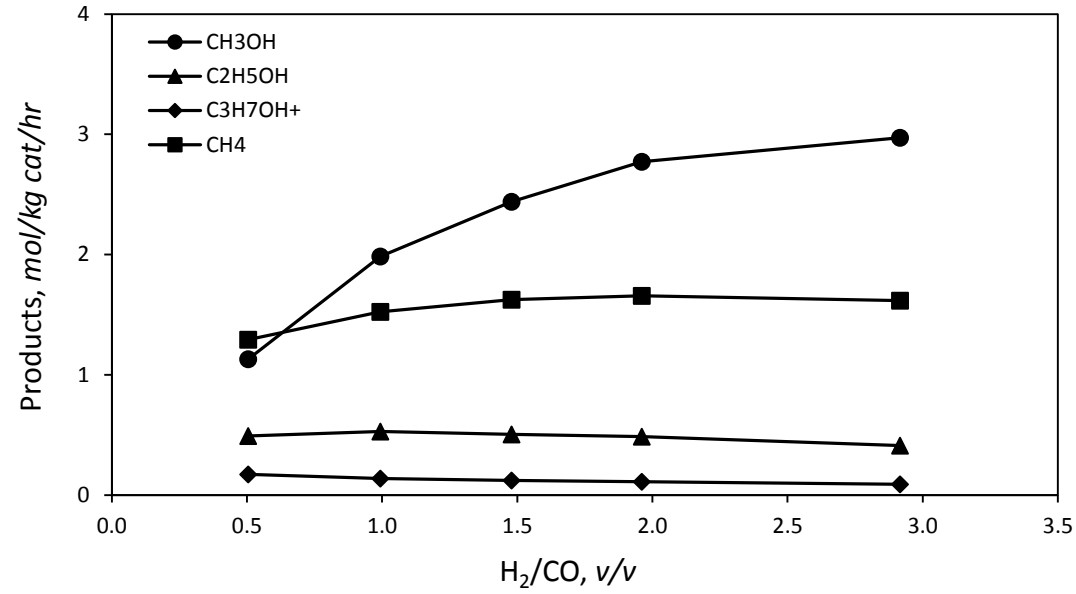

[redacted]

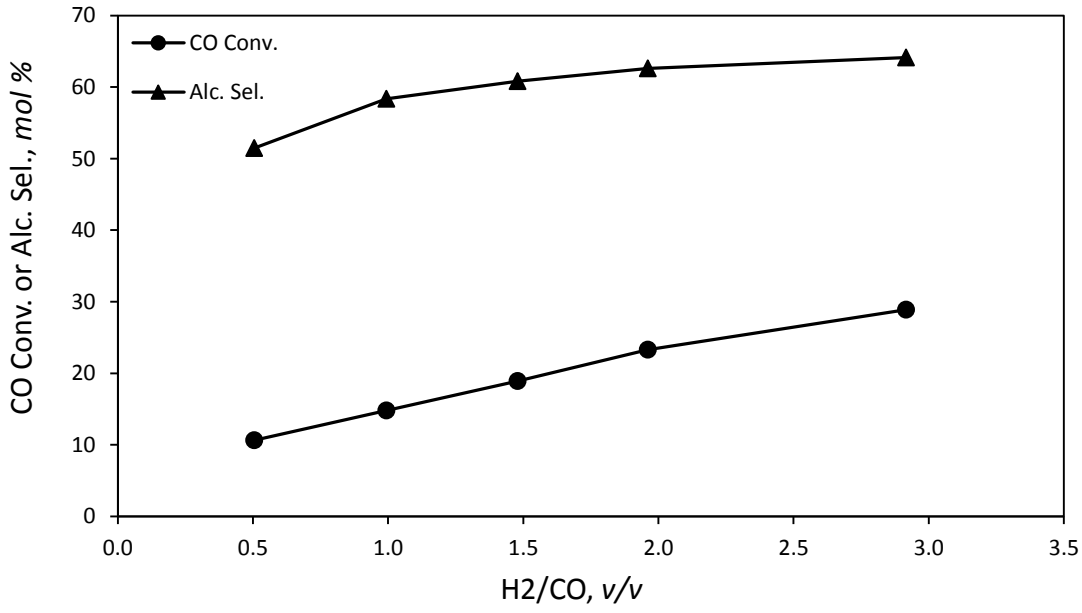

[redacted]

Cat. #	Testing Conditions			Products, *mol/kg cat/hr*				C_2^+/C_1 *alcohol, w/w*	CO Conv, *%*	Alc. Sel., m*ol %*
	T, *°K*	Pressure, *bar*	Time, *hr*	CH_3OH	C_2H_5OH	$C_3H_7OH^+$	CH_4			
3	589	85.9	61.0	1.749	0.494	0.189	2.317	0.62	18.68	46.92
14	582	85.8	51.0	1.633	0.554	0.123	1.499	0.63	13.68	56.05
17	589	85.1	43.6	1.519	0.506	0.137	1.610	0.65	13.94	53.12
13	589	84.3	16.5	0.617	0.201	0.032	1.173	0.56	9.82	35.08
	601	84.6	21.2	0.695	0.263	0.096	1.815	0.82	15.57	30.19
	612	84.6	26.0	0.764	0.277	0.142	2.495	0.89	20.52	25.97
16	590	85.8	59.7	0.464	0.410	0.148	1.761	1.91	20.72	27.82
	608	85.4	63.3	0.489	0.538	0.218	2.796	2.47	31.75	22.72
	620	85.6	67.9	0.455	0.620	0.283	3.892	3.21	43.17	18.46

GHSV of 2992.9 *L/kg cat/hr*, and H_2/CO ratio of 0.993 *v/v* was used for all the cases.

Table 3.4. Lab-scale testing results of oxide and sulfide based catalysts.

Catalyst number 14 and catalyst number 17 shows improved alcohol selectivity, ethanol yield, and C_2^+/C_1 ratio. Addition of cobalt (catalyst number 16) dramatically suppresses the methanol yield. Further increase in reaction temperature increases ethanol, propanol$^+$, and methane yield. At reaction temperature of 620 *°K*, the ethanol yield and C_2^+/C_1 alcohol ratio increases to 0.620 *mol/kg cat/hr* and 3.21 *w/w* respectively and alcohol selectivity decreases to 18.46 *mol %*. Presence of oxides in the catalyst favors hydrocarbon formations; as a result, oxide based catalysts shows poor selectivity for alcohols compared to sulfide based catalysts. Increases in CO conversion for oxide based catalysts are due to increase in hydrocarbon yields.

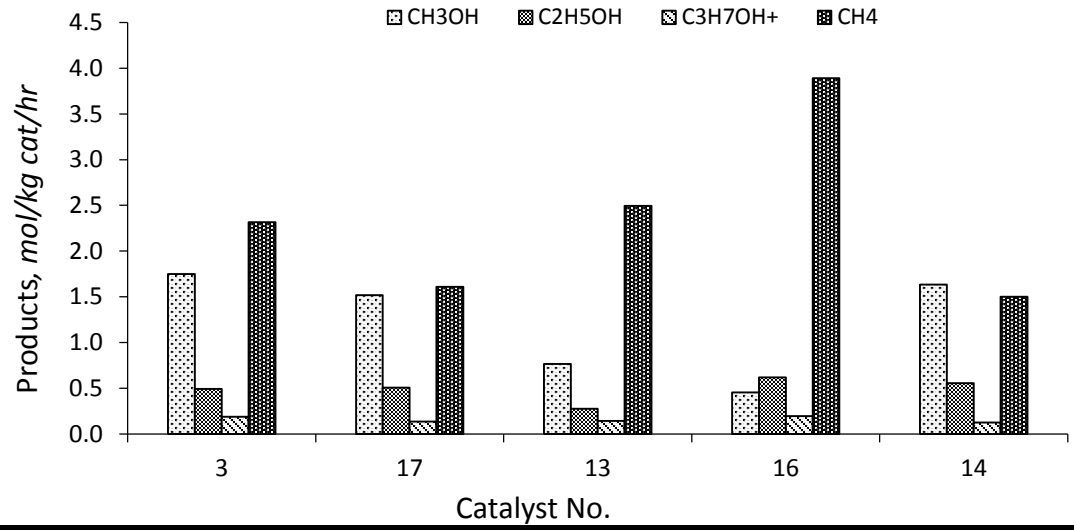

[redacted]

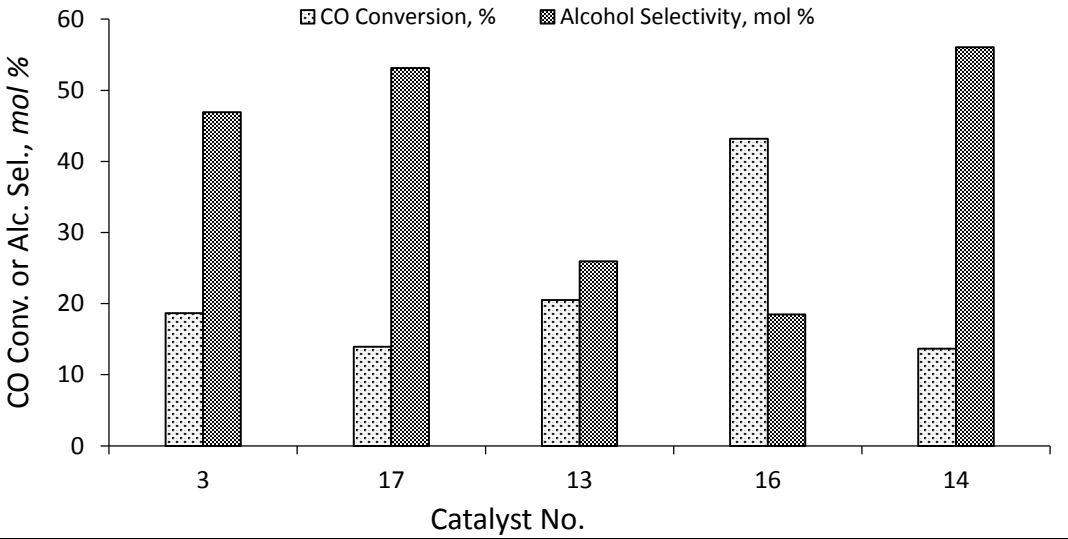

[redacted]

3.3.3. Optimum Catalyst Composition and Catalytic Performance

The optimum catalyst compositions, operating conditions and steady-state results of Cs promoted carbon supported molybdenum sulfide catalysts are summarized in Table 3.5.

Optimum Catalyst Preparation Process Parameters		**Optimum Catalyst Operating Conditions**		**Steady-State Results**	
Mo Content[#*], *wt %*	12 – 17	Temperature, *°K*	580 – 610	CO Conversion, *%*	5 – 25
Cs/Mo, *mol/mol*	0.23 – 1.58 (0.7)	Pressure, *bar*	> 50	Alcohol Selectivity, *mol %*	45 – 75
Batch Size, *gm*	5 – 50	GHSV, *L/kg cat/hr*	3000 – 10000	Alcohol Production, *mol/kg cat/hr*	2.0 – 5.4
Calcination Temp., *°K*	773.15	H_2/CO, *v/v*	0.5 – 2.0 (1.0)	C_2^+/Methanol, *w/w*	0.3 – 1.0
Sulfidation Temp., *°K*	923.15	Stabilization time, *hr*	5 – 25	Ethanol/Methanol, *w/w*	0.3 – 0.7
Ramp, *°K/min*	5 – 10	Stability time, *hr*	> 600		

[*] based on MoO_2/AC after the calcination step
[#] not optimized
( ) optimum value
C_2^+ ethanol plus higher alcohols

Table 3.5. Optimum catalyst composition, operating conditions and steady-state results of Cs/MoS_2/AC catalysts.

3.4. Conclusions

The cesium promoted molybdenum based supported catalysts were prepared by employing different sulfidation temperatures and tested for higher alcohol synthesis. The increase in alcohol yields, alcohol selectivity, and catalyst activity was observed with increase in sulfidation temperature of the calcined pellets. In another attempt, the process was simplified by employing high temperature direct sulfidation of AMT promoted AC pellets. The catalyst prepared by direct sulfidation was tested extensively for more than 600 *hrs*. The loss of catalyst activity and the presence of water and sulfur compounds in the product were not observed during these periods. The experimental data needed for kinetic analysis was collected after 385 *hrs* of reactions. The catalyst was also successfully prepared by using molybdenum dioxydiacetylacetonate as an alternative molybdenum precursor, instead of AMT and tested for higher alcohol synthesis. The cobalt containing molybdenum oxide catalyst shifts the production towards higher alcohols with the expense of overall alcohol selectivity.

3.5. Acknowledgement

The financial support from AMCS Corporation is gratefully acknowledged.

3.6. Appendix

Appendix 3A: Example Catalyst Composition Calculation

Mass balance of catalyst preparation process for catalyst number 10

Step: Support Preparation

AC used for acid wash = 44.5 *g*

Acis washed, vacuum dried, clean AC = 43.28 *g*

Step: AMT Impregnation

Clean AC pellets used (AC) = 42.0 *g*

AMT used = 17.00 *g*

Vacuum dried AMT promoted AC pellets (AMT/AC) = 55.53 *g*

Step: Direct Sulfidation

AMT promoted AC pellets used (AMT/AC) = 13.5 *g*

Sulfidized pellets (MoS_2/AC) = 13.04 *g*

Calcination of 13.5 *g* gives 12.66 *g* of calcined MoO_2/AC pellets

Amount of C in sulfidized pellets = 42/55.53×13.5 = 10.2107 *g*

Amount of MoS_2 and S in sulfidized pellets = 13.5 – 10.2107 = 2.8293 *g*

Amount of Mo in sulfidized pellets = (12.66 – 10.2107)/127.939×95.94 = 1.8367 *g*

Amount of S in sulfidized pellets = 2.8293 – 1.8367 = 0.992596 *g*

Composition of C in sulfidized pellets = 10.2107/13.04×100 = 78.30 *wt%*

Composition of Mo in sulfidized pellets = 1.8367/13.04×100 = 14.085 *wt%*

Composition of S in sulfidized pellets = 0.992596/13.04×100 = 7.61 *wt%*

Calculated sulfur to molybdenum ratio, S/Mo = (7.61/32.065)/(14.085/95.94) = **1.617**

Step: CsCOOH Promotion

Sulfidized pellets used = 12.5 *g*

CsCOOH (98%) used = 2.536 *g*

Final weight of the catalyst = 15.08 *g*

Amount of Cs in the final catalyst = 2.536×0.98/177.9229×132.905 = 1.8564 *g*

Amount of formate (-COOH) = 2.536×0.98 – 1.8564 = 0.6288 *g*

Amount of Mo in the final catalyst = 12.5×14.085/100 = 1.7606 *g*

Amount of S in the final catalyst = 12.5×7.61/100 = 0.9515 *g*

Amount of C in the final catalyst = 12.5×78.30/100 + 0.6288/45.017×12.011= 9.9556 *g*

Amount of O in the final catalyst = 0.6288/45.017×2×15.999 = 0.4469 *g*

Amount of H in the final catalyst = 0.6288/45.017×1.008 = 0.0141 *g*

Calculated total weight of the catalyst = 14.99 *g*

Calculated cesium to molybdenum ratio, Cs/Mo = (1.8564/132.905)/(1.7606/95.94) = **0.76**

Final Catalyst Composition

Composition of catalyst number 10 calculated from mass balance is given in Table 3A.

Elements	C	Mo	S	O	Cs	H	S/Mo	Cs/Mo
Catalyct # 10	66.44	11.75	6.35	2.98	12.39	0.09	1.617	0.761

Table 3A. Elemental composition of catalyst number 10 calculated from mass balance.

Appendix 3B: Example of the Calculation of Product Yields, Carbon Monoxide Conversion, and Alcohol Selectivity from the GC Area Data.

The GC results obtained from the testing of catalyst number 14 (prepared by high temperature direct sulfidation) are used to illustrate the procedure involved in the determination of product yields (*mol/kg cat/hr*), CO conversion (*%*), and alcohol selectivity (*mol %*) from carbon balance. The results were also checked for consistency against the oxygen balance. Six GC injections were made for each data point between 483.2 and 485.3 *hrs* of reactions and the average GC area values were used for the calculations. The operating conditions during this period were: T = 590.15 *°K*, P = 84.21 *bar*, H_2/CO = 0.993 *v/v*, and GHSV = 2992.9 *L/kg cat/hr*.

- GHSV and H_2/CO ratio: Observed CO and H_2 flows were determined from the mass flow controller calibration lines. The mass flow controllers were calibrated at about reaction pressure of 85 *bar* and room temperature of 298.15 *°K*. Fig. 3B (1-2) shows the calibration curves for CO and H_2 respectively. Observed flows were used to determine the GHSV, *L/kg cat/hr* and H_2/CO ratio, *v/v*. A 3 *g* catalyst was used for each of the experiments.

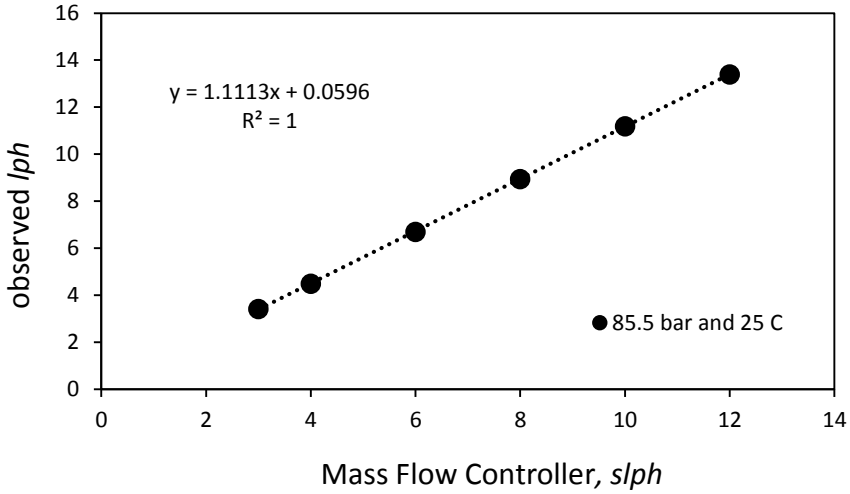

[redacted]

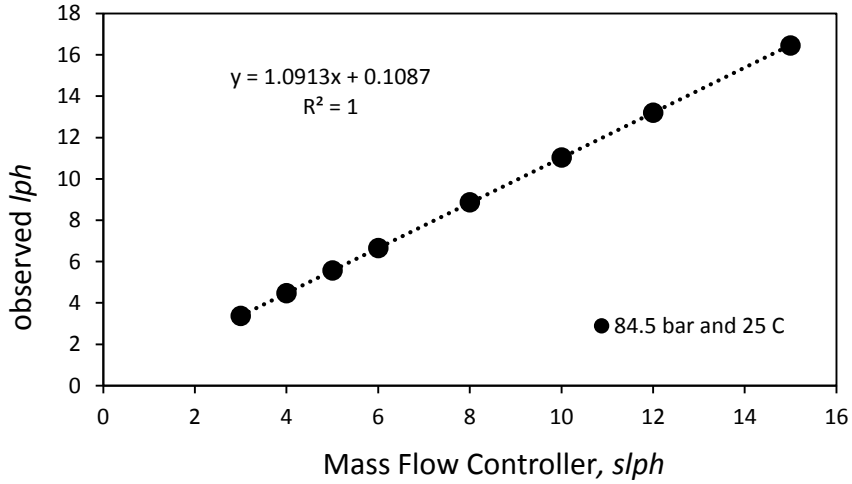

[redacted]

- Composition of the outlet stream: The average GC areas were corrected for the sensitivities of each component by dividing the areas by the respective thermal response factors (TRFs) and then normalizing these results to give the percent molar concentrations. The mole percentage of a component, *i* can be calculated from,

$$y_i = \frac{\left(GC\ Area/_{TRF}\right)_i}{\sum_i \left(GC\ Area/_{TRF}\right)_i} \times 100 \qquad (3B-1)$$

Table 3B (1) shows the calculation of mole percentages from GC area data.

Components	Average GC Area	TRF from Table 2E (8)	Area/TRF	*mol %*
CO	464860.8	30.10	15445.90	88.044
CH_4	13202.5	32.15	410.69	2.341
CO_2	47420.8	55.37	856.36	4.881
C_2H_6	2934.2	43.36	67.67	0.386
C_3H_8	1193.2	45.16	26.42	0.151
CH_3OH	18674.2	33.37	559.63	3.190
C_2H_5OH	8652.0	61.28	141.18	0.805
C_3H_7OH	2745.7	77.25	35.55	0.203

Table 3B (1). Calculation of the mole percentages from GC area data.

- Carbon Balance: The material balance is based on the number of carbon atoms entering and leaving the reactor at steady state. The number of C and O atoms entering the reactor is,

$$C_{in} = O_{in} = GHSV \times \frac{1}{22.414} \times \frac{273.15}{(25 + 273.15)} \times \frac{1}{\left(1 + \frac{H_2}{CO}\right)}, \quad \frac{mol}{(kg\ cat.hr)} \qquad (3B-2)$$

It is assumed that, all the inlet C atoms are distributed among the products. The absolute yield, *mol/kg cat/hr* of the carbon containing products can be calculated using the *mol %* of the products determined from GC area data,

$$F_i = \frac{y_i}{\sum_i n_{c,i} y_i} \times C_{in}, \qquad \frac{mol}{(kg\ cat.hr)} \qquad (3B-3)$$

Where, F_i is the yield or production rate of carbon containing component i, $n_{c,i}$ is the number of carbon atoms in each carbon containing components.

Similar procedure can be used to calculate yield of products from O balance,

$$F_i = \frac{y_i}{\sum_i n_{o,i} y_i} \times O_{in}, \qquad \frac{mol}{(kg\ cat.hr)} \qquad (3B-4)$$

Where, F_i is the yield or production rate of oxygen containing component i, $n_{o,i}$ is the number of oxygen atoms in each oxygen containing components. Table 3B (2) shows the calculation of product yields.

Percentage error on C and O,

$$\%\ error\ on\ C\ = \left(\frac{C_{in} - C_{out}}{C_{in}}\right) \times 100 = 0.0507 \qquad (3B-5)$$

$$\%\ error\ on\ O\ = \left(\frac{O_{in} - O_{out}}{O_{in}}\right) \times 100 = -0.0526 \qquad (3B-6)$$

Components	*mol %*	Yield from C balance	Yield from O balance	Average Yield
		mol/kg cat/hr		
CO	88.044	53.032	52.977	53.004
CH_4	2.341	1.410		1.410
CO_2	4.881	2.940	2.937	2.939
C_2H_6	0.386	0.232		0.232
C_3H_8	0.151	0.091		0.091
CH_3OH	3.190	1.921	1.919	1.920
C_2H_5OH	0.805	0.485	0.484	0.484
C_3H_7OH	0.203	0.122	0.122	0.122
H_2				51.293

Table 3B (2). Calculation of the product yields.

Amount of hydrogen in the product is calculated from the hydrogen atom balance.

$$H_{in} = GHSV \times \frac{1}{22.414} \times \frac{273.15}{(25 + 273.15)} \times \frac{\left(\frac{H_2}{CO}\right)}{\left(1 + \frac{H_2}{CO}\right)}, \quad \frac{mol}{(kg\ cat.hr)} \qquad (3B-7)$$

$$F_{H_2,product} = \left(H_{in} - \sum_i n_{H,i} \times F_i\right)\Big/_2 \qquad (3B-8)$$

Where, F_i is the yield or production rate of component *i* (except hydrogen), $n_{H,i}$ is the number of hydrogen atoms in each hydrogen containing components.

Overall mass balance error is,

$$Overall\ mass\ balance\ error, \% = \frac{(mass\ in - mass\ out)}{mass\ in} \times 100 = -0.0077 \qquad (3B-9)$$

- CO conversion and Alcohol selectivity are,

$$CO_{conversion} = \frac{CO_{in} - CO_{out}}{CO_{in}} \times 100 = 13.64\ \% \qquad (2.3)$$

$$Alcohol_{Selectivity} = \frac{\sum\left(\frac{mol}{kg\ cat.hr}\right)_{alcohols}}{\sum\left(\frac{mol}{kg\ cat.hr}\right)_{alcohols} + \sum\left(\frac{mol}{kg\ cat.hr}\right)_{Hydrocarbons}} \times 100 = 59.32\ mol\ \% \qquad (2.4)$$

Appendix 3C: Testing Results of the Catalysts

3C.1. Catalyst # 11 results

Time, *hr*	*P*, *bar*	*T*, *°K*	H_2/CO, *v/v*	GHSV, *L/kg cat/hr*	Products, *mol/kg cat/hr*												CO Conv., *%*	Alc. Sel., *mol %*
					CO	H_2	CH_3OH	C_2H_5OH	C_3H_7OH	CH_4	C_2H_6	C_3H_8	CO_2	H_2O	Tot. Alc.	Tot. HCs		
25.0	84	585	0.99	2993	47.42	46.08	1.96	0.65	0.19	2.80	0.40	0.14	5.42	0.00	2.87	3.35	22.7	46.1
100.8	84	584	0.99	2993	49.92	48.38	2.05	0.61	0.16	2.08	0.32	0.10	4.31	0.00	2.88	2.50	18.7	53.5
140.8	84	572	0.99	2993	53.93	52.17	1.83	0.57	0.11	1.12	0.16	0.05	2.52	0.00	2.53	1.33	12.1	65.6
145.2	84	590	0.99	2993	48.93	47.51	2.04	0.59	0.17	2.19	0.37	0.12	4.68	0.00	2.87	2.69	20.3	51.7
149.5	84	567	0.99	2993	55.20	53.50	1.68	0.51	0.09	0.86	0.12	0.03	2.02	0.00	2.29	1.01	10.1	69.4

Table 3C (1). Operating conditions and testing results of catalyst # 11.

3C.2. Catalyst # 12 results

Time, *hr*	*P*, *bar*	*T*, *°K*	H_2/CO, *v/v*	GHSV, *L/kg cat/hr*	Products, *mol/kg cat/hr*												CO Conv., *%*	Alc. Sel., *mol %*
					CO	H_2	CH_3OH	C_2H_5OH	C_3H_7OH	CH_4	C_2H_6	C_3H_8	CO_2	H_2O	Tot. Alc.	Tot. HCs		
18.1	85	587	0.99	2993	54.28	53.48	0.93	0.44	0.10	1.26	0.21	0.08	2.73	0.00	1.46	1.55	11.6	48.4
34.6	85	587	0.99	2993	54.06	53.12	1.12	0.47	0.10	1.33	0.22	0.08	2.83	0.00	1.69	1.63	11.9	50.8
46.0	85	593	0.99	2993	52.26	51.41	1.18	0.48	0.12	1.66	0.29	0.11	3.55	0.00	1.79	2.07	14.9	46.5
50.0	85	605	0.99	2993	47.96	47.83	1.18	0.46	0.15	2.47	0.50	0.23	5.55	0.00	1.85	3.20	21.9	36.6
53.8	85	576	0.99	2993	56.63	55.64	0.89	0.41	0.07	0.81	0.12	0.01	1.75	0.00	1.38	0.93	7.7	59.6
59.1	85	593	0.99	4461	82.74	80.99	1.58	0.58	0.12	1.53	0.28	0.11	3.42	0.00	2.28	1.91	9.7	54.4
63.1	103	594	0.99	4461	79.49	77.45	2.12	0.76	0.18	2.19	0.37	0.13	4.68	0.00	3.06	2.69	13.3	53.2
67.3	102	595	0.99	6664	124.44	120.97	2.53	0.85	0.19	2.16	0.38	0.13	4.56	0.00	3.57	2.67	9.2	57.2
71.9	102	595	0.99	8867	169.70	165.13	2.75	0.93	0.18	2.09	0.36	0.13	4.48	0.00	3.86	2.57	7.0	60.0
89.2	85	594	0.99	4461	82.42	80.48	1.72	0.57	0.13	1.62	0.29	0.11	3.47	0.00	2.42	2.02	10.1	54.5
94.3	86	595	0.99	6664	127.50	124.39	1.98	0.66	0.15	1.55	0.29	0.11	3.41	0.00	2.79	1.94	7.0	58.9
98.9	85	594	0.99	2993	51.94	50.82	1.46	0.47	0.13	1.64	0.29	0.11	3.54	0.00	2.08	2.05	15.4	50.3

Table 3C (2). Operating conditions and testing results of catalyst # 12.

3C.3. Catalyst # 13 results

Time, *hr*	*P*, *bar*	*T*, *°K*	H_2/CO, *v/v*	GHSV, *L/kg cat/hr*	Products, *mol/kg cat/hr*												CO Conv., *%*	Alc. Sel., *mol %*
					CO	H_2	CH_3OH	C_2H_5OH	C_3H_7OH	CH_4	C_2H_6	C_3H_8	CO_2	H_2O	Tot. Alc.	Tot. HCs		
16.5	84	589	0.99	2993	55.35	55.33	0.62	0.20	0.03	1.17	0.28	0.12	2.83	0.00	0.85	1.57	9.8	35.1
21.2	85	601	0.99	2993	51.82	52.17	0.70	0.26	0.08	1.81	0.44	0.18	4.37	0.00	1.05	2.44	15.6	30.2
26.0	85	612	0.99	2993	48.78	49.60	0.76	0.28	0.10	2.49	0.60	0.27	5.90	0.00	1.18	3.37	20.5	26.0
30.5	85	578	0.99	2993	57.52	57.14	0.54	0.14	0.05	0.68	0.16	0.07	1.69	0.00	0.73	0.91	6.3	44.7

Table 3C (3). Operating conditions and testing results of catalyst # 13.

3C.5. Catalyst # 15 results

Time, *hr*	*P*, *bar*	*T*, *°K*	H_2/CO, *v/v*	GHSV, *L/kg cat/hr*	Products, *mol/kg cat/hr*												CO Conv., *%*	Alc. Sel., *mol %*
					CO	H_2	CH_3OH	C_2H_5OH	C_3H_7OH	CH_4	C_2H_6	C_3H_8	CO_2	H_2O	Tot. Alc.	Tot. HCs		
20.0	85	582	0.99	2993	49.53	48.09	1.88	0.54	0.14	2.23	0.36	0.13	4.45	0.00	2.61	2.72	19.3	49.0
36.9	84	583	0.99	2993	50.02	48.51	1.91	0.54	0.15	2.06	0.33	0.11	4.19	0.00	2.66	2.50	18.5	51.5
41.0	85	589	0.99	2993	48.02	46.85	1.92	0.53	0.16	2.59	0.43	0.16	5.23	0.00	2.68	3.18	21.8	45.7
45.5	85	571	0.99	2993	53.60	51.85	1.84	0.53	0.11	1.28	0.18	0.06	2.68	0.00	2.49	1.52	12.7	62.1
59.9	85	564	0.99	2993	55.37	53.68	1.61	0.48	0.08	0.89	0.12	0.03	1.95	0.00	2.18	1.04	9.8	67.7
66.7	85	565	0.99	2993	55.27	53.54	1.66	0.49	0.09	0.88	0.12	0.03	1.98	0.00	2.24	1.04	10.0	68.3

Table 3C (5). Operating conditions and testing results of catalyst # 15.

3C.4. Catalyst # 14 results

Time, *hr*	*P*, *bar*	*T*, *°K*	H_2/CO, *v/v*	GHSV, *L/kg cat/hr*	Products, *mol/kg cat/hr*												CO Conv., *%*	Alc. Sel., *mol %*
					CO	H_2	CH_3OH	C_2H_5OH	C_3H_7OH	CH_4	C_2H_6	C_3H_8	CO_2	H_2O	Tot. Alc.	Tot. HCs		
0.9	89	586	0.99	2993	46.87	46.87	1.42	0.58	0.15	2.50	0.57	0.25	6.12	0.00	2.17	3.32	23.6	39.5
1.7	87	585	0.99	2993	50.01	49.21	1.47	0.60	0.15	1.98	0.39	0.16	4.51	0.00	2.24	2.53	18.5	47.0
2.5	86	585	0.99	2993	50.43	49.52	1.46	0.60	0.14	1.94	0.36	0.14	4.29	0.00	2.22	2.44	17.8	47.7
3.3	86	585	0.99	2993	50.73	49.79	1.44	0.59	0.14	1.88	0.35	0.13	4.14	0.00	2.19	2.35	17.3	48.2
4.0	86	585	0.99	2993	50.94	49.99	1.45	0.60	0.13	1.80	0.33	0.12	4.05	0.00	2.20	2.26	17.0	49.3
4.7	86	584	0.99	2993	50.81	49.78	1.44	0.60	0.14	1.89	0.33	0.12	4.05	0.00	2.21	2.34	17.2	48.5
6.1	87	585	0.99	2993	50.96	49.91	1.43	0.60	0.14	1.88	0.32	0.12	3.99	0.00	2.18	2.32	17.0	48.5
7.1	87	585	0.99	2993	51.03	49.96	1.43	0.59	0.14	1.87	0.32	0.11	3.95	0.00	2.18	2.31	16.9	48.6
18.3	87	584	0.99	2993	52.39	51.16	1.53	0.59	0.12	1.66	0.27	0.09	3.45	0.00	2.24	2.02	14.6	52.6
18.7	88	583	0.99	2993	52.33	51.09	1.54	0.60	0.13	1.67	0.27	0.09	3.48	0.00	2.26	2.02	14.7	52.7
19.1	88	583	0.99	2993	52.71	51.48	1.49	0.58	0.12	1.59	0.25	0.08	3.31	0.00	2.19	1.93	14.1	53.2
19.7	88	582	0.99	2993	52.59	51.36	1.51	0.58	0.12	1.62	0.26	0.08	3.37	0.00	2.22	1.96	14.3	53.1
20.1	88	582	0.99	2993	52.68	51.45	1.48	0.58	0.12	1.60	0.25	0.08	3.33	0.00	2.18	1.94	14.2	53.0
20.5	88	582	0.99	2993	52.87	51.56	1.52	0.58	0.12	1.55	0.24	0.08	3.21	0.00	2.21	1.87	13.9	54.2
22.8	88	582	0.99	2993	52.88	51.57	1.52	0.57	0.12	1.56	0.24	0.08	3.21	0.00	2.21	1.88	13.8	54.1
24.8	88	582	0.99	2993	52.89	51.54	1.53	0.57	0.12	1.57	0.24	0.08	3.19	0.00	2.22	1.89	13.8	54.1
25.2	87	581	0.99	2993	52.89	51.50	1.55	0.58	0.12	1.56	0.24	0.08	3.17	0.00	2.25	1.88	13.8	54.5
25.6	87	582	0.99	2993	53.13	51.75	1.51	0.56	0.12	1.51	0.23	0.07	3.06	0.00	2.19	1.82	13.4	54.7
26.0	86	582	0.99	2993	53.04	51.66	1.53	0.57	0.11	1.53	0.24	0.08	3.10	0.00	2.21	1.85	13.6	54.5
26.6	86	582	0.99	2993	53.07	51.72	1.52	0.55	0.11	1.54	0.23	0.08	3.12	0.00	2.19	1.85	13.5	54.2
27.8	86	582	0.99	2993	52.74	51.34	1.57	0.58	0.12	1.60	0.24	0.08	3.23	0.00	2.27	1.93	14.1	54.1
28.1	86	582	0.99	2993	52.91	51.53	1.54	0.56	0.12	1.57	0.24	0.08	3.17	0.00	2.22	1.89	13.8	54.0
28.9	86	582	0.99	2993	52.93	51.54	1.54	0.57	0.12	1.56	0.24	0.08	3.14	0.00	2.23	1.88	13.8	54.2
29.3	86	582	0.99	2993	52.71	51.28	1.59	0.58	0.12	1.61	0.25	0.08	3.23	0.00	2.29	1.93	14.1	54.2
30.2	86	582	0.99	2993	52.65	51.25	1.60	0.59	0.12	1.59	0.25	0.08	3.26	0.00	2.31	1.92	14.2	54.7

Contd.

30.6	86	582	0.99	2993	53.11	51.73	1.54	0.56	0.11	1.50	0.23	0.07	3.08	0.00	2.22	1.81	13.5	55.0
31.4	86	582	0.99	2993	52.70	51.28	1.62	0.58	0.12	1.58	0.25	0.08	3.23	0.00	2.32	1.90	14.1	54.9
51.0	86	582	0.99	2993	52.98	51.52	1.63	0.55	0.12	1.50	0.24	0.08	3.09	0.00	2.31	1.81	13.7	56.1
75.6	86	582	0.99	2993	53.09	51.60	1.68	0.54	0.12	1.45	0.24	0.07	3.03	0.00	2.34	1.76	13.5	57.1
116.0	86	581	0.99	2993	53.46	51.86	1.73	0.51	0.11	1.36	0.22	0.07	2.83	0.00	2.36	1.64	12.9	59.0
120.0	86	581	0.99	2993	53.48	51.87	1.77	0.52	0.11	1.31	0.22	0.07	2.81	0.00	2.41	1.59	12.9	60.2
164.2	86	581	0.99	2993	53.73	52.12	1.78	0.51	0.11	1.21	0.21	0.07	2.70	0.00	2.40	1.48	12.5	61.8
173.8	87	582	0.99	2993	53.58	51.94	1.82	0.51	0.11	1.25	0.21	0.07	2.75	0.00	2.44	1.53	12.7	61.6
188.1	86	580	0.99	2993	53.96	52.34	1.77	0.49	0.11	1.17	0.19	0.06	2.60	0.00	2.37	1.43	12.1	62.4
194.7	86	580	0.99	2993	54.18	52.49	1.75	0.48	0.10	1.16	0.18	0.06	2.48	0.00	2.33	1.41	11.7	62.4
221.7	86	580	0.99	2993	54.22	52.55	1.77	0.47	0.11	1.12	0.18	0.06	2.47	0.00	2.35	1.36	11.7	63.4
242.9	86	580	0.99	2993	54.43	52.75	1.76	0.46	0.10	1.08	0.17	0.06	2.38	0.00	2.32	1.31	11.3	63.9
264.7	86	580	0.99	2993	54.51	52.82	1.76	0.46	0.10	1.06	0.17	0.05	2.34	0.00	2.32	1.28	11.2	64.4
268.8	86	580	0.99	2993	54.43	52.72	1.80	0.46	0.10	1.06	0.17	0.05	2.36	0.00	2.36	1.29	11.3	64.7
283.9	86	579	0.99	2993	54.72	53.02	1.76	0.45	0.09	1.00	0.16	0.05	2.25	0.00	2.31	1.21	10.8	65.5
292.4	86	580	0.99	2993	54.64	52.89	1.80	0.46	0.09	1.02	0.16	0.05	2.26	0.00	2.36	1.22	11.0	65.8
307.9	86	579	0.99	2993	54.92	53.21	1.76	0.44	0.09	0.96	0.15	0.05	2.16	0.00	2.28	1.16	10.5	66.4
318.8	86	580	0.99	2993	54.80	53.06	1.78	0.45	0.09	0.99	0.15	0.05	2.19	0.00	2.32	1.19	10.7	66.0
361.3	86	580	0.99	2993	55.32	53.61	1.67	0.42	0.08	0.91	0.14	0.04	1.99	0.00	2.18	1.09	9.9	66.7
364.0	87	580	0.99	2993	53.74	52.02	1.81	0.50	0.11	1.23	0.20	0.08	2.64	0.00	2.42	1.51	12.4	61.6
384.0	86	588	0.99	2993	52.23	50.58	1.95	0.53	0.14	1.56	0.27	0.10	3.32	0.00	2.61	1.93	14.9	57.5
418.2	86	589	0.99	2993	52.29	50.61	1.98	0.53	0.14	1.52	0.26	0.10	3.28	0.00	2.65	1.89	14.8	58.4
484.2	84	590	0.99	2993	53.04	51.28	1.92	0.48	0.12	1.41	0.23	0.09	2.94	0.00	2.53	1.73	13.6	59.3
544.0	84	587	0.99	2993	53.07	51.35	1.97	0.50	0.12	1.31	0.23	0.09	2.94	0.00	2.59	1.63	13.5	61.4
621.7	84	587	0.99	2993	53.57	51.77	1.93	0.48	0.11	1.25	0.20	0.08	2.69	0.00	2.53	1.54	12.7	62.2
397.8	86	589	0.50	3002	72.87	32.22	1.13	0.49	0.14	1.29	0.28	0.12	3.38	0.00	1.79	1.69	10.7	51.5
418.2	86	589	0.99	2993	52.29	50.61	1.98	0.53	0.14	1.52	0.26	0.10	3.28	0.00	2.65	1.89	14.8	58.4
410.5	86	589	1.48	2988	39.95	61.58	2.44	0.50	0.12	1.62	0.26	0.09	3.09	0.00	3.06	1.97	18.9	60.8
388.7	86	590	1.96	2984	31.60	68.85	2.77	0.49	0.11	1.66	0.26	0.09	3.05	0.00	3.37	2.01	23.3	62.6
393.4	86	589	2.92	2980	22.11	78.87	2.97	0.41	0.09	1.62	0.24	0.08	2.58	0.00	3.47	1.94	28.9	64.1
578.3	49	586	0.99	2993	57.32	56.29	0.89	0.27	0.06	0.60	0.13	0.05	1.41	0.00	1.23	0.79	6.6	60.8
459.0	57	587	0.99	2993	55.76	54.54	1.22	0.33	0.08	0.88	0.19	0.08	1.99	0.00	1.64	1.14	9.2	58.9
477.3	71	587	0.99	2993	54.78	53.39	1.53	0.40	0.10	0.99	0.20	0.08	2.35	0.00	2.03	1.27	10.8	61.6

Contd.

484.2	84	590	0.99	2993	53.04	51.28	1.92	0.48	0.12	1.41	0.23	0.09	2.94	0.00	2.53	1.73	13.6	59.3
453.0	91	589	0.99	2993	52.16	50.34	2.08	0.54	0.14	1.56	0.26	0.10	3.28	0.00	2.76	1.92	15.0	59.0
599.9	96	587	0.99	2993	51.96	49.98	2.27	0.57	0.14	1.55	0.24	0.09	3.31	0.00	2.98	1.88	15.3	61.3
653.3	106	587	0.99	2993	51.34	49.10	2.55	0.60	0.14	1.65	0.24	0.09	3.46	0.00	3.28	1.99	16.3	62.3
500.0	84	589	1.00	2259	38.26	37.10	1.64	0.43	0.12	1.41	0.23	0.09	2.93	0.00	2.20	1.73	17.3	56.0
484.2	84	590	0.99	2993	53.04	51.28	1.92	0.48	0.12	1.41	0.23	0.09	2.94	0.00	2.53	1.73	13.6	59.3
525.1	84	589	0.99	3360	60.85	58.82	2.02	0.50	0.11	1.29	0.22	0.09	2.76	0.00	2.63	1.59	11.7	62.3
505.9	84	590	0.99	4461	82.69	79.95	2.31	0.60	0.12	1.37	0.24	0.09	2.98	0.00	3.03	1.70	9.8	64.1
510.5	84	590	0.99	6664	127.70	123.76	2.68	0.68	0.12	1.27	0.25	0.09	2.95	0.00	3.48	1.61	6.8	68.4
604.3	84	589	0.99	8867	173.29	168.47	2.86	0.71	0.12	1.19	0.24	0.00	2.93	0.00	3.69	1.43	5.0	72.0
535.1	84	561	0.99	2993	57.99	56.73	1.08	0.28	0.04	0.43	0.07	0.00	1.06	0.00	1.41	0.49	5.5	74.1
539.6	84	573	0.99	2993	56.09	54.48	1.51	0.39	0.07	0.72	0.12	0.05	1.68	0.00	1.97	0.89	8.6	68.8
544.0	84	587	0.99	2993	53.07	51.35	1.97	0.50	0.12	1.31	0.23	0.09	2.94	0.00	2.59	1.63	13.5	61.4
548.6	84	603	0.99	2993	48.67	47.38	2.00	0.54	0.18	2.26	0.42	0.17	4.87	0.00	2.77	2.85	20.7	49.3
553.1	84	620	0.99	2993	43.38	43.60	1.47	0.44	0.21	3.56	0.75	0.35	7.71	0.00	2.22	4.66	29.3	32.3
563.1	84	630	0.99	2993	38.41	40.40	1.00	0.30	0.21	5.35	1.16	0.49	10.80	0.00	1.64	7.01	37.4	19.0
433.7	86	589	1.96	4448	51.11	107.20	3.36	0.60	0.11	1.54	0.27	0.09	3.02	0.00	4.07	1.90	16.7	68.2
585.0	97	588	0.99	4461	81.58	78.52	2.69	0.68	0.13	1.56	0.24	0.09	3.31	0.00	3.51	1.89	11.0	65.0
629.7	104	588	0.99	6664	125.83	121.27	3.40	0.78	0.14	1.57	0.26	0.10	3.50	0.00	4.32	1.93	8.2	69.1
648.8	104	587	0.99	4461	81.36	78.14	2.94	0.67	0.13	1.53	0.23	0.10	3.35	0.00	3.74	1.86	11.2	66.8
364.0	87	580	0.99	2993	53.74	52.02	1.81	0.50	0.11	1.23	0.20	0.08	2.64	0.00	2.42	1.51	12.4	61.6
621.7	84	587	0.99	2993	53.57	51.77	1.93	0.48	0.11	1.25	0.20	0.08	2.69	0.00	2.53	1.54	12.7	62.2
529.7	84	590	0.99	5930	113.36	109.91	2.48	0.61	0.11	1.14	0.22	0.09	2.72	0.00	3.20	1.45	7.0	68.7
462.2	69	589	0.99	10335	204.84	199.99	2.34	0.65	0.11	0.93	0.23	0.00	2.59	0.00	3.11	1.16	3.7	72.9

Table 3C (4). Operating conditions and testing results of catalyst # 14.

3C.6. Catalyst # 16 results

Time, *hr*	*P*, *bar*	*T*, *°K*	H_2/CO, *v/v*	GHSV, *L/kg cat/hr*	Products, *mol/kg cat/hr*												CO Conv., *%*	Alc. Sel., *mol %*
					CO	H_2	CH_3OH	C_2H_5OH	C_3H_7OH	CH_4	C_2H_6	C_3H_8	CO_2	H_2O	Tot. Alc.	Tot. HCs		
38.5	86	550	0.99	2993	56.47	57.53	0.23	0.16	0.07	0.52	0.21	0.13	2.82	0.00	0.47	0.86	8.0	35.4
42.4	86	570	0.99	2993	46.59	51.14	0.40	0.37	0.11	1.44	0.59	0.36	8.52	0.01	0.93	2.39	24.1	28.0
59.7	86	590	0.99	2993	48.66	51.15	0.46	0.41	0.11	1.76	0.59	0.30	6.70	0.01	1.02	2.65	20.7	27.8
63.3	85	608	0.99	2993	41.89	45.94	0.49	0.54	0.16	2.80	0.98	0.46	10.23	0.08	1.24	4.23	31.8	22.7
67.9	86	620	0.99	2993	34.88	41.11	0.45	0.62	0.20	3.89	1.45	0.66	14.34	0.15	1.36	6.00	43.2	18.5

Table 3C (6). Operating conditions and testing results of catalyst # 16.

3C.7. Catalyst # 17 results

Time, *hr*	*P*, *bar*	*T*, *°K*	H_2/CO, *v/v*	GHSV, *L/kg cat/hr*	Products, *mol/kg cat/hr*												CO Conv., *%*	Alc. Sel., *mol %*
					CO	H_2	CH_3OH	C_2H_5OH	C_3H_7OH	CH_4	C_2H_6	C_3H_8	CO_2	H_2O	Tot. Alc.	Tot. HCs		
19.2	85	578	0.99	2993	55.01	53.76	1.28	0.48	0.09	1.12	0.15	0.04	2.33	0.00	1.84	1.31	10.4	58.4
43.6	85	589	0.99	2993	52.82	51.65	1.52	0.51	0.12	1.61	0.22	0.07	3.32	0.00	2.16	1.91	13.9	53.1

Table 3C (7). Operating conditions and testing results of catalyst # 17.

Appendix 3D: Example Indexing and Quantitative Analysis using GSAS (EXPGUI Interface) and Rigaku PDXL Software

Following are the examples of phase identification and phase composition calculations using GSAS (EXPGUI interface) and Rigaku PDXL software for a sulfidized sample (Calcination followed by sulfidation, calcined at 773.15 °K and sulfidized at 923.15 °K).

Example GSAS

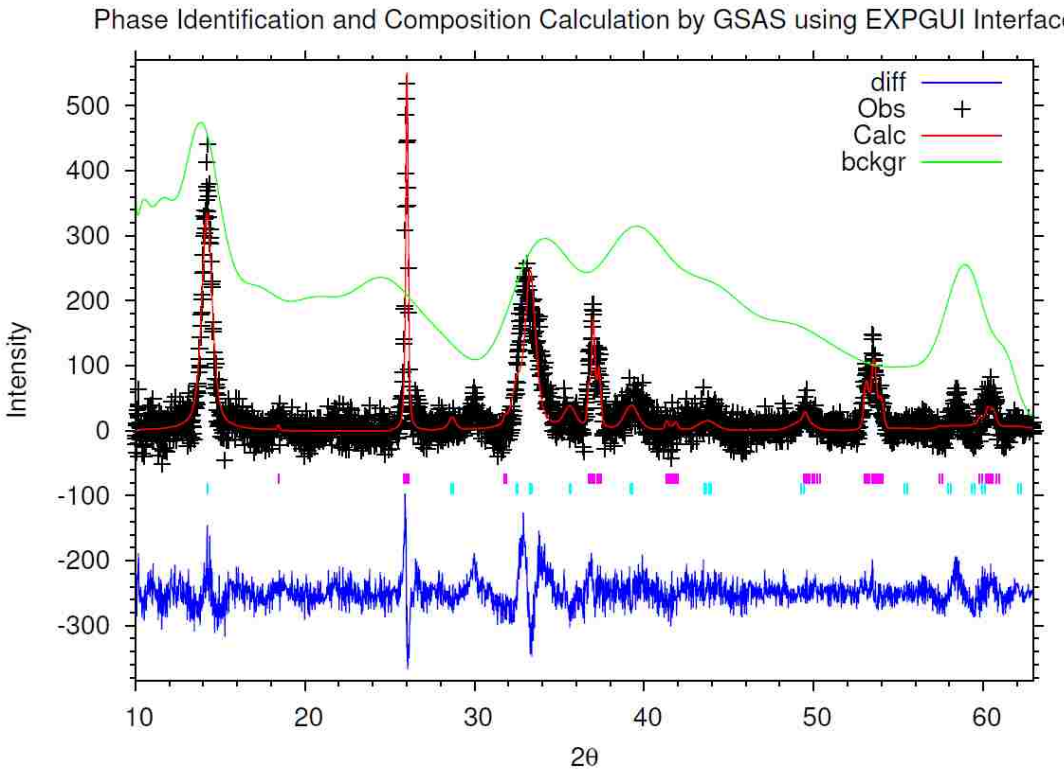

Example Rigaku PDXL

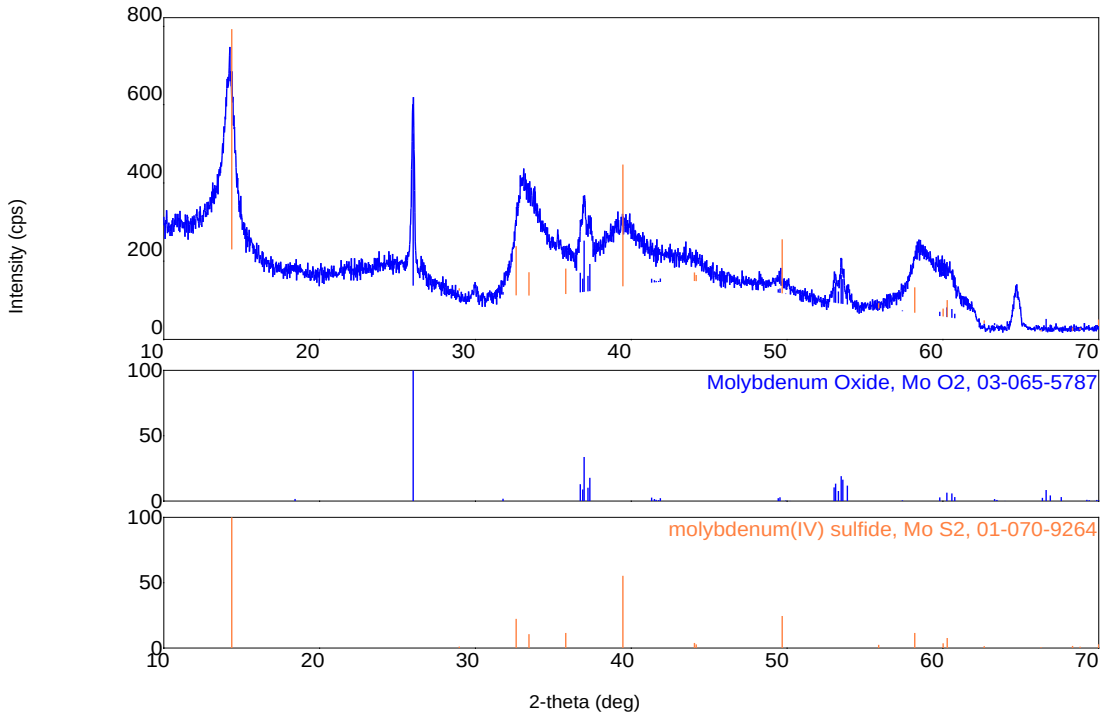

Phase composition by RIR method

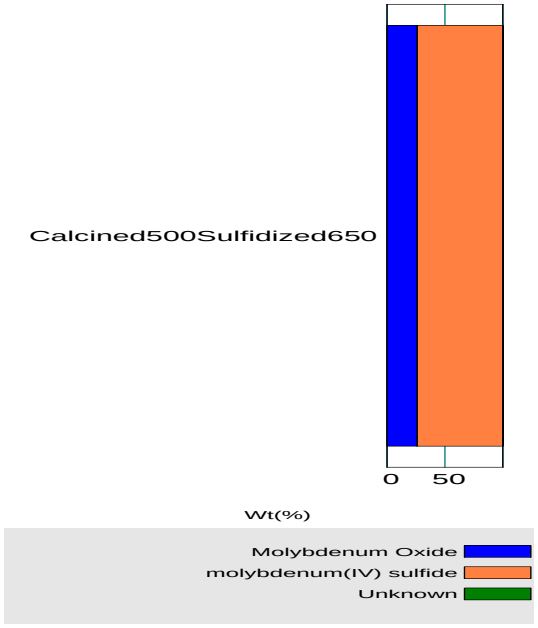

[redacted]

3.7. References

1. Farag, H., *Effect of Sulfidation Temperatures on the Bulk Structures of Various Molybdenum Precursors.* Energy & Fuels, 2002. **16**: p. 944-950.
2. Van Hengstum, A., et al., *Preparation of supported vanadium and molybdenum oxide catalysts using metal acetylacetonate complexes.* Applied Catalysis, 1983. **5**(2): p. 207-217.
3. Mohamed, M., S. Halawy, and M. Ebrahim, *The non-isothermal decomposition of cobalt acetate tetrahydrate.* Journal of Thermal Analysis and Calorimetry, 1994. **41**(2): p. 387-404.
4. Larson, A.C. and R.B. Von Dreele, *Gsas.* General Structure Analysis System. LANSCE, MS-H805, Los Alamos, New Mexico, 1994.
5. Toby, B.H., *EXPGUI, a graphical user interface for GSAS.* Journal of Applied Crystallography, 2001. **34**(2): p. 210-213.
6. *Integrated X-ray powder diffraction software PDXL, 2010.* The Rigaku Journal. **26**(1): p. 23-27.

Chapter 4

Steady-State Kinetic Analysis of Higher Alcohol Synthesis from Syngas over Activated Carbon Supported Cesium-Promoted Molybdenum Sulfide Catalysts

The work described in this chapter has been titled "Steady-State Kinetic Analysis of Higher Alcohol Synthesis from Syngas over Activated Carbon Supported Cesium-Promoted Molybdenum Sulfide Catalysts" by Ranjan K. Sahoo, Hugo S. Caram, Divyanshu R. Acharya, and Richard G. Herman, *manuscript in preparation.*

Abstract

The cesium promoted molybdenum sulfide based supported catalyst was prepared by direct sulfidation of the calcined pellets and tested extensively under higher alcohol synthesis conditions. The steady-state experimental data were collected between 385 to 655 hours of reaction. The four operating variables; reaction temperature, pressure, gas hourly space velocity, and hydrogen to carbon monoxide ratio were varied around a center point or base condition of 590 °K, 84 bar, 3000 L/kg cat/hr, and hydrogen to carbon monoxide ratio of 1.0 v/v. At least five different values of the operating conditions between 560-630 °K, 50-110 bar, 2000-9000 L/kg cat/hr, and hydrogen to carbon monoxide ration between 0.5-3.0 v/v were used for steady-state data collections. The alcohol and hydrocarbon products follow aderson-schultz-flory distribution. The chain growth probability of 0.297 and 0.235 was calculated at the base condition for alcohol and the sum of alcohol and hydrocarbon products respectively. Two different types of

kinetic models (power-law type and langmuir-hinshelwood type) were developed based on seven reactions; methanol, ethanol, propanol, methane, ethane, propane, and carbon dioxide formation reactions. It was assumed that the hydrocarbons are formed from decomposition of the corresponding carbon number alcohols and the higher alcohols are formed from the immediate lower carbon number alcohols via carbon monoxide insertion mechanism, whereas the methanol was formed directly from syngas. The gross rate of production of products was used instead of net productions for kinetic analysis. The apparent activation energy of 61.3, 73.0, 121.70 kJ/mol was calculated from the arrhenius plots for methanol, ethanol, and propanol formation reactions respectively, whereas, a relatively higher activation energy of 97.3, 104.8, 120.1, and 116.9 kJ/mol was calculated for carbon dioxide, methane, ethane, and propane reactions respectively. The power-law expressions, relating the gross rate of production of products to reaction temperature and partial pressures of hydrogen and carbon monoxide were used. From the power-law exponents it was concluded that, the formation of CH_3O surface species is the rate-determining step for methanol formation, and the formations of corresponding acyl ($C_nH_{2n+1}CO$*) and alkyl (C_nH_{2n+1}*) species are the rate-determining steps for higher alcohols ($C_nH_{2n+1}OH$) and hydrocarbon (C_nH_{2n+2}) formation reactions respectively. Based on these rate-determining steps, a micro-kinetics was proposed and the corresponding Langmuir-hinshelwood type rate expressions for the gross rate of production of products were developed. The net production of products was calculated from the gross rate of production of products. The singular value decomposition was applied for the first time to the higher alcohol reaction network to determine the minimum number of reactions required and the corresponding reaction stoichiometry to*

sufficiently describe the effect of four operating conditions (temperature, pressure, gas hourly space velocity, and hydrogen to carbon monoxide ratio) on alcohol and hydrocarbon yields. Only two empirical forward reactions: formations of alcohols, hydrocarbons, and carbon dioxide directly from hydrogen and carbon monoxide and formations of hydrocarbons, higher alcohols, and carbon dioxide by decomposition of alcohols and addition of carbon monoxide. An empirical kinetic model based on these two empirical reactions with langmuir-hinshelwood type rate expressions was developed. A genetic algorithm minimization tool was used to estimate the kinetic parameters associated with the power-law, langmuir-hinshelwood, and empirical kinetic models. Both the langmuir-hinshelwood and empirical model can predict the experimental data quite reasonably well, both qualitatively and quantitatively, with the latter being required only two forward reactions and eleven kinetic parameters, whereas the former one required more complex formulations involving seven reaction with one of the reaction is reversible reaction and eighteen kinetic parameters.

4.1. Objective

The higher alcohol synthesis reactions are complex and it involves many series and parallel reactions. The objective of this chapter is:

- To develop simplified and accurate kinetic models to describe the catalytic behavior with respect to change in reaction conditions, such as, temperature, pressure, gas hourly space velocity, and hydrogen to carbon monoxide ratio at steady-state.

4.2. Experimental Section

4.2.1. Catalyst Preparation

Activated Carbon (AC) was cut and sieved to approximately 3 *mm* cylindrical pellets (aspect ratio of 1) and washed with a 1.0 *M* HNO_3 solution to remove any metal impurities present in the AC. The acid washed, dried AC was promoted with an aqueous solution of Ammonium Molybdate Tetrahydrate (AMT) using a solution rate of 15-20 *ml/hr* in a Rotovap, simulating spray drying technique under vacuum. The AMT solution prepared by dissolving 17 *g* of AMT in 80 *ml* of de-ionized (DI) water was used to impregnate 42 *g* of acid washed AC. The dried, AMT promoted pellet was sulfidized at 923.15 °*K* and atmospheric pressure with 5 % H_2S in H_2 flowing through a quartz tube reactor at 100 *ml/min*. The sulfidation process was followed by monitoring the water and H_2S content of the exit gas by chromatography. The sulfidation time was determined by disappearance of H_2O at outlet of the reactor and when the outlet concentration of H_2S equals the inlet concentration of H_2S. The sulfidized pellet was promoted with an aqueous solution of Cs formate using a solution feed rate of 12 *ml/hr* in a Rotovap similar to the AMT impregnation step. The Cs formate solution was prepared by dissolving 10 g of Cs formate in 300 *ml* DI water. A 75 *ml* Cs formate solution was used to promote 12.5 *g* of sulfidized pellets. Drying operation after Acid wash, AMT promotion and Cs formate promotion was performed in a vacuum oven maintained at 343.15 °*K* and 20-25 *in Hg* vacuum for at least 24 *hr*. The dried catalyst pellet was stored in a N_2 purged bottle. Detailed description of each catalyst preparation steps were described in section 2.2.3 of chapter 2 and section 3.2.2 of chapter 3.

The approximate composition of the catalyst as calculated by performing mass balance for the catalyst preparation process (weight difference before and after each catalyst preparation steps) was, 11.75 *wt%* Mo, *12.39 wt%* Cs and *6.35 % S* (target Mo/Cs was 1 *w/w*). Mass balance of catalyst preparation process is given in Appendix 3A of chapter 3.

4.2.2. Experimental Design

The catalyst testing was performed in a single pass lab-scale tubular reactor. Detailed descriptions of catalyst testing unit and analytical procedures are given in section 2.3 of chapter 2. A 3 *g* of catalyst was used for the testing. Four operating variables; reactor temperature, pressure, gas hourly space velocity (GHSV), and H_2/CO ratio, were varied around a center point condition of 590.15 *°K*, 84 *bar*, 3000 *L/kg cat/hr* and H_2/CO = 1 *v/v*. At least five different values of temperature, pressure, GHSV and H_2/CO in the ranges of 560 – 630 *°K*, 50 – 110 *bar*, 2000 – 9000 *L/kg cat/hr*, and 0.5 – 3.0 *v/v*, respectively were used for the analysis. The catalyst testing results were taken after 385 *hrs* of reaction to ensure that the catalyst was reached steady-state. Operating conditions and steady-state results obtained between 385 – 655 *hrs* of continuous run are reported in Table 4.1. The average values from carbon and oxygen balance were used. The bold faced row in the pressure variation section was used as the center point condition for kinetic analysis. The atomic balance errors were with in ± 0.6 *%* as shown in the Fig. 4.1. The pictorial representation of effect of temperature, pressure, GHSV, and H_2/CO ratio on product yields, CO conversion, and alcohol selectivity are shown in Fig. 3.10 – 3.17 of chapter 3.

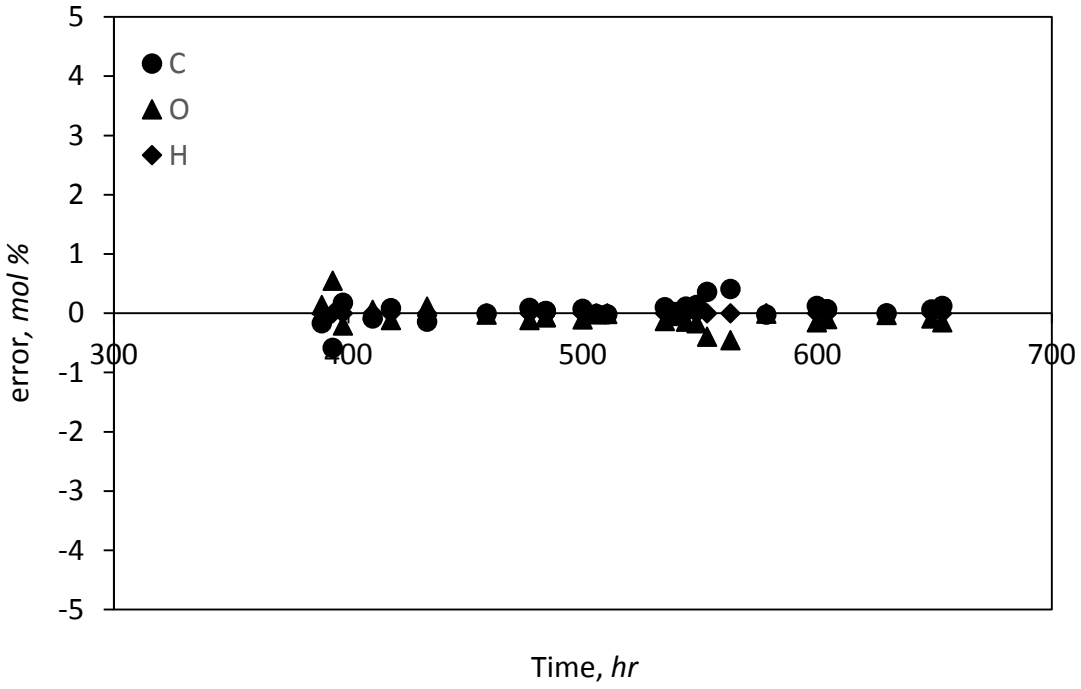

[redacted]

Sl. No.	Time, *hr*	*P*, *bar*	*T*, *°K*	H_2/CO, *v/v*	GHSV, *L/kg cat/hr*	Products, *mol/kg cat/hr*												CO Conv., *%*	Alc. Sel., *mol %*
						CO	H_2	CH_3OH	C_2H_5OH	C_3H_7OH	C_4H_9OH	CH_4	C_2H_6	C_3H_8	CO_2	Tot. Alc.	Tot. HCs		
Effect of Temperature																			
1	535.1	84	561	1.0	2993	57.93	56.73	1.08	0.28	0.04	0.00	0.43	0.07	0.00	1.06	1.40	0.49	5.6	74.1
2	539.6	84	573	1.0	2993	56.07	54.48	1.51	0.39	0.07	0.00	0.72	0.12	0.05	1.68	1.97	0.89	8.6	68.8
3	544.0	84	587	1.0	2993	53.00	51.37	1.97	0.50	0.12	0.00	1.31	0.23	0.09	2.93	2.59	1.63	13.6	61.4
4	548.6	84	603	1.0	2993	48.91	47.81	2.01	0.54	0.18	0.05	2.27	0.43	0.18	4.89	2.79	2.87	20.3	49.3
5	553.1	84	620	1.0	2993	43.81	44.45	1.49	0.45	0.21	0.09	3.60	0.75	0.35	7.78	2.24	4.70	28.6	32.3
6	563.1	84	630	1.0	2993	38.41	40.40	1.00	0.30	0.21	0.13	5.35	1.16	0.49	10.8	1.64	7.01	37.4	19.0
Effect of Pressure																			
7	578.3	49	586	1.0	2993	57.32	56.29	0.89	0.27	0.06	0.00	0.60	0.13	0.05	1.41	1.23	0.79	6.6	60.8
8	459.0	57	587	1.0	2993	55.76	54.54	1.22	0.33	0.08	0.00	0.88	0.19	0.08	1.99	1.64	1.14	9.2	58.9
9	477.3	71	587	1.0	2993	54.72	53.40	1.53	0.40	0.10	0.00	0.99	0.20	0.08	2.35	2.03	1.27	10.8	61.6
10	**484.2**	**84**	**590**	**1.0**	**2993**	**53.01**	**51.29**	**1.92**	**0.48**	**0.12**	**0.00**	**1.41**	**0.23**	**0.09**	**2.94**	**2.53**	**1.73**	**13.6**	**59.3**
11	599.9	96	587	1.0	2993	51.89	49.99	2.27	0.57	0.14	0.00	1.55	0.24	0.09	3.30	2.97	1.88	15.5	61.3
12	653.3	106	587	1.0	2993	51.27	49.12	2.54	0.60	0.14	0.00	1.65	0.24	0.09	3.46	3.28	1.99	16.5	62.3
Effect of GHSV																			
13	500.0	84	589	1.0	2259	38.22	37.11	1.64	0.42	0.12	0.02	1.41	0.23	0.09	2.93	2.20	1.73	17.3	56.0
14	484.2	84	590	1.0	2993	53.01	51.29	1.92	0.48	0.12	0.00	1.41	0.23	0.09	2.94	2.53	1.73	13.6	59.3
15	505.9	84	590	1.0	4461	82.69	79.95	2.31	0.60	0.12	0.00	1.37	0.24	0.09	2.98	3.03	1.70	9.8	64.1
16	510.5	84	590	1.0	6664	127.70	123.76	2.68	0.68	0.12	0.00	1.27	0.25	0.09	2.95	3.48	1.61	6.8	68.4
17	604.3	84	589	1.0	8867	173.15	168.48	2.85	0.71	0.12	0.00	1.19	0.24	0.00	2.92	3.69	1.43	5.1	72.0
Effect of H_2/CO																			
18	397.8	86	589	0.5	3002	73.14	32.76	1.13	0.49	0.14	0.03	1.30	0.28	0.12	3.39	1.80	1.69	10.3	51.5
19	418.2	86	589	1.0	2993	52.24	50.62	1.98	0.53	0.14	0.00	1.52	0.26	0.10	3.28	2.65	1.89	14.9	58.4
20	410.5	86	589	1.5	2988	39.98	61.57	2.44	0.50	0.12	0.00	1.63	0.26	0.09	3.10	3.07	1.98	18.9	60.8
21	388.7	86	590	2.0	2984	31.65	68.83	2.78	0.49	0.11	0.00	1.66	0.26	0.09	3.05	3.38	2.02	23.2	62.6
22	393.4	86	589	2.9	2980	22.23	78.81	2.99	0.41	0.09	0.00	1.63	0.24	0.08	2.60	3.49	1.95	28.5	64.1
Additional Results at various combinations of Temperature, Pressure, GHSV and H_2/CO																			
23	433.7	86	589	2.0	4448	51.17	107.18	3.37	0.60	0.11	0.00	1.54	0.27	0.09	3.03	4.08	1.91	16.6	68.2
24	629.7	104	588	1.0	6664	125.81	121.27	3.40	0.78	0.14	0.00	1.57	0.26	0.10	3.49	4.32	1.93	8.2	69.1
25	648.8	104	587	1.0	4461	81.30	78.15	2.94	0.67	0.13	0.00	1.53	0.23	0.10	3.35	3.74	1.85	11.3	66.8

Table 4.1. Operating conditions and steady-state testing results of $Cs/MoS_2/AC$ catalyst obtained after 385 hr (cat. # 14).

4.3. Kinetic Model Development

The objective of the present analysis is to formulate simplified rate expressions describing the nature of observed rate of formation of alcohols and hydrocarbons with respect to change in operating variables, such as, reaction pressure, temperature, GHSV and H_2/CO.

4.3.1. Product Distribution

Only linear alcohols, hydrocarbons and carbon dioxide along with un-reacted carbon monoxide and hydrogen were observed in the product. Major alcohols and hydrocarbons observed are: methanol, ethanol, propanol, methane, ethane and propane. Small amount of butanol observed in the products are lumped together with propanol for kinetic analysis.

Experimental observations shows that the formation of alcohols, hydrocarbons and sum of alcohols and hydrocarbons decreases exponentially with increase in carbon number as described by the Anderson-Schultz-Flory (ASF) distribution [1],

$$y_n = (1-\alpha)\alpha^{n-1} \;\Rightarrow\; \ln(y_n) = ln\left(\frac{1}{\alpha}-1\right) + nln(\alpha) \qquad (4.1)$$

Where, y_n is the mole fraction of alcohol or hydrocarbon or sum of alcohol and hydrocarbon, n is the carbon number and α is the chain-growth probability.

The ASF distribution of the alcohols and the sum of alcohols and hydrocarbons at the operating condition of 603 °*K*, 84 *bar*, 2993 *L/kg cat/hr* GHSV and H_2/CO =1 is show in Fig. 4.2. The average value of chain-growth probability obtained from the

intercept and slope of the plot is 0.297 for the alcohols and 0.235 for the sum of alcohols and hydrocarbons.

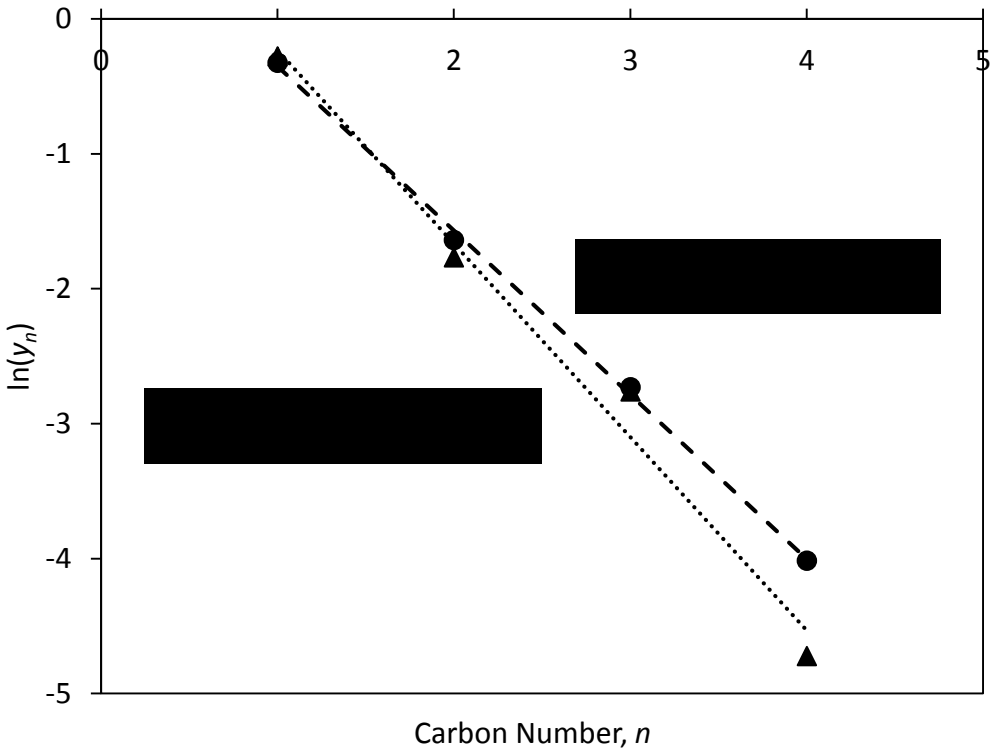

4.3.2. Reaction Scheme

The overall reaction network is shown in Fig. 4.3. It is assumed that the hydrocarbons are formed by decomposition of corresponding alcohols; methane, ethane and propane are formed by hydrogenation of methanol, ethanol and propanol, respectively [1]. Alcohols are formed *via* CO insertion mechanism; ethanol and propanol are formed respectively from methanol and ethanol by CO insertion mechanism [2]. Methanol formation reaction is a reversible reaction. We do not see any water in the products, except very negligible amount at high temperature reaction conditions. It is assumed that, all the water formed during reaction is converted to carbon dioxide by a forward water gas shift reaction [2].

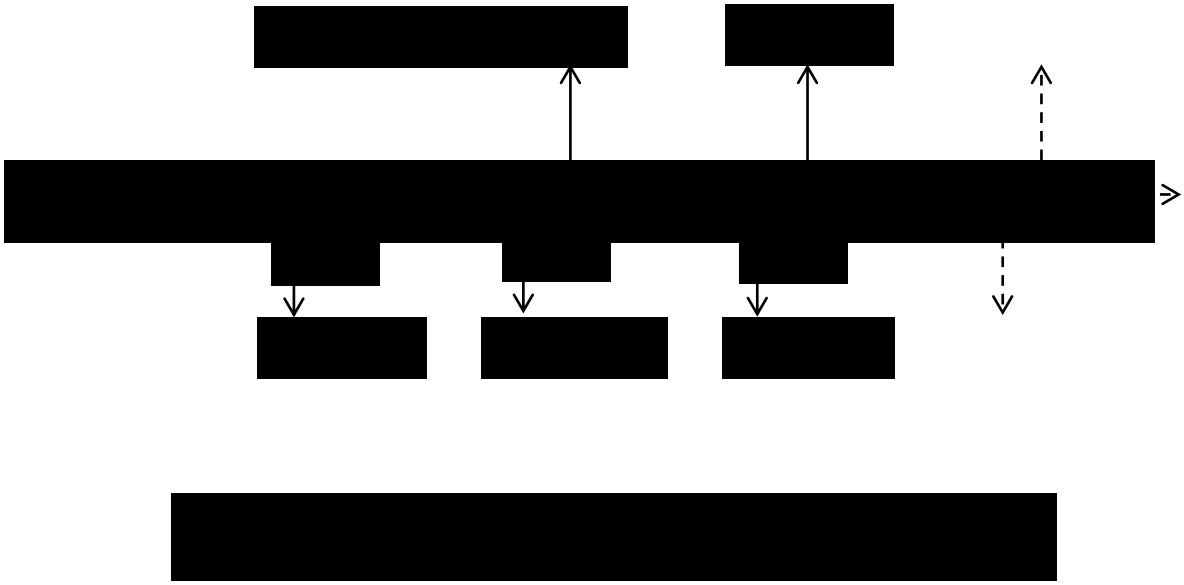

Based on these assumptions and as the series of alcohols and hydrocarbons follow ASF distribution, the simplified reaction scheme for higher alcohol synthesis can be written as;

$$CO + 2H_2 \rightleftarrows CH_3OH \tag{4.2}$$

$$CH_3OH + CO + 2H_2 \longrightarrow C_2H_5OH + H_2O \tag{4.3}$$

$$C_2H_5OH + CO + 2H_2 \longrightarrow C_3H_7OH + H_2O \tag{4.4}$$

$$CH_3OH + H_2 \longrightarrow CH_4 + \mathrm{H_2O} \tag{4.5}$$

$$C_2H_5OH + H_2 \longrightarrow C_2H_6 + \mathrm{H_2O} \tag{4.6}$$

$$C_3H_7OH + H_2 \longrightarrow C_3H_8 + \mathrm{H_2O} \tag{4.7}$$

$$CO + H_2\mathrm{O} \longrightarrow CO_2 + H_2 \tag{4.8}$$

The observed (or net) rate of productions of alcohols, hydrocarbons and CO_2 can be obtained from the gross rate of production of alcohols for the simplified reaction scheme presented in the previous section as [3],

$$r_{CH_4} = r^g_{CH_4} \tag{4.9}$$

$$r_{C_2H_6} = r^g_{C_2H_6} \tag{4.10}$$

$$r_{C_3H_8} = r^g_{C_3H_8} \tag{4.11}$$

$$r_{CH_3OH} = r^g_{CH_3OH} - r^g_{C_2H_5OH} - r_{CH_4} \tag{4.12}$$

$$r_{C_2H_5OH} = r^g_{C_2H_5OH} - r^g_{C_3H_7OH} - r_{c_2H_6} \tag{4.13}$$

$$r_{C_3H_7OH} = r^g_{C_3H_7OH} - r_{C_3H_8} \tag{4.14}$$

$$r_{CO_2} = r^g_{CO_2} = r^g_{C_2H_5OH} + r^g_{C_3H_7OH} + r_{CH_4} + r_{c_2H_6} + r_{C_3H_8} \tag{4.15}$$

The gross rate of production of methanol is equal to the sum of observed rate of production of methanol, ethanol, propanol, methane, ethane and propane. The gross rate of production of ethanol is equal to the sum of observed rate of production of ethanol, propanol, ethane and propane. Similarly, the gross rate of production of propanol is equal to the sum of observed rate of production of propanol and propane. The rate of production of CO_2 is equal to the sum of the rate of production of water from ethanol, propanol, and hydrocarbon reactions [2].

4.3.3. Apparent Activation Energy

Arrhenius plots for the gross rate of formation of alcohols, hydrocarbons and CO_2 are shown in Fig. 4.4 and Fig. 4.5. The activation energies and pre-exponential factors were calculated from slope and intercept of these plots and reported in Table 4.2. Activation energies of hydrocarbons are found to be higher compared to that of alcohols.

Components	A_i , ***mol/kg cat/hr***	E_i , ***kJ/mol***	**Coefficient of determination,** r^2
CH_3OH	4.046	61.31	0.977
C_2H_5OH	0.937	73.02	0.986
C_3H_7OH	0.205	121.70	0.961
CO_2	3.088	97.34	0.998
CH_4	1.370	104.84	0.996
C_2H_6	0.244	120.09	0.998
C_3H_8	0.108	116.89	0.998

Table 4.2. Activation energies and pre-exponential factors calculated from arrhenius plots.

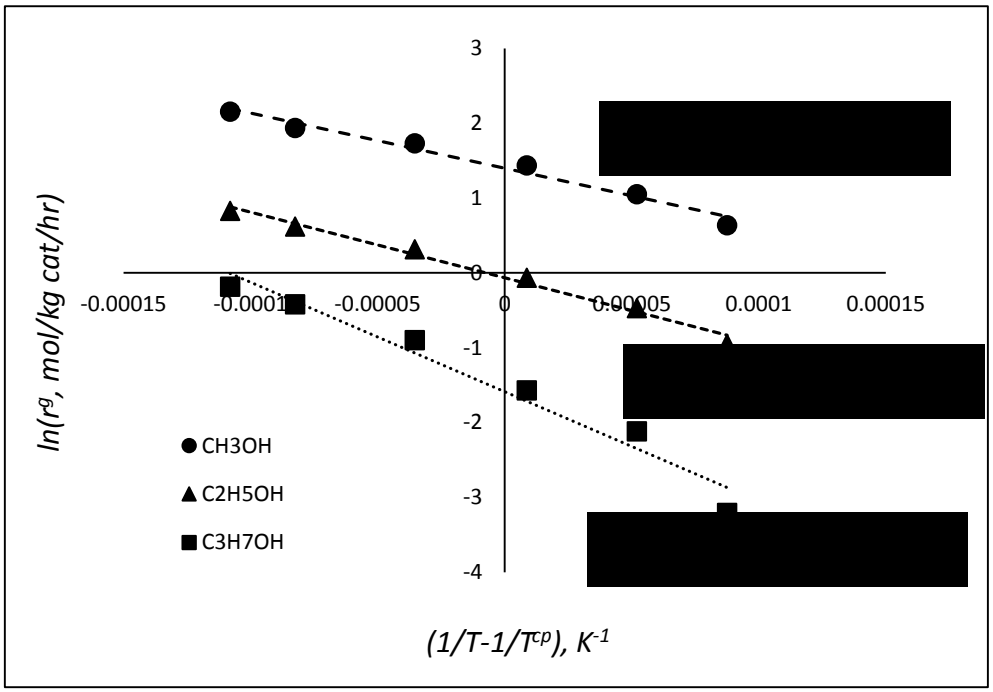
3
2
1
0
-1
-2
-3
-4
-0.00015
-0.0001
-0.00005
0
0.00005
0.0001
0.00015
ln(r^g, mol/kg cat/hr)
CH3OH
C2H5OH
C3H7OH
(1/T-1/T^cp), K^-1

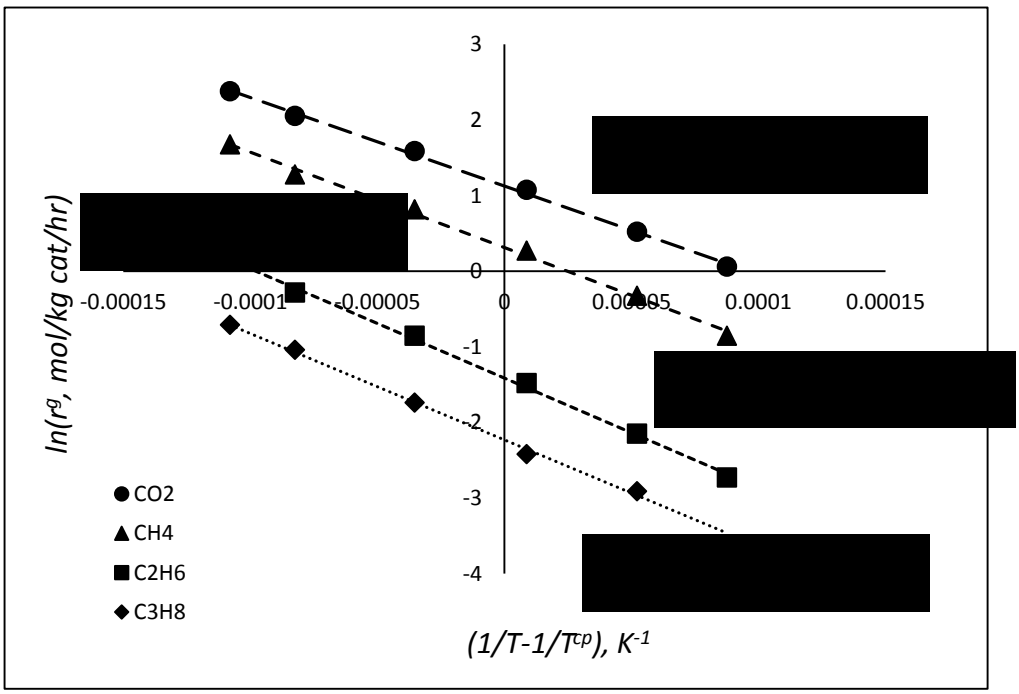
3
2
1
0
-1
-2
-3
-4
-0.00015
-0.0001
-0.00005
0
0.00005
0.0001
0.00015
ln(r^g, mol/kg cat/hr)
CO2
CH4
C2H6
C3H8
(1/T-1/T^cp), K^-1

4.3.4. Power-Law Model

The rate expressions of the following power-law type were used to determine reaction orders in CO and H_2 for each of the reactions 4.2 – 4.8 [4]. The experimental data from Table 4.1 was used for the analysis.

$$r_i^g = A_i e^{-\left(\frac{E_i}{R}\right)\left(\frac{1}{T}-\frac{1}{T^{cp}}\right)} \left(\frac{p_{CO}}{p_{CO}^{cp}}\right)^{a_i} \left(\frac{p_{H_2}}{p_{H_2}^{cp}}\right)^{b_i} \tag{4.16}$$

Where, r_i^g is the gross rate of production of component *i*, A_i is the pre-exponential factor, E_i is the activation energy, *p* denotes the partial pressure of the reactant, p^{cp} is the partial pressure of the reactant at a center point operating condition ($p_{CO}^{cp} = 40.035\ bar\ and\ p_{H_2}^{cp} = 38.737\ bar$), and a_i and b_i are the reaction orders in CO and H_2.

Genetic Algorithm (GA) was employed separately to each of the components to calculate the reaction orders by minimizing the following objective function [5],

$$f = 100\ \text{sqrt}\left[\frac{1}{m}\sum_{1}^{m}\left(r_{i,expt.}^g - r_{i,est.}^g\right)^2\right] \tag{4.17}$$

$m = \#\ of\ data\ sets, i = components$

Where, $r_{i,expt.}^g$ and $r_{i,est.}^g$ are respectively the experiential and the predicted gross rate of production of component *i*. Detailed description of GA for kinetic parameter

estimation is presented in section 4.4.2. The activation energies, pre-exponential factors and reaction orders calculated for power-law model are given in Table 4.3. The upper and lower bound used for GA minimization and the corresponding value of objective function is also given in Table 4.3. The number of population and the number of generation used are 500 and 100 respectively.

By looking at the ratio of reaction orders for the methanol formation reaction, it can be inferred that the formation of CH_3O^* species could be the possible rate-determining step for methanol formation. The ratio of reaction orders for methane formation reaction is also close to 3. It indicates the formation of methanol and methane *via* common surface species. For both alcohols and hydrocarbons the ratio of reaction orders decreases with increase in chain length; as chain length increases by CO insertion mechanism. Partial pressure of CO dominates the formation of C_2^+ components (Ethanol, ethane, propanol and propane). Activation energy increases with increase in chain length.

Kinetic Parameters	Lower Bound	Upper Bound	Optimized Value	Kinetic Parameters	Lower Bound	Upper Bound	Optimized Value	Objective Function, f	$\frac{b_i}{a_i}$	Possible rate limiting reaction
A_{CH_3OH}	3	6	4.47	E_{CH_3OH}	50	80	63.48	0.29	3.33	formation of CH_3O*
a_{CH_3OH}	0	1	0.32	b_{CH_3OH}	0	2	1.05			
$A_{C_2H_5OH}$	0	2	1.01	$E_{C_2H_5OH}$	60	90	74.27	0.06	1.01	formation of CH_3CO* by CO insertion
$a_{C_2H_5OH}$	0	1	0.48	$b_{C_2H_5OH}$	0	1	0.48			
$A_{C_3H_7OH}$	0	0.5	0.23	$E_{C_3H_7OH}$	100	150	110.63	0.03	0.30	formation of C_2H_5CO* by CO insertion
$a_{C_3H_7OH}$	0	1	0.49	$b_{C_3H_7OH}$	0	1	0.15			
A_{CH_4}	1	3	1.41	E_{CH_4}	90	120	110.48	0.12	3.22	formation of CH_3* from CH_3O*
a_{CH_4}	0	1	0.23	b_{CH_4}	0	1	0.74			
$A_{C_2H_6}$	0	0.5	0.25	$E_{C_2H_6}$	100	140	121.91	0.12	1.71	formation of C_2H_5* from CH_3CO*
$a_{C_2H_6}$	0	1	0.17	$b_{C_2H_6}$	0	1	0.30			
$A_{C_3H_8}$	0	0.25	0.10	$E_{C_3H_8}$	100	150	133.01	0.02	0.57	formation of C_3H_7* from C_2H_5CO*
$a_{C_3H_8}$	0	1	0.27	$b_{C_3H_8}$	0	1	0.15			
A_{CO_2}	1	5	3.12	E_{CO_2}	80	120	105.03	0.20	0.96	$OH*+CO*$
a_{CO_2}	0	1	0.45	b_{CO_2}	0	1	0.44			

Table 4.3. Kinetic parameters of power-law model.

4.3.5. Langmuir-Hinshelwood (LH) Model

Simplified reaction scheme as described in the previous section has been used. Reversible nature of the methanol formation reaction was taken into considerations. Each of the reactions 4.2 – 4.7 were considered separately.

Adsorption and desorption reactions in micro-kinetics are assumed to be so fast compared to alkyl (C_nH_{2n+1}*) and acyl ($C_nH_{2n+1}CO$*) formation reactions that they achieve equilibrium. Alkyl and acyl formation reactions are rate controlling for hydrocarbon and alcohol formations respectively, except for methanol formation reaction. Most likely rate-determining step for methanol formation is the formation of CH_3O^* surface species. The micro-kinetics for higher alcohol synthesis reactions can be written as,

Initiation

$$CO(g) + * \overset{K_{CO}}{\leftrightarrow} CO*, \qquad quasi-equilibrated \tag{4.18}$$

$$H_2(g) + 2* \overset{K_H}{\leftrightarrow} 2H*, \qquad quasi-equilibrated \tag{4.19}$$

Methanol Formation

$$CO* + 3H* \rightleftharpoons CH_3O* + 3*, \qquad rate-determining\ step,\ k^+_{CH_3O}, k^-_{CH_3O} \tag{4.20}$$

$$CH_3O* + H* \overset{K_{CH_3O}}{\longleftrightarrow} CH_3OH(g) + 2*, \qquad quasi-equilibrated \tag{4.21}$$

Methane Formation

$$CH_3O* + H* \rightarrow CH_3* + OH*, \qquad rate-determining\ step, k_{CH_3} \tag{4.22}$$

$$CH_3* + H* \rightarrow CH_4(g) + 2* \tag{4.23}$$

Ethanol Formation

$$CH_3O* + CO* + H* \rightarrow CH_3CO* + OH* + *, rate-determining\ step, k_{CH_3CO} \tag{4.24}$$

$$CH_3CO* + 3H* \overset{K_{CH_3CO}}{\longleftrightarrow} C_2H_5OH(g) + 4*, \qquad quasi-equilibrated \tag{4.25}$$

Ethane Formation

$$CH_3CO* + 3H* \rightarrow C_2H_5* + OH* + 2*, \qquad rate-determining\ step, k_{C_2H_5} \tag{4.26}$$

$$C_2H_5* + H* \rightarrow C_2H_6(g) + 2* \tag{4.27}$$

Propanol Formation

$$CH_3CO* + CO* + 3H* \rightarrow C_2H_5CO* + OH* + 3*,$$

$$rate-determining\ step, k_{C_2H_5CO} \tag{4.28}$$

$$C_2H_5CO* + 3H* \overset{K_{C_2H_5CO}}{\longleftrightarrow} C_3H_7OH(g) + 4*, \qquad quasi-equilibrated \tag{4.29}$$

Propane Formation

$$C_2H_5CO* + 3H* \rightarrow C_3H_7* + OH* + 2*, \qquad rate-determining\ step, k_{C_3H_7} \tag{4.30}$$

$$C_3H_7* + H* \rightarrow C_3H_8(g) + 2* \tag{4.31}$$

$Carbon\ Dioxide\ Formation$

$$OH* + CO* \rightarrow CO_2* + H* \tag{4.32}$$

$$CO_2* \rightarrow CO_2(g) + * \tag{4.33}$$

Carbon monoxide adsorption, dissociative adsorption of hydrogen, and desorption of alcohols are assumed to be in equilibrium. The pictorial representation of the micro-kinetics is shown in Fig. 4.6.

4.3.5.1. Gross Rate of Methanol Formation

The gross rate of formation of methanol can be expressed in terms of the rate-determining step 4.20 as,

$$r^{g}_{CH_3OH} = k^{+}_{CH_3O}[CO*][H*]^3 - k^{-}_{CH_3O}[CH_3O*][*]^3 \tag{4.34}$$

The equilibrium relationships for CO adsorption, eq. 4.18, H_2 adsorption, eq. 4.19 and CH_3O* formation from methanol decomposition, eq. 4.21 are,

$$K_{CO} = \frac{[CO*]}{p_{co}[*]} \Rightarrow [CO*] = K_{CO}p_{co}[*] \tag{4.35}$$

$$K_H = \frac{[H*]^2}{p_{H_2}[*]^2} \Rightarrow [H*] = K_{H_2}p_{H_2}^{0.5}[*];\ K_{H_2} = K_H^{0.5} \tag{4.36}$$

$$K_{CH_3O} = \frac{p_{CH_3OH}[*]^2}{[CH_3O*][H*]} \Rightarrow [CH_3O*] = K'_{CH_3O}\frac{p_{CH_3OH}[*]}{p_{H_2}^{0.5}};\ K'_{CH_3O} = \frac{1}{K_{CH_3O}K_{H_2}} \tag{4.37}$$

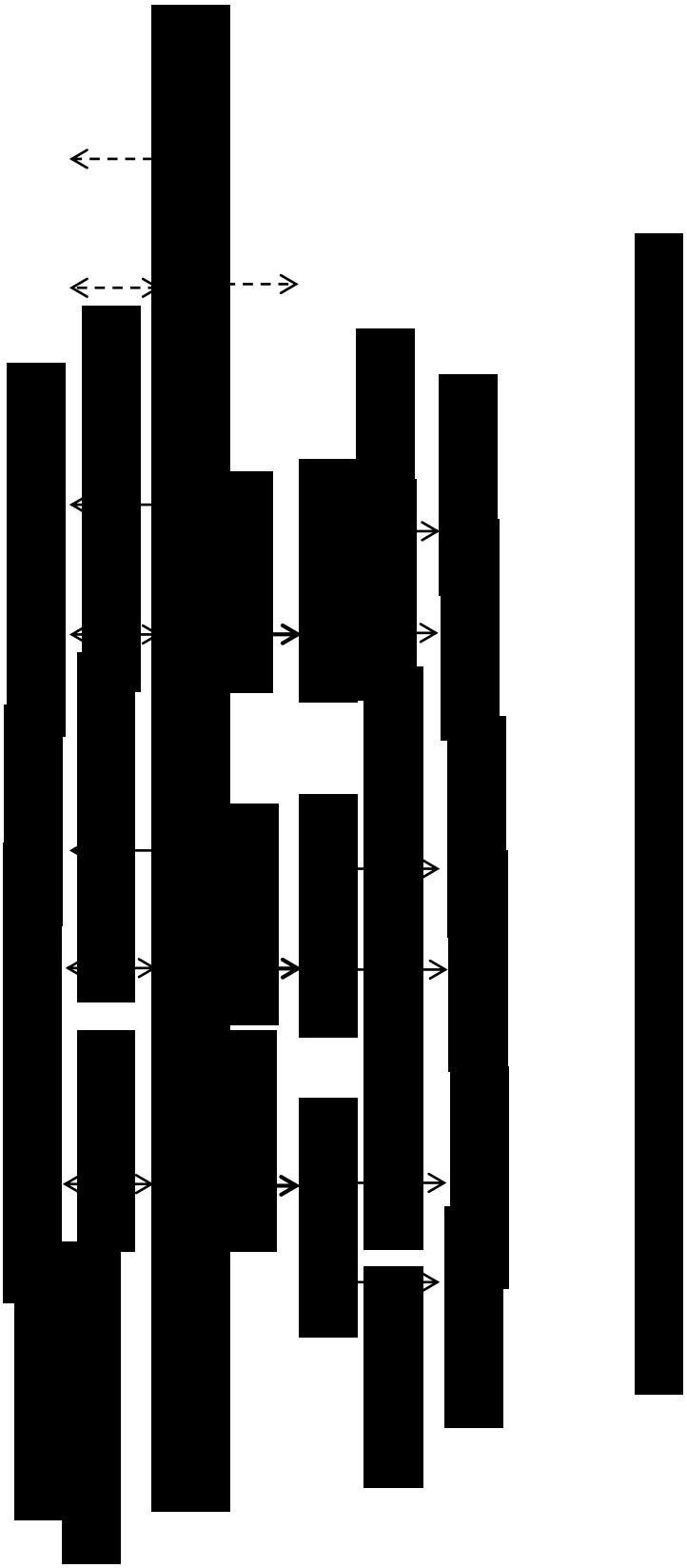

Where [ ] denotes surface concentrations of adsorbed species, p_i is the partial pressure of gaseous species *i*, *k* is the rate constant, and *K*'s are equilibrium constants. The concentration of vacant site [*] can be determined from the site balance. Surface species participating in the rate-determining reaction step of methanol formation reaction were considered for site balance. Effect of other surface species related to higher alcohols, hydrocarbons and water-gas-shift reactions are assumed to be negligible for methanol formation and *vice versa*.

$$[s]_{CH_3OH} = [*] + [CO\,*] + [H\,*] + [CH_3O\,*] \tag{4.38}$$

Substituting equilibrium relationships 4.35 – 4.37 and solving for [∗],

$$[*] = \frac{[s]_{CH_3OH}}{\left(1 + K_{CO}p_{co} + K_{H_2}p_{H_2}^{0.5} + K'_{CH_3O}\frac{p_{CH_3OH}}{p_{H_2}^{0.5}}\right)} \tag{4.39}$$

Solving rate equation 4.34, equilibrium relationships 4.35 – 4.37, and site balance equation 4.39 simultaneously and eliminating [∗] to obtain gross rate of formation of methanol, $r_{CH_3OH}^{g}$ in-terms of partial pressures, rate constant and equilibrium constants,

$$r^{g}_{CH_3OH} = \frac{k_{CH_3OH}\left[p_{CO}p^{1.5}_{H_2} - \frac{1}{K_{CH_3OH}}\frac{p_{CH_3OH}}{p^{0.5}_{H_2}}\right]}{\left(1 + K_{CO}p_{co} + K_{H_2}p^{0.5}_{H_2} + K'_{CH_3O}\frac{p_{CH_3OH}}{p^{0.5}_{H_2}}\right)^4} \tag{4.40}$$

$$where, \qquad k_{CH_3OH} = k^{+}_{CH_3O}K_{CO}K_{H_2}[s]^4_{CH_3OH}, \qquad K_{CH_3OH} = \frac{k^{+}_{CH_3O}}{k^{-}_{CH_3O}}\frac{K_{CO}K_{H_2}}{K'_{CH_3O}}$$

For the calculation purpose, the gross rate of production of methanol in-terms of dimensionless partial pressures can be written as [6],

$$r^{g}_{CH_3OH} = \frac{k'_{CH_3OH}\left[\left(\frac{p_{CO}}{p^{cp}_{CO}}\right)\left(\frac{p_{H_2}}{p^{cp}_{H_2}}\right)^{1.5} - \frac{1}{K'_{CH_3OH}}\left(\frac{p_{CH_3OH}}{p^{cp}_{CH_3OH}}\right)\left(\frac{p^{cp}_{H_2}}{p_{H_2}}\right)^{0.5}\right]}{\left[1 + K_{CO}\left(\frac{p_{CO}}{p^{cp}_{CO}}\right) + K_{H_2}\left(\frac{p_{H_2}}{p^{cp}_{H_2}}\right)^{0.5} + K'_{CH_3O}\left(\frac{p_{CH_3OH}}{p^{cp}_{CH_3OH}}\right)\left(\frac{p^{cp}_{H_2}}{p_{H_2}}\right)^{0.5}\right]^2} \tag{4.41}$$

$$k'_{CH_3OH} = A_{CH_3OH}e^{-\left(\frac{E_{CH_3OH}}{R}\right)\left(\frac{1}{T}-\frac{1}{T^{cp}}\right)}, \qquad Arrhenius'equation$$

Where, A_{CH_3OH} and E_{CH_3OH} refer to pre-exponential factor and activation energy for methanol synthesis reaction. Partial pressures at a center point conditions are denoted by p^{cp}_i for component *i*. The non-dimensional equilibrium constant K'_{CH_3OH} in the numerator can be given by [6],

$$K'_{CH_3OH} = \frac{K_{eq,CH_3OH}}{K_\gamma K^{cp}_{CH_3OH}};\ K^{cp}_{CH_3OH} = \frac{p^{cp}_{CH_3OH}}{p^{cp}_{CO}\left(p^{cp}_{H_2}\right)^2} \tag{4.42}$$

The fugacity correction factor K_γ is assumed to be constant and it is estimated from regression analysis. The equilibrium constant, K_{eq,CH_3OH} is obtained from CHEMEQ.BAS software developed by Sandler [7]. The estimated equilibrium constants at different temperatures are shown in the Table 4.4, and correlated to,

$$K_{eq,CH_3OH} = e^{\left(\frac{-\Delta G^{\circ}_{CH_3OH}}{RT}\right)} \tag{4.43}$$

$$\Delta G^{\circ}_{CH_3OH} = -98.517 + 0.2401T, \frac{KJ}{mol} \tag{4.44}$$

$$R = 8.314 \times 10^{-3}, \frac{KJ}{mol.K}$$

$\Delta G^{\circ}_{CH_3OH}$ is the Gibb's free energy, *T* and *P* represents temperature and pressure respectively, and *R* is the universal gas constant.

T, °K	$K_{eq,CH_3OH} \times 10^5$ [7]
523	198.400
548	70.910
573	27.570
598	11.540
623	5.516
648	2.444

Table 4.4. Methanol equilibrium constant at different temperature.

4.3.5.2. Gross Rate of Ethanol Formation

The gross rate of formation of ethanol in terms of the rate-determining step 4.24 can be written as,

$$r^{g}_{C_2H_5OH} = k_{CH_3CO}[CH_3O*][CO*] \tag{4.45}$$

The concentration of vacant site [*] for ethanol formation reactions can be determined from the site balance. Surface species participating in the rate-determining reaction step of ethanol formation reaction were considered for site balance. Contributions from other surface species are negligible.

$$[s]_{C_2H_5OH} = [*] + [CO*] + [CH_3O*] \tag{4.46}$$

Substituting equilibrium relationships 4.35, 4.37 and solving for $[*]$,

$$[*] = \frac{[s]_{C_2H_5OH}}{\left(1 + K_{CO}p_{co} + K'_{CH_3O}\frac{p_{CH_3OH}}{p^{0.5}_{H_2}}\right)} \tag{4.47}$$

Solving rate equation 4.45, equilibrium relationships 4.35, 4.37, and site balance equation 4.47 simultaneously and eliminating $[*]$ to obtain gross rate of formation of ethanol, $r^{g}_{C_2H_5OH}$ in-terms of partial pressures, rate constant and equilibrium constants,

$$r_{C_2H_5OH}^{g} = \frac{k_{C_2H_5OH}\dfrac{p_{CH_3OH}\,p_{co}}{p_{H_2}^{0.5}}}{\left(1 + K_{CO}p_{co} + K'_{CH_3O}\dfrac{p_{CH_3OH}}{p_{H_2}^{0.5}}\right)^2} \tag{4.48}$$

$$where, \qquad k_{C_2H_5OH} = k_{CH_3CO}K'_{CH_3O}K_{CO}[s]^2_{C_2H_5OH}$$

The gross rate of production of ethanol in-terms of dimensionless partial pressures for calculation purpose can be written as,

$$r_{C_2H_5OH}^{g} = \frac{A_{C_2H_5OH}e^{-\left(\frac{E_{C_2H_5OH}}{R}\right)\left(\frac{1}{T}-\frac{1}{T^{cp}}\right)}\left(\dfrac{p_{CH_3OH}}{p_{CH_3OH}^{cp}}\right)\left(\dfrac{p_{CO}}{p_{CO}^{cp}}\right)\left(\dfrac{p_{H_2}^{cp}}{p_{H_2}}\right)^{0.5}}{\left[1 + K_{CO}\left(\dfrac{p_{CO}}{p_{CO}^{cp}}\right) + K'_{CH_3O}\left(\dfrac{p_{CH_3OH}}{p_{CH_3OH}^{cp}}\right)\left(\dfrac{p_{H_2}^{cp}}{p_{H_2}}\right)^{0.5}\right]^2} \tag{4.49}$$

Where, $A_{C_2H_5OH}$ and $E_{C_2H_5OH}$ refer to pre-exponential factor and activation energy for ethanol synthesis reaction.

4.3.5.3. Gross Rate of Propanol Formation

The gross rate of formation of propanol in terms of the rate-determining step 4.28 can be written as,

$$r_{C_3H_7OH}^{g} = k_{C_2H_5CO}[CH_3CO*][CO*] \tag{4.50}$$

The equilibrium relationship for CH_3CO* can be obtained from the ethanol decomposition reaction 4.25,

$$K_{CH_3CO} = \frac{p_{C_2H_5OH}[*]^4}{[CH_3CO*][H*]^3}$$

$$\Rightarrow [CH_3CO*] = K'_{CH_3CO}\frac{p_{C_2H_5OH}[*]}{p_{H_2}^{1.5}};\ K'_{CH_3CO} = \frac{1}{K_{CH_3CO}K_{H_2}^3} \tag{4.51}$$

Surface species participating in the rate-determining reaction step of propanol formation reaction were considered for site balance. Contributions from other surface species are negligible.

$$[s]_{C_3H_7OH} = [*] + [CO*] + [CH_3CO*] \tag{4.52}$$

Substituting equilibrium relationships 3.35, 3.51 and solving for $[*]$,

$$[*] = \frac{[s]_{C_3H_7OH}}{\left(1 + K_{CO}p_{co} + K'_{CH_3CO}\frac{p_{C_2H_5OH}}{p_{H_2}^{1.5}}\right)} \tag{4.53}$$

Solving rate equation 4.50, equilibrium relationships 4.35, 4.51, and site balance equation 4.53 simultaneously and eliminating $[*]$ to obtain gross rate of formation of ethanol, $r^g_{C_3H_7OH}$ in-terms of partial pressures, rate constant and equilibrium constants,

$$r^{g}_{C_3H_7OH} = \frac{k_{C_3H_7OH}\dfrac{p_{C_2H_5OH}\,p_{co}}{p_{H_2}^{1.5}}}{\left(1 + K_{CO}p_{co} + K'_{CH_3CO}\dfrac{p_{C_2H_5OH}}{p_{H_2}^{1.5}}\right)^2} \tag{4.54}$$

$where, \qquad k_{C_3H_7OH} = k_{C_2H_5CO}K'_{CH_3CO}K_{CO}[s]^2_{C_3H_7OH}$

The gross rate of production of propanol in-terms of dimensionless partial pressures for calculation purpose can be written as,

$$r^{g}_{C_3H_7OH} = \frac{A_{C_3H_7OH}e^{-\left(\frac{E_{C_3H_7OH}}{R}\right)\left(\frac{1}{T}-\frac{1}{T^{cp}}\right)}\left(\dfrac{p_{C_2H_5OH}}{p^{cp}_{C_2H_5OH}}\right)\left(\dfrac{p_{CO}}{p^{cp}_{CO}}\right)\left(\dfrac{p^{cp}_{H_2}}{p_{H_2}}\right)^{1.5}}{\left[1 + K_{CO}\left(\dfrac{p_{CO}}{p^{cp}_{CO}}\right) + K'_{CH_3CO}\left(\dfrac{p_{CH_3OH}}{p^{cp}_{CH_3OH}}\right)\left(\dfrac{p^{cp}_{H_2}}{p_{H_2}}\right)^{1.5}\right]^2} \tag{4.55}$$

Where, $A_{C_3H_7OH}$ and $E_{C_3H_7OH}$ refer to pre-exponential factor and activation energy for propanol synthesis reaction.

4.3.5.4. Rate of Methane Formation

The rate of formation of methane can be expressed in terms of the rate-determining step 4.22 as,

$$r_{CH_4} = k_{CH_3}[CH_3O*] \tag{4.56}$$

Site balance for methane formation reaction can be written as,

$$[s]_{CH_4} = [*] + [CH_3O*] \tag{4.57}$$

Substituting the equilibrium relationship 4.37 and solving for $[*]$,

$$[*] = \frac{[s]_{CH_4}}{\left(1 + K'_{CH_3O}\frac{p_{CH_3OH}}{p_{H_2}^{0.5}}\right)} \tag{4.58}$$

Solving the rate equation, 4.56 and equilibrium relationship, 4.37 and the site balance equation, 4.58 simultaneously and eliminating $[*]$ to obtain rate of formation of methane, r_{CH_4},

$$r_{CH_4} = \frac{k_{CH_4}\frac{p_{CH_3OH}}{p_{H_2}^{0.5}}}{1 + K'_{CH_3O}\frac{p_{CH_3OH}}{p_{H_2}^{0.5}}} \tag{4.59}$$

$where, \quad k_{CH_4} = k_{CH_3} K'_{CH_3O}[s]_{CH_4}$

The rate of production of methane in terms of dimensionless partial pressures can be written as,

$$r_{CH_4} = \frac{A_{CH_4} e^{-\left(\frac{E_{CH_4}}{R}\right)\left(\frac{1}{T}-\frac{1}{T^{cp}}\right)} \left(\frac{p_{CH_3OH}}{p^{cp}_{CH_3OH}}\right)\left(\frac{p^{cp}_{H_2}}{p_{H_2}}\right)^{0.5}}{1 + K'_{CH_3O}\left(\frac{p_{CH_3OH}}{p^{cp}_{CH_3OH}}\right)\left(\frac{p^{cp}_{H_2}}{p_{H_2}}\right)^{0.5}} \tag{4.60}$$

Where, A_{CH_4} and E_{CH_4} refer to pre-exponential factor and activation energy for methane synthesis reaction.

4.3.5.5. Rate of Ethane, Propane, and Carbon Dioxide Formation

The rate of formation of ethane and propane can be expressed in terms of the rate-determining step 4.26 and 4.30 respectively as,

$$r_{C_2H_6} = k_{C_2H_5}[CH_3CO*] \tag{4.61}$$

$$r_{C_3H_8} = k_{C_3H_7}[C_2H_5CO*] \tag{4.62}$$

The equilibrium relationship for C_2H_5CO* can be obtained from the propanol decomposition reaction 4.29,

$$K_{C_2H_5CO} = \frac{p_{C_3H_7OH}[*]^4}{[C_2H_5CO*][H*]^3}$$

$$\Rightarrow [C_2H_5CO\ *] = K'_{C_2H_5CO}\frac{p_{C_3H_7OH}[*]}{p_{H_2}^{1.5}};\ K'_{C_2H_5CO} = \frac{1}{K_{C_2H_5CO}K_{H_2}^3} \tag{4.63}$$

Site balance for ethane and propane formation reactions can be written as,

$$[s]_{C_2H_6} = [*] + [CH_3CO\ *] \tag{4.64}$$

$$[s]_{C_3H_8} = [*] + [C_2H_5CO\ *] \tag{4.65}$$

Solving the rate equation, equilibrium relationship and the site balance equation simultaneously and eliminating $[*]$ to obtain the rate of formation of methane, $r_{C_2H_6}$ and ethane, $r_{C_3H_8}$,

$$r_{C_2H_6} = \frac{k_{C_2H_6}\frac{p_{C_2H_5OH}}{p_{H_2}^{1.5}}}{1 + K'_{CH_3CO}\frac{p_{C_2H_5OH}}{p_{H_2}^{1.5}}} \tag{4.66}$$

$$where, \qquad k_{C_2H_6} = k_{C_2H_5}K'_{CH_3CO}[s]_{C_2H_6}$$

$$r_{C_3H_8} = \frac{k_{C_3H_8}\frac{p_{C_3H_7OH}}{p_{H_2}^{1.5}}}{1 + K'_{C_2H_5CO}\frac{p_{C_3H_7OH}}{p_{H_2}^{1.5}}} \tag{4.67}$$

$$where, \qquad k_{C_3H_8} = k_{C_3H_7}K'_{C_2H_5CO}[s]_{C_3H_8}$$

The rate of production of ethane and propane in terms of dimensionless partial pressures for the calculation purposes can be written as,

$$r_{C_2H_6} = \frac{A_{C_2H_6} e^{-\left(\frac{E_{C_2H_6}}{R}\right)\left(\frac{1}{T}-\frac{1}{T^{cp}}\right)} \left(\frac{p_{C_2H_5OH}}{p^{cp}_{C_2H_5OH}}\right)\left(\frac{p^{cp}_{H_2}}{p_{H_2}}\right)^{1.5}}{1 + K'_{CH_3CO}\left(\frac{p_{C_2H_5OH}}{p^{cp}_{C_2H_5OH}}\right)\left(\frac{p^{cp}_{H_2}}{p_{H_2}}\right)^{1.5}} \tag{4.68}$$

$$r_{C_3H_8} = \frac{A_{C_3H_8} e^{-\left(\frac{E_{C_3H_8}}{R}\right)\left(\frac{1}{T}-\frac{1}{T^{cp}}\right)} \left(\frac{p_{C_3H_7OH}}{p^{cp}_{C_3H_7OH}}\right)\left(\frac{p^{cp}_{H_2}}{p_{H_2}}\right)^{1.5}}{1 + K'_{C_2H_5CO}\left(\frac{p_{C_3H_7OH}}{p^{cp}_{C_3H_7OH}}\right)\left(\frac{p^{cp}_{H_2}}{p_{H_2}}\right)^{1.5}} \tag{4.69}$$

Where, $A_{C_2H_6}, A_{C_3H_8}$ and $E_{C_2H_6}, E_{C_3H_8}$ refer to pre-exponential factor and activation energy for ethane and propane synthesis reactions respectively.

The amount of water formed during the reactions is negligible (below the detection limit of TCD gas chromatography) and hence ignored for the calculations. The rate of production of CO_2 for this case is equal to the sum of the rate of formation of OH* from equation 4.22, 4.24, 4.26, 4.28, and 4.30. The rate of formation of CO_2 can be obtained from OH* balance as,

$$r_{CO_2} = r^g_{C_2H_5OH} + r^g_{C_3H_7OH} + r_{CH_4} + r_{c_2H_6} + r_{C_3H_8} \tag{4.15}$$

4.3.6. Empirical (EMP) Model

In the previous section, kinetic expressions were developed based on given set of reactions with fixed reaction stoichiometry. There are other powerful techniques, such as Singular Value Decomposition (SVD) is available, that can be utilized to estimate the number of reactions required and the corresponding reaction stoichiometry to describe the given set of experimental results. The application of SVD has been limited to biochemical [8], batch fermentation [9], and metabolic reactions [10]. This is the first time, we are applying SVD to a HAS reaction network.

4.3.6.1. Application of Singular Value Decomposition (SVD)

The SVD can be utilized to decompose the given matrix containing the experimental data into two matrices: one is containing stoichiometry of the reactions, and other containing the extent of reactions. The SVD can also be used to identify the minimum number of independent reactions required to adequately describe the given experimental data. The *svd* subroutine in MATLAB was used for this purpose.

$$[U, S, V] = svd(D) \tag{4.70}$$

SVD of a given experimental data matrix, *D*, produces a diagonal matrix, *S*, with non-negative diagonal elements in decreasing order, and unitary matrices *U* and *V* so that,

$$D = USV' \tag{4.71}$$

The columns of V represent the stoichiometry of the reactions. The number of independent reactions required to adequately describe the experimental data can be determined by the singular values contained in the matrix S. Number of significant singular values in the matrix S determines the number of reactions required. Once the number of reactions is fixed, corresponding singular vectors from matrix V can be used as initial estimate for reaction stoichiometry α. The corresponding reaction extents can be calculated by [9];

$$X = D\alpha \tag{4.72}$$

Predicted values can be calculated, by;

$$\mathbb{D} = X\alpha' = D\alpha\alpha' \tag{4.73}$$

There are multiple singular vectors; any linear combinations can be possible that can equally predict the experimental results. The objective is to select most suitable linear combinations that are most likely correspond to independent part of the reaction network, e.g. alcohols and hydrocarbons formation reaction from CO and H_2 (primary reaction) and decomposition of alcohols to hydrocarbons and/or linear chain growth by CO insertion mechanism (secondary reaction) to higher alcohols, can be used as two independent part of the reaction network for $Cs/MoS_2/AC$ alcohol synthesis

catalysts. If possible, try to make all the entries in the extent of reaction matrix, X positive, in other words, try to make the reactions irreversible and try to eliminate entries in the stoichiometry matrix, α. These objectives can be achieved by using a transformation matrix, T_r

$$T_r = \frac{1}{cos(\beta - \gamma)} \begin{bmatrix} cos\beta & -sin\gamma \\ sin\beta & cos\gamma \end{bmatrix} \tag{4.74}$$

Where β, and γ are selected, to get different linear combinations of singular vectors that can equally predict the experimental results. The modified extent of reaction matrix, X_t and corresponding stoichiometry matrix, α_t can be evaluated by applying the transformation matrix,

$$\mathbb{D} = X\alpha' = D\alpha' = (XT_r)\left(\alpha T_r'^{-1}\right)' = X_t\alpha_t' \tag{4.75}$$

The experimental results shown in Table 4.1 were used for the SVD analysis. Amount of butanol produced is very small compared to methanol, ethanol and propanol, and hence, butanol is lumped together with propanol and considered as propanol. The experimental data matrix, D as used is presented in Table 4.5.

Experimental Data Matrix (*mol/kg cat/hr*), *D*									Extent of Reaction	
CO	H_2	CH_3OH	C_2H_5OH	C_3H_7OH	CH_4	C_2H_6	C_3H_8	CO_2	X_p	X_s
-8.42	-8.37	1.13	0.49	0.17	1.30	0.28	0.12	3.40	8.46	2.49
-9.14	-10.34	1.98	0.53	0.14	1.52	0.26	0.10	3.28	10.35	2.04
-9.29	-11.28	2.44	0.50	0.12	1.63	0.26	0.09	3.10	11.22	1.68
-9.54	-11.95	2.78	0.49	0.11	1.66	0.26	0.09	3.05	11.88	1.50
-8.86	-11.89	2.99	0.41	0.09	1.63	0.24	0.08	2.60	11.75	1.02
-4.05	-4.67	0.89	0.27	0.06	0.60	0.13	0.05	1.41	4.66	0.85
-5.62	-6.42	1.22	0.33	0.08	0.88	0.19	0.08	1.99	6.41	1.22
-6.66	-7.56	1.53	0.40	0.10	0.99	0.20	0.08	2.35	7.59	1.41
-8.37	-9.67	1.92	0.48	0.12	1.41	0.23	0.09	2.94	9.66	1.76
-9.49	-10.96	2.27	0.57	0.14	1.55	0.24	0.09	3.30	10.99	1.94
-10.10	-11.84	2.54	0.60	0.14	1.65	0.24	0.09	3.46	11.87	1.96
-8.01	-8.97	1.64	0.42	0.14	1.41	0.23	0.09	2.93	8.97	1.88
-8.37	-9.67	1.92	0.48	0.12	1.41	0.23	0.09	2.94	9.66	1.76
-8.97	-10.74	2.31	0.60	0.12	1.37	0.24	0.09	2.98	10.73	1.62
-9.38	-11.54	2.68	0.68	0.12	1.27	0.25	0.09	2.95	11.55	1.44
-9.36	-11.42	2.85	0.71	0.12	1.19	0.24	0.00	2.92	11.53	1.36
-3.45	-4.22	1.08	0.28	0.04	0.43	0.07	0.00	1.06	4.27	0.48
-5.30	-6.47	1.51	0.39	0.07	0.72	0.12	0.05	1.68	6.49	0.83
-8.37	-9.59	1.97	0.50	0.12	1.31	0.23	0.09	2.93	9.63	1.74
-12.47	-13.15	2.01	0.54	0.23	2.27	0.43	0.18	4.89	13.16	3.44
-17.57	-16.51	1.49	0.45	0.31	3.60	0.75	0.35	7.78	16.55	6.19
-22.97	-20.56	1.00	0.30	0.34	5.35	1.16	0.49	10.80	20.50	9.04
-10.20	-13.25	3.37	0.60	0.11	1.54	0.27	0.09	3.03	13.20	1.23
-11.27	-14.03	3.40	0.78	0.14	1.57	0.26	0.10	3.49	14.05	1.62
-10.36	-12.55	2.94	0.67	0.13	1.53	0.23	0.10	3.35	12.59	1.70

Table 4.5. Experimental Data Matrix, *D* used for SVD analysis and Calculated Extent of Reaction Matrix, *X*.

The nine singular values obtained from SVD of the matrix *D* are:

[79.301 8.327 0.927 0.215 0.146 0.100 0.062 0.003 0.002]

Last seven singular values are very small compared to the first two singular values; indicating only two reactions should be adequate to describe the experimental data. Only two reactions were selected for the analysis.

Following two reactions were obtained by selecting, β = 140.125° and γ=175.0°,

Primary Reaction

$$0.684\ CO + H_2 \rightarrow 0.309\ CH_3OH + 0.066\ C_2H_5OH + 0.007\ C_3H_7OH + 0.07\ CH_4 + 0.006\ C_2H_6 + 0.149\ CO_2 \qquad (4.76a)$$

Secondary Reaction

$$0.590\ CH_3OH + 0.103\ C_2H_5OH + CO \rightarrow 0.026\ C_3H_7OH + 0.411\ CH_4 + 0.109\ C_2H_6 + 0.054\ C_3H_8 + 0.857\ CO_2 \qquad (4.77a)$$

The corresponding extent of reaction matrix is shown in Table 4.5. All the entries are positive, suggesting only forward reactions are sufficient to describe the experimental data. Pictorial representation of predicted values and experimental results with respect to reactor temperature, pressure, GHSV and H_2/CO are shown in the Fig. 4.7 - 4.10.

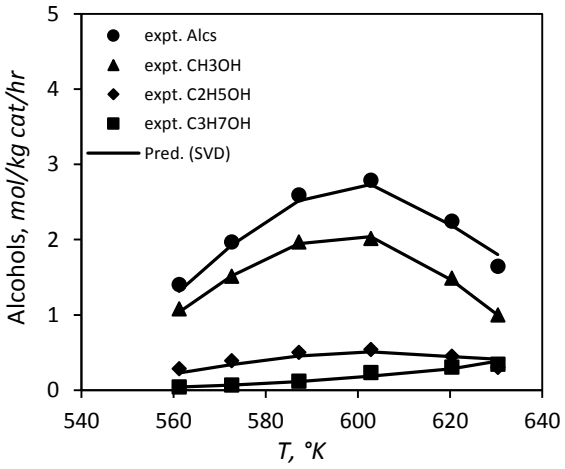

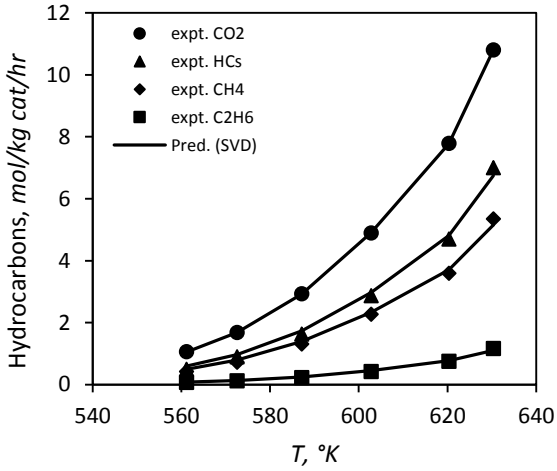

[redacted]

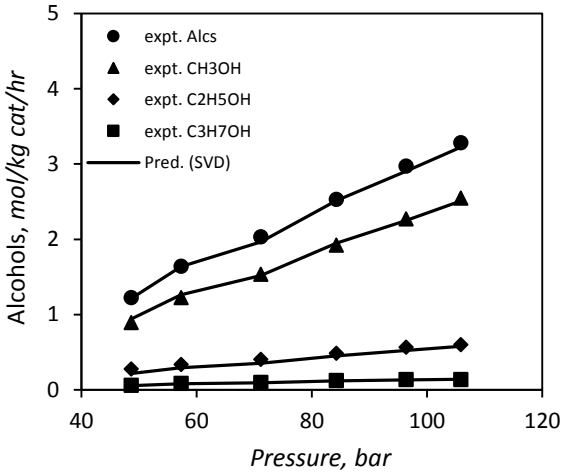

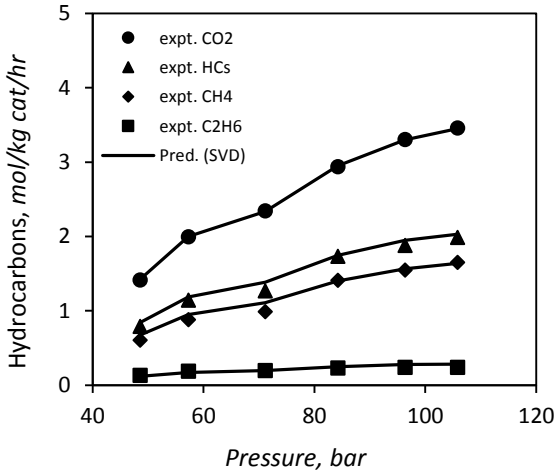

[redacted]

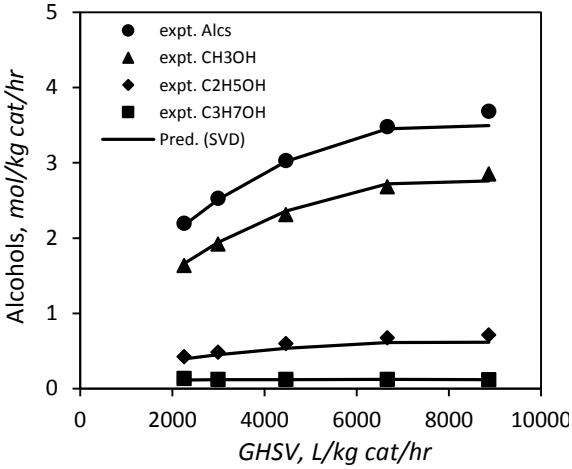

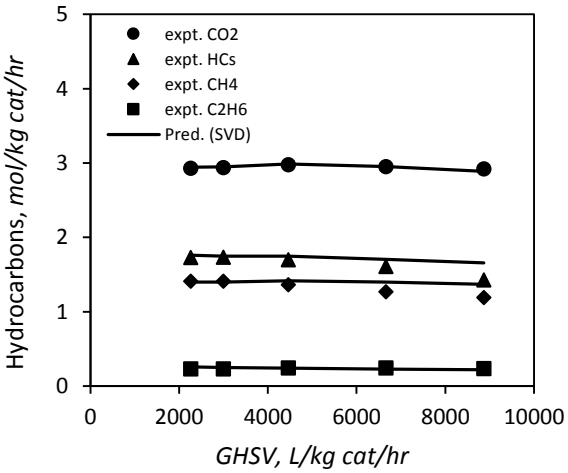

[redacted]

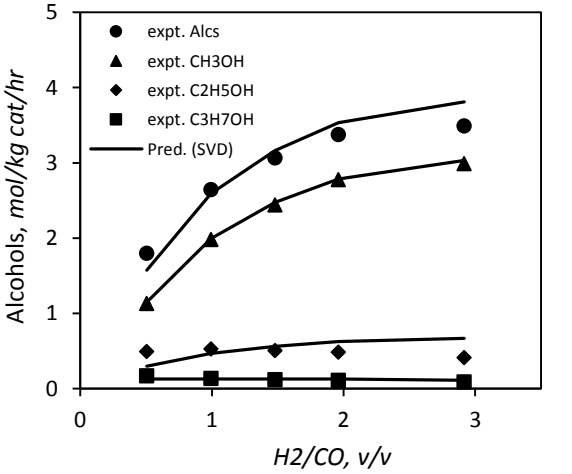

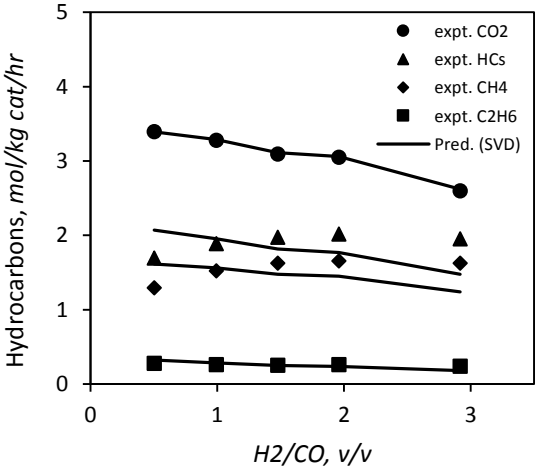

[redacted]

As we can see, given experimental results from testing of $Cs/MoS_2/AC$ catalysts can be represented by only two independent reactions;

- *Primary reaction*: Formation of alcohols, hydrocarbons and associated CO_2 directly from CO and H_2. Chain growth reactions by CO insertion mechanism and water-gas shift reaction are coupled in this reaction. Primary reaction accounts for 70-92 *mol%* of the overall reaction.

- *Secondary reaction*: Decomposition of methanol and ethanol to hydrocarbons. Small amount of higher carbon number components such as propanol, and propane were observed due to chain growth reaction and thereby decomposition of higher alcohols such as ethanol and propanol. Formation of CO_2 by water-gas shift reaction is also included in the reaction. Secondary reaction accounts for 8-30 *mol%* of the overall reaction, with higher end is mostly at high temperature reaction and lower H_2 to CO ratio.

Once we got the empirical reactions, our next step is to fit the extent of reaction entries to rate expression models, such as LH type models to describe the extent of reactions in terms of partial pressures and kinetic parameter terms.

4.3.6.2. Rate Expressions

Empirical reactions obtained from SVD analysis were slightly off in C, O, and H balance. Balanced reactions consistent with the simplified reaction scheme, reactions 4.2 - 4.8 can be written as,

$Primary\ Reaction$

$$0.705\ CO + H_2 \rightarrow 0.308\ CH_3OH + 0.066\ C_2H_5OH + 0.007\ C_3H_7OH + 0.07\ CH_4 + 0.006\ C_2H_6 + 0.162\ CO_2 \qquad (4.76b)$$

$Secondary\ Reaction$

$$0.5905\ CH_3OH + 0.103\ C_2H_5OH + 0.8405\ CO \rightarrow 0.03\ C_3H_7OH + 0.41\ CH_4 + 0.11\ C_2H_6 + 0.055\ C_3H_8 + 0.752\ CO_2 \qquad (4.77b)$$

Rate expressions of L-H type can be written for these two forward reactions as,

$Primary\ Reaction$

$$r_{gen} = \frac{A_{gen} e^{-\left(\frac{E_{gen}}{R}\right)\left(\frac{1}{T}-\frac{1}{T^{cp}}\right)} \left(\frac{p_{CO}}{p_{CO}^{cp}}\right)^{0.705} \left(\frac{p_{H_2}}{p_{H_2}^{cp}}\right)}{\left[1 + K_1\left(\frac{p_{CO}}{p_{CO}^{cp}}\right) + K_2\left(\frac{p_{H_2}}{p_{H_2}^{cp}}\right)^{0.5}\right]^{n_{gen}}} \qquad (4.78)$$

Secondary Reaction

$$r_{dec} = \frac{A_{dec} e^{-\left(\frac{E_{dec}}{R}\right)\left(\frac{1}{T}-\frac{1}{T^{cp}}\right)} \left(\frac{p_{CO}}{p_{CO}^{cp}}\right)\left(\frac{p_{CH_3OH}}{p_{CH_3OH}^{cp}}\right)\left(\frac{p_{C_2H_5OH}}{p_{C_2H_5OH}^{cp}}\right)}{\left[1 + K_3\left(\frac{p_{CO}}{p_{CO}^{cp}}\right) + K_4\left(\frac{p_{CH_3OH}}{p_{CH_3OH}^{cp}}\right) + K_5\left(\frac{p_{C_2H_5OH}}{p_{C_2H_5OH}^{cp}}\right)\right]^{n_{dec}}} \quad (4.79)$$

The $A_i$terms in the rate equations are refer to pre-exponential factors and the E_i, terms represents activation energies. *K*'s in the denominator represent adsorption constants. Partial pressures of components *i*, are denoted by p_i, and partial pressures at center point conditions are denoted by p_i^{cp}. The exponential terms, *n's*, in the denominator are estimated from regression analysis.

4.4. Application of Genetic Algorithm (GA) for the Kinetic Parameter Estimation

4.4.1 Reactor Model

Isothermal plug-flow reactor model was used in the kinetic study of Cs/MoS_2/AC catalyst. The following differential mole balance equations can be written for a one-dimensional model [11],

$$\frac{dx_j}{d\tau} = r_j^g; x = \frac{X}{F_o}; \tau = \frac{w}{F_o}; j = reactions \quad (4.80)$$

$$\frac{F_i}{F_o} = y_{o,i} + \alpha_{ij} x_j; i = components \quad (4.81)$$

X is the extent of reaction, F_o is the total inlet molar flow rate, F_i is the molar flow rate of components *i*, $y_{o,i}$, is the mole fraction of component *i* in the feed stream.

α_{ij}, is the matrix of reaction coefficients, and w is the weight of catalyst = 3 g for the lab-scale reactor used.

4.4.2. Genetic Algorithm Minimization

The differential equations were solved using *ode15s* routines in MATLB, and simultaneously the objective function f was minimized using Genetic Algorithm (GA). As GA is only for maximization, for minimizing the errors between experimental and predicted values, the objective function can be defined as [5],

$$max.f = -100 \text{ sqrt}\left[\frac{1}{m\sum_i^c w_i}\sum_i^c w_i \sum_1^m \left(\frac{F_{i,expt.}}{F_o} - \frac{F_{i,est.}}{F_o}\right)^2\right] \quad (4.82)$$

$m = \#\ of\ data\ sets, i = components\ and$

$c = \#\ of\ components = 6\ (methanol, ethanol, propanol, methane, ethane\ and\ propane)$

The kinetic parameters: pre-exponential factors, *A*'s, activation energies, *E*'s, equilibrium/adsorption constants, *K*'s, fugacity correction factor, K_γ, and exponents, *n*'s, were estimated by fitting the experimental data by minimizing the error between predicted and experimental molar flow rates of alcohols and hydrocarbons. w_i, is the weight factor used for component *i*, high value of weight factors (3, 10, and 5 for methanol, ethanol and propanol, respectively) were used for the alcohols compared to a value of one was used for the hydrocarbons (1 for methane, ethane and propane).

GA is a method that searches for the global optima of an objective function through the use of simulated evolution, the survival of the fittest strategy. Unlike most of

the optimization methods, GA does not require any initial guess but only the upper and lower bounds of the variables; in our case kinetic parameters, such as the pre-exponential factors, activation energies, fugacity correction factor, adsorption/equilibrium constants, and the powers in the denominators. GA explores all regions of the solution space and exponentially exploits promising areas through selection, crossover and mutation operations applied to kinetic parameters in the population. Float genetic algorithm (FGA) was used for the estimation of kinetic parameters [12]. Flow diagram for FGA is shown in Fig. 4.11. The FGA starts with initial populations of fixed size, P_{pop}. Kinetic parameters in the initial populations are generated randomly. Normalized geometric ranking, a probabilistic selection method, is used for the selection of populations. This method selects populations for next generation based on their fitness to the objective function; *f*. Remainder populations are randomly generated. Size of the population remains same in each generation. In each generation, new populations are generated using genetic operators; crossover and mutation. GA moves from generation to generation until a termination criterion is met. The most frequently used stopping criterion is a specified maximum number of generations, G_{max}. Finally GA gives best population of kinetic parameters which is available at the top of the list as organized by the ranking method from final generation as the required solution.

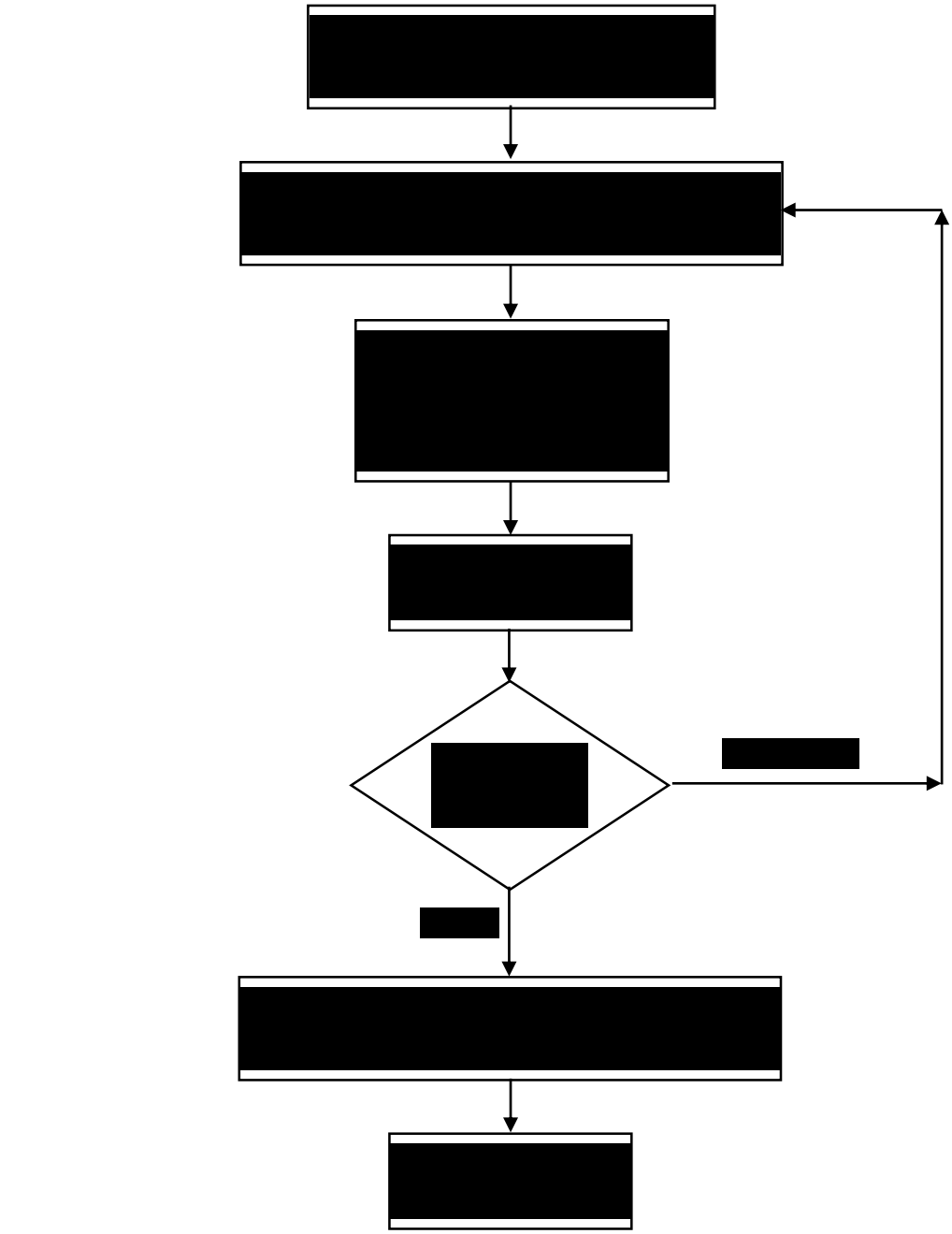

4.5. Results and Discussions

The variation of absolute objective function values for both LH and EMP model with a population size of 1000 is shown against the number of generation in Fig. 4.12. Methanol, ethanol, propanol (propanol plus butanol), methane, ethane, and propane are considered for objective function minimization, as amount of CO_2 is constrained by reactions 4.2 - 4.7 for the LH model and reactions 4.76b and 4.77b for the EMP model. It is observed that, 500th generation is sufficient to give a very good set of parameters; further generations only seem to improve marginally upon the solution obtained. Therefore, population size of 1000 and maximum generation number of 500 was used for optimization. It can also be noted that the objective function for the EMP model reaches quickly to a minimum value compared to the LH model.

Optimized kinetic parameters along with corresponding upper and lower bounds for LH and EMP model are respectively shown in Table 4.6 and Table 4.7.

Example MATLAB code for GA optimization using EMP model is given in Appendix 4A. Pictorial representation of the experimental results and the predicted values by LH and EMP model with respect to change in reactor temperature, pressure, GHSV, and H_2/CO ratio are shown in Fig. 4.13 - 4.16.

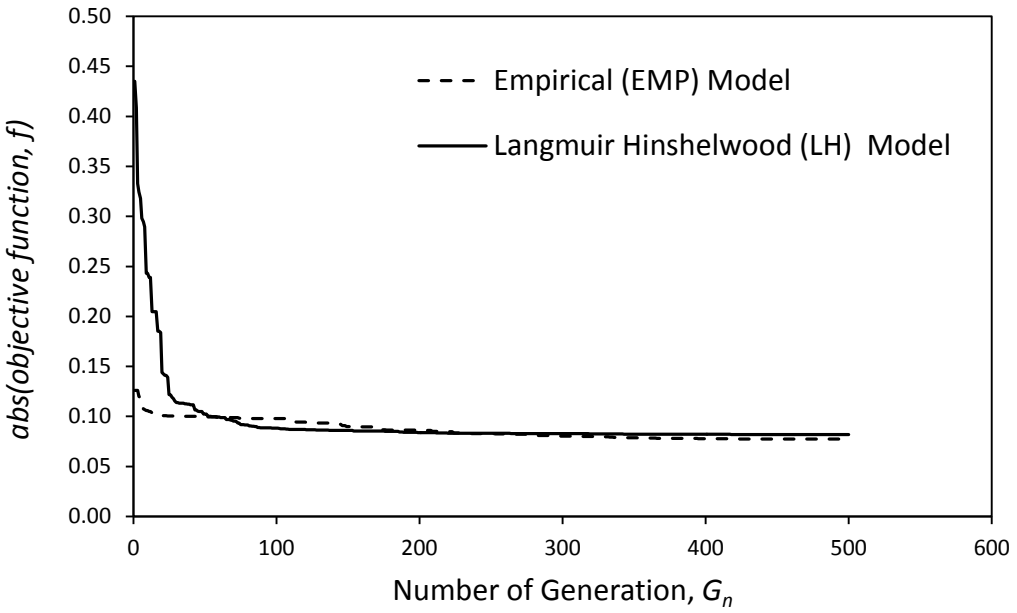
0.50
0.45
0.40
0.35
0.30
0.25
0.20
0.15
0.10
0.05
0.00
abs(objective function, f)
Empirical (EMP) Model
Langmuir Hinshelwood (LH) Model
0
100
200
300
400
500
600
Number of Generation, G_n

Kinetic Parameters	Lower Bound	Upper Bound	Optimized Value	Kinetic Parameters	Lower Bound	Upper Bound	Optimized Value	Kinetic Parameters	Lower Bound	Upper Bound	Optimized Value
A_{CH_3OH}	1	15	14.154	E_{CH_3OH}	50	120	96.93	K_γ	0.1	1	0.6443
$A_{C_2H_5OH}$	0.5	10	2.331	$E_{C_2H_5OH}$	50	100	65.90	K_{CO}	0.001	3	0.2316
$A_{C_3H_7OH}$	0.05	2	0.715	$E_{C_3H_7OH}$	90	150	109.29	K_{H_2}	0.001	3	0.0205
A_{CH_4}	0.5	12	2.277	E_{CH_4}	80	120	88.89	K'_{CH_3O}	0.001	3	0.1655
$A_{C_2H_6}$	0.05	2	0.602	$E_{C_2H_6}$	90	150	93.35	K'_{CH_3CO}	0.001	3	0.3161
$A_{C_3H_8}$	0.01	1	0.302	$E_{C_3H_8}$	90	160	126.79	$K'_{C_2H_5CO}$	0.001	3	1.8255

A's mol/kg cat/hr, E's kJ/mol, K's and n's are dimensionless

Table 4.6. Optimized kinetic parameters of LH Model.

Kinetic Parameters	Lower Bound	Upper Bound	Optimized Value	Kinetic Parameters	Lower Bound	Upper Bound	Optimized Value	Kinetic Parameters	Lower Bound	Upper Bound	Optimized Value
A_{gen}	1	50	18.596	K_1	0.001	3	0.4183	n_{gen}	1	3	1.730
A_{dec}	1	100	86.653	K_2	0.001	3	0.0679	n_{dec}	1	3	2.192
E_{gen}	40	100	64.79	K_3	0.001	3	1.0911				
E_{dec}	75	175	123.68	K_4	0.001	3	1.3744				
				K_5	0.001	3	1.1913				

A's mol/kg cat/hr, E's kJ/mol, K's and n's are dimensionless

Table 4.7. Optimized kinetic parameters of EMP Model.

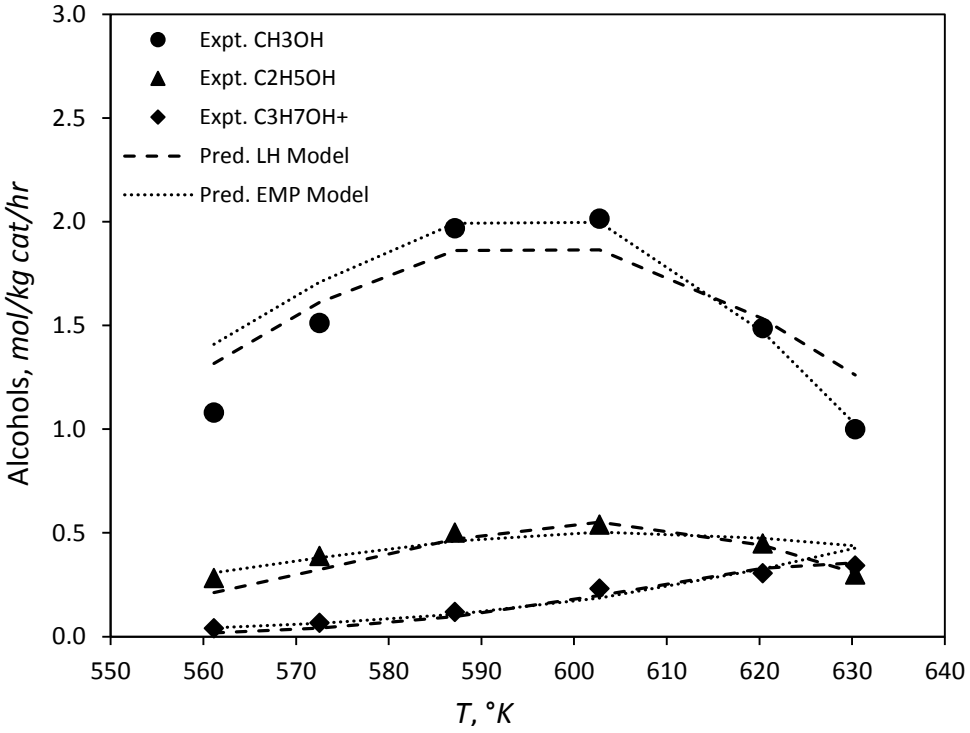
Expt. CH3OH
Expt. C2H5OH
Expt. C3H7OH+
Pred. LH Model
Pred. EMP Model
Alcohols, mol/kg cat/hr
T, °K
3.0
2.5
2.0
1.5
1.0
0.5
0.0
550
560
570
580
590
600
610
620
630
640

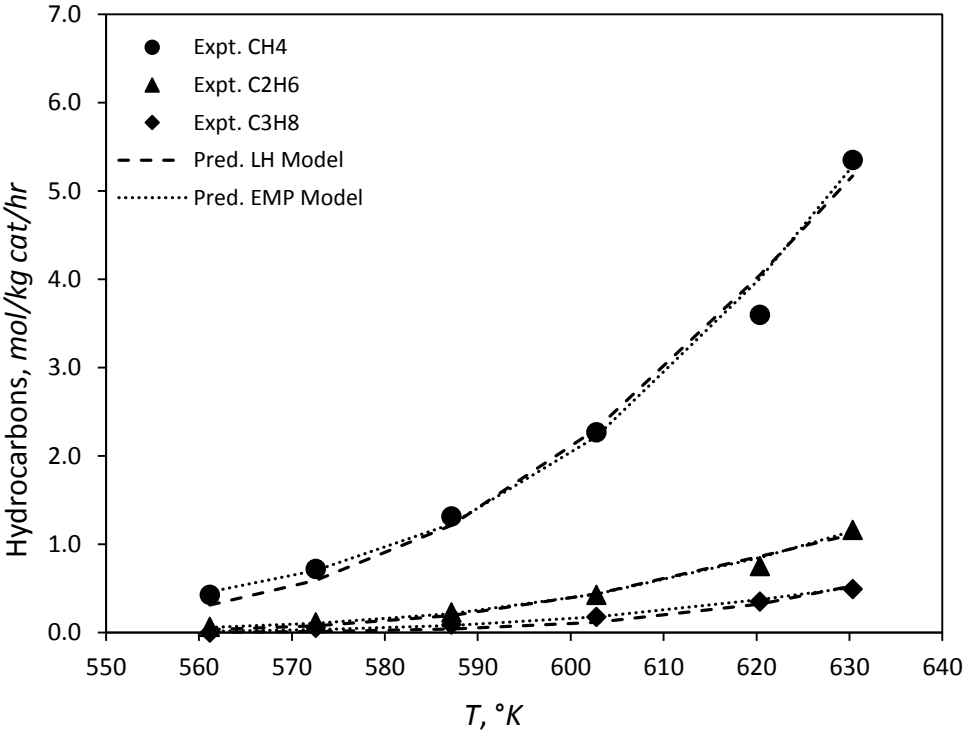
Expt. CH4
Expt. C2H6
Expt. C3H8
Pred. LH Model
Pred. EMP Model
Hydrocarbons, mol/kg cat/hr
T, °K
7.0
6.0
5.0
4.0
3.0
2.0
1.0
0.0
550
560
570
580
590
600
610
620
630
640

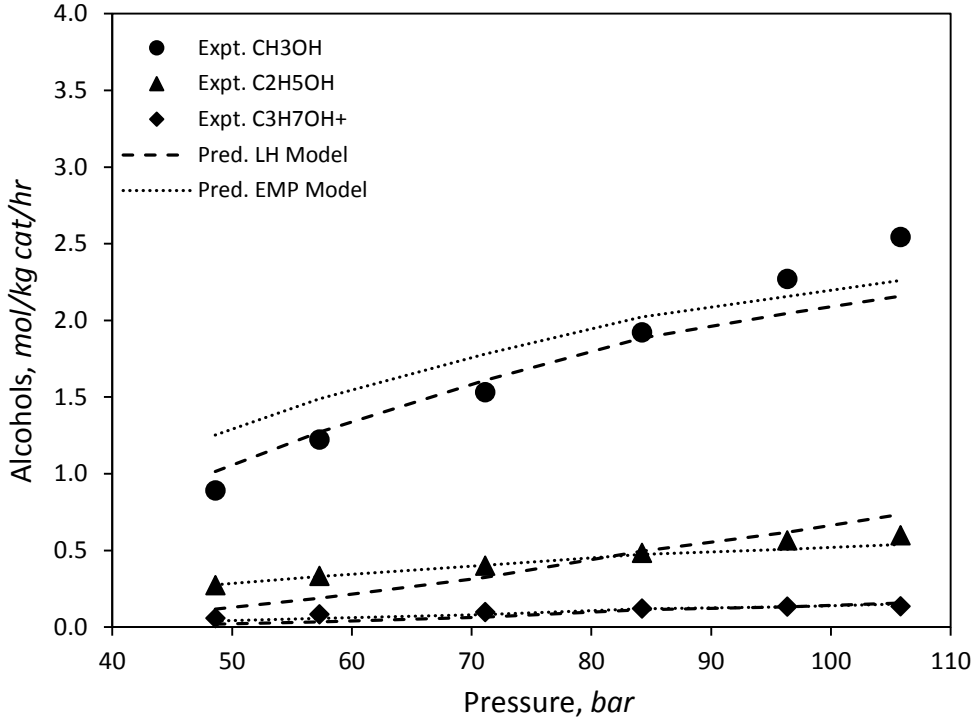
Expt. CH3OH
Expt. C2H5OH
Expt. C3H7OH+
Pred. LH Model
Pred. EMP Model
Alcohols, mol/kg cat/hr
Pressure, bar
4.0
3.5
3.0
2.5
2.0
1.5
1.0
0.5
0.0
40
50
60
70
80
90
100
110

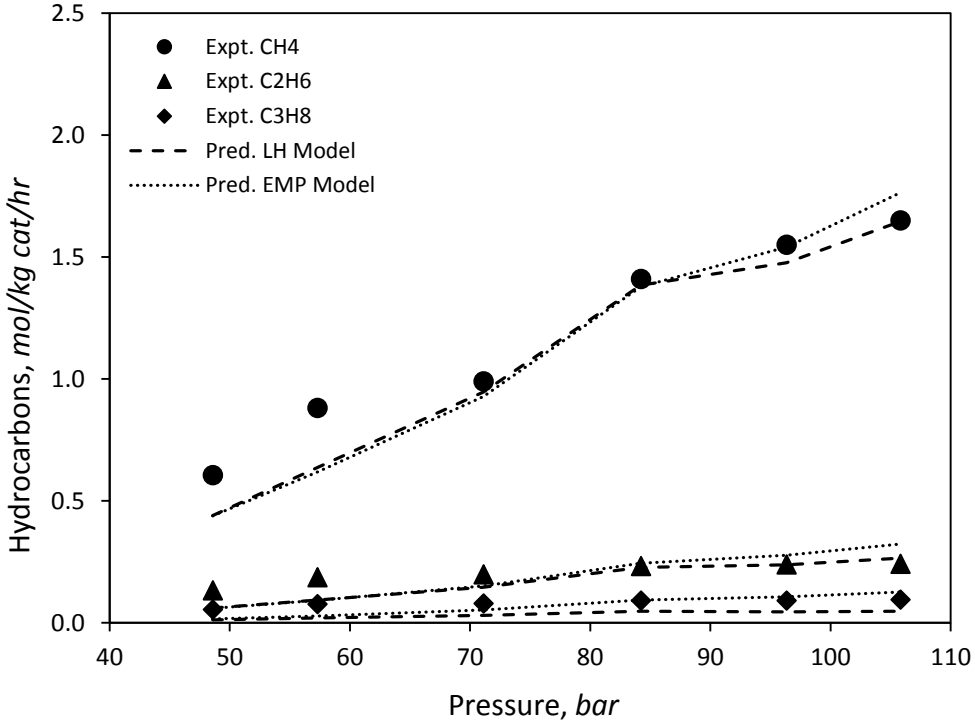
Expt. CH4
Expt. C2H6
Expt. C3H8
Pred. LH Model
Pred. EMP Model
Hydrocarbons, mol/kg cat/hr
Pressure, bar
2.5
2.0
1.5
1.0
0.5
0.0
40
50
60
70
80
90
100
110

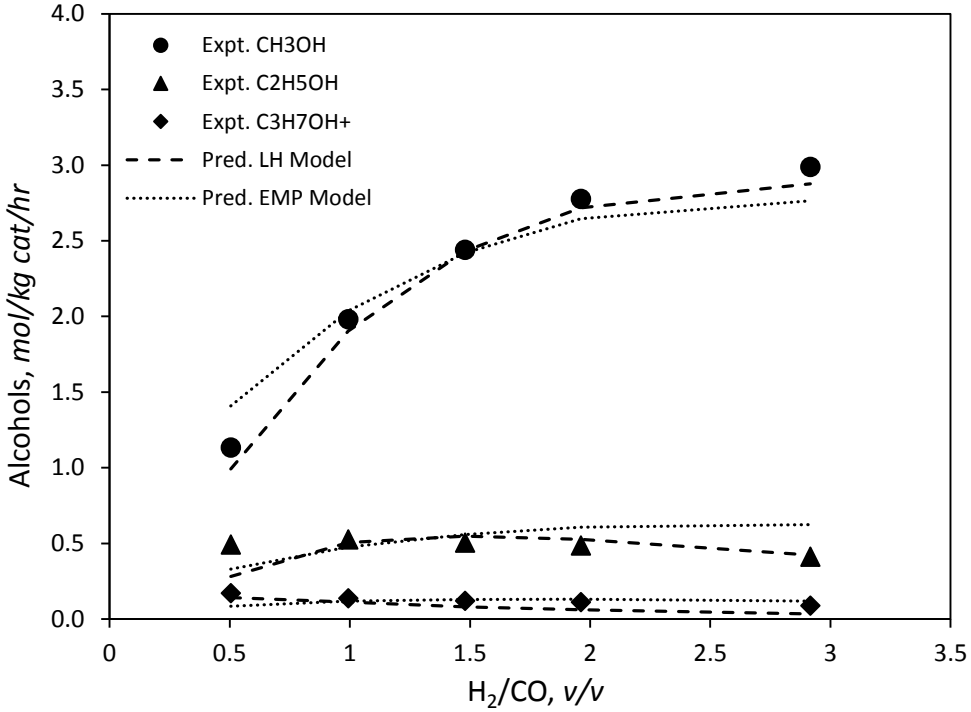
Expt. CH3OH
Expt. C2H5OH
Expt. C3H7OH+
Pred. LH Model
Pred. EMP Model
Alcohols, mol/kg cat/hr
H2/CO, v/v

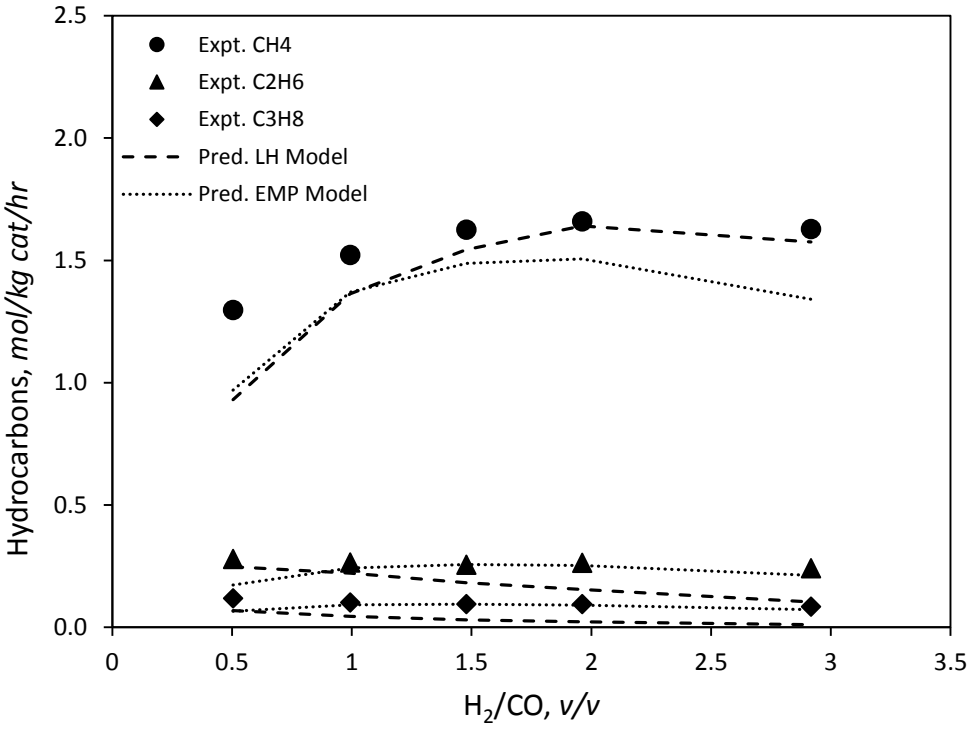
Expt. CH4
Expt. C2H6
Expt. C3H8
Pred. LH Model
Pred. EMP Model
Hydrocarbons, mol/kg cat/hr
H2/CO, v/v

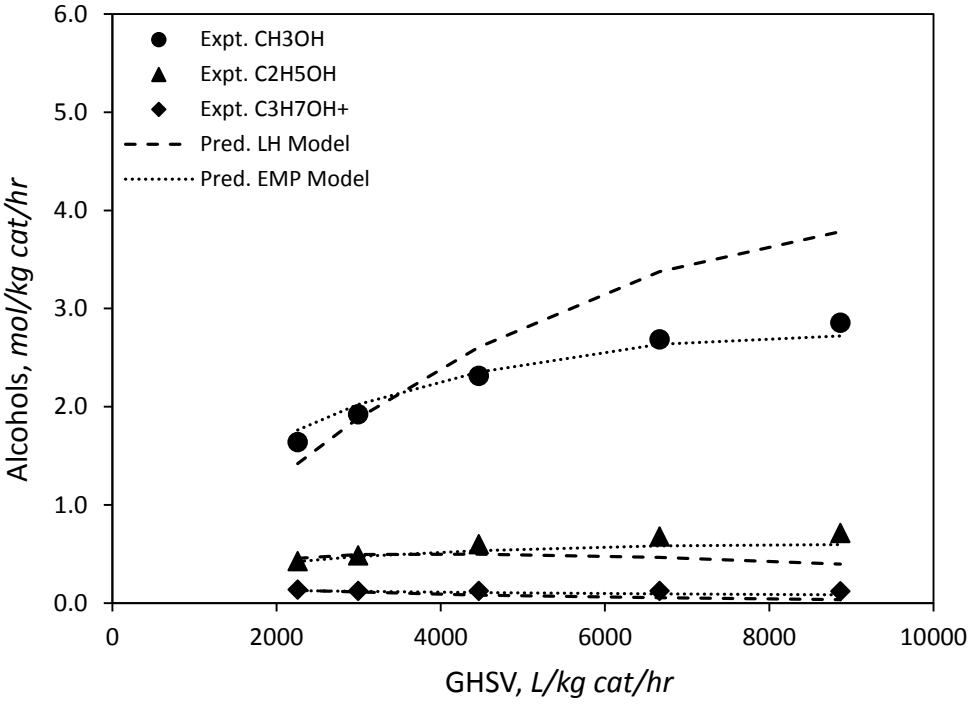
Expt. CH3OH
Expt. C2H5OH
Expt. C3H7OH+
Pred. LH Model
Pred. EMP Model
Alcohols, mol/kg cat/hr
GHSV, L/kg cat/hr
0.0
1.0
2.0
3.0
4.0
5.0
6.0
0
2000
4000
6000
8000
10000

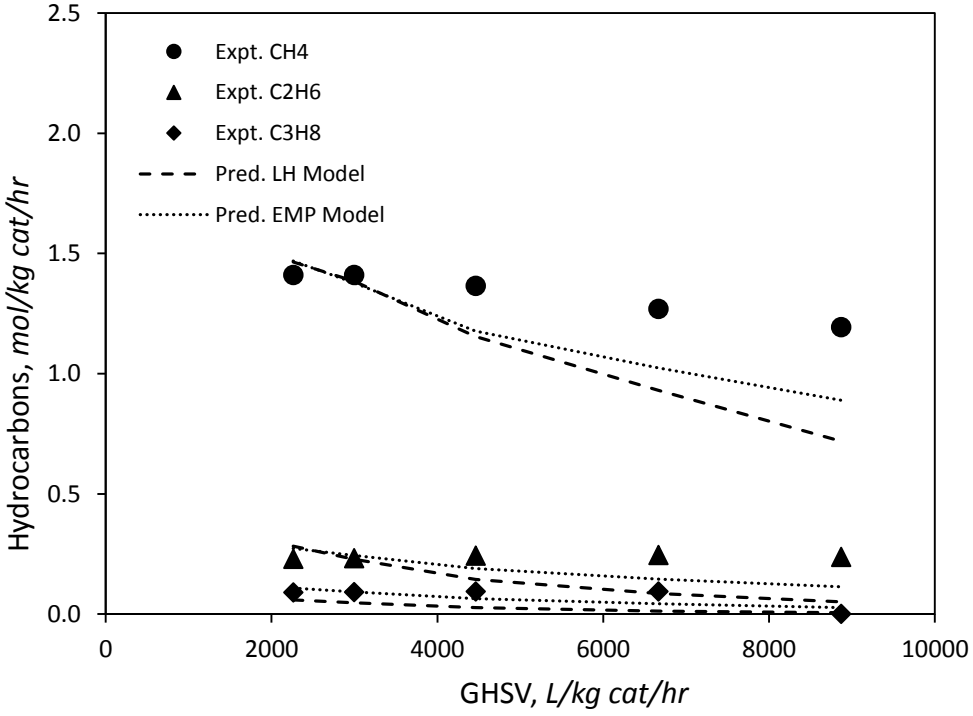
Expt. CH4
Expt. C2H6
Expt. C3H8
Pred. LH Model
Pred. EMP Model
Hydrocarbons, mol/kg cat/hr
GHSV, L/kg cat/hr
0.0
0.5
1.0
1.5
2.0
2.5
0
2000
4000
6000
8000
10000

The reversible nature of methanol reaction was considered for LH model, whereas for EMP model, reversible methanol, water-gas shift reaction, alcohols and hydrocarbon formation reactions were coupled together and represented by two forward reactions only. Both LH and EMP model can predict the experimental data quite reasonably well, both qualitatively and quantitatively. Added advantages of EMP model over LH model are,

- Only two reactions are sufficient to represent the higher alcohol synthesis reaction network.
- The reactions are forward reactions; no reversible reaction. This eliminates the additional kinetic parameters used for the LH model.

4.6. Conclusions

The kinetic models of the power-law and Langmuir-hinshelwood type rate expressions based on seven reactions were developed for higher alcohol synthesis reactions over cesium promoted molybdenum sulfide based supported catalyst. The singular value decomposition was applied for the first time to a higher alcohol synthesis reactions network. Only two reactions are sufficient to describe the catalyst behavior under the influence of reaction temperature, pressure, gas hourly space velocity, and hydrogen to carbon monoxide ratio. An empirical kinetic model based on these two reactions was developed. A genetic algorithm minimization tool was applied to estimate the kinetic parameters associated with the power-law, langmuir-hinshelwood, and empirical kinetic models.

4.7. Appendix

Appendix 4A: Example MATLAB Code for GA Minimization using the Empirical Model

Main Function

```
clear all;
clc;
format short g;
npop=1000;
ngen=500;
initPop=initializega(npop,[1 50;1 100;40 100;75 175;0.001 3;0.001 3;0.001 3;0.001 3;0.001
3;1 3;1 3],'ObjSVDLH');
[BestX, endPop, bpop, traceinfo] = ga([1 50;1 100;40 100;75 175;0.001 3;0.001 3;0.001
3;0.001 3;0.001 3;1 3;1 3],'ObjSVDLH',[],initPop,[1e-8 1 1],'maxGenTerm',ngen);
BestX
xlswrite('BestX',BestX);
```

Function `ObjSVDLH` (Objective function)

```
function [b, val] = ObjSVDLH(b,options)
% clear all;
% clc;

%%%%%%%%%%%%%     Estimated Parameters     %%%%%%%%%
%Different CO adsorption coefficient
% b=[19.053 61.102 64.749 128.04 0.63262 0.170390 0.44658 2.5557 1.9701 1.2061 1.7181];
%error = -0.078314 %workspace THESISFINAL1
% b=[18.596 86.653 64.786 123.68 0.41834 0.067884 1.09110 1.3744 1.1913 1.7301 2.1917];
%error = -0.077448 %workspace THESISFINAL2
% b=[18.596 86.653 64.786 123.68 0.41834 0.067884 1.09110 1.3744 1.1913 1.7301 2.1917];
%error = -0.077448 %workspace THESISFINAL3 ANSWER


global alpha pcp Tcp rxn
W=3e-3;                             %Catalyst weight, kg

%%%%%%%%%%%%     Reaction Stoichiometry     %%%%%%%%%%
% [Methanol, Ethanol, Propanol, Butanol, Methane, Ethane,Propane, Carbon Dioxide, Carbon
Monoxide, Hydrogen]
alpha=[0.3080  0.0660 0.0070 0.0000 0.0700 0.0060 0.0000 0.1620 -0.7050  -1.0000; %CO+H2-
->CH3OH+C2H5OH+C3H7OH+CH4+C2H6+CO2
      -0.5905 -0.1030 0.0300 0.0000 0.4100 0.1100 0.0550 0.7520 -0.8405
0.0000];%CO+CH3OH+C2H5OH-->C3H7OH+CH4+C2H6+C3H8+CO2

MW=[32.04146 46.06804 60.09462 16.04246 30.06904 44.09562 44.0087 18.01488 28.0097
2.01588];
```

```
rxn=2;

% E=xlsread('Input');

%%%%%%%%%%%%%%%     Input Data     %%%%%%%%%%%%%
E=[1    397.7833333 85.87675267 589.15  0.504270696 3001.788889 81.56451373 41.13059415
73.14217595 32.75622173 1.133005753 0.49345548  0.172042842 0   1.296218623 0.279315054
0.118740703 3.394954346 1.798504075 1.694274381 10.32598295 51.49207423;
2   418.1805556 85.87675267 589.15  0.99314065  2992.9  61.37639281 60.95539065
52.2374026  50.61746426 1.981178642 0.527249701 0.137064614 0   1.521974986 0.264221384
0.101934548 3.281275501 2.645492958 1.888130917 14.89007385 58.35272248;
3   410.5027778 86.22149267 589.15  1.478787309 2987.566667 49.26352026 72.85026856
39.97570983 61.57290316 2.441391594 0.504647174 0.120567338 0   1.62522826  0.255592038
0.094915498 3.095684507 3.066606106 1.975735796 18.85332267 60.81709979;
4   388.6888889 86.22149267 589.65  1.961242447 2984.011111 41.1882719  80.78018716
31.65127978 68.83118087 2.776822322 0.487035441 0.111653762 0   1.658970324 0.263516369
0.094373987 3.051127311 3.375511525 2.01686068  23.15463038 62.59789564;
5   393.3916667 85.646926   589.15  2.916703181 2979.566667 31.09421144 90.69258541
22.23333368 78.80564591 2.988454107 0.413014264 0.088713624 0   1.627314073 0.241093079
0.084082281 2.599522152 3.490181995 1.952489433 28.4968724  64.12626669;
6   578.3   48.587376   586.15  0.99314065  2992.9  61.37639281 60.95539065 57.32428792
56.28782682 0.892139803 0.274770848 0.058664339 0   0.604658722 0.133148005 0.053550897
1.414517826 1.225574989 0.791357624 6.60205774  60.76430026;
7   458.9633333 57.274824   587.15  0.99314065  2992.9  61.37639281 60.95539065
55.75673468 54.5394845  1.223320185 0.334912784 0.084090495 0   0.880616591 0.186851258
0.076268258 1.994228052 1.642323464 1.143736108 9.156058017 58.94789473;
8   477.2611111 71.11038933 587.4833333 0.99314065  2992.9  61.37639281 60.95539065
54.71992336 53.40020925 1.532985332 0.40167507  0.09769559  0   0.989781385 0.198764524
0.079066518 2.347020597 2.032355992 1.267612427 10.8453253  61.5871346;
9   484.2472222 84.21050933 590.15  0.99314065  2992.9  61.37639281 60.95539065
53.0072054  51.28867432 1.921546652 0.48470135  0.122051267 0   1.410061214 0.232360464
0.090720705 2.94011792  2.528299269 1.733142382 13.63584113 59.32967;
10  599.9458333 96.333866   587.4   0.99314065  2992.9  61.37639281 60.95539065
51.88638802 49.99317699 2.271192024 0.566383305 0.135028581 0   1.550237379 0.238453507
0.090882739 3.304375206 2.972603911 1.879573625 15.46197871 61.26329651;
11  653.3333333 105.814216  587.15  0.99314065  2992.9  61.37639281 60.95539065
51.27275954 49.11846282 2.544683971 0.599639526 0.135743529 0   1.650488751 0.242140847
0.094271726 3.457660814 3.280067025 1.986901324 16.46175803 62.27618637;
12  499.9595238 84.29259029 589.15  0.996787977 2258.7  46.23530213 46.08679327
38.22137177 37.11190957 1.637642794 0.424956159 0.135049153 0   1.409323928 0.229806064
0.090103198 2.931324507 2.197648106 1.72923319  17.33292524 55.96421028;
13  484.2472222 84.21050933 590.15  0.99314065  2992.9  61.37639281 60.95539065
53.0072054  51.28867432 1.921546652 0.48470135  0.122051267 0   1.410061214 0.232360464
0.090720705 2.94011792  2.528299269 1.733142382 13.63584113 59.32967;
14  505.8733333 83.9577 590.15  0.98946101  4461.3  91.65857419 90.69258541 82.68534503
79.95047453 2.312810901 0.597392668 0.121972624 0   1.365026414 0.242636663 0.094133955
2.976447526 3.032176193 1.701797032 9.789841526 64.05140141;
15  510.51  84.440336   590.15  0.986989753 6663.9  137.0818463 135.2983776 127.7042065
123.7557382 2.684454612 0.677903626 0.121425506 0   1.269380103 0.245507998 0.094013129
2.952087825 3.483783743 1.60890123  6.840905629 68.40760348;
16  604.3166667 84.440336   588.75  0.985748626 8866.5  182.5051183 179.9041697
173.1459282 168.4809556 2.854646801 0.71227577  0.11893044  0   1.193252581 0.236935256 0
2.9239489   3.685853011 1.430187837 5.128179554 72.04502701;
17  535.1133333 84.164544   561.15  0.99314065  2992.9  61.37639281 60.95539065
57.92711486 56.73489423 1.080959252 0.282501521 0.040501427 0   0.426131165 0.065145325 0
1.061686233 1.4039622   0.49127649  5.619877285 74.07838428;
18  539.6033333 84.440336   572.55  0.99314065  2992.9  61.37639281 60.95539065
56.07472448 54.48341954 1.51325139  0.389081904 0.066572257 0   0.721938829 0.116455169
0.054344087 1.679895215 1.968905551 0.892738085 8.637960128 68.80331032;
19  544.0233333 84.30244    587.15  0.99314065  2992.9  61.37639281 60.95539065
53.00442918 51.36579456 1.969270617 0.502265831 0.11929812  0   1.313145012 0.227918599
0.08894677  2.933355025 2.590834568 1.630010381 13.6403644  61.38189389;
20  548.5833333 84.026648   602.75  0.99314065  2992.9  61.37639281 60.95539065
48.90627485 47.80781814 2.014849742 0.541009488 0.232098847 0   2.26714505  0.425849948
0.175792268 4.892411082 2.787958076 2.868787265 20.31745006 49.2855504;
21  553.08  83.750856   620.35  0.99314065  2992.9  61.37639281 60.95539065 43.81004839
44.44673972 1.488017048 0.44934892  0.306528756 0   3.596579139 0.753215393 0.352533275
7.781183925 2.243894724 4.702327808 28.6206856  32.30381281;
```

```
22  563.08  83.750856   630.35  0.99314065  2992.9  61.37639281 60.95539065 38.41
40.395  1   0.3 0.343136561 0   5.353131029 1.160871935 0.491680941 10.8    1.643136561
7.005683905 37.41893546 18.99838906;
23  433.675 85.991666   588.9833333 1.962151483 4447.966667 61.37639281 120.4297802
51.17438237 107.1841106 3.365370568 0.602473491 0.10972359  0   1.543795084 0.26870331
0.093081847 3.027023036 4.077567649 1.90558024  16.62204306 68.15087517;
24  629.68  104.29736   588.15  0.986989753 6663.9  137.0818463 135.2983776 125.8089526
121.2686979 3.398514146 0.780858089 0.138752798 0   1.572072015 0.259172393 0.10261975
3.494893262 4.318125034 1.933864158 8.223476679 69.06801821;
25  648.8   103.883672  587.15  0.98946101  4461.3  91.65857419 90.69258541 81.29808575
78.14533184 2.936833038 0.669908533 0.132693068 0   1.529510382 0.229056893 0.096253207
3.350619369 3.739434639 1.854820482 11.30334891 66.84419209];


C(:,1)=E(:,5);                                          %H2/CO, v/v
C(:,2)=E(:,2);                                          %Time, hr
C(:,3)=W./(E(:,6)'/22.414*W*273.15/(273.15+25));        %GHSV converted to kg/(mol/hr)
C(:,4)=E(:,4);                                          %Temp in K
C(:,5)=E(:,3);                                          %Pressure in bar
C(:,6)=E(:,6);                                          %GHSV, L/kgcat/hr
C(:,21)=E(:,7).*C(:,3);                                 %COin, (mol/hr)/(molf/hr)
C(:,22)=E(:,8).*C(:,3);                                 %Hydrogenin, (mol/hr)/(molf/hr)
C(:,7)=E(:,21);                                         %CO conv, %
C(:,11)=E(:,11).*C(:,3);                                %Methanol, (mol/hr)/(molf/hr)
C(:,12)=E(:,12).*C(:,3);                                %Ethanol, (mol/hr)/(mol/hr)
C(:,13)=E(:,13).*C(:,3);                                %Propanol, (mol/hr)/(mol/hr)
C(:,14)=E(:,14).*C(:,3);                                %Butanol, (mol/hr)/(mol/hr)
C(:,15)=E(:,15).*C(:,3);                                %Methane, (mol/hr)/(mol/hr)
C(:,16)=E(:,16).*C(:,3);                                %Ethane, (mol/hr)/(mol/hr)
C(:,17)=E(:,17).*C(:,3);                                %Propane, (mol/hr)/(mol/hr)
C(:,18)=E(:,18).*C(:,3);                                %CO2, (mol/hr)/(mol/hr)
% C(:,19)=E(:,19);                                        %Water, (mol/hr)/(mol/hr)
C(:,19)=E(:,9).*C(:,3);                                 %CO, (mol/hr)/(mol/hr)
C(:,20)=E(:,10).*C(:,3);                                %Hydrogen, (mol/hr)/(mol/hr)
C(:,9)=E(:,19).*C(:,3);                                 %Total Alcohols, (mol/hr)/(mol/hr)
C(:,10)=E(:,20).*C(:,3);                                %Total Hydrocarbons,
(mol/hr)/(mol/hr)
C(:,8)=E(:,22);                                         %Alcohol Selectivity, mol/mol

NFoexpt=[C(:,11:20)];
T=C(:,4)';
Tcp=C(9,4);                                 %Center Point Temp, K
Pcp=C(9,5);                                 %Center Point Pressure, bar
pcp=Pcp*NFoexpt(9,:)/sum(NFoexpt(9,:));     %bar (a)
[m n]=size(C);
c=length(NFoexpt(2,:)');
XFoj=zeros;
WFoj=zeros;
% XFoc=zeros;
Fo=C(:,6)'/22.414*273.15/(273.15+25);       %molf/kg cat/hr

HCO=C(:,1)';
P=C(:,5)';

%%%%%%%%%%%%%%%  ODE   %%%%%%%%%%%%%%
for i=1:1:m
    xzero=[0 0 T(i)];
    wspan=[0 C(i,3)];
    op=[HCO(i) Fo(i) T(i) P(i)]; %ratio(v/v),Fo (molf/kg cat/hr), K, bar(a)
    [WF0,XF0]=ode15s(@(WF0,XF0)KineticsSVDLH(WF0,XF0,b,op),wspan,xzero);
    for j = 1:length(WF0)
         for l=1:length(xzero)
             XFoj(j,i,l) = XF0(j,l);
         end
    WFoj(j,i)=WF0(j,1);
    end
end

[r,s]=size(XFoj);
```

```
for i=1:1:s
    XFoc(i)=XFoj(find(XFoj(:,i),1,'last'),i);
end
XFo=[XFoc(1:m); XFoc(m+1:2*m); XFoc(2*m+1:3*m)]';

[t,u]=size(WFoj);
for i=1:1:u
    WFo(i)=WFoj(find(WFoj(:,i),1,'last'),i);
end

yo=[zeros(c-2,m);(1./(C(:,1)+1))';(C(:,1)./(C(:,1)+1))'];

for i=1:1:m
    NrFo(:,i)=alpha'*XFo(i,1:rxn)';
    No(:,i)=Fo(i)*yo(:,i);
    Nr(:,i)=Fo(i)*NrFo(:,i);
    N(:,i)=No(:,i)+Nr(:,i);
    NFoest(:,i)=N(:,i)/Fo(i);
end
NFoex=NFoexpt';
Nest=N';

for i=1:1:m
    NMest(:,i)=bsxfun(@times,N(:,i),MW');
    NMex(:,i)=NFoex(:,i)*Fo(i);
    NMexp(:,i)=bsxfun(@times,NMex(:,i),MW');
end
NFocal=NFoest';
NMcal=NMest';
NMexpt=NMexp';
Nexp=NMex';

%%%%%%% Results %%%%%%
% xlswrite('ExpSVDLHmol',Nexp);
% xlswrite('CalSVDLHmol',Nest);
% xlswrite('ExpSVDLHmass',NMexpt);
% xlswrite('CalSVDLHmass',NMcal);

%%%%%%% Objective Function %%%%%%%%%
errorch3oh=sum((bsxfun(@minus,NFoexpt(:,1),NFocal(:,1))).^2);
errorc2h5oh=sum((bsxfun(@minus,NFoexpt(:,2),NFocal(:,2))).^2);
errorc3h7oh=sum((bsxfun(@minus,NFoexpt(:,3),NFocal(:,3))).^2);
% errorc4h9oh=sum((bsxfun(@minus,NFoexpt(:,4),NFocal(:,4))).^2);
errorch4=sum((bsxfun(@minus,NFoexpt(:,5),NFocal(:,5))).^2);
errorc2h6=sum((bsxfun(@minus,NFoexpt(:,6),NFocal(:,6))).^2);
errorc3h8=sum((bsxfun(@minus,NFoexpt(:,7),NFocal(:,7))).^2);
% errorco2=sum((bsxfun(@minus,NFoexpt(:,8),NFocal(:,8))).^2);

error=3*errorch3oh+10*errorc2h5oh+5*errorc3h7oh+1*(errorch4+errorc2h6+errorc3h8);

rms=sqrt((error)/(m*21))*100;
val=rms;
val=-val;

%%%%%%%%%%%     rmsds    %%%%%%%%%%%
rmsdfo=sqrt((sum(sum((bsxfun(@minus,NFoexpt,NFocal)).^2)))/(m*c));
Nexpalcs=bsxfun(@plus,(bsxfun(@plus,Nexp(:,1),Nexp(:,2))),Nexp(:,3));
Nestalcs=bsxfun(@plus,(bsxfun(@plus,Nest(:,1),Nest(:,2))),Nest(:,3));
Nexphcs=bsxfun(@plus,(bsxfun(@plus,Nexp(:,5),Nexp(:,6))),Nexp(:,7));
Nesthcs=bsxfun(@plus,(bsxfun(@plus,Nest(:,5),Nest(:,6))),Nest(:,7));

rmsdalcs=sqrt((sum((bsxfun(@minus,Nexpalcs(:,1),Nestalcs(:,1))).^2))/m);
rmsdhcs=sqrt((sum((bsxfun(@minus,Nexphcs(:,1),Nesthcs(:,1))).^2))/m);
rmsdch3oh=sqrt((sum((bsxfun(@minus,Nexp(:,1),Nest(:,1))).^2))/m);
rmsdc2h5oh=sqrt((sum((bsxfun(@minus,Nexp(:,2),Nest(:,2))).^2))/m);
rmsdc3h7oh=sqrt((sum((bsxfun(@minus,Nexp(:,3),Nest(:,3))).^2))/m);
rmsdch4=sqrt((sum((bsxfun(@minus,Nexp(:,5),Nest(:,5))).^2))/m);
rmsdc2h6=sqrt((sum((bsxfun(@minus,Nexp(:,6),Nest(:,6))).^2))/m);
rmsdc3h8=sqrt((sum((bsxfun(@minus,Nexp(:,7),Nest(:,7))).^2))/m);
```

```
rmsdco2=sqrt((sum((bsxfun(@minus,Nexp(:,8),Nest(:,8))).^2))/m);


RMSD=[rmsdch3oh rmsdc2h5oh rmsdc3h7oh rmsdalcs rmsdch4 rmsdc2h6 rmsdhcs rmsdco2];


%%%%%%%%%%     Parity plots      %%%%%%%%%%%
NFoexptHC=bsxfun(@plus,(bsxfun(@plus,NFoexpt(:,5),NFoexpt(:,6))),NFoexpt(:,7));
NFocalHC=bsxfun(@plus,(bsxfun(@plus,NFocal(:,5),NFocal(:,6))),NFocal(:,7));
NFoexptprohplus=bsxfun(@plus,NFoexpt(:,3),NFoexpt(:,4));
NFocalprohplus=bsxfun(@plus,NFocal(:,3),NFocal(:,4));

% figure(1); hold on
% plot(NFoexpt,NFocal,'bo'); hold on
% plot((0:0.01:0.75),(0:0.01:0.75),'--')
% axis([0,0.75,0,0.75]);
% xlabel 'Fexpt/Fo (mol/mol)',ylabel 'Fest/Fo (mol/mol)'
% legend('Parity plot of products'); hold off
%
% figure(2)
% subplot(221)
% plot(NFoexpt(:,1),NFocal(:,1),'bo'); hold on
% plot((0.00:0.001:0.03),(0.00:0.001:0.03),'--')
% axis([0.00,0.03,0.00,0.03])
% xlabel 'Methanol, Fexpt/Fo (mol/mol)',ylabel 'Fest/Fo (mol/mol)'
% subplot(222)
% plot(NFoexpt(:,2),NFocal(:,2),'bo'); hold on
% plot((0.00:0.001:0.007),(0.00:0.001:0.007),'--')
% axis([0.00,0.007,0.00,0.007])
% xlabel 'Ethanol, Fexpt/Fo (mol/mol)',ylabel 'Fest/Fo (mol/mol)'
% subplot(223)
% plot(NFoexptprohplus,NFocalprohplus,'bo'); hold on
% plot((0:0.0001:0.0025),(0:0.0001:0.0025),'--')
% axis([0,0.0025,0,0.0025])
% xlabel 'Propanol+, Fexpt/Fo (mol/mol)',ylabel 'Fest/Fo (mol/mol)'
% subplot(224)
% plot(NFoexptHC,NFocalHC,'bo'); hold on
% plot((0:0.001:0.03),(0:0.001:0.03),'--')
% axis([0,0.03,0,0.03])
% xlabel 'HC, Fexpt/Fo (mol/mol)',ylabel 'Fest/Fo (mol/mol)'
```

Function KineticsSVDLH (reaction kinetics)

```
function xprime=KineticsSVDLH(~,x,b,op)

global alpha pcp Tcp rxn

R=8.3145e-3;                %KJ/(mol.K)


%%%%%%%%%%%%%%          REACTION PARAMETERS     %%%%%%%%%%%%%%%%%%

%METHANOL
Agen=b(1);                  %mol/(Kgcat.hr)
Egen=b(3);                  %KJ/mol
ngen=b(10);
k=[b(5) b(6) b(7) b(8) b(9)];    %Adsorption/Qquilibrium Constants

%HYDROCARBONS
Adec=b(2);
Edec=b(4);
```

```
ndec=b(11);

%PARTIAL PRESSURE
yo=[0 0 0 0 0 0 0 0 1/(1+op(1)) op(1)/(1+op(1))];
ye=yo'+alpha'*x(1:rxn);
y=ye/sum(ye);
p=y*op(4);


%%%%%%%%%%%%%%%%%% Rate Expressions %%%%%%%%%%%%%%

rgengn=(p(9)/pcp(9))^0.705*(p(10)/pcp(10));
rgengd=(1+k(1)*(p(9)/pcp(9))+k(2)*(p(10)/pcp(10))^0.5)^ngen;
rgeng=Agen*exp(-(Egen/R)*(1/op(3)-1/Tcp))*rgengn/rgengd;

rdecg=Adec*exp(-(Edec/R)*(1/op(3)-
1/Tcp))*((p(1)/pcp(1))*(p(2)/pcp(2))*(p(9)/pcp(9)))/((1+k(4)*(p(1)/pcp(1))+k(5)*(p(2)/pcp
(2))+k(3)*(p(9)/pcp(9)))^ndec);

xprime=[rgeng; rdecg; 0]; %Iso-thermal reactor
```

4.8. References

1. Herman, R.G. *Classical and non-classical routes for alcohol synthesis*. in *Studies in Surface Science and Catalysis, New Trends in CO Activation*. 1991. Elsevier.
2. Santiesteban, J.G., *Alcohol Synthesis from Carbon Monoxide and Hydrogen over MoS_2-based Catalysts*, in *Chemistry*. 1989, Lehigh University.
3. Gunturu, A.K., et al., *A kinetic model for the synthesis of high-molecular-weight alcohols over a sulfided Co-K-Mo/C catalyst.* Industrial & engineering chemistry research, 1998. **37**(6): p. 2107-2115.
4. Christensen, J.M., et al., *Effects of H_2S and process conditions in the synthesis of mixed alcohols from syngas over alkali promoted cobalt-molybdenum sulfide.* Applied Catalysis A: General, 2009. **366**(1): p. 29-43.
5. Sahoo, R.K., et al., *Improved binary parameters using GA for multi-component aromatic extraction: NRTL model without and with closure equations.* Fluid Phase Equilibria, 2006. **239**(1): p. 107-119.

6. Gunturu, A.K., et al., *The Economical Production of Alcohol Fuels from Coal-Derived Synthesis Gas: Chapter 5 A Kinetic Model for the Synthesis of High-Molecular-Weight Alcohols over a Sulfided Co-K-Mo/C Catalyst*. 1999, West Virginia University Research Corporation. p. 87-117.
7. Sandler, S.I., *Chemical and Engineering Thermodynamics -- 3rd Edition*. 1999: John Wiley & Sons.
8. Harmon, J., P. Duboc, and D. Bonvin, *Factor analytical modeling of biochemical data.* Computers & chemical engineering, 1995. **19**(12): p. 1287-1300.
9. Hamer, J.W., *Stoichiometric interpretation of multireaction data: application to fed-batch fermentation data.* Chemical Engineering Science, 1989. **44**(10): p. 2363-2374.
10. Famili, I. and B.O. Palsson, *Systemic metabolic reactions are obtained by singular value decomposition of genome-scale stoichiometric matrices.* Journal of theoretical biology, 2003. **224**(1): p. 87-96.
11. Froment, G.F., K.B. Bischoff, and J.D. Wilde, *Chemical Reactor Analysis and Design*. Third ed. 2011: John Wiley & Sons, Inc.
12. Houck, C.R., J.A. Joines, and M.G. Kay, *A genetic algorithm for function optimization: a MATLAB implementation. NCSU-IE TR 95-09.* 1995.

Chapter 5

Modeling and Simulation of Fixed-Bed Higher Alcohol Synthesis Reactor from Syngas over Activated Carbon Supported Cesium-Promoted Molybdenum Sulfide Catalysts

The work described in this chapter has been titled "Modeling and Simulation of Fixed-Bed Higher Alcohol Synthesis Reactor from Syngas over Activated Carbon Supported Cesium-Promoted Molybdenum Sulfide Catalysts" by Ranjan K. Sahoo, Hugo S. Caram, Divyanshu R. Acharya, and Richard G. Herman, *manuscript in preparation.*

Abstract

A one-dimensional pseudo-homogeneous fixed bed tubular reactor model was developed using the two reaction empirical kinetic model for higher alcohol synthesis from syngas over cesium-promoted molybdenum sulfide based activated carbon supported catalyst. The heat transfer coefficient was calculated by leva's correlation. An overall heat transfer coefficient of 507.6 W/m^2/°K was calculated for a 0.066 m reactor (inside diameter), at a reaction condition of 588.15 °K, 100 bar, gas hourly space velocity of 4500 L/kg cat/hr, and hydrogen to carbon monoxide ratio of 1.0 v/v. The higher alcohol synthesis reactions are highly exothermic in nature and hence, it is required to remove the excess heat generated in-order to avoid any runaway situations. The reactor simulation results from MATLAB were verified with the aspen plus simulation results, as well as with the experimental results obtained from an isothermal lab scale reactor. For a plant scale reactor, a runaway situation may be possible at a gas

hourly space velocity below 2000 L/kg cat/hr, and a reactor diameter of larger than 0.075 m. The aspen plus reactor simulation was further extended to incorporate the recycle stream from out let of the reactor. Initial simulation results shows that, it is required to purge at least 15 % of the recycle stream to keep the methane level less than 10 % and remove at least 50 % of the carbon dioxide present in the recycle stream to keep the carbon dioxide level below 7 % at inlet of the reactor. The overall carbon monoxide conversion and alcohol selectivity of at least 50.3 % and 48.3 mol% respectively was predicted. The total alcohol of 405 g/kg active materials/hr, with ethanol and higher alcohols of 95.3 g/kg active materials/hr and 133.5 g/kg active materials/hr respectively was predicted for the alcohol synthesis process configuration and the reaction conditions employed for the simulation.

5.1. Objective

The objective of this chapter is:

- To develop a fixed bed reactor model using the simplified governing equations and the kinetic models.
- Verify the MATLAB simulation results with the lab-scale experimental results.
- Simulation of the alcohol synthesis reactor and higher alcohol synthesis process in a commercial simulator, such as, aspen plus and hysys.

5.2. Reactor Modeling

5.2.1. Reaction Kinetics

Two reaction empirical kinetic model (EMP) developed in Chapter 4 for higher alcohol synthesis over Cs/MoS_2/AC catalyst was used. The empirical reactions are:

$Primary\ reaction$

$$0.705CO + H_2 \rightarrow 0.308CH_3OH + 0.066C_2H_5OH + 0.007C_3H_7OH + 0.07CH_4 + 0.006C_2H_6 + 0.162CO_2 \quad (5.1)$$

$Secondary\ reaction$

$$0.5905CH_3OH + 0.103C_2H_5OH + 0.8405CO \rightarrow 0.03C_3H_7OH + 0.41CH_4 + 0.11C_2H_6 + 0.055C_3H_8 + 0.752CO_2 \quad (5.2)$$

First reaction accounts for the formation of alcohols and hydrocarbons whereas second reaction accounts for the decomposition of alcohols to hydrocarbons and formation of higher alcohols at high temperatures and/or low space velocities.

Rate expressions for the two reactions are:

$Primary\ reaction$

$$r_{gen} = \frac{A_{gen} e^{-\left(\frac{E_{gen}}{R}\right)\left(\frac{1}{T}-\frac{1}{T^{cp}}\right)} \left(\frac{p_{CO}}{p_{CO}^{cp}}\right)^{0.705} \left(\frac{p_{H_2}}{p_{H_2}^{cp}}\right)}{\left[1 + K_1\left(\frac{p_{CO}}{p_{CO}^{cp}}\right) + K_2\left(\frac{p_{H_2}}{p_{H_2}^{cp}}\right)^{0.5}\right]^{n_{gen}}} \quad (5.3)$$

$$Secondary\ reaction$$

$$r_{dec} = \frac{A_{dec} e^{-\left(\frac{E_{dec}}{R}\right)\left(\frac{1}{T}-\frac{1}{T^{cp}}\right)} \left(\frac{p_{CO}}{p_{CO}^{cp}}\right)\left(\frac{p_{CH_3OH}}{p_{CH_3OH}^{cp}}\right)\left(\frac{p_{C_2H_5OH}}{p_{C_2H_5OH}^{cp}}\right)}{\left[1 + K_3\left(\frac{p_{CO}}{p_{CO}^{cp}}\right) + K_4\left(\frac{p_{CH_3OH}}{p_{CH_3OH}^{cp}}\right) + K_5\left(\frac{p_{C_2H_5OH}}{p_{C_2H_5OH}^{cp}}\right)\right]^{n_{dec}}} \quad (5.4)$$

The r_{gen} and r_{dec} are the rate of formation and rate of decomposition respectively. The A_i terms are refer to pre-exponential factors and the E_i, terms represents activation energies. The *K*'s in the denominator represent adsorption constants. The *n*'s in the denominator are exponents to the adsorption terms. Partial pressures of components *i* are denoted by p_i, and partial pressures and temperature at center point conditions are denoted by p_i^{cp} and T^{cp} respectively. The center point conditions are; $T^{cp} = 590.15\ °K$, $P^{cp} = 84.211\ bar$, $p_{CH_3OH}^{cp} = 1.451\ bar$, $p_{C_2H_3OH}^{cp} = 0.366\ bar$, $p_{CO}^{cp} = 40.035\ bar$, $p_{CO}^{cp} = 38.737\ bar$

The kinetic parameters for rate expressions 5.3 and 5.4 are given in Table 5.1.

Kinetic Parameters	Value	Kinetic Parameters	Value
A_{gen}	18.596	K_3	1.0911
A_{dec}	86.653	K_4	1.3744
E_{gen}	64.79	K_5	1.1913
E_{dec}	123.68	n_{gen}	1.730
K_1	0.4183	n_{dec}	2.192
K_2	0.0679		

A's mol/kg cat/hr, E's kJ/mol, K's and n's are dimensionless

Table 5.1. Kinetic parameters of Empirical (EMP) Model.

5.2.2. Reactor Models

The differential gas phase mass and energy balance equations of the one-dimensional pseudo-homogeneous fixed-bed tubular reactor model can be written as [1],

$Mass\ balance$

$$\frac{dx_j}{d\tau} = r_j; x = \frac{X}{F_o}; \tau = \frac{w}{F_o}; j = reactions \tag{5.5}$$

$$\frac{F_i}{F_o} = y_{o,i} + \alpha_{ij} x_j; i = components \tag{5.6}$$

$Energy\ balance$

$$\frac{dT}{d\tau} = \sum_j r_j \left(\frac{-\Delta H_j}{C_{p,mix}}\right) - \frac{4}{\rho_b C_{p,mix}} \left(\frac{U}{d_t}\right)(T - T_c) \tag{5.7}$$

The initial conditions for the inlet bulk phase were:

$$At\ \tau = 0: T = T_{in}, and\ x_j = 0 \tag{5.8}$$

Where, X_j is the extent of reaction j, F_o is the total inlet molar flow rate, F_i is the molar flow rate of component i, $y_{o,i}$ is the mole fraction of component i in the feed stream, α_{ij} is the matrix of reaction coefficients, r_j is the rate of formation of reaction j, T is the temperature of the reactor, ΔH_j is the heat of formation of reaction j, T_c is the outside reactor temperature, $C_{p,mix}$ is the heat capacity of the gas mixture, ρ_b is the bulk density of the catalyst, d_t is the inside reactor diameter, and w is the weight of catalyst. Pressure drop across the bed is insignificant with the particle size and flow rates employed for this study [2]. It is also assumed that, the change in heat capacity of the

reaction mixture along the catalyst bed is negligible and assumed to be constant and calculated from the inlet conditions.

The overall heat transfer coefficient, U in the energy balance equation is defined as,

$$\frac{1}{U} = \frac{1}{h_b} + \frac{t}{\lambda_s} \tag{5.9}$$

Where, t and λ_s are the thickness and the heat conductivity of reactor wall respectively.

The heat transfer coefficient on the bed side, h_b can be obtained from Leva's correlation. For cooling up the reaction mixture [1, 3]:

$$\frac{h_b d_t}{k_{mix}} = 3.5\left(R_{ep}\right)^{0.7} e^{\left(-\frac{4.6 d_p}{d_t}\right)}; R_{ep} = \frac{d_p v_s \rho_g}{\mu_{mix}} \tag{5.10}$$

Where, k_{mix} is the thermal conductivity of the gas mixture, R_{ep} is the particle Reynolds number, d_p is the equivalent particle diameter of the catalyst, v_s is the superficial velocity through the reactor, ρ_g is the density of the gas mixture, and μ_{mix} is the dynamic viscosity of the gas mixture.

Semi empirical equation developed by Eucken for a polyatomic gas was used for the calculation of thermal conductivity,

$$k = \left(C_p + \frac{5}{4}R\right)\frac{\mu}{M} \tag{5.11}$$

The dynamic viscosity, μ of a polyatomic gas of molecular weight M can be calculated from the equation [4],

$$\mu = 2.6693 \times 10^{-6} \frac{\sqrt{MT}}{\sigma^2 \Omega_\mu}, \qquad \frac{kg}{m.s} \tag{5.12}$$

Where, σ is the collision diameter.

The dimensionless collision integral quantity, Ω_μ can be obtained from,

$$\Omega_\mu = \frac{1.16145}{\left(\frac{\kappa T}{\epsilon}\right)^{0.14874}} + \frac{0.52487}{e^{0.7732\frac{\kappa T}{\epsilon}}} + \frac{2.16178}{e^{2.43787\frac{\kappa T}{\epsilon}}} \tag{5.13}$$

Where, κ is the Boltzmann constant, and ε is a characteristic energy term.

The Chapman-Enskog model for a multi component mixture was used for the prediction of thermal conductivity, k and dynamic viscosity, μ of a gas mixture,

$$\mu_{mix} = \sum_i \frac{y_{o,i}\mu_i}{\sum_j y_{o,j}\phi_{ij}} \tag{5.14}$$

$$k_{mix} = \sum_i \frac{y_{o,i}k_i}{\sum_j y_{o,j}\phi_{ij}} \tag{5.15}$$

The dimensionless quantities $\phi_{ij}'s$ are,

$$\phi_{ij} = \frac{1}{\sqrt{8}}\left(1+\frac{M_i}{M_j}\right)^{-\frac{1}{2}}\left[1+\left(\frac{\mu_i}{\mu_j}\right)^{\frac{1}{2}}\left(\frac{M_j}{M_i}\right)^{\frac{1}{4}}\right]^2 \tag{5.16}$$

Temperature dependent properties, k_{mix}, μ_{mix}, C_p and ρ_g of the gaseous mixture are calculated based on inlet CO and H_2 compositions, as the compositions of other components along the catalyst bed are negligible compared to CO and H_2 composition.

The Lennard-Jones parameters, σ and ε/κ, for CO and H_2 used for our calculations are given in Table 5.2 [4].

Components	***σ, Å***	***ε/κ, °K***
CO	2.915	38.0
H_2	3.590	110.0

Table 5.2. Lennard-Jones parameters for CO and H_2.

Molar heat capacity of a gas mixture can be obtained from,

$$C_{p,mix} = \sum_i y_{o,i} C_{p,i} \tag{5.17}$$

$$\frac{C_p}{R} = A + BT + \frac{C}{T^2} \tag{5.18}$$

Where R is the universal gas constant, R=8.3145 × 10^{-3} *kJ/mol/°K*.

Constants in the equation 5.18 for CO and H_2 are given in Table 5.3.

Components	A	$B \times 10^3$	$C \times 10^{-5}$
CO	3.376	0.557	-0.031
H_2	3.249	0.422	0.083

Table 5.3. Heat capacity parameters for CO and H_2.

Heat of formations, H_f of the components are calculated from Aspen Plus property estimation technique using *ideal* as the property method [5], and correlated by following series of equations,

$$H_f = AT - B, \frac{kJ}{mol} \tag{5.19}$$

Constants *A* and *B* are given in Table 5.4.

Components	A	B
CH_3OH	0.0734	228.13
C_2H_5OH	0.1179	278.99
C_3H_7OH	0.1588	314.23
C_4H_9OH	0.2032	351.43
CH_4	0.0579	96.041
C_2H_6	0.0986	121.27
C_3H_8	0.1418	158.67
CO_2	0.0492	410.03
CO	0.0312	120.28
H_2	0.0294	8.8418

Table 5.4. Heat of formation parameters.

5.3. Results and Discussion

The mass and energy balance equations 5.5, 5.6 and 5.7 were solved using *ode15s* routine in MATLAB. The code developed in MATLAB for a single tube reactor model is given in Appendix 5A. This model can predict the product distributions and temperature profile along the catalyst bed for a given inlet conditions of temperature, H_2/CO, reactor pressure, GHSV and outside reactor wall temperature. The reactor parameters and operating conditions used for our simulations for a lab-scale and plant-scale unit are given in Table 5.5. The l_b is the catalyst bed length for a given catalyst weight, catalyst bulk density and inside reactor diameter. Simulations were performed on a single tube of an industrial methanol reactor [6]. Non-isothermal (adiabatic and non-adiabatic) condition is assumed for the plant-scale unit as there is a considerable change in reactor temperature is expected along the length of catalyst bed due to highly exothermic nature of the higher alcohol synthesis reactions. Temperature variations for the lab-scale unit are negligible for such a small amount of catalyst and assumed to be in an isothermal condition. Isothermal lab-scale experimental results were used to validate the simplified reactor models developed in MATLAB and Aspen plus. The code developed can easily be extended for a multi tube reactor.

Reactor Parameters and Operating Conditions	Plant-scale (non-Isothermal reactor)	Lab-scale (Isothermal reactor)
Diameter of catalyst particle (*m*), d_p	0.003	0.003
Bulk density of catalyst bed (kg/m^3), ρ_b	750	750
Mass of catalyst (*kg*), *w*	27 (l_b = 10.512 *m*)	0.003 (l_b = 0.0316 *m*)
Inside diameter of tube (*m*), d_t	0.066	0.0127
Tube wall thickness (*m*), *t*	0.004	0.0032
Heat conductivity of wall material (*w/m/°K*), λ_s (steel)	50.2	
GHSV (*L/kg cat/hr*)	4500 (F_o = 4.968 *kmol/hr*)	2993
Inlet feed temperature (°*K*), T_{in}	588.15	590.15
Outside wall temperature (°*K*), T_c	588.15	590.15
H_2/CO ratio at inlet (*v/v*)	1	0.993
Reactor pressure (*bar*), *P*	100	84.211

Table 5.5. Reactor parameters and operating conditions used for simulation.

5.3.1. Adiabatic Reactor Simulation

Only the first term on right hand side of the energy balance equation 5.7 was considered for adiabatic reactor simulation. Fig. 5.1 shows the effect of inlet feed temperature on reactor temperature, total hydrocarbons (HCs), total alcohols, ethanol, alcohol selectivity and CO conversion profiles along the length of the reactor expressed as *kg* of catalyst. Plant-scale single tube reactor specifications and operating conditions as given in Table 5.5 was used for the simulation. Our goal is to keep the reactor

temperature between 580 °*K* and 610 °*K*, the optimum temperature conditions for higher alcohol productions and catalyst activity. Less activity of the catalyst was observed below 580 °*K*, whereas exponential increase in hydrocarbon productions and decrease in alcohol productions were observed above 610 °*K*. For an inlet feed temperature of 523.15 °*K* and 526.15 °*K*, the hydrocarbon productions are small and hence reactor temperature is under control, only 100 °*K* rise in temperature was predicted for an inlet feed temperature of 526.15 °*K*. However, a small increase in inlet feed temperature to 529.15 °*K* results in rapid increase in reactor temperature to 846 °*K*, results in exponential increase of hydrocarbon productions and thereby decreases the catalyst selectivity for alcohols. Rapid decrease in total alcohols as well as ethanol productions was also observed at very high temperatures. It is difficult to maintain the reactor temperature between the specified optimum temperature ranges due to highly exothermic nature of the reactions. In order to keep the reactor within specified optimum temperature range, heat generated due to exothermic reactions must be removed. This can be achieved by keeping the outside reactor tube temperature to a desired value by using a suitable heat transfer fluid such as, dowtherm, boiling water etc.

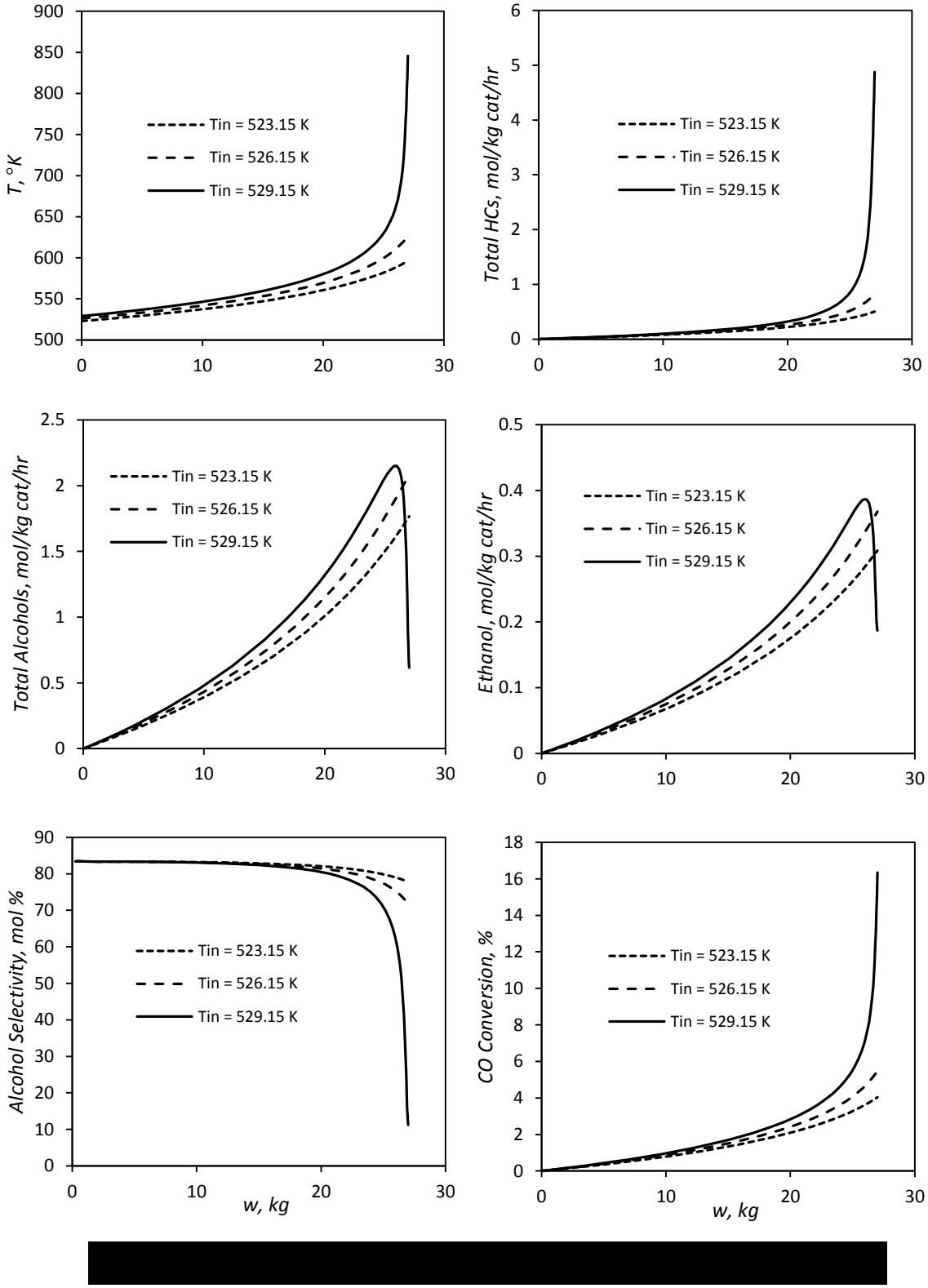
T, °K
Tin = 523.15 K
Tin = 526.15 K
Tin = 529.15 K
Total HCs, mol/kg cat/hr
Total Alcohols, mol/kg cat/hr
Ethanol, mol/kg cat/hr
Alcohol Selectivity, mol %
CO Conversion, %
w, kg

5.3.2. Non-Adiabatic Reactor Simulation

Energy balance equation 5.7, containing the additional heat balance term is solved simultaneously with mass balance equations 5.5 and 5.6 for a non-adiabatic reactor. Again the specifications given in Table 5.5, for a plant-scale reactor tube was used for the simulation. The reactor inlet temperature and the outside reactor tube temperature were assumed to be same and kept at 588.15 °*K*. Reactor tube diameter and inlet feed flow rate, expressed in terms of GHSV were used for the simulation study. Reactor tube diameter is explicitly appeared in the energy balance equation. Effect of reactor tube diameter on reactor temperature, total hydrocarbons, total alcohols, ethanol, alcohol selectivity and CO conversion profiles along the reactor length (in terms of catalyst weight) is shown in Fig. 5.2. Single tube simulations were performed for different inside diameter of the reactor tube at a fixed catalyst amount (27 *kg*) and feed flow rate (GHSV = 4500 *L/kg cat/hr*). Increase in reactor temperature was observed with increase in reactor diameter, after a certain diameter reactor temperature increases rapidly. A 20 % increase in reactor diameter from a base case reactor diameter of 0.066 *m* can increase the reactor exit temperature by 36 °*K*. This is due to the less heat transfer area available for a larger diameter reactor. Further increase in reactor diameter results in rapid rise of reactor temperature. The overall heat transfer coefficient calculated for reactor diameter of d_t = 0.066 *m* and 1.24d_t are 507.64 and 331.88 $W/m^2/°K$, respectively. As seen in the adiabatic case, rapid rise of reactor temperature, above the optimum temperature range increases hydrocarbon productions and decreases alcohol productions.

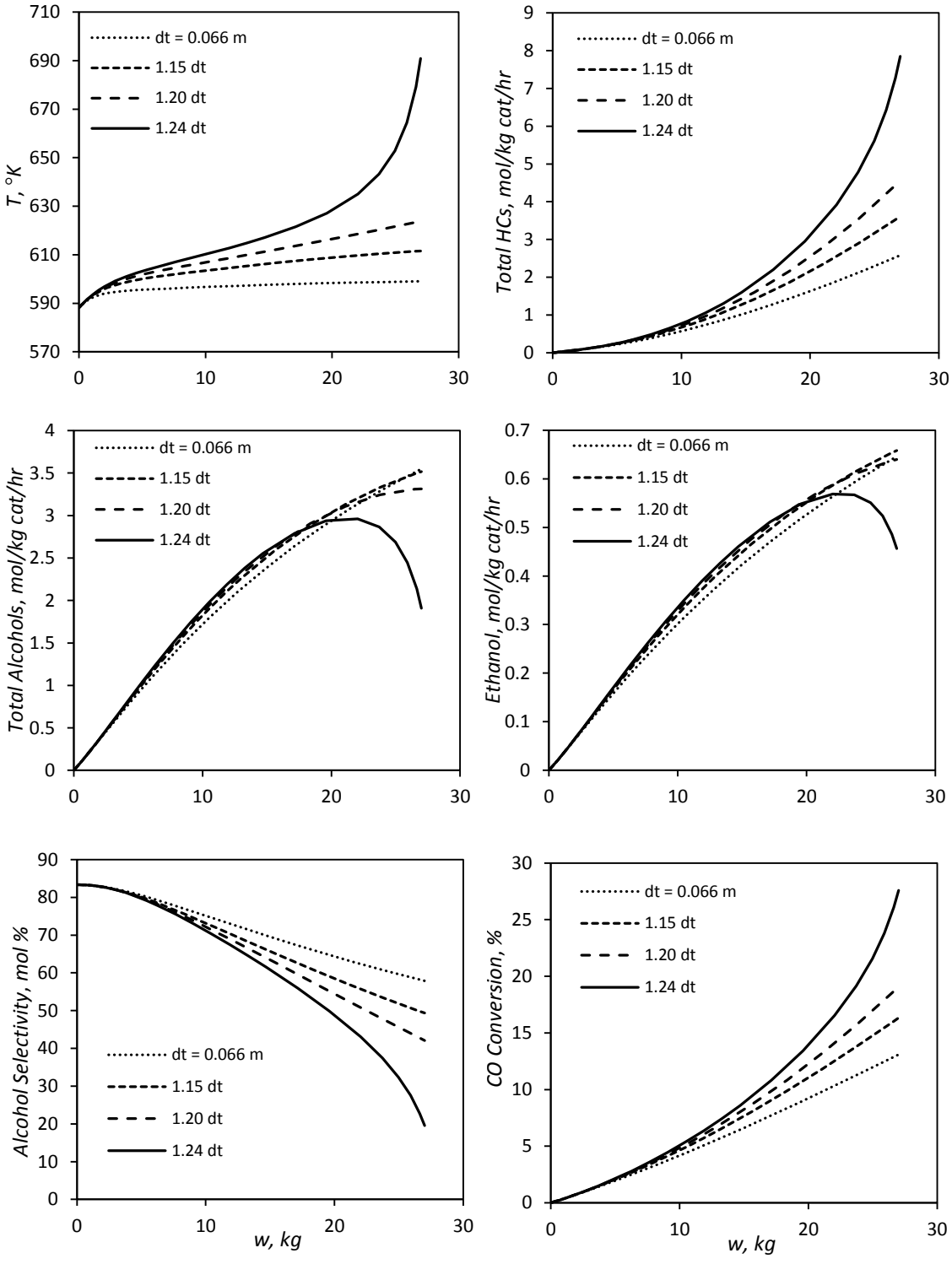
T, °K
dt = 0.066 m
1.15 dt
1.20 dt
1.24 dt
Total HCs, mol/kg cat/hr
Total Alcohols, mol/kg cat/hr
Ethanol, mol/kg cat/hr
Alcohol Selectivity, mol %
CO Conversion, %
w, kg

Effect of feed flow rate (GHSV) on reactor temperature, total hydrocarbons, total alcohols, ethanol, alcohol selectivity and CO conversion profiles along the reactor length (catalyst weight) is shown in Fig. 5.3. Reactor temperature increases and reaches a maximum value at some axial position for lower feed rates. A feed rate of 1810 *L/kg cat/hr* can results in rapid rise of reactor temperature to a maximum value of 683 °*K* at about mid-point of the reactor length. We can see the corresponding effect of temperature variations on the production of alcohols and hydrocarbons along the length of the reactor. Alcohol productions decrease with rapid rise in reactor temperature above 610 °*K* and increases again with decrease in reactor temperature. A feed flow rate of 3000 *L/kg cat/hr* or above can keep the reactor temperature within the limit of the optimum temperature range (580 °*K* - 610 °*K*). Overall heat transfer coefficient calculated for flow rates 1810, 3000, 4500 and 6000 *L/kg cat/hr* are 273.88, 387.13, 507.64 and 614.62 $W/m^2/°K$, respectively.

5.3.3. Aspen Plus Simulation

Aspen plus *RPlug* reactor module was selected for the simulation of tubular reactors. Simulations can be performed as an isothermal, adiabatic or a non-adiabatic reactor by selecting appropriate reactor configurations; select constant-temperature reactor for isothermal, adiabatic reactor for adiabatic and reactor with constant coolant temperature for a non-adiabatic reactor with constant outside wall temperature.

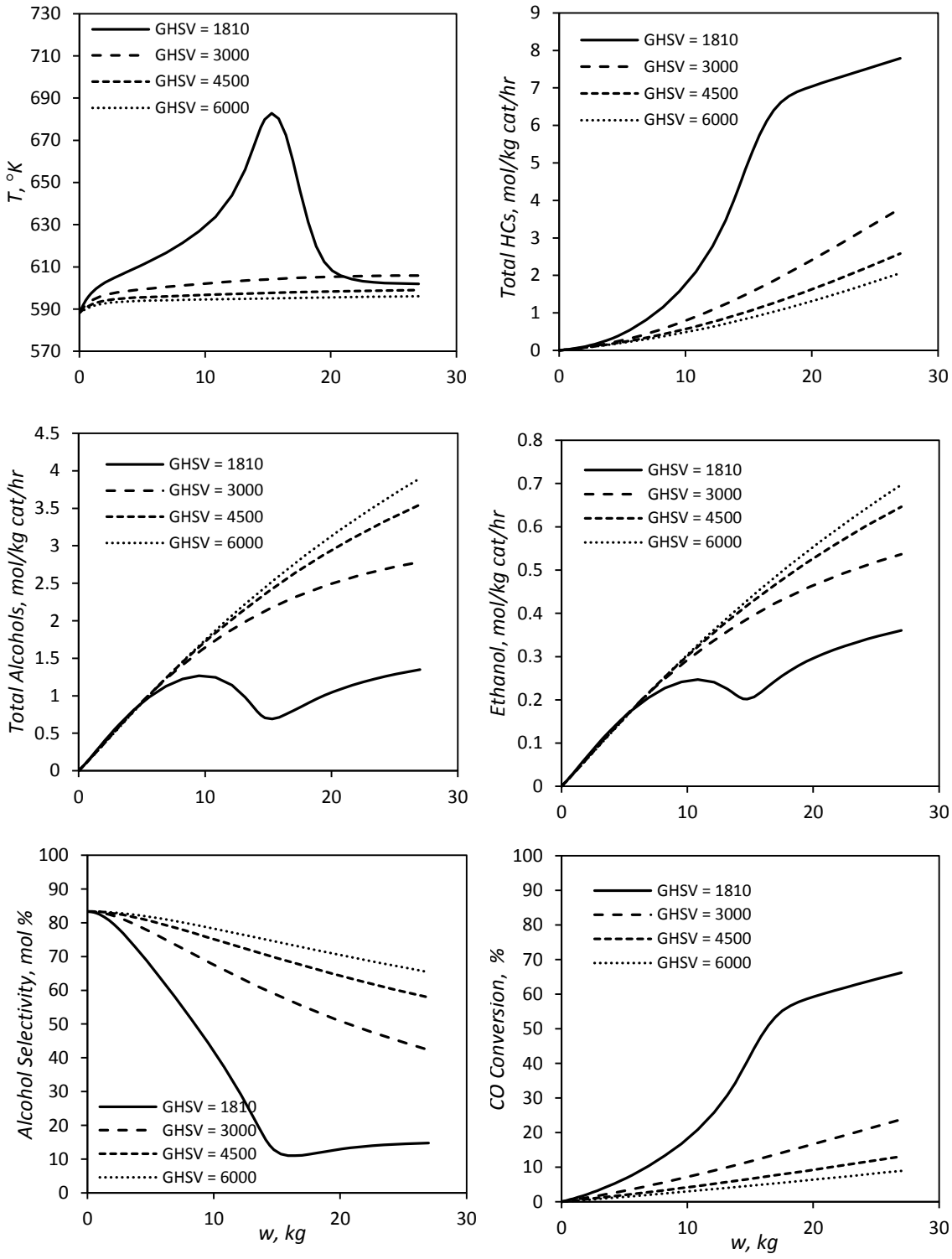
T, °K
GHSV = 1810
GHSV = 3000
GHSV = 4500
GHSV = 6000
Total HCs, mol/kg cat/hr
Total Alcohols, mol/kg cat/hr
Ethanol, mol/kg cat/hr
Alcohol Selectivity, mol %
CO Conversion, %
w, kg

[redacted]

The IDEAL property method was selected for the Aspen plus simulations. MATLAB and Aspen plus simulation results were validated with experimental results obtained from a lab-scale reactor unit. Lab-scale reactor parameters and operating conditions are given in Table 5.5.

Overall heat transfer coefficient calculated from equation 5.9 and 5.10 for a given operating conditions was used for non-adiabatic aspen plus simulations. Overall heat transfer coefficient value of 507.64 $W/m^2/°K$ for the conditions and reactor parameters specified in Table 5.5 for a plant-scale reactor was used. Since Aspen plus reactor kinetics input form only accepts SI units, reaction parameters (Table 5.1) for the rate expressions 5.3 and 5.4 were converted to SI units.

The rate expressions can be re-written as,

$$r_{gen} = \frac{A'_{gen} e^{-\left(\frac{E_{gen}}{R}\right)\left(\frac{1}{T}-\frac{1}{T^{cp}}\right)} {p_{CO}}^{0.705} p_{H_2}}{\left[1 + K'_1 p_{CO} + K'_2 {p_{H_2}}^{0.5}\right]^{n_{gen}}} \tag{5.19}$$

$$r_{dec} = \frac{A'_{dec} e^{-\left(\frac{E_{dec}}{R}\right)\left(\frac{1}{T}-\frac{1}{T^{cp}}\right)} p_{CO} p_{CH_3OH} p_{C_2H_5OH}}{\left[1 + K'_3 p_{CO} + K'_4 p_{CH_3OH} + K'_5 p_{C_2H_5OH}\right]^{n_{dec}}} \tag{5.20}$$

The kinetic parameters in SI units used in Aspen plus simulation are given in Table 5.6. Aspen plus input form for reaction kinetics and input specifications were given in Appendix 5B.

Kinetic Parameters	Value	Kinetic Parameters	Value
$A'_{gen}, \frac{kmol}{kg\ cat.s.(Pa)^{1.705}}$	2.953×10^{-17}	$ln(K'_3, Pa^{-1})$	-15.115
$A'_{dec}, \frac{kmol}{kg\ cat.s.(Pa)^{3}}$	1.132×10^{-21}	$ln(K'_4, Pa^{-1})$	-11.567
$E_{gen}, J/kmol$	64.79×10^{6}	$ln(K'_5, Pa^{-1})$	-10.333
$E_{dec}, J/kmol$	123.68×10^{6}	n_{gen}	1.730
$ln(K'_1, Pa^{-1})$	-16.074	n_{dec}	2.192
$ln(K'_2, Pa^{-0.5})$	-10.275		

Table 5.6. Empirical (EMP) model kinetic parameters in SI units for aspen plus simulation.

5.3.3.1. Isothermal Reactor

Simulation results for an isothermal lab-scale reactor are presented in Table 5.7. It is compared with the results obtained from MATLAB simulation and experimental results. The simulation results perfectly match the experimental results for alcohols, hydrocarbons and CO_2 productions. Once the MATLAB and Aspen plus models are validated with the experimental results for a lab-scale isothermal reactor, these models can be used for plant-scale non-isothermal reactor simulations.

Products, *mol/kg cat/hr*	Experimental	MATLAB Simulation	Aspen plus Simulation
CH_3OH	1.922	2.023	2.026
C_2H_5OH	0.485	0.473	0.474
C_3H_7OH	0.122	0.119	0.119
CH_4	1.410	1.378	1.376
C_2H_6	0.232	0.244	0.244
C_3H_8	0.091	0.093	0.093
CO_2	2.940	2.857	2.853
CO	53.007	53.046	53.085
H_2	51.289	51.151	51.186
CO Conv., *%*	13.64	13.57	13.26
Alcohol Sel, *mol %*	59.33	60.39	60.46

Operating Conditions = 590.15 *°K*, 84.21 *bar*, H_2/CO = 0.993 and GHSV = 2993 *L/kg cat/hr*

Table 5.7. Simulations and experimental results for a lab-scale reactor.

5.3.3.2. Non-Isothermal Reactor (Adiabatic and Non-Adiabatic)

Temperature profiles as estimated along the length of the reactor (expressed as weight of the catalyst) by MATLAB and Aspen plus simulation runs for a non-isothermal plant-scale reactor is shown in Fig. 5.4. Individual component flow rates are shown in Table 5.8. The predicted Aspen plus temperature profile perfectly matches the temperature profile obtained from the MATLAB simulation. A temperature rise of 11 °*K* was predicted at the outlet of the reactor. Reactor model developed in Aspen plus can further be extended for mixed alcohol plant simulations and cost optimizations

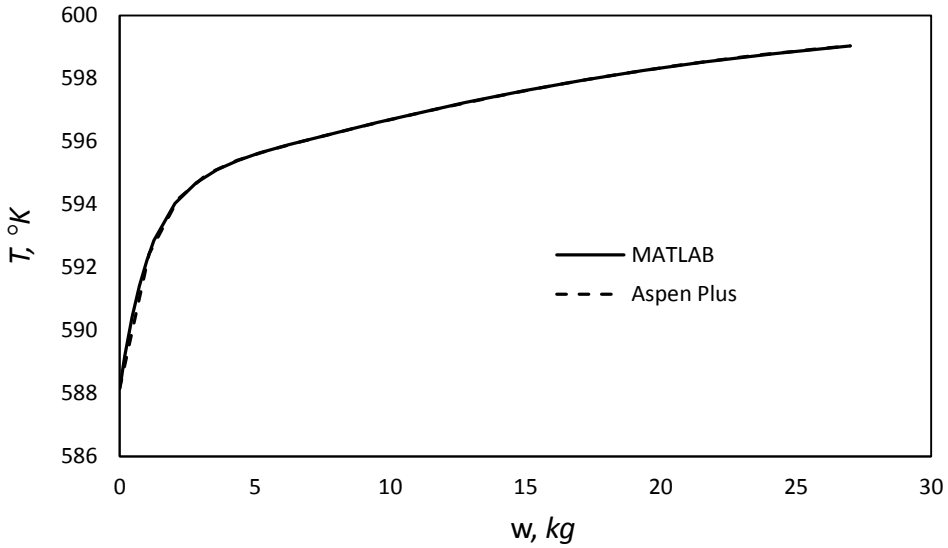

[redacted]

Products, *mol/kg cat/hr*	MATLAB Simulation	Aspen plus Simulation
CH_3OH	2.725	2.725
C_2H_5OH	0.646	0.646
C_3H_7OH	0.177	0.177
CH_4	2.061	2.061
C_2H_6	0.375	0.375
C_3H_8	0.146	0.146
CO_2	4.248	4.248
CO	79.922	79.923
H_2	78.040	78.041
CO Conv., *%*	13.10	13.10
Alcohol Sel., *mol %*	57.88	57.88
T_{out}, *°K*	599.03	599.04

Operating Conditions = 588.15 *°K*, 100 *bar*, H_2/CO = 1 and GHSV = 4500 *L/kg cat/hr*

Table 5.8. MATLAB and aspen plus simulation results for a plant-scale reactor.

Fig. 5.5 shows the effect of overall heat transfer coefficient, *U* on the outlet reactor temperature (also the maximum reactor temperature for the case considered) obtained from Aspen plus sensitivity analysis (Appendix 5B). Exponential increase in reactor exit temperature can be predicted at lower heat transfer coefficient values. Overall heat transfer coefficient is dependent on superficial gas velocity through the reactor and inside reactor tube diameter (eq. 5.10). It increases with increase in feed flow rate and decreases with increase in reactor diameter, and vice versa. On the other hand, smaller diameter tubes can increase pressure drop across the reactor and a higher feed flow rate can results in decrease of catalytic conversion to alcohols.

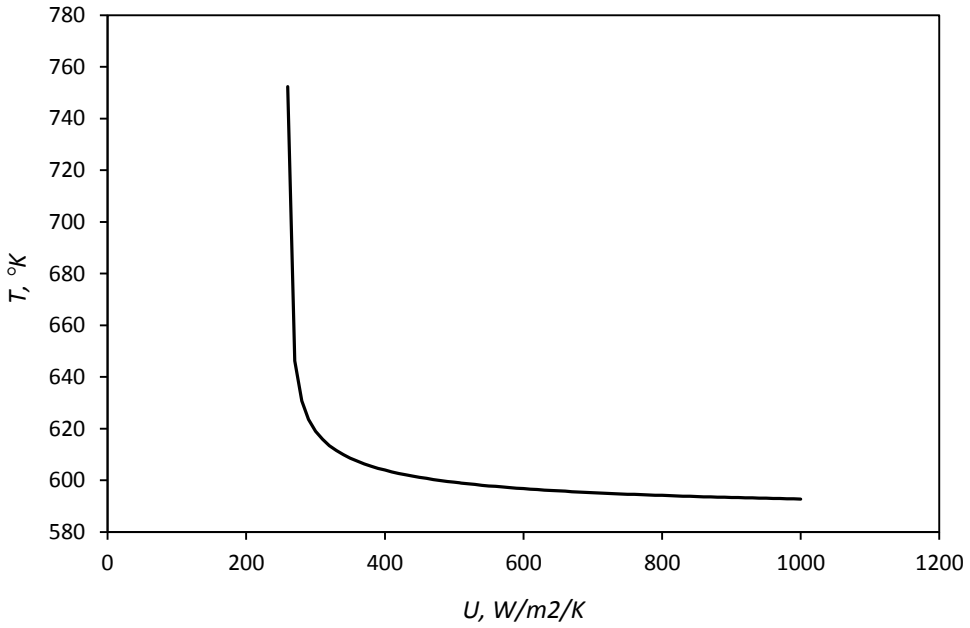

[redacted]

5.3.4. Aspen Plus Simulation with Recycle

A simplified aspen plus process flow diagram for higher alcohol synthesis is shown in Fig. 5.6. The syngas composition, as given in Table 5.9, can be obtained from gasification and steam reforming of biomass [7], was used for the simulation.

Components	***mol % (dry)***
CO	41.7
H_2	44.7
CO_2	11.4
CH_4	1.4
N_2	0.8

Table 5.9. Syngas composition obtained from Biomass.

The syngas and the recycle gas was compressed separately to a reaction pressure of 125 *bar* and mixed together and heated to a reaction temperature of 588.15 °*K* before it fed to the alcohol reactor. The aspen plus *RPlug* reactor model was selected to simulate a multi-tube shell and tube reactor with a constant coolant temperature. The catalyst was placed inside the tubes. The product stream from the reactor was flashed at 50 *bar* and 283.15 °*K* to separate the gases from the liquid alcohols. The liquid alcohols can be processed through a series of fractionation units to obtain high purity methanol, ethanol, and propanol/higher alcohols.

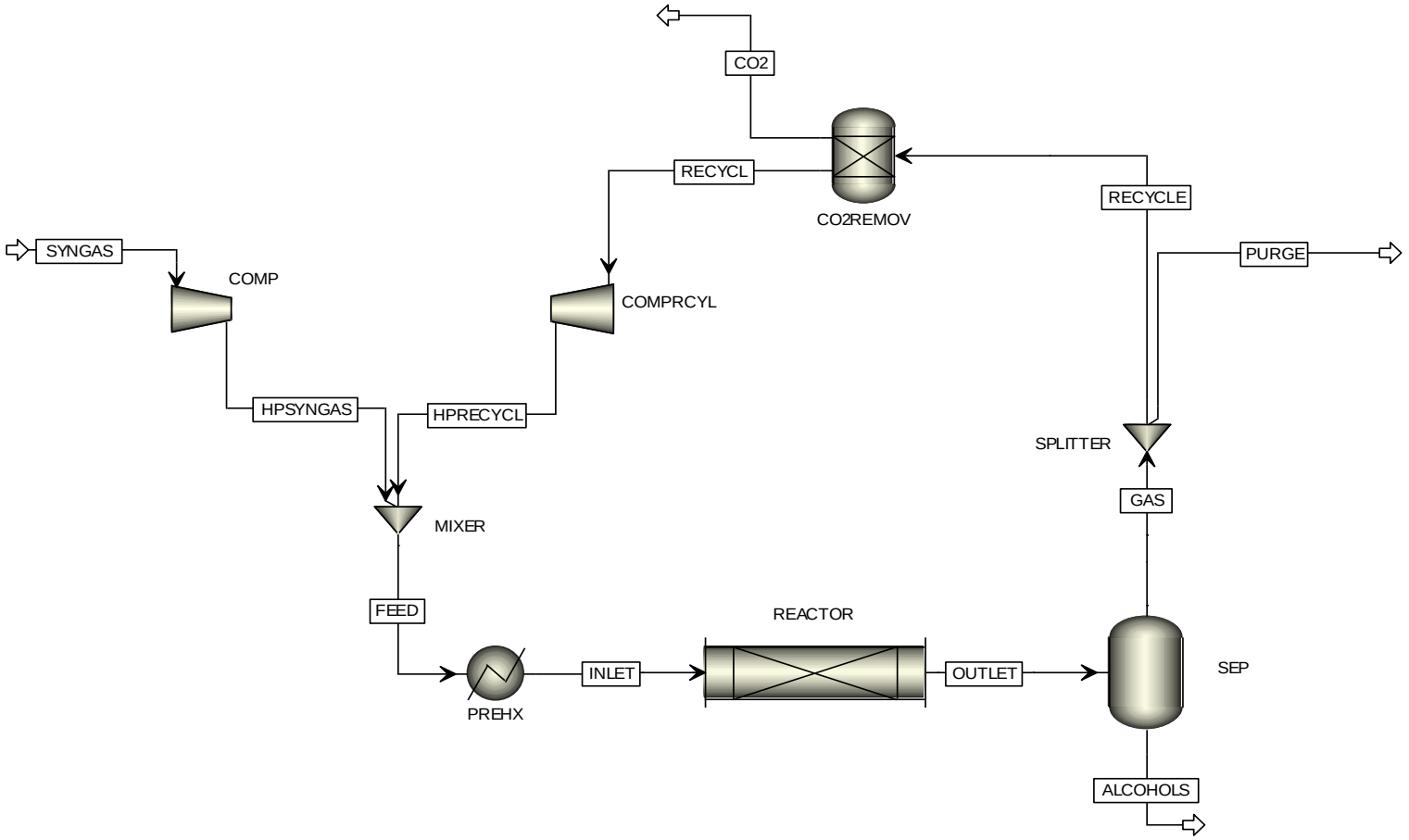
CO2
RECYCL
CO2REMOV
RECYCLE
SYNGAS
COMP
COMPRCYL
PURGE
HPSYNGAS
HPRECYCL
SPLITTER
GAS
MIXER
FEED
REACTOR
INLET
OUTLET
SEP
PREHX
ALCOHOLS

The gases from the separator are primarily a mixture of CO_2, CH_4, CO and H_2. Part of the gas was purged to avoid excess accumulation of CH_4 in the recycle loop. A split ratio of 0.15 was sufficient to keep CH_4 concentration below 10 *mol%* in the recycle loop. Some portion of the CO_2 from the recycle stream was also removed in a CO_2 removal unit to avoid excess accumulation of CO_2 in the recycle stream. It is required to remove 50 *mol%* of the CO_2 present in the recycle stream to keep the CO_2 concentration below 7 *mol%* in the recycle loop. The recycle stream was compressed and mixed with compressed syngas and fed to the alcohol reactor. The peng-robinson equation of state was selected as the global property method for aspen plus simulation.

The aspen plus input parameters and the key simulation results are summarized in Table 5.10. The alcohol productions were also compared with the target set by National Renewable Energy Laboratory (NREL) [8, 9]. The individual stream results are given in Appendix 5C. A slight decrease in H_2/CO ratio at outlet of the reactor was observed for the simulation parameters used in the simulation. The total alcohol production surpassed the target set by NREL, whereas the ethanol and higher alcohol production is lower than the target. It should be noted that the reaction pressure used by NREL is 207 *bar*, higher than the reaction pressure used in the present case. Higher pressure promotes higher alcohol productions and also increases the overall alcohol productions. The catalyst used by the NREL is cobalt promoted sulfide based Dow catalyst. Cobalt increases the selectivity towards ethanol and higher alcohols

Aspen plus Parameters	**This Work**	**NREL [8, 9]**
Catalyst	$Cs/MoS_2/AC$ (30.49 *wt%* active material*)	$K/Co/MoS_2$ (Dow)
Property method	Peng-Robinson EOS	
Syngas H_2/CO molar ratio	1.072	1.247
Reactor inlet temperature, *°K*	588.15	586.15
Shell side temperature, *°K*	588.15	578.15
Reactor pressure, *bar*	125	207
GHSV, *L/kg cat/hr*	4500 (3375 hr^{-1})	5000 hr^{-1}
Number of reactor	1	2 (parallel)
Total number of tubes	5000	9579
Inside diameter of tube, *m*	0.066	0.03
Reactor tube length, *m*	10.512	18.288
Mass of catalyst/tube, *kg*	27	
Split ratio, purge/(purge + recycle)	0.15	0.12
CO_2 Removal Unit Efficiency, *mol%*	50	
Overall heat transfer coefficient, $w/m^2/°K$	507.64	
Simulation Results		
Reactor outlet temperature, *°K*	599.66	595.15
Reactor inlet gas composition, *mol%*		
H_2	41.58	45.0
CO	40.53	30.0
CO_2	6.69	14.0
CH_4	8.20	7.7
CH_3OH	0.13	2.6
N_2	1.40	
Single pass CO conversion, *%*	14.14	29
Overall CO conversion, *%*	52.32 – 99.9	79
Alcohol Selectivity, *mol%*	48.3 – 98.7 (64.1 – 99 *wt %*)	81
Total Alcohol Productivity, *g/kg act. mat/hr*	404.86	368[#]
Ethanol Productivity, *g/kg act. mat/hr*	95.31	160[#]
Ethanol[+] Productivity, *g/kg act. mat/hr*	133.48	

* Active material refers to weight percent of Mo, Cs and S content of the catalyst.

[#] *g/kg cat/hr*, composition of active materials are not reported, it is assumed that the catalyst is a un-supported/powder catalyst

[+] Ethanol[+] refers to the combined production of ethanol and propanol.

Table 5.10. Aspen plus parameters and simulation results for higher alcohol synthesis from syngas.

The ranges of CO conversion and alcohol selectivity were reported. The purge line can be sent to a reformer for the generation of syngas and it can recycle back to the reactor. The upper values of CO conversion and alcohol selectivity were calculated by considering the complete recycle of purge line, whereas, the lower values were calculated without considering the purge recycle. The overall CO conversion and alcohol selectivity can be between 52.32 – 99.9 % and 48.3 – 98.7 *mol%*, depending on the reformer efficiency for the conversion of purge gas to syngas.

5.4. Conclusions

A non-isothermal reactor model was developed by using the simplified governing equations and the two reaction empirical model developed for higher alcohol synthesis. The MATLAB simulation results were verified with the experimental results and the simulation results obtained from aspen plus for an isothermal lab scale reactor. The aspen plus simulation results were also verified with the MATLB results for the case of non-isothermal plant scale reactor. The aspen plus simulation flow sheet of a single pass reactor was then extended to accommodate the multi tubular reactor with recycle stream. The process flow sheet developed in aspen plus is not yet optimized. Further work on process modification, optimization and cost optimization can be performed by using this flow sheet as a starting point.

5.5. Appendix

Appendix 5A: Example MATLAB Code for Non-Isothermal Reactor using the Empirical Model

Main Function

```
clear all;
clc;
format short g

%Estimated Parameters from Iso-thermal model using GA
%A's, mol/kg cat/hr, E's, KJ/mol
b=[18.596 86.653 64.786 123.68 0.41834 0.067884 1.09110 1.3744 1.1913 1.7301 2.1917];
%error = -0.077448 %workspace THESISFINAL3 ANSWER


global alpha pcp Tcp rxn rho dp R dt MW W t lambda factor L

factor=1;

%Input%

%%%%%%%%%%%%  Unit Dimesions (Reactor & Catalyst) %%%%%%%%%%%%

R=8.3145e-3;                                %KJ/(mol.K)
rho=750;                                    %Catalyst density, kg/m3
dp=3/1000;                                  %Particle dia, m
lambda=50.2/1000*3600;                      %Therml conductivity of steel at 500 C,
KJ/(hr.m.K)
% W=3e-3;                                       %lab-scale Catalyst weight, kg
% dt=0.5*2.54/100;                              %Tube inside dia, m
% t=0.125*2.54/100;                             %Tube thickness, m
% L=0.0315849;                                    %Length of Tube, m
% W=100e-3;                                     %bench-scale Catalyst weight, kg
% dt=0.834*2.54/100;                            %Tube inside dia, m
% t=0.0830*2.54/100;                            %Tube thickness, m
W=27;                                       %plant-scale Catalyst weight, kg
dt=2.6*2.54/100;                            %Tube inside dia, m
L=10.512;                                           %Length of Tube, m
t=0.15748*2.54/100;                         %Tube thickness, m


%%%%%%%%%%%%  Feed, Cooling Medium & Operating Conditions %%%%%%%%%%%%

GHSV=4500;                                 %Gas Hourly Space Velocity, L/kg cat/hr
% GHSV=2992.9;
Fo=GHSV/22.414*273.15/(273.15+25)*W         %Feed Flow, mol/hr
Tin=315+273.15;                             %Inlet Temp in K %Adiabatic 247 C, 252 C, 255
C
% Tin=590.15;
H2CO=1;                                     %H2/CO, v/v
% H2CO=0.99314065;
P=100;                                      %Reactor pressure, bar
% P=84.21050933;
Tc=315+273.15;                              %Coolant temperature, K

%%%%%%%%% REACTION STOICHIOMETRIES, KINETICS & OTHER PARAMETERS %%%%%%%%%%%%%
```

```
MW=[32.04146 46.06804 60.09462 74.1212 16.04246 30.06904 44.09562 44.0087 28.0097
2.01588];
rxn=2;
% [Methanol, Ethanol, Propanol, Butanol, Methane, Ethane,Propane, Carbon Dioxide, Carbon
Monoxide, Hydrogen]
alpha=[0.3080  0.0660 0.0070 0.0000 0.0700 0.0060 0.0000 0.1620 -0.7050  -1.0000; %CO+H2-
->CH3OH+C2H5OH+C3H7OH+CH4+C2H6+CO2
      -0.5905 -0.1030 0.0300 0.0000 0.4100 0.1100 0.0550 0.7520 -0.8405
0.0000];%CO+CH3OH+C2H5OH-->C3H7OH+CH4+C2H6+C3H8+CO2
Tcp=590.15;                              %Center Point Temp, K

Pcp=84.2105;                              %Center Point Pressure, bar

pcp=[1.4513 0.3661 0.0922 0 1.0650 0.1755 0.0685 2.2206 40.0347 38.7367]; %bar

%%%%%%%%%% ODE EVALUATION %%%%%%%
m=1;
c=length(MW);
%
XFoj=zeros;
WFoj=zeros;
% XFoc=zeros;
tau=W/Fo;               %kg.hr/molf

for i=1:1:m
    xzero=[0 0 Tin];
    wspan=[0 tau];
    op=[H2CO 1/tau Tc P]; %ratio(v/v),Fo (molf/kg cat/hr), K, bar(a)
    [WF0,XF0]=ode15s(@(WF0,XF0)ReactorKineticsNonIso(WF0,XF0,b,op),wspan,xzero);
    for j = 1:length(WF0)
         for l=1:length(xzero)
             XFoj(j,i,l) = XF0(j,l);
         end
    WFoj(j,i)=WF0(j,1);
    end
end

[r,s]=size(XFoj);
for i=1:1:s
    XFoc(i)=XFoj(find(XFoj(:,i),1,'last'),i);
end
XFo=[XFoc(1:m); XFoc(m+1:2*m)]';

[t,u]=size(WFoj);
for i=1:1:u
    WFo(i)=WFoj(find(WFoj(:,i),1,'last'),i);
end

yo=[zeros(c-2,m);(1/(H2CO+1));(H2CO/(H2CO+1))];

for i=1:1:m
    NrFo(:,i)=alpha'*XFo(i,1:rxn)';
    No(:,i)=Fo(i)*yo(:,i);
    Nr(:,i)=Fo(i)*NrFo(:,i);
    N(:,i)=No(:,i)+Nr(:,i);
    NFoest(:,i)=N(:,i)/Fo(i);
end
Nest=N/W;
Ncal=Nest';
y=N/sum(N);
Sel=(sum(N(1:4,:))/sum(N(1:7,:)))*100;
Conv=((1/tau*(1/(1+H2CO)))-Nest(9,:))/(1/tau*(1/(1+H2CO)))*100;
Tout=XFoc(m+2:3*m);
Tmax=max(XF0(:,3));

for i=1:1:m
    NMest(:,i)=bsxfun(@times,N(:,i),MW')/W;
end
NFocal=NFoest';
```

```
NMcal=NMest';

Conv
Sel %mol %
NMcal %g/kg cat/hr
NMT=NMcal*W % gm/hr
Ncal %mol/kg cat/hr
Tout %K
Tmax %K



% %
% figure(1)
% plot(WF0,XF0(:,1),'bo'); hold on
% plot(WF0,XF0(:,2),'bo');
% xlabel 'W/Fo, Kg/(mol/hr)',ylabel 'X (mol/kg cat/hr)'
%

WF0;
Np=(alpha'*XF0(:,1:2)')'/W*Fo % mol/kg cat/hr
dW=WF0*Fo % kg
Tp=XF0(:,3) %Temp Profile
Flow=Fo/W
% np=bsxfun(@times,Np,Fo);

figure(2)
plot(dW,XF0(:,3),'bo'); hold on
xlabel 'w (Kg)',ylabel 'T (K)'
%
% figure(3)
% plot(dW,Np(:,1),'bo'); hold on
% plot(dW,Np(:,2),'bo');
% plot(dW,Np(:,3),'bo');
% plot(dW,Np(:,4),'bo');
% plot(dW,Np(:,5),'bo');
% plot(dW,Np(:,6),'bo');
% plot(dW,Np(:,7),'bo');
% plot(dW,Np(:,8),'bo');
% xlabel 'w (Kg)',ylabel 'Fi (mol/kg cat/hr)'
```

Function ReactorKineticsNonIso (reaction kinetics)

```
function xprime=ReactorKineticsNonIso(~,x,b,op)

global alpha pcp Tcp rxn rho dp R dt MW W t lambda factor L

rhomol=op(4)*1e5/R*1e-3/x(3);           %mol/m3
rhogas=((MW(9)*1/(1+op(1))+MW(10)*op(1)/(1+op(1))))*rhomol*1e-3; %kg/m3

%%% CALCULATION OF GAS VISCOSITY %%%%

sigmaH2=2.915;                      % Angstrom
sigmaCO=3.590;                      % Angstrom
epskH2=38.0;                        % K
epskCO=110.0;                       % K

sigmamuH2=1.16145/((x(3)/epskH2)^0.14874)+0.52487/exp(0.77320*x(3)/epskH2)+2.16178/exp(2.
43787*x(3)/epskH2);
sigmamuCO=1.16145/((x(3)/epskCO)^0.14874)+0.52487/exp(0.77320*x(3)/epskCO)+2.16178/exp(2.
43787*x(3)/epskCO);

muCO=2.6693e-6*sqrt(MW(9)*x(3))/sigmaCO^2/sigmamuCO;          %Pa.s or kg/(m.s)
muH2=2.6693e-6*sqrt(MW(10)*x(3))/sigmaH2^2/sigmamuH2;         %Pa.s or kg/(m.s)
```

```
mumix=muCO/(1+(op(1)/(1+op(1)))/(1/(1+op(1)))/2/sqrt(2)*(1+(muCO/muH2)^0.5*(MW(10)/MW(9))
^0.25)^2/(1+MW(9)/MW(10))^0.5)+muH2/(1+(1/(1+op(1)))/(op(1)/(1+op(1)))/2/sqrt(2)*(1+(muH2
/muCO)^0.5*(MW(9)/MW(10))^0.25)^2/(1+MW(10)/MW(9))^0.5);  %Pa.s or or kg/(m.s)



%%% CALCULATION OF IDEAL HEAT CAPACITY  & HEAT OF FORMATION%%%

% Cp=3.5*R                  %KJ/(mol.K) for diatomic gas
CpCO=(3.376+0.557*x(3)*1e-3-0.031*1e5/x(3)^2)*R;
CpH2=(3.249+0.422*x(3)*1e-3+0.083*1e5/x(3)^2)*R;
%
CpCO=(2.9108e4+8.7730e3*((3.0851e3/x(3))/(sinh(3.0851e3/x(3))))+8.4553e3*((1.5382e3/x(3))
/(sinh(1.5382e3/x(3)))))*1e-6; %KJ/(mol.K)
%
CpH2=(2.7617e4+9.5600e3*((2.4660e3/x(3))/(sinh(2.4660e3/x(3))))+3.7600e3*((5.6760e3/x(3))
/(sinh(5.6760e3/x(3)))))*1e-6; %KJ/(mol.K)
Cp=CpCO*1/(1+op(1))+CpH2*op(1)/(1+op(1));

% Hf=[-201.3 -235.3 -255 -275.349 -74.87 -84.68 -103.85 -393.5 -110.5 0.0];   %KJ/mol

%Calculated from Aspen Plus
% Hf=[-184.94 -209.63 -220.84 -231.92 -61.958 -63.301 -75.249 -381.11 -101.95 8.46793];
%KJ/mol at 315 C

Hfch3oh=0.0734*x(3)-228.13;
Hfc2h5oh=0.1179*x(3)-278.99;
Hfc3h7oh=0.1588*x(3)-314.23;
Hfc4h9oh=0.2032*x(3)-351.43;
Hfch4=0.0579*x(3)-96.041;
Hfc2h6=0.0986*x(3)-121.27;
Hfc3h8=0.1418*x(3)-158.67;
Hfco2=0.0492*x(3)-410.03;
Hfco=0.0312*x(3)-120.28;
Hfh2=0.0294*x(3)-8.8418;

Hf=[Hfch3oh Hfc2h5oh Hfc3h7oh Hfc4h9oh Hfch4 Hfc2h6 Hfc3h8 Hfco2 Hfco Hfh2]; %KJ/mol


%%% CALCULATION OF THERMAL CONDUCTIVITY %%%

kH2=(Cp/R+5/4)*R*muH2/MW(10)*1e6;          %J/(K.m.s)
kCO=(Cp/R+5/4)*R*muCO/MW(9)*1e6;           %J/(K.m.s)

kmix=kCO/(1+(op(1)/(1+op(1)))/(1/(1+op(1)))/2/sqrt(2)*(1+(muCO/muH2)^0.5*(MW(10)/MW(9))^0
.25)^2/(1+MW(9)/MW(10))^0.5)+kH2/(1+(1/(1+op(1)))/(op(1)/(1+op(1)))/2/sqrt(2)*(1+(muH2/mu
CO)^0.5*(MW(9)/MW(10))^0.25)^2/(1+MW(10)/MW(9))^0.5);  %J/(s.m.K)


%%% Heat TRANSFER COEFFICIENT %%%%%

Vsup=op(2)/rhomol/3600*W/(pi/4*dt^2) %m/s
Rep=dp*Vsup*rhogas/mumix


alphaic=3.50*kmix/dt*exp(-4.6*dp/dt)*Rep^0.7*1e-3*3600;            % KJ/(hr.m2.K) for
Cooling
alphaih=0.813*kmix/dt*exp(-6*dp/dt)*Rep^0.9*1e-3*3600;           % KJ/(hr.m2.K) for
Heating

Uoh=(0.01545+0.6885e-6/dp*Rep)*1000;           % W/(m2.K)
%KJ/(hr.m2.K)

Ulevah=1/(1/alphaih+t/lambda);
Ulevac=1/(1/alphaic+t/lambda);
Ulub=Uoh;

Uc=Ulevac/3600*1000 %W/(m2.K)
```

```
Uh=Ulevah/3600*1000; %W/(m2.K)

fac=Ulevac/dt*factor;
delH=alpha*Hf';



%%%%%%%%%%%%%%          REACTION PARAMETERS     %%%%%%%%%%%%%%%%%%

%METHANOL
Agen=b(1);                      %mol/(Kgcat.hr)
Egen=b(3);                      %KJ/mol
ngen=b(10);
k=[b(5) b(6) b(7) b(8) b(9)];

%HYDROCARBONS
Adec=b(2);
Edec=b(4);
ndec=b(11);

%PARTIAL PRESSURE
yo=[0 0 0 0 0 0 0 0 1/(1+op(1)) op(1)/(1+op(1))];
ye=yo'+alpha'*x(1:rxn);
% Fi=ye*op(2);
y=ye/sum(ye);
p=y*op(4);

%ODEs

rgengn=(p(9)/pcp(9))^0.705*(p(10)/pcp(10));
rgengd=(1+k(1)*(p(9)/pcp(9))+k(2)*(p(10)/pcp(10))^0.5)^ngen;
rgeng=Agen*exp(-(Egen/R)*(1/x(3)-1/Tcp))*rgengn/rgengd;

rdecg=Adec*exp(-(Edec/R)*(1/x(3)-
1/Tcp))*((p(1)/pcp(1))*(p(2)/pcp(2))*(p(9)/pcp(9)))/((1+k(4)*(p(1)/pcp(1))+k(5)*(p(2)/pcp
(2))+k(3)*(p(9)/pcp(9)))^ndec);

rg=[rgeng rdecg];

rT=rg*(-delH)/Cp-4/rho/Cp*fac*(x(3)-op(3));

xprime=[rgeng; rdecg; rT]; %Non / Iso-thermal
```

Appendix 5B: Aspen Plus Entry Form for the Reaction Kinetics, and the effect of Overall Heat Transfer Coefficient on Reactor Outlet Temperature

Reaction kinetics entry form

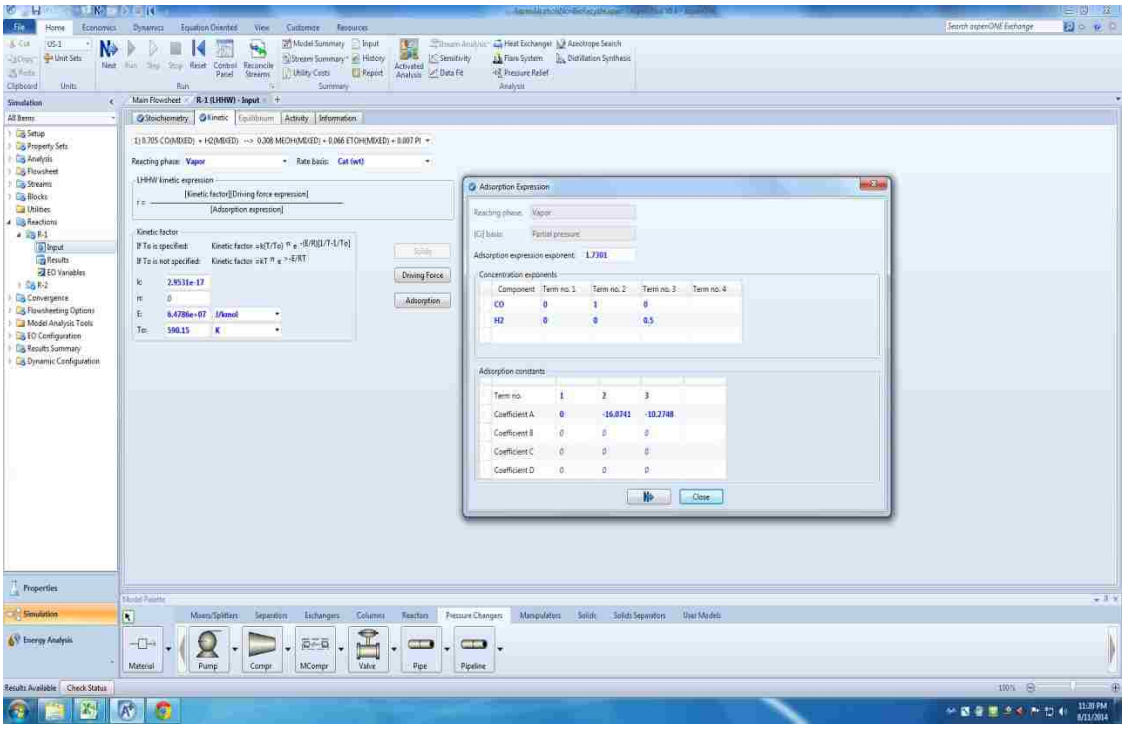

[redacted]

Overall Heat Transfer Coefficient

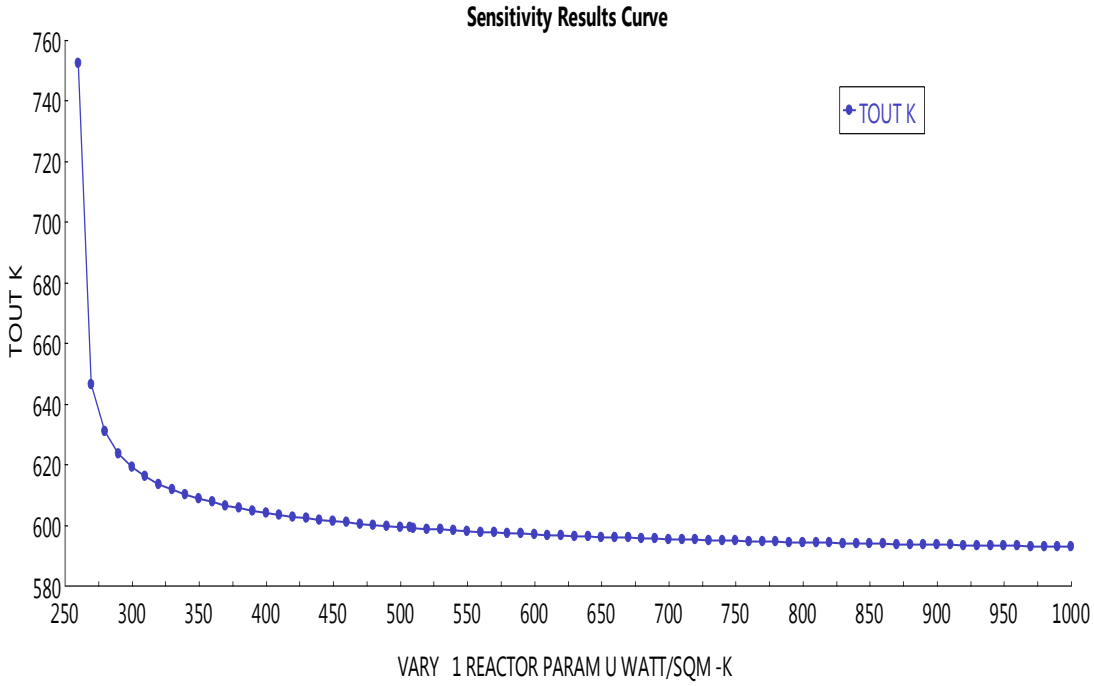

Appendix 5C: Aspen Plus Input Specifications and the Stream Results for Higher Alcohol Synthesis Process

Input Summary

```
;
;
;Input Summary created by Aspen Plus Rel. 30.0 at 18:43:29 Wed Aug 13, 2014
;Directory   Filename H:\.....\AspenPlus\aspenalcoholsnonisorecyclefinal.inp
;


DYNAMICS
   DYNAMICS RESULTS=ON

TITLE 'SVD for Higher Alcohol Synthesis'

IN-UNITS SI MASS-FLOW='gm/hr'

DEF-STREAMS CONVEN ALL

SIM-OPTIONS MASS-BAL-CHE=YES

MODEL-OPTION

DATABANKS 'APV84 PURE28' / 'APV84 AQUEOUS' / 'APV84 SOLIDS' /  &
      'APV84 INORGANIC' / NOASPENPCD

PROP-SOURCES 'APV84 PURE28' / 'APV84 AQUEOUS' / 'APV84 SOLIDS' &
       / 'APV84 INORGANIC'

COMPONENTS
   CH3OH CH4O /
   C2H5OH C2H6O-2 /
   C3H7OH+ C3H8O-1 /
   CH4 CH4 /
   C2H6 C2H6 /
   C3H8 C3H8 /
   CO2 CO2 /
   CO CO /
   H2 H2 /
   N2 N2 /
   H2O H2O /
   O2 O2

SOLVE
   RUN-MODE MODE=SIM

FLOWSHEET
   BLOCK REACTOR IN=INLET OUT=OUTLET
   BLOCK SPLITTER IN=GAS OUT=PURGE RECYCLE
   BLOCK SEP IN=OUTLET OUT=GAS ALCOHOLS
   BLOCK MIXER IN=HPSYNGAS HPRECYCL OUT=FEED
   BLOCK PREHX IN=FEED OUT=INLET
   BLOCK COMP IN=SYNGAS OUT=HPSYNGAS
   BLOCK COMPRCYL IN=RECYCL OUT=HPRECYCL
   BLOCK CO2REMOV IN=RECYCLE OUT=CO2 RECYCL

PROPERTIES PENG-ROB
   PROPERTIES IDEAL / RK-ASPEN

PROP-DATA PRKBV-1
   IN-UNITS SI MASS-FLOW='gm/hr'
```

```
  PROP-LIST PRKBV
  BPVAL CH3OH C2H6 .0270000000 0.0 0.0 0.0 1000.000000
  BPVAL C2H6 CH3OH .0270000000 0.0 0.0 0.0 1000.000000
  BPVAL CH3OH CO2 .0230000000 0.0 0.0 0.0 1000.000000
  BPVAL CO2 CH3OH .0230000000 0.0 0.0 0.0 1000.000000
  BPVAL C2H5OH C3H8 .0315000000 0.0 0.0 0.0 1000.000000
  BPVAL C3H8 C2H5OH .0315000000 0.0 0.0 0.0 1000.000000
  BPVAL CH4 C2H6 -2.6000000E-3 0.0 0.0 0.0 1000.000000
  BPVAL C2H6 CH4 -2.6000000E-3 0.0 0.0 0.0 1000.000000
  BPVAL CH4 C3H8 .0140000000 0.0 0.0 0.0 1000.000000
  BPVAL C3H8 CH4 .0140000000 0.0 0.0 0.0 1000.000000
  BPVAL CH4 CO2 .0919000000 0.0 0.0 0.0 1000.000000
  BPVAL CO2 CH4 .0919000000 0.0 0.0 0.0 1000.000000
  BPVAL CH4 CO .0300000000 0.0 0.0 0.0 1000.000000
  BPVAL CO CH4 .0300000000 0.0 0.0 0.0 1000.000000
  BPVAL CH4 H2 .0156000000 0.0 0.0 0.0 1000.000000
  BPVAL H2 CH4 .0156000000 0.0 0.0 0.0 1000.000000
  BPVAL C2H6 C3H8 1.10000000E-3 0.0 0.0 0.0 1000.000000
  BPVAL C3H8 C2H6 1.10000000E-3 0.0 0.0 0.0 1000.000000
  BPVAL C2H6 CO2 .1322000000 0.0 0.0 0.0 1000.000000
  BPVAL CO2 C2H6 .1322000000 0.0 0.0 0.0 1000.000000
  BPVAL C2H6 CO -.0226000000 0.0 0.0 0.0 1000.000000
  BPVAL CO C2H6 -.0226000000 0.0 0.0 0.0 1000.000000
  BPVAL C2H6 H2 -.0667000000 0.0 0.0 0.0 1000.000000
  BPVAL H2 C2H6 -.0667000000 0.0 0.0 0.0 1000.000000
  BPVAL C3H8 CO2 .1241000000 0.0 0.0 0.0 1000.000000
  BPVAL CO2 C3H8 .1241000000 0.0 0.0 0.0 1000.000000
  BPVAL C3H8 CO .0259000000 0.0 0.0 0.0 1000.000000
  BPVAL CO C3H8 .0259000000 0.0 0.0 0.0 1000.000000
  BPVAL C3H8 H2 -.0833000000 0.0 0.0 0.0 1000.000000
  BPVAL H2 C3H8 -.0833000000 0.0 0.0 0.0 1000.000000
  BPVAL CO2 H2 -.1622000000 0.0 0.0 0.0 1000.000000
  BPVAL H2 CO2 -.1622000000 0.0 0.0 0.0 1000.000000
  BPVAL CO H2 .0919000000 0.0 0.0 0.0 1000.000000
  BPVAL H2 CO .0919000000 0.0 0.0 0.0 1000.000000
  BPVAL CH3OH N2 -.2141000000 0.0 0.0 0.0 1000.000000
  BPVAL N2 CH3OH -.2141000000 0.0 0.0 0.0 1000.000000
  BPVAL CH4 N2 .0311000000 0.0 0.0 0.0 1000.000000
  BPVAL N2 CH4 .0311000000 0.0 0.0 0.0 1000.000000
  BPVAL C2H6 N2 .0515000000 0.0 0.0 0.0 1000.000000
  BPVAL N2 C2H6 .0515000000 0.0 0.0 0.0 1000.000000
  BPVAL C3H8 N2 .0852000000 0.0 0.0 0.0 1000.000000
  BPVAL N2 C3H8 .0852000000 0.0 0.0 0.0 1000.000000
  BPVAL CO2 N2 -.0170000000 0.0 0.0 0.0 1000.000000
  BPVAL N2 CO2 -.0170000000 0.0 0.0 0.0 1000.000000
  BPVAL CO N2 .0307000000 0.0 0.0 0.0 1000.000000
  BPVAL N2 CO .0307000000 0.0 0.0 0.0 1000.000000
  BPVAL H2 N2 .1030000000 0.0 0.0 0.0 1000.000000
  BPVAL N2 H2 .1030000000 0.0 0.0 0.0 1000.000000

DEF-STREAMS LOAD

PROP-SET PS-1 HIG SUBSTREAM=MIXED

STREAM SYNGAS
  SUBSTREAM MIXED TEMP=25. <C> PRES=50. <bar> MOLE-FLOW=2.207
  MOLE-FRAC CH4 0.014 / CO2 0.114 / CO 0.417 / H2 0.447 / &
    N2 0.008

BLOCK MIXER MIXER
  PARAM PRES=125. <bar> NPHASE=1 PHASE=V T-EST=0. <C>
  PROPERTIES PENG-ROB FREE-WATER=STEAM-TA SOLU-WATER=3  &
    TRUE-COMPS=YES
  BLOCK-OPTION FREE-WATER=NO

BLOCK SPLITTER FSPLIT
  PARAM NPHASE=1 PHASE=V
  FRAC PURGE 0.15
```

```
  PROPERTIES PENG-ROB FREE-WATER=STEAM-TA SOLU-WATER=3  &
    TRUE-COMPS=YES
  BLOCK-OPTION FREE-WATER=NO

BLOCK CO2REMOV SEP
  PARAM NPHASE=1 PHASE=V
  FRAC STREAM=RECYCL SUBSTREAM=MIXED COMPS=CO2 FRACS=0.5
  FLASH-SPECS CO2 TEMP=25. <C>
  FLASH-SPECS RECYCL TEMP=100. <C>
  BLOCK-OPTION FREE-WATER=NO

BLOCK PREHX HEATER
  PARAM TEMP=588.15 PRES=125. <bar> NPHASE=1 PHASE=V
  PROPERTIES PENG-ROB FREE-WATER=STEAM-TA SOLU-WATER=3  &
    TRUE-COMPS=YES
  BLOCK-OPTION FREE-WATER=NO

BLOCK SEP FLASH2
  PARAM TEMP=10. <C> PRES=50. <bar>
  PROPERTIES PENG-ROB FREE-WATER=STEAM-TA SOLU-WATER=3  &
    TRUE-COMPS=YES

BLOCK REACTOR RPLUG
  PARAM TYPE=TCOOL-SPEC NTUBE=5000 LENGTH=10.512 DIAM=2.6 <in>  &
    PDROP=0.0 U=507.64 NPOINT=25 CATWT=135001.5312  &
    IGN-CAT-VOL=YES CAT-PRESENT=YES CAT-RHO=750.
  COOLANT TEMP=315. <C>
  PROPERTIES PENG-ROB FREE-WATER=STEAM-TA SOLU-WATER=3  &
    TRUE-COMPS=YES / PENG-ROB FREE-WATER=STEAM-TA  &
    SOLU-WATER=3 TRUE-COMPS=YES
  REACTIONS RXN-IDS=R-1 R-2

BLOCK COMP COMPR
  PARAM TYPE=ISENTROPIC PRES=125. <bar> NPHASE=1 SB-MAXIT=30  &
    SB-TOL=0.0001
  PROPERTIES PENG-ROB FREE-WATER=STEAM-TA SOLU-WATER=3  &
    TRUE-COMPS=YES
  BLOCK-OPTION FREE-WATER=NO

BLOCK COMPRCYL COMPR
  PARAM TYPE=ISENTROPIC PRES=125. <bar> SB-MAXIT=30  &
    SB-TOL=0.0001

EO-CONV-OPTI

REPORT INPUT NOINSERT NOADA BLOCKS STREAMS

BLOCK-REPORT NONEWPAGE COMPBAL

STREAM-REPOR MOLEFLOW MASSFLOW MOLEFRAC NOMASSFRAC

REACTIONS R-1 LHHW
  REAC-DATA 1 PHASE=V CBASIS=PARTIALPRES RBASIS=CAT-WT
  RATE-CON 1 PRE-EXP=2.9531E-017 ACT-ENERGY=64786000.  &
    T-REF=590.15
  STOIC 1 MIXED CO -0.705 / H2 -1. / CH3OH 0.308 /  &
    C2H5OH 0.066 / C3H7OH+ 0.007 / CH4 0.07 / C2H6  &
    0.006 / CO2 0.162
  DFORCE-EXP-1 1 MIXED CO 0.705 / MIXED H2 1. / MIXED  &
    CH3OH 0. / MIXED C2H5OH 0. / MIXED C3H7OH+ 0. /  &
    MIXED CH4 0. / MIXED C2H6 0. / MIXED CO2 0.
  DFORCE-EQ-1 REACNO=1 A=0.
  DFORCE-EQ-2 REACNO=1 A=-9000000000.
  ADSORP-EXP REACNO=1 CID=CO SSID=MIXED EXPONENT=0. 1. 0. /  &
    REACNO=1 CID=H2 SSID=MIXED EXPONENT=0. 0. 0.5
  ADSORP-EQTER REACNO=1 TERM= 1 A=0. / REACNO=1 TERM= 2  &
    A=-16.07413282 / REACNO=1 TERM= 3 A=-10.27481138
  ADSORP-POW REACNO=1 EXPONENT=1.7301
```

```
   PARAM NTERM-ADS=3

REACTIONS R-2 LHHW
   REAC-DATA 1 PHASE=V CBASIS=PARTIALPRES RBASIS=CAT-WT
   RATE-CON 1 PRE-EXP=1.1316E-021 ACT-ENERGY=123680000.  &
      T-REF=590.15
   STOIC 1 MIXED CH3OH -0.5905 / C2H5OH -0.103 / CO  &
      -0.8405 / C3H7OH+ 0.03 / CH4 0.41 / C2H6 0.11 /  &
      C3H8 0.055 / CO2 0.752
   DFORCE-EXP-1 1 MIXED CH3OH 1. / MIXED C2H5OH 1. / MIXED  &
      CO 1. / MIXED C3H7OH+ 0. / MIXED CH4 0. / MIXED  &
      C2H6 0. / MIXED C3H8 0. / MIXED CO2 0.
   DFORCE-EQ-1 REACNO=1 A=0.
   DFORCE-EQ-2 REACNO=1 A=-9000000000.
   ADSORP-EXP REACNO=1 CID=CH3OH SSID=MIXED EXPONENT=0. 1. 0.  &
      0. / REACNO=1 CID=C2H5OH SSID=MIXED EXPONENT=0. 0. 1.  &
      0. / REACNO=1 CID=CO SSID=MIXED EXPONENT=0. 0. 0. 1.
   ADSORP-EQTER REACNO=1 TERM= 1 A=0. / REACNO=1 TERM= 2  &
      A=-11.5673679 / REACNO=1 TERM= 3 A=-10.33303156 /  &
      REACNO=1 TERM= 4 A=-15.11548568
   ADSORP-POW REACNO=1 EXPONENT=2.1917
   PARAM NTERM-ADS=4

PROP-TABLE PURE-1 PROPS
   IN-UNITS SI MASS-FLOW='gm/hr' PRESSURE=bar TEMPERATURE=C  &
      PDROP='N/sqm'
   MOLE-FLOW CH3OH 1 / C2H5OH 1 / C3H7OH+ 1 / CH4 1 /  &
      C2H6 1 / C3H8 1 / CO2 1 / CO 1 / H2 1
   PROPERTIES IDEAL FREE-WATER=STEAM-TA SOLU-WATER=3  &
      TRUE-COMPS=YES
   VARY TEMP
   RANGE LOWER=250. UPPER=600. NPOINT= 15
   VARY PRES
   RANGE LIST=100.
   PARAM
   TABULATE PROPERTIES=PS-1
;
;
```

Stream Results

Substream: MIXED	SYNGAS	HPSYNGAS	RECYCL	HPRECYCL	FEED	INLET	OUTLET	GAS	RECYCLE	CO2	PURGE	ALCOHOLS
Mole Flow kmol/sec												
CH3OH	0.00E+00	1.12E-02	1.12E-02	1.12E-02	1.12E-02	1.12E-02	1.10E-01	1.32E-02	1.12E-02	0.00E+00	1.97E-03	9.68E-02
C2H5OH	0.00E+00	1.48E-03	1.48E-03	1.48E-03	1.48E-03	1.48E-03	2.54E-02	1.74E-03	1.48E-03	0.00E+00	2.61E-04	2.37E-02
C3H7OH+	0.00E+00	2.27E-04	2.27E-04	2.27E-04	2.27E-04	2.27E-04	7.53E-03	2.68E-04	2.27E-04	0.00E+00	4.01E-05	7.26E-03
CH4	3.09E-02	6.58E-01	6.58E-01	6.58E-01	6.89E-01	6.89E-01	7.75E-01	7.74E-01	6.58E-01	0.00E+00	1.16E-01	6.33E-04
C2H6	0.00E+00	8.84E-02	8.84E-02	8.84E-02	8.84E-02	8.84E-02	1.04E-01	1.04E-01	8.84E-02	0.00E+00	1.56E-02	4.86E-04
C3H8	0.00E+00	3.32E-02	3.32E-02	3.32E-02	3.32E-02	3.32E-02	3.96E-02	3.91E-02	3.32E-02	0.00E+00	5.86E-03	5.42E-04
CO2	2.52E-01	3.11E-01	3.11E-01	3.11E-01	5.62E-01	5.62E-01	7.38E-01	7.31E-01	6.21E-01	3.11E-01	1.10E-01	7.21E-03
CO	9.20E-01	2.48E+00	2.48E+00	2.48E+00	3.40E+00	3.40E+00	2.92E+00	2.92E+00	2.48E+00	0.00E+00	4.38E-01	4.46E-04
H2	9.87E-01	2.51E+00	2.51E+00	2.51E+00	3.49E+00	3.49E+00	2.95E+00	2.95E+00	2.51E+00	0.00E+00	4.42E-01	1.46E-04
N2	1.77E-02	9.98E-02	9.98E-02	9.98E-02	1.18E-01	1.18E-01	1.18E-01	1.17E-01	9.98E-02	0.00E+00	1.76E-02	3.54E-05
H2O	0.00E+00	0.00E+00	0.00E+00	0.00E+00	0.00E+00	0.00E+00	0.00E+00	0.00E+00	0.00E+00	0.00E+00	0.00E+00	0.00E+00
O2	0.00E+00	0.00E+00	0.00E+00	0.00E+00	0.00E+00	0.00E+00	0.00E+00	0.00E+00	0.00E+00	0.00E+00	0.00E+00	0.00E+00
Mole Frac												
CH3OH	0.0000	0.0018	0.0018	0.0018	0.0013	0.0013	0.0141	0.0017	0.0017	0.0000	0.0017	0.7056
C2H5OH	0.0000	0.0002	0.0002	0.0002	0.0002	0.0002	0.0033	0.0002	0.0002	0.0000	0.0002	0.1723
C3H7OH+	0.0000	0.0000	0.0000	0.0000	0.0000	0.0000	0.0010	0.0000	0.0000	0.0000	0.0000	0.0529
CH4	0.0140	0.1062	0.1062	0.1062	0.0820	0.0820	0.0995	0.1012	0.1012	0.0000	0.1012	0.0046
C2H6	0.0000	0.0143	0.0143	0.0143	0.0105	0.0105	0.0134	0.0136	0.0136	0.0000	0.0136	0.0035
C3H8	0.0000	0.0054	0.0054	0.0054	0.0040	0.0040	0.0051	0.0051	0.0051	0.0000	0.0051	0.0039
CO2	0.1140	0.0501	0.0501	0.0501	0.0669	0.0669	0.0947	0.0955	0.0955	1.0000	0.0955	0.0525
CO	0.4170	0.4011	0.4011	0.4011	0.4053	0.4053	0.3753	0.3820	0.3820	0.0000	0.3820	0.0033
H2	0.4470	0.4047	0.4047	0.4047	0.4158	0.4158	0.3786	0.3853	0.3853	0.0000	0.3853	0.0011
N2	0.0080	0.0161	0.0161	0.0161	0.0140	0.0140	0.0151	0.0154	0.0154	0.0000	0.0154	0.0003
H2O	0.0000	0.0000	0.0000	0.0000	0.0000	0.0000	0.0000	0.0000	0.0000	0.0000	0.0000	0.0000
O2	0.0000	0.0000	0.0000	0.0000	0.0000	0.0000	0.0000	0.0000	0.0000	0.0000	0.0000	0.0000

Stream Results Contd.

Mass Flow gm/hr												
CH3OH	0.00E+00	1.29E+06	1.29E+06	1.29E+06	1.29E+06	1.29E+06	1.27E+07	1.52E+06	1.29E+06	0.00E+00	2.28E+05	1.12E+07
C2H5OH	0.00E+00	2.45E+05	2.45E+05	2.45E+05	2.45E+05	2.45E+05	4.21E+06	2.88E+05	2.45E+05	0.00E+00	4.32E+04	3.92E+06
C3H7OH+	0.00E+00	4.92E+04	4.92E+04	4.92E+04	4.92E+04	4.92E+04	1.63E+06	5.79E+04	4.92E+04	0.00E+00	8.68E+03	1.57E+06
CH4	1.78E+06	3.80E+07	3.80E+07	3.80E+07	3.98E+07	3.98E+07	4.47E+07	4.47E+07	3.80E+07	0.00E+00	6.71E+06	3.65E+04
C2H6	0.00E+00	9.56E+06	9.56E+06	9.56E+06	9.56E+06	9.56E+06	1.13E+07	1.13E+07	9.56E+06	0.00E+00	1.69E+06	5.26E+04
C3H8	0.00E+00	5.28E+06	5.28E+06	5.28E+06	5.28E+06	5.28E+06	6.29E+06	6.21E+06	5.28E+06	0.00E+00	9.31E+05	8.60E+04
CO2	3.99E+07	4.92E+07	4.92E+07	4.92E+07	8.91E+07	8.91E+07	1.17E+08	1.16E+08	9.84E+07	4.92E+07	1.74E+07	1.14E+06
CO	9.28E+07	2.50E+08	2.50E+08	2.50E+08	3.43E+08	3.43E+08	2.95E+08	2.95E+08	2.50E+08	0.00E+00	4.42E+07	4.50E+04
H2	7.16E+06	1.82E+07	1.82E+07	1.82E+07	2.53E+07	2.53E+07	2.14E+07	2.14E+07	1.82E+07	0.00E+00	3.21E+06	1.06E+03
N2	1.78E+06	1.01E+07	1.01E+07	1.01E+07	1.19E+07	1.19E+07	1.19E+07	1.18E+07	1.01E+07	0.00E+00	1.78E+06	3.57E+03
H2O	0.00E+00	0.00E+00	0.00E+00	0.00E+00	0.00E+00	0.00E+00	0.00E+00	0.00E+00	0.00E+00	0.00E+00	0.00E+00	0.00E+00
O2	0.00E+00	0.00E+00	0.00E+00	0.00E+00	0.00E+00	0.00E+00	0.00E+00	0.00E+00	0.00E+00	0.00E+00	0.00E+00	0.00E+00
Total Flow kmol/sec	2.21E+00	6.19E+00	6.19E+00	6.19E+00	8.40E+00	8.40E+00	7.79E+00	7.65E+00	6.50E+00	3.11E-01	1.15E+00	1.37E-01
Total Flow gm/hr	1.43E+08	3.82E+08	3.82E+08	3.82E+08	5.26E+08	5.26E+08	5.26E+08	5.08E+08	4.32E+08	4.92E+07	7.62E+07	1.80E+07
Total Flow cum/sec	1.0948	2.2000	3.8872	2.2000	2.8439	3.4316	3.2375	3.5489	3.0166	0.1016	0.5323	0.0061
Temperature K	298.15	510.8439	373.15	510.8439	486.8746	588.15	599.6615	283.15	283.15	298.15	283.15	283.15
Pressure N/sqm	5.00E+06	1.25E+07	5.00E+06	1.25E+07	1.25E+07	1.25E+07	1.25E+07	5.00E+06	5.00E+06	5.00E+06	5.00E+06	5.00E+06
Vapor Frac	1	1	1	1	1	1	1	1	1	1	1	0
Liquid Frac	0	0	0	0	0	0	0	0	0	0	0	1
Solid Frac	0	0	0	0	0	0	0	0	0	0	0	0
Enthalpy J/kmol	-9.22E+07	-6.74E+07	-7.20E+07	-6.74E+07	-7.29E+07	-6.95E+07	-8.15E+07	-9.02E+07	-9.02E+07	-3.96E+08	-9.02E+07	-2.58E+08
Enthalpy J/kg	-5.11E+06	-3.93E+06	-4.20E+06	-3.93E+06	-4.20E+06	-4.00E+06	-4.35E+06	-4.89E+06	-4.89E+06	-9.00E+06	-4.89E+06	-7.07E+06
Enthalpy Watt	-2.04E+08	-4.17E+08	-4.46E+08	-4.17E+08	-6.13E+08	-5.84E+08	-6.35E+08	-6.90E+08	-5.87E+08	-1.23E+08	-1.04E+08	-3.54E+07
Entropy J/kmol-K	1.22E+04	1.06E+04	8.02E+03	1.06E+04	1.21E+04	1.85E+04	1.40E+04	-1.58E+03	-1.58E+03	-3.64E+04	-1.58E+03	-2.64E+05
Entropy J/kg-K	675.02	619.86	467.80	619.86	693.09	1066.41	745.19	-85.87	-85.87	-826.75	-85.87	-7236.97
Density kmol/cum	2.0160	2.8150	1.5931	2.8150	2.9536	2.4478	2.4056	2.1559	2.1559	3.0553	2.1559	22.4519
Density kg/cum	36.383	48.279	27.323	48.279	51.352	42.558	45.109	39.740	39.740	134.461	39.740	819.345
Average MW	18.047	17.151	17.151	17.151	17.386	17.386	18.751	18.433	18.433	44.010	18.433	36.493
Liq Vol 60F cum/sec	0.1182	0.3354	0.3354	0.3354	0.4536	0.4536	0.4205	0.4142	0.3520	0.0166	0.0621	0.0064

Table 5C. Aspen plus simulation stream results of higher alcohol synthesis process.

5.5. References

1. Froment, G.F., K.B. Bischoff, and J.D. Wilde, *Chemical Reactor Analysis and Design*. Third ed. 2011: John Wiley & Sons, Inc.
2. Emrani, A.S., M. Saber, and F. Farhadi, *Modeling and Optimization of Fixed-Bed Fischer-Tropsch Synthesis using Genetic Algorithm.* Journal of Chemical and Petroleum Engineering, Unversity of Tehran, 2012. **46**(1): p. 1-11.
3. Balakrishnan, A.R. and D.C.T. Pei, *Heat Transfer in Gas-Solid Packed Bed Systems. 1. A Critical Review.* Ind. Eng. Chem. Process Des. Dev., 1979. **18**(1): p. 30-40.
4. Bird, R.B., W.E. Stewart, and E.N. Lightfoot, *Transport phenomena*. Second ed. 2007: John Wiley & Sons.
5. *Aspen plus V8.0, Aspen Technology, Inc., MA, 2012*.
6. Yusup, S., P.N. Anh, and H. Zabiri, *A Simulation Study of an Industrial Methanol Reactor based on Simplified Steady-State Model.* IJRRAS, 2010. **5**(3): p. 213-222.
7. Phillips, S.D., *Technoeconomic Analysis of a Lignocellulosic Biomass Indirect Gasification Process to Make Ethanol via Mixed Alcohols Synthesis.* Ind. Eng. Chem. Res., 2007. **46**: p. 8887-8897.
8. Dutta, A., et al., *Techno-economics for conversion of lignocellulosic biomass to ethanol by indirect gasification and mixed alcohol synthesis.* Environmental Progress & Sustainable Energy, 2012. **31**(2): p. 182-190.

9. Dutta, A., et al., *Process Design and Economics for Conversion of Lignocellulosic Biomass to Ethanol: Thermochemical Pathway by Indirect Gasification and Mixed Alcohol Synthesis*. 2011, National Renewable Energy Laboratory.

Chapter 6

Summary and Future Work

6.1. Summary

The present work relates to the catalytic conversion of syngas into mixed alcohols with molybdenum based catalysts supported on activated carbon. The sulfide based catalyst was chosen for its tolerance of sulfur. The primary focus has been on the development and optimization of catalyst preparation process, kinetic model development of alcohol synthesis reactions, and modeling and simulation of alcohol synthesis process. The main features of this work are summarized below.

1. A method has been developed for the preparation of a cesium promoted molybdenum disulfide catalyst supported on activated carbon. The steps involved are molybdenum precursor, e.g. ammonium molybdate tetrahydrate (AMT) or molybdenum dioxydiacetylacetonate ($MoO_2(acac)_2$) promotion, calcination, sulfidation, and cesium formate promotion. Similar method has also been applied for the preparation of cobalt promoted oxide catalysts supported on activated carbon. The decomposition temperature of AMT to MoO_2 on an activated carbon support was found to be 773.15 $°K$ in an inert atmosphere.
2. The amount of cesium loading on the catalyst was varied in order to find the optimum cesium to molybdenum ratio. As the cesium loading increases, the

alcohol yields passes through a maximum, while the hydrocarbon formation were progressively suppressed. The optimum atomic ratio of cesium to molybdenum was found to be around 0.7 – 0.8.

3. The total alcohol production of 576.62 – 942.2 *g/kg metals/hr* with C_2^+/C_1 alcohol ratio of 0.39 – 0.74 *w/w* was achieved at a reaction pressure of about 100 *bar*.
4. The catalyst was tested extensively at higher alcohol synthesis (HAS) reaction conditions. The catalyst was tested for more than 600 *hrs* without injecting any sulfur species in the syngas feed. Loss of catalyst activity and formation of water was not observed during this period.
5. The scalability of the catalyst was successfully evaluated on a 100 *g* scaled-up unit. The catalyst preparation and testing process are reproducible.
6. The presence of cobalt in the cesium promoted molybdenum based oxide catalysts supported on activated carbon promotes the ethanol and higher alcohol productions with the expense of alcohol selectivity. A C_2^+/C_1 alcohol ratio of 3.21 *w/w* was achieved with an expense of alcohol selectivity to 18.46 *mol %*.
7. Combined x-ray photoelectron spectroscopy (XPS) and x-ray diffraction (XRD) analyses reveals dramatic changes on surface and bulk composition of the catalyst at different stages of catalyst preparation and testing process. Crystalline MoO_2 is the only phase present after calcination of AMT, promoted on an activated carbon support, at 773.15 °*K* in an inert atmosphere. It was found that the complete conversion of MoO_2 to MoS_2 is not possible at a lower sulfidaton temperature of 673.15 °*K*. A longer sulfidation time of 52 *hrs* was not helpful at this temperature. The XRD of the sulfidized sample shows the presence of crystalline MoO_2 and

amorphous or poorly crystalline MoS_2 phase. The XPS reveals the presence of MoS_2 at the surface of the catalyst. Even though the sulfidized sample has the bulk structure of MoO_2, its surface is covered with MoS_2. Molybdenum carbide was not observed at any stages of the catalyst preparation and testing process.

8. The XRD and XPS studies revealed the surface oxidation of MoO_2 to MoO_3, when the calcined pellets were exposed to atmospheric conditions. Although the MoS_2 is a stable component at atmospheric conditions, XPS reveals that, it oxidizes to MoO_3 upon exposure to atmosphere after the catalyst is promoted with cesium formate. The XRD and XPS also reveal that, the exposure of cesium promoted catalysts to atmosphere produce unwanted sulfate species, such as crystalline Cs_2SO_4. It should be noted that, Cs_2SO_4 is not the active component for alcohol synthesis and it forms only when the catalyst is exposed to atmosphere. The sulfate species were not detected on the surface of tested catalyst stored in an inert atmosphere. It is important to keep the catalyst away from atmosphere oxygen and moisture at any time once it is promoted with cesium formate.
9. The effect of sulfidation temperature on catalyst composition and performance was studied. Complete conversion of MoO_2 or AMT to MoS_2 on an activated carbon support was achieved at a higher sulfidation temperature of 923.15 $°K$. Increase in MoS_2 in the catalyst improves the catalyst activity and alcohol selectivity.
10. The presence of methanol and ethanol in the syngas feed was studied on catalyst performance and product distributions. These results were coupled with methanol

and ethanol decompositions in an inert atmosphere to understand the reaction pathways involved during alcohol synthesis reactions. A slight increase in the production of higher alcohols were observed upon introduction of methanol or ethanol into the syngas feed. In addition to the established CO insertion reactions, it was found that the additional butanol was formed by ethanol coupling reactions. Methanol coupling was not observed. At least a part of the hydrocarbons formed are formed as secondary products from the alcohols. Aldehydes are one of the products formed, when the system was deprived from syngas. It is believed that, the alcohols are formed *via* aldehyde route. The catalyst regains its activity once the external injection of methanol or ethanol was stopped.

11. The HAS reactions are very complex; it involves many series and parallel reactions. This reaction network can be described by a minimum number of independent reactions. A steady-state kinetic model of the power-law type was developed. The exponents of the partial pressure terms in the power-law model were used to determine the rate determining steps and these results were subsequently used for the development of Langmuir Hinshelwood (LH) type kinetic models. Both power law and LH models were developed by using seven independent reactions.
12. Singular value decomposition (SVD) was applied for the first time to HAS reactions. The reaction network was successfully described by two empirical forward reactions only. This reduces the computational effort required for the estimation of kinetic parameters. An empirical (EMP) model involving LH type rate expression was developed.

13. A genetic algorithm minimization technique was used for the estimation of power-law, LH, and EMP model kinetic parameters. The predicted results were compared with the experimental results by pictorial representations describing the effect of reaction temperature, pressure, gas hourly space velocity, and hydrogen to carbon monoxide ratio on product yields. The EMP model was preferred over LH model because it involves only two reactions, and less kinetic parameters.
14. A non-isothermal alcohol synthesis reactor model using the two reaction EMP model was developed in MATLAB. Leva's correlation for cooling up the reaction mixture was used for the calculation of the overall heat transfer coefficient. The overall heat transfer coefficient of 507.64 $W/m^2/°K$ was calculated for a single tube plant scale tubular reactor of dimension 0.066 *m* (ID) × 10.512 *m* (length) × 0.004 *m* (wall thickness) operating at a HAS operating condition of 588.15 °*K*, 100 *bar*, 4500 *L/kg cat/hr* GHSV, H_2/CO of 1.0 *v/v*, and a constant outside reactor wall temperature of 588.15 °*K*. Effect of reactor diameter and GHSV on product yields and reactor temperature were studied. A reactor diameter of 0.066 *m* or less and a GHSV of 2000 *L/kg cat/hr* or more is recommended for the present catalyst. Further increase in reactor diameter or decrease in GHSV may leads to runaway situations.
15. The reactor dimensions determined from MATLAB simulations was used in Aspen plus reactor simulation and validated with aspen plus results. The aspen plus reactor model is further extended to incorporate recycle of unreacted syngas from outlet of the reactor back to the syngas feed. Preliminary aspen plus simulation shows, a 15 % purge followed by 50 % removal of carbon dioxide

from recycle stream can keep the methane and carbon dioxide level below 10 *mol %* and 7 *mol %* respectively at inlet of the reactor for the reaction conditions used. At these conditions, the overall CO conversion and alcohol selectivity are calculated to be 52.32 *%* and 48.3 *mol %* respectively. These values can be improved by recycling the purge stream back to the syngas feed after reforming. The HAS process is not optimized; further work on process and cost optimization should be performed.

6.2. Future Work

Although the present study provided significant information about HAS process with molybdenum based sulfide catalysts supported on activated carbon, there are potential scopes for further improvement of catalyst activity by modifying the catalyst preparation and testing process, *in situ* characterization of the catalyst during alcohol synthesis reaction, ex situ characterization of the catalyst at various stages of catalyst preparation and testing process, improvement on kinetic models of alcohol synthesis reactions, and optimization of integrated HAS processes from the syngas source, such as biomass, natural gas, or landfill gas to high purity alcohols. Research opportunities, unfinished work, and new directions to follow the present work are summarized as follows:

1. The present catalyst consists of 20 – 30 *wt %* active material (combined weight of molybdenum, sulfur, and cesium). The effect of active material loading, specifically the molybdenum loading, on catalyst performance must be evaluated. It is expected that, the optimum cesium to molybdenum atomic ratio won't change with increase or decrease of molybdenum loading [1], and complete

conversion of MoO_2 to MoS_2 invariably fixes the sulfur concentration (sulfur to molybdenum atomic ratio of approximately 2.0) in the catalyst.

2. Sulfidation of MoO_2 to MoS_2 requires a higher sulfidation temperature of 923.15 *°K*, whereas MoO_3 can be sulfidized to MoS_2 at relatively a lower temperature of 673.15 *°K*, under reducing atmosphere of 5 *vol %* H_2S in hydrogen [2-4]. A catalyst preparation process involving alumina as a support can be proposed. It involves AMT promotion on an alumina support, calcination to MoO_3 in the presence of flowing air or oxygen, sulfidation of MoO_3 to MoS_2 at a temperature of 673.15 *°K* or lower, and cesium promotion. It may require additional cesium to counter the acidic sites that might be present in alumina support. Hydrotalcite is another potential support could be tried. Both hydrotalcite and molybdenum disulfide have layered structure. The idea is to deposit molybdenum disulfide onto the relatively high surface area hydrotalcite support as an epitaxial extension of the hydrotalcite structure.
3. The sulfidation time is a function of batch size. A larger batch requires a longer sulfidation time for a fixed flow rate of sulfidizing and reducing agent. Additional experiments can be designed to relate sulfidation time with bath size, and develop correlations for the break through curves relating transient behavior of exit concentrations etc. These information will be helpful in determining the sulfidation time and the amount of sulfidizing agent required for a given batch size. Other sulfidizing agents, such as dimethyl disulfide and dimethyl sulfide in hydrogen could be tried. Dimethyl disulfide and dimethyl sulfide are less polluting agents than hydrogen sulfide, which is indeed a highly toxic compound.

4. The cesium promotion is always being the last step for the present catalyst. Different order of promotion can be tried. It was observed that the addition of cobalt can increase the C_2^+/C_1 alcohol ratio to 3.21 *w/w*. Further work on effect of transition metals, such as cobalt, nickel, iron, cupper, manganese, and rhodium on the catalyst performance can be explored. A combination of these metals can also be used. Effect of other alkali metals, such as potassium, lithium, rubidium, and sodium can also be compared with cesium. Potassium and cobalt are the most used promoters on molybdenum sulfide based catalysts for alcohol synthesis.
5. The sulfidation temperatures used for the present catalysts are 723.15 °*K* or 923.15 °*K*. It is possible that, the direct sulfidation of AMT to MoS_2 may require a sulfidation temperature lower than 923.15 °*K*. It is expected that, the MoS_2 crystal size will increase with increase in sulfidation temperature. Increase in crystal size may cause sintering of the catalyst [5, 6]. The catalyst activity should go through a maximum value with increase in sulfidation temperature. The optimum sulfidation temperature can be determined.
6. The alcohol synthesis reactions are high pressure reactions and high pressure favors the total alcohol as well as higher alcohol productions. The catalyst performance at a reaction pressure above 100 *bar* should be explored. In the literature, pressure up to 200 *bars* was used [7-9].
7. The catalyst was tested continuously for 600 *hrs* at HAS conditions. Decline in catalyst activity was not observed during this period. The catalyst should be tested for a longer period of time (few thousand hours) to ensure the long-term stability

of the present catalyst. Effect of sulfur species (H_2S) in the feed on catalyst performance must also be explored.

8. Higher alcohols over cesium promoted MoS_2 catalysts supported on activated carbon are formed by CO insertion mechanism, whereas the higher alcohols are formed by aldol condensation or coupling mechanism over cesium promoted Cu/Zn/Al catalysts supported on hydrotacite. Increase in chain length from C_1 to C_2 is the rate limiting step for HAS over cesium modified Cu/Zn/Al catalysts (slowest step), subsequent increase in chain lengths are very quick. Therefore, the primary product from these catalysts is methanol. Preliminary ethanol injection experiments into syngas shows the complete consumption of methanol product to higher alcohols; primarily ethanol, propanol, and butanol. Considering the different reaction mechanisms of cesium modified Cu/Zn/Al and cesium promoted MoS_2 catalysts, one can design a double bed testing process with sulfide based catalyst being the first bed and Cu/Zn/Al catalyst as the second bed operating in a series, wherein ethanol from the first bed can react with methanol from the second bed and produce higher alcohols.
9. The active species of the catalyst and the surface intermediates during HAS reactions are still unknown. *In situ* characterization of the catalyst during HAS reactions can give insight about the active species and surface intermediates. The techniques such as extended x-ray absorption fine structure (EXAFS), infrared (IR) and raman spectroscopy, and XRD can be used for *in situ* characterization of the catalyst.

10. The catalyst surface changes after each stage of preparation and testing processes. Coupling XRD and XPS with scanning electron microscopy (SEM), energy dispersive x-ray spectroscopy (EDS or EDX), and transmission electron microscopy (TEM) is a good method for surface analysis of a catalyst. The XRD was used to determine bulk crystal structure and chemical phase composition, whereas the XPS was used to determine the surface oxidation states and semi quantitative elemental composition at the surface. The SEM, EDS, and TEM can be used for high resolution imaging and quantitative measurement of the surface elements. The other techniques such as x-ray fluorescence spectroscopy (XRF) or inductively coupled plasma mass spectroscopy (ICP-MS) can be used for the determination of bulk elemental composition of the catalyst. The surface area, pore volume, and average pore diameter of the catalysts can be measured by widely accepted brunauer, emmett and teller (BET) method. The temperature programmed reduction (TPR) can be used to determine the reduction temperature of AMT promoted on an activated carbon support. It can also give the oxidation states of the surface and bulk of the catalyst. The particle size distribution can also be determined by SEM or TEM or any other optical imaging techniques.
11. The cesium promoted MoS_2 supported catalyst was tested under the influence of feed and recycles impurities such as methanol, ethanol, carbon dioxide, and methane. The short-term exposure to these impurities does not deteriorate the catalyst performance. However, a long term testing under the influence of these impurities must be examined to ensure the long-term stability of the catalyst.

12. The kinetic parameters estimated for HAS reactions are based on the steady-state results, where the feed is free from impurities. Effect of external injections of methanol, ethanol, carbon dioxide, and methane were not taken into considerations. These results can be included in the model parameters estimation to simulate a real case of alcohol synthesis reactions.
13. The steady-state kinetic models developed for alcohol synthesis reactions can further be extended to include the transient behavior of the catalyst. These models can give important information during start-up and shut down of the reactor.
14. The simplified process developed in aspen plus can be used as a starting point to develop a fully integrated alcohol synthesis process. The present process can be integrated with a syngas production process and recycling of purge gas etc. The combined cost and process optimization of the integrated unit can be performed.

6.3. References

1. *The Economical Production of Alcohol Fuels from Coal-Derived Synthesis Gas, 1999*. West Virginia University Research Corporation.
2. Boer, M.d., et al., *The Structure of Highly Dispersed SiO_2-Supported Molybdenum Oxide Catalysts during Sulfidation.* J. Phys. Chem., 1994. **98**: p. 7862-7870.
3. Jong, A.M.d., et al., *Sulfidation Mechanism of Molybdenum Catalysts Supported on a SiO_2/Si(100) Model Support Studied by Surface Spectroscopy.* J. Phys. Chem., 1993. **97**: p. 6477-6483.

4. Weber, T., et al., *Basic Reaction Steps in the Sulfidation of Crystalline MoO_3 to MoS_2, As Studies by X-ray Photoelectron and Infrared Emission Spectroscopy.* J. Phys. Chem., 1996. **100**: p. 14144-14150.

5. Silvy, R.P., et al., *Influence of Sulfidation Temperature on the Dispersion and Activity of Cobalt-Molybdenum Catalysts Supported on γ-Alumina.* Bull. Soc. Chim. Belg., 1984. **93**(8-9): p. 775-782.

6. Li, Z., et al., *Effect of sulfidation temperature on the catalytic behavior of unsupported MoS_2 catalysts for synthetic natural gas production from syngas.* Journal of Molecular Catalysis A: Chemical, 2013. **378**: p. 99-108.

7. Iranmahboob, J., *Formation of Ethanol and Higher Alcohols from Syngas*, in *Chemical Engineering*. 1999, Mississippi State University.

8. Iranmahboob, J. and D.O. Hill, *Alcohol synthesis from syngas over $K_2CO_3/CoS/MoS_2$ on activated carbon.* Catalysis Letters, 2002. **78**(1-4): p. 49-55.

9. Dutta, A., et al., *Process Design and Economics for Conversion of Lignocellulosic Biomass to Ethanol: Thermochemical Pathway by Indirect Gasification and Mixed Alcohol Synthesis*. 2011, National Renewable Energy Laboratory.

Vita

Ranjan K. Sahoo was born in Rourkela, India. He earned a Bachelor of Technology in Chemical Engineering from National Institute of Technology Rourkela, India in 2003. From May 2003 to September 2005, he was awarded a National Fellowship to pursue a Master of Technology in Chemical Engineering at Indian Institute of Technology Kanpur, India. He entered graduate study in Chemical Engineering at Lehigh University, Bethlehem, Pennsylvania in the fall of 2008 and awarded with a PhD in January 2015. He accepted employment in October 2014 as a Research Engineer with AMCS Corporation, New Jersey.